Using ultrasound to investigate relaxation and resonance phenomena in wheat flour dough

By

Yuanzhong Fan

A Thesis submitted to the Faculty of Graduate Studies of the University of Manitoba

In partial fulfillment of the requirements of the degree of

MASTER OF SCIENCE

Department of Physics and Astronomy

University of Manitoba

Winnipeg

Table of Contents

List of Tables

List of Figures

Abstract

This thesis is based on observations of the physical properties of wheat flour dough using ultrasonic measurements. Three frequency ranges were used in the study, low frequencies (near 40 kHz), intermediate frequencies (1 to 5 MHz, where bubble resonance effects are apparent), and high frequencies (near 20 MHz). Doughs mixed under different head space air pressures, from vacuum to atmospheric pressure, as well as under nitrogen, were studied at low frequency to investigate their relaxation behavior. Subsamples from ambient dough and vacuum dough displayed differences in the dependence of velocity and attenuation on time after compression, but no post mixing relaxation effect was apparent. A critical headspace pressure of approximately 0.16 atmospheres determined whether vacuum-like or ambient-like relaxation was observed. A peak in attenuation and changes in ultrasonic velocity were observed around the bubble resonance frequency, and these ultrasonic parameters changed substantially as a function of time. A bubble resonance model was used to interpret the results around the bubble resonance frequency, and bubble size distributions were estimated for ambient and vacuum dough from the ultrasonic data. For the high frequency range, a molecular relaxation model was used to interpret the results. Different fast relaxation times were observed for ambient dough (5 ns) and vacuum dough (1 ns). This relaxation time may be associated with conformational rearrangements in glutenin inside the dough matrix. These experiments have enabled dough relaxation to be probed over a very wide range of time scales (from ns to hours), and will lead to a better understanding of the role of dough matrix and gas cell effects on the physical properties of wheat flour doughs.

Acknowledgements

With a deep sense of gratitude, I wish to express my sincere thanks to both of my supervisors, Dr. J. H. Page and Dr. M. G. Scanlon, for their valuable counsel, constant guidance, encouragement and financial support during the course of this work. Without their advice, extreme hard work and patience on reading and commenting constructively on the thesis, it would have been impossible to complete the thesis in this manner. I also would like to thank Dr. Andrew Frederiksen for agreeing to be member of my examining committee and for his encouragement to me to start using Matlab, with which I did all the computational analysis in this thesis.

Special thanks go to Dr. Valentin Leroy for his suggestions and patient explanation of the bubble model that we used to explain the frequency dependence of ultrasonic parameters around the bubble resonance frequency, and for writing the Matlab program used to compare this model's predictions with experiment. I also wish to thank G. Roy, Department of Physics and Astronomy, for all the help he provided on using the mechanical equipment.

Thanks also go to all my friends who gave me technical suggestions and help in everyday life.

Last but not least, I would like to thank my mother, father, and brother for their support and understanding throughout the course of my thesis work. Special thanks go to my wife for her emotional support. She made the long trip from China and took care of my everyday life for the last four months that I was in Winnipeg.

DEDICATION

This is dedicated to my parents and my wife Jing

Chapter 1 Introduction

1.1. The importance of studying dough properties

Wheat is the world's most widely cultivated food plant. It is eaten in various forms by more than 1000 million human beings, and makes a larger contribution to the calories and protein available to man than any other food (Aykroyd and Doughty, 1970). Figure 1.1 shows some of the foods made from wheat flour.

Figure 1.1. Some foods made from wheat flour (Faridi and Faubion, 1995)

Dough is one of the principal intermediate stages in the transformation of wheat (Bloksma, 1971), through flour, to other end-use foods. One of the most important dough end-use foods is bread. The significance of bread in human life was clearly reviewed by Scanlon and Zghal (Scanlon and Zghal, 2001). The mixture of wheat-flour, water, yeast and other ingredients produces dough with specific viscoelastic

characteristics (combining the properties of a Hookean solid with those of a non-Newtonian viscous fluid (Faubion and Hoseney, 1989)), capable of retaining gas and therefore producing aerated goods (Garcia-Alvarez *et al.*, 2006). A rheological knowledge of dough is essential to better control the food making process (e.g., extrusion, lamination, etc.) and to produce high quality final products (Létang *et al*., 1999). Many empirical instruments (e.g. farinographs, mixographs) and fundamental instruments (e.g. rheometers) are used to evaluate the mechanical properties of doughs for these purposes (Walker and Hazelton, 1996). Because of the viscoelastic nature of the dough, time-dependent changes in its properties have been a major focus of experimental studies (Bloksma, 1990, Létang *et al*., 1999).

1.2. Basic structure of dough and the importance of bubbles in breadmaking

At the microscopic level, dough is a heterogeneous material, consisting of a concentrated suspension of almost spherical solid particles (starch granules) in a viscoelastic matrix (hydrated gluten), but also containing air (Létang *et al.,* 1999). Figure 1.2 shows the microscopic structure of dough and bubbles in dough. Basically, for the purposes of this thesis, we can consider dough to be a two-phase material containing a continuous viscoelastic matrix containing the starch granules and the isolated air bubbles.

a. The continuous phase: The glutenin forms a three dimensional matrix with disulfide

bonds, tyrosine crosslinks (Tilley *et al.,* 2001), hydrogen bonds and many other kinds of interactions. Other smaller gluten polymers (the gliadins) are associated with the glutenin network. The gluten network makes the framework of the dough. Starch granules are buried in the matrix.

b. Dispersed phase: The air bubbles are dispersed in the dough with a size distribution which is influenced by the type of mixer, and by the rate and intensity of the mixing action, as well as by the viscosity of the dough (MacRitchie, 1985).

Figure 1.2. Scanning electron micrographs of dough (A, B and C) (Pyler, 1973) and images of bubbles in dough (Bugusu *et al.*, 2002).

Air bubbles incorporated in dough during mixing are fundamental and important to breadmaking. All the nuclei for developing gas cells that make up the air phase in the bread crumb must be generated in the mixer (Scanlon and Zghal, 2001), and in the subsequent operations, including fermentation (if leavening agents are present), cutting or sheeting, no more gas cells are generated (Baker and Mize, 1941). Aeration during dough mixing is critical to achieving a baked loaf of good volume, structure, and texture (Campbell *et al*., 1998) and it affects the dough rheology not only through the physical presence of bubbles in dough but also through the contribution of oxygen during mixing (Chin *et al*., 2005).

1.3. Ultrasound as a tool for investigating the physical properties of dough

Traditional methods for dough testing are slow and off-line and do not provide fundamental rheological information (Garcia-Alvarez *et al.*, 2006). There is a need to develop new techniques that can perform precise evaluations of the quality of doughs and the use of ultrasound is really novel and promising for this purpose (Létang *et al.*, 2001).

Ultrasonic testing has many advantages, including:

a. It is a non-destructive test.

b. It takes rapid measurements and can get real time results. Therefore it has a great potential as an on-line quality control tool (Forrest, 1996; Saggin and Coupland, 2001)

c. It can propagate in optically opaque materials.

d. It is relatively less expensive than many other non-destructive measurement techniques.

e. The large impedance mismatch between air and most materials means that ultrasound is very sensitive to the presence of bubbles.

Although ultrasonic techniques are commonly used in materials science for investigating the mechanical properties of inorganic materials, their applications to biological systems are less well established (Elmehdi, 2001). Biological materials are generally complex, heterogeneous and their properties are time dependent. The more complex the system, the more difficult the theoretical interpretation of the experimental data will be (Létang *et al.*, 2001). From above, it is clear that biomaterials, such as dough, are generally multiphase, and this multiphase nature leads to the existence of an internal structure of the materials that influences the macroscopic properties. The attenuation and phase velocity of ultrasonic waves in the biomaterial will thus be affected (Kaczmarek *et al.*, 2000).

1.4. The aim of the research

The aim of this thesis is to use ultrasound to investigate the physical properties of bread dough, specifically the effect of gas cells on the properties of the dough. To reduce the complexity of the system, the only ingredients used in dough preparation are flour, water and salt.

The research can be divided into three parts:

a. Investigations of the effect of different concentrations of air bubbles in the dough on the relaxation behavior of ultrasonic parameters.

b. Investigations of the effect of different gases (air and nitrogen) on the relaxation behavior of ultrasonic parameters.

c. Investigations of the distribution of air bubbles in dough mixed under ambient pressure conditions and under vacuum (to attain very low bubble concentrations) and a study of the temporal evolution of the bubble distribution.

In each part of the research, two different kinds of relaxation behavior were investigated, post mixing relaxation (the evolution in properties with the time after mixing), and sample preparation relaxation (the evolution in properties with the time after compressing the sample of dough from a ball-shape to a plate-shape (so that it is suitable for ultrasonic transmission experiments)).

1.5. Thesis outline

The thesis contains five chapters. The first chapter introduces the research topic. The second chapter describes the sample preparation and ultrasonic measurement apparatus. Chapter 3 is a detailed description of the data analysis method. The first part of Chapter 3 explains how the two important ultrasonic parameters (phase velocity and attenuation coefficient) were obtained and corrected due to the impedance mismatching of the transducer and the dough samples. The second part of Chapter 3 is a

computational simulation of one of the analysis methods. This simulation helps us to understand the uncertainty, reliability and limitations of the method and it will be helpful for future work. All the results and discussion are included in chapter 4 which contains three parts. The first part of the chapter reports on the low frequency measurements (40 kHz measurements). The relaxation behavior was found to be opposite in the vacuum and ambient mixed doughs. The relaxation behavior of doughs mixed at various headspace pressures was also studied in this part. In addition, a comparison of the properties of nitrogen mixed dough and ambient mixed dough was covered at the end of the first part. The second part of Chapter 4 reports on the high frequency measurement results for both ambient mixed dough and vacuum mixed dough, from 1 MHz to 20 MHz. Both the post mixing relaxation and post sample preparation relaxations are shown individually at each frequency range. The whole frequency spectrum of phase velocity and attenuation for ambient mixed dough and vacuum mixed dough were dealt with at the end of this part of the chapter. The third part of Chapter 4 is the interpretation of the frequency and time dependent response of the behavior of the dough. Two models are introduced, one to explain the bubble effect around the bubble resonance frequency range, and the other to interpret the high frequency end results, which allow us to describe the properties of the matrix. The distribution of bubble sizes was estimated from the ultrasonic results for ambient mixed dough and vacuum mixed dough. Although the bubble size distribution obtained from the bubble model was different to the distribution obtained from an x-ray tomography experiment, a very clear changing of bubble sizes

(disproportionation) was found by ultrasound. Using the model for interpreting the frequency dependence of the dough at frequencies where matrix properties will dominate, two different relaxation times were obtained - one for ambient dough (about 5 ns) and one for vacuum dough (about 1 ns). On the basis of examining molecular and structural events reported to occur in dough, I propose that these relaxation times might be associated with the conformational rearrangements in glutenin inside the dough matrix, and so point to differences in matrix properties as a result of inclusion of air bubbles in the dough.

Chapter 2 Apparatus and Experimental Procedure

2.1. Dough preparation

The sample preparation entails mainly mixing of dough. Mixing makes an apparently homogeneous mass from dough ingredients (Bloksma, 1988). During mixing, the dough ingredients are first blended together and ingredients are hydrated or solubilized. The second set of events that happens during mixing is the development of the gluten polymers into a viscoelastic film that will retain gas, and the occlusion of air nuclei into the dough from the headspace of the mixer (Elmehdi, 2001). There are two popularly used methods for characterizing the development of the dough, Farinograph and Mixograph. In 1932, Brabender reported on the development of the Farinograph, while the following year, Swanson and Working (1933) described another recording dough mixer, which later became known as the Mixograph (Walker *et al.*, 1997).

The Farinograph employs broad, sigmoid-shaped paddles and measures dough consistency as it is kneaded between two of these blades (Walker *et al.*, 1997). Figure 2.1 is a typical Farinograph curve, which is known as a farinogram (resistance to the mixer rotation exerted by the developing dough is measured in Brabender units [BU] versus time in minutes). We can obtain a number of different parameters from the figure. One of them is the Farinograph absorption, which is also called optimum water absorption of the flour. The more water added to the flour and other ingredients, the lower the peak value of the farinogram, since dough of higher water content generally offers less resistance to mixing. Conventionally, the amount of water when the

farinogram peak is centered on the 500 BU line is taken as the optimum water absorption for this flour.

Figure 2.1. A typical farinogram, with some commonly measured indices indicated (Reprinted from Atwell (2001)).

For some strong flours, the Farinograph cannot provide enough mixing intensity. Compared to the Farinograph, the Mixograph's vertically oriented planetary pin design provided higher shear rates and more intensive mixing (Walker *et al.*, 1997). However, the Mixograph cannot be used to give the optimum water absorption of a flour.

Figure 2.2 is a typical mixogram of wheat flour dough. The y-axis is a measure of the dough's resistance to extension (torque) caused by the passage of the mixing pins. The *x*-axis represents the time over which the dough has been mixed. The peak point is the "mixing time" of the flour. It has also been called the point of minimum mobility or the point of optimum mixing time (Elmehdi, 2001). For mixing time to the left of the peak, the dough is undermixed and to the right of the peak the dough is overmixed.

Figure 2.2. A typical mixogram, labeled to show the development (hydration), optimum (peak), and breakdown stages (Reprinted from Atwell (2001)).

In all my experiments a mixer operating on similar principles to the mixograph was chosen to mix dough. The samples were mixed under different headspace pressures. The following figure showed the mixograph I used, a GRL 200 recording mixer. More details have been provided by Hlynka and Anderson (1955).

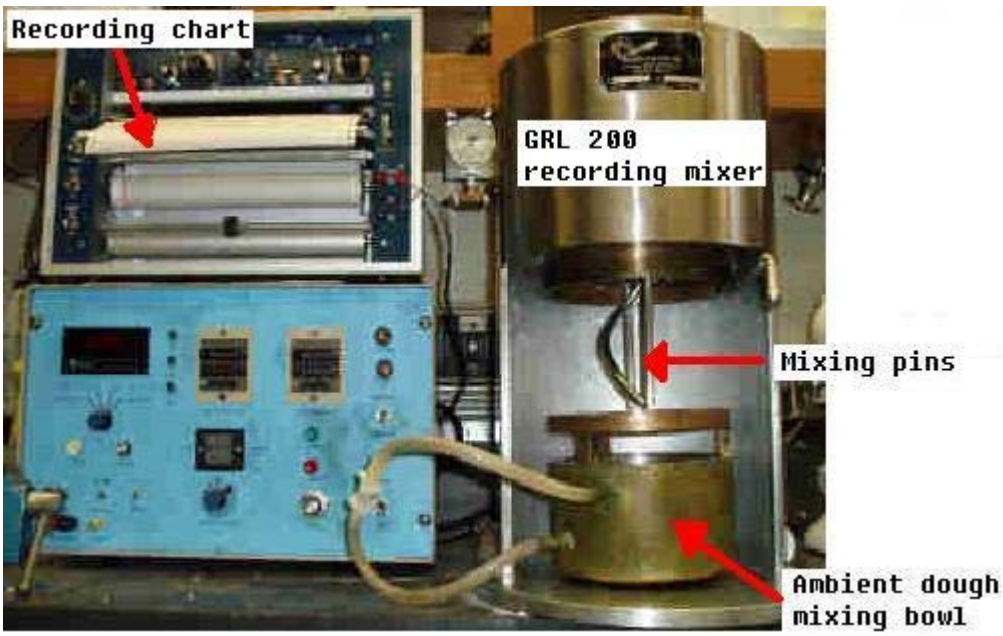

Figure 2.3. The mixer used in the experiments.

2.1.1. Ambient dough mixing

The ingredients I used in my experiment were 100 g of a strong breadmaking flour (CWRS), 2.4 g of NaCl, 61 ml of distilled water. The salt was dissolved in water first and then mixed with the flour in the mixing bowl for 5.5 minutes.

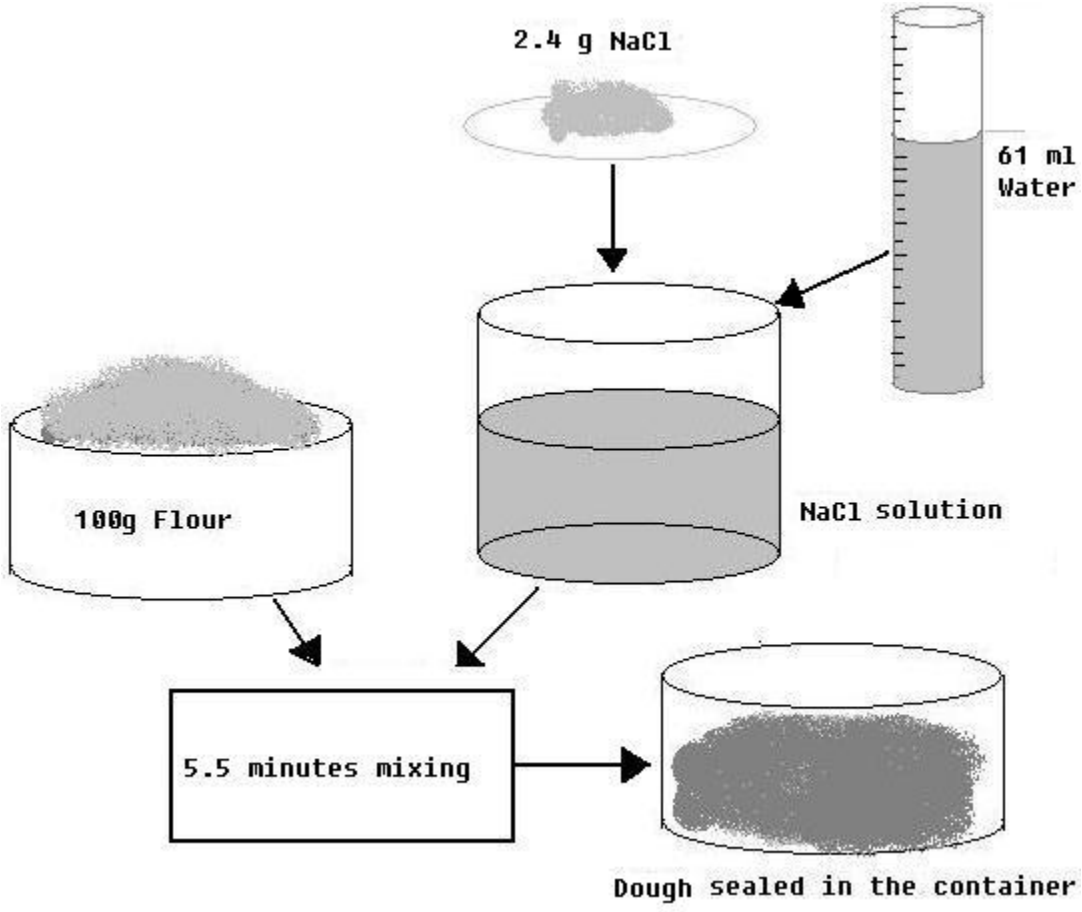

Figure 2.4. Dough making process.

The speed of the mixer was controlled by a Focus 1 Analog DC Drive. The DC Drive was set to be 9, which means 225 RPM. The optimum mixing time was 5.5 minutes for my flour as assessed when mixed at atmospheric pressure. After mixing the dough was saved in a sealed container.

In the ultrasound measurements, subsamples were cut from the dough piece with scissors. The size of the dough subsample was chosen according to the thickness that the subsample was to be compressed to. The mass of the container with the dough piece was measured before and after cutting the subsample. The difference of the mass gave the mass of the subsample. This process was the same for dough mixed under different conditions.

2.1.2. Vacuum dough mixing

To mix doughs under vacuum the set-up shown in figure 2.5 was used and attached to the GRL-200 mixer.

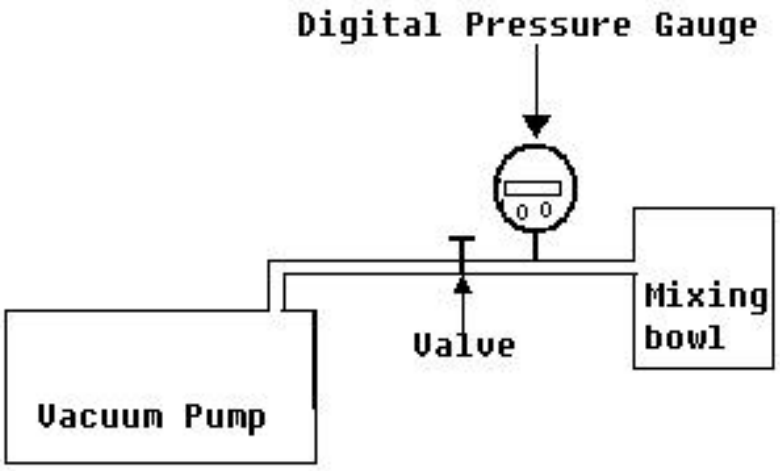

Figure 2.5. Diagram of vacuum mixing system.

The sample ingredients I used for the vacuum mixed dough were the same as the ambient dough, but the mixing bowl for vacuum mixing was slightly different (figure 2.6).

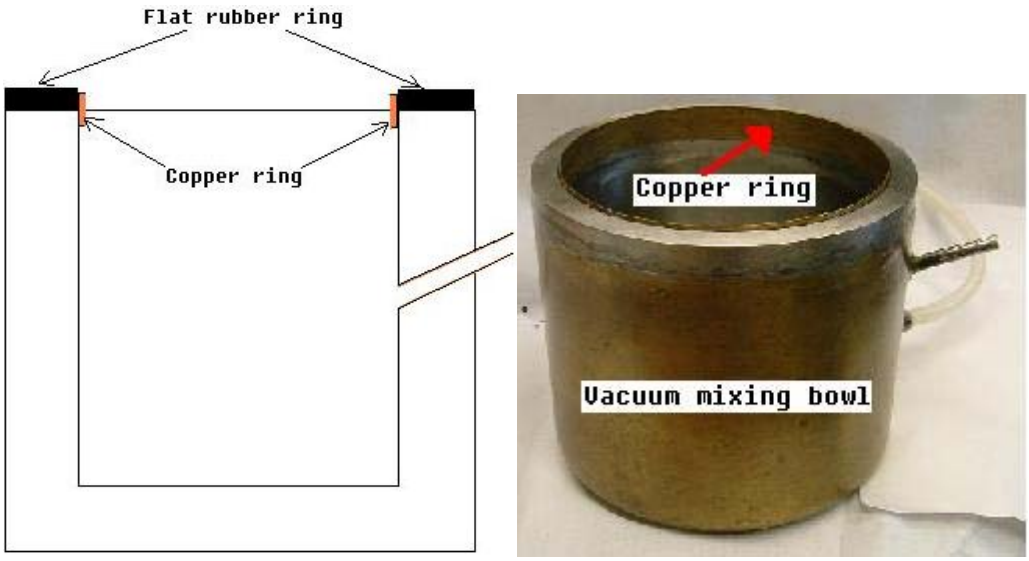

Figure 2.6. Vacuum mixing bowl.

The vacuum mixing bowl was sealed during mixing. Vacuum grease was used on the two surfaces of the flat rubber ring. I designed a thin copper ring to stop the flat rubber ring being sucked into the bowl during mixing. This copper ring needed to be very thin in order to not touch the mixing pins.

The ingredients were mixed for one minute before the vacuum pump was turned on. This allowed the flour to be mixed first with water (with added salt) so that the flour particles would not be sucked out by the pump. The pump was switched on for the last 4.5 minutes of mixing. The headspace pressure during evacuation was recorded by a digital vacuum gauge.

2.1.3. Nitrogen mixing

To vary the composition of gas occluded into the dough during mixing, a nitrogen mixing system was devised (figure 2.7)

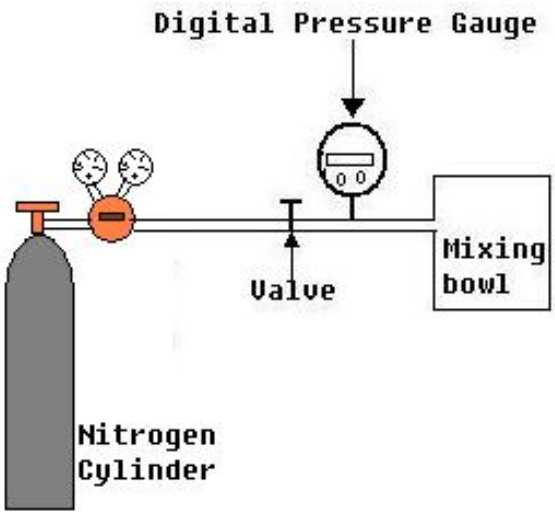

Figure 2.7. Diagram of nitrogen system.

The vacuum mixing bowl was used in nitrogen mixing. Dry flour is mixed in a nitrogen flow at a pressure of about 680 Pa (0.2 inch Hg) above ambient pressure for 2 minutes. The pressure should not be higher than this, since the flour could be blown out of the bowl by the nitrogen flow. This procedure removed air entrapped in the void spaces of the flour and replaced it with nitrogen. After this, the NaCl solution was added into the bowl and the dough continually mixed for 5.5 minutes. The pressure of the nitrogen flow was gradually increased to 2700 Pa (0.8 inch Hg) above ambient at the end of the first minute of mixing and then remained the same.

2.2. Ultrasonic measurement

2.2.1. Apparatus

After dough was mixed, the ultrasonic measurements were started. In my experiment I used two sets of apparatus. One was for low frequency measurements, namely those at 40 kHz. The other one was for high frequency measurements, which was from 500 kHz up to 20 MHz. Two block diagrams of the apparatus are shown in figure 2.8 and figure 2.9. All the connections in the experiment were made with 50 Ω BNC cables.

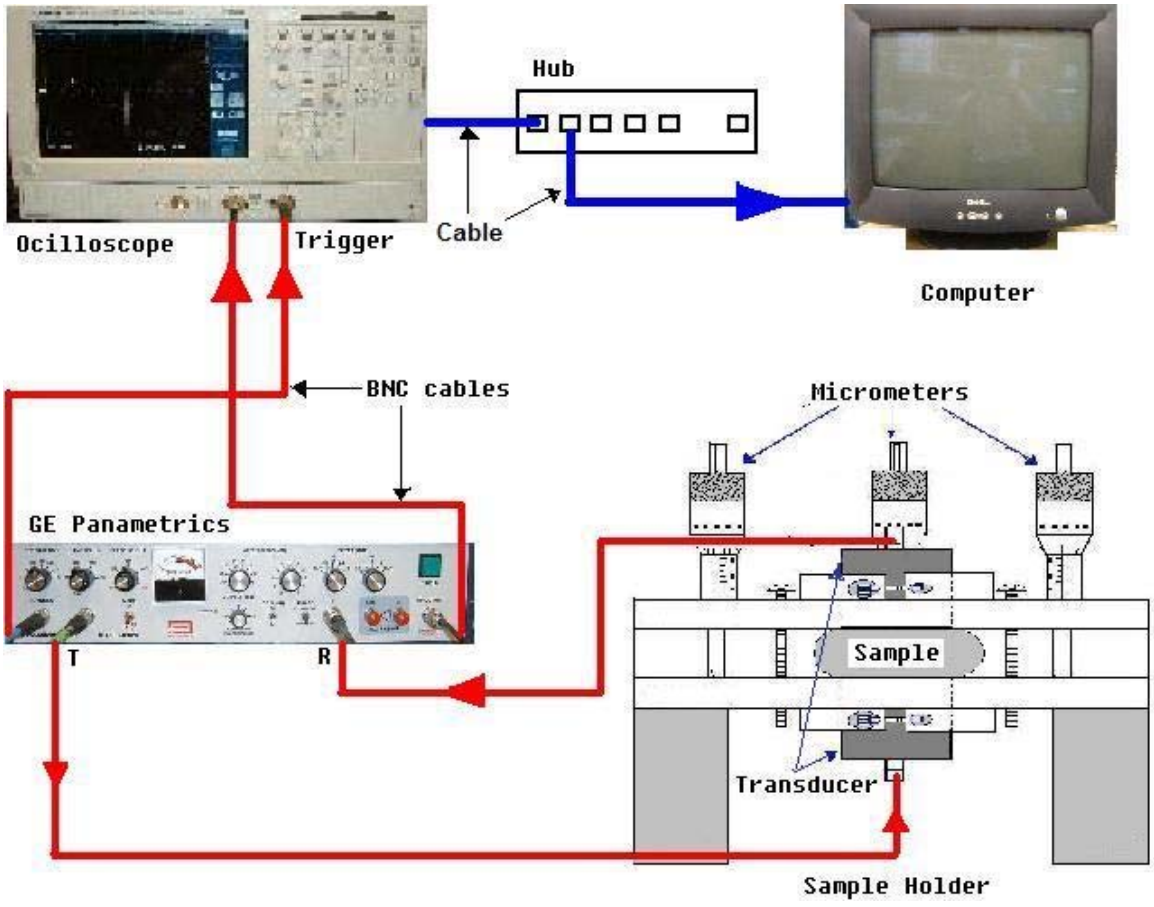

Figure 2.8. 40 kHz experiment setup.

In the 40 kHz setup, a GE Panametrics high voltage pulse receiver was used to

generate an electromagnetic (EM) pulse. The pulse was then sent to the generating transducer, which transformed the EM signal to an ultrasonic signal with a central frequency determined by the resonant frequency of the transducers. The dough sample was sandwiched between two piezoelectric transducers. The generated ultrasonic signal traveled through the sample and was detected by the other transducer. This transducer converted the transmitted ultrasonic signal back into an EM signal. The EM signal then was amplified, signal averaged and displayed on a digital oscilloscope (Tektronix TDS 5052 Digital Phosphor Oscilloscope), and recorded on a computer by a program called **TDSWAVE**. For recording signals at regular intervals over a long period of time, two Matlab programs (**fan1** and **fan2)** were used. (See section 2.2.3)

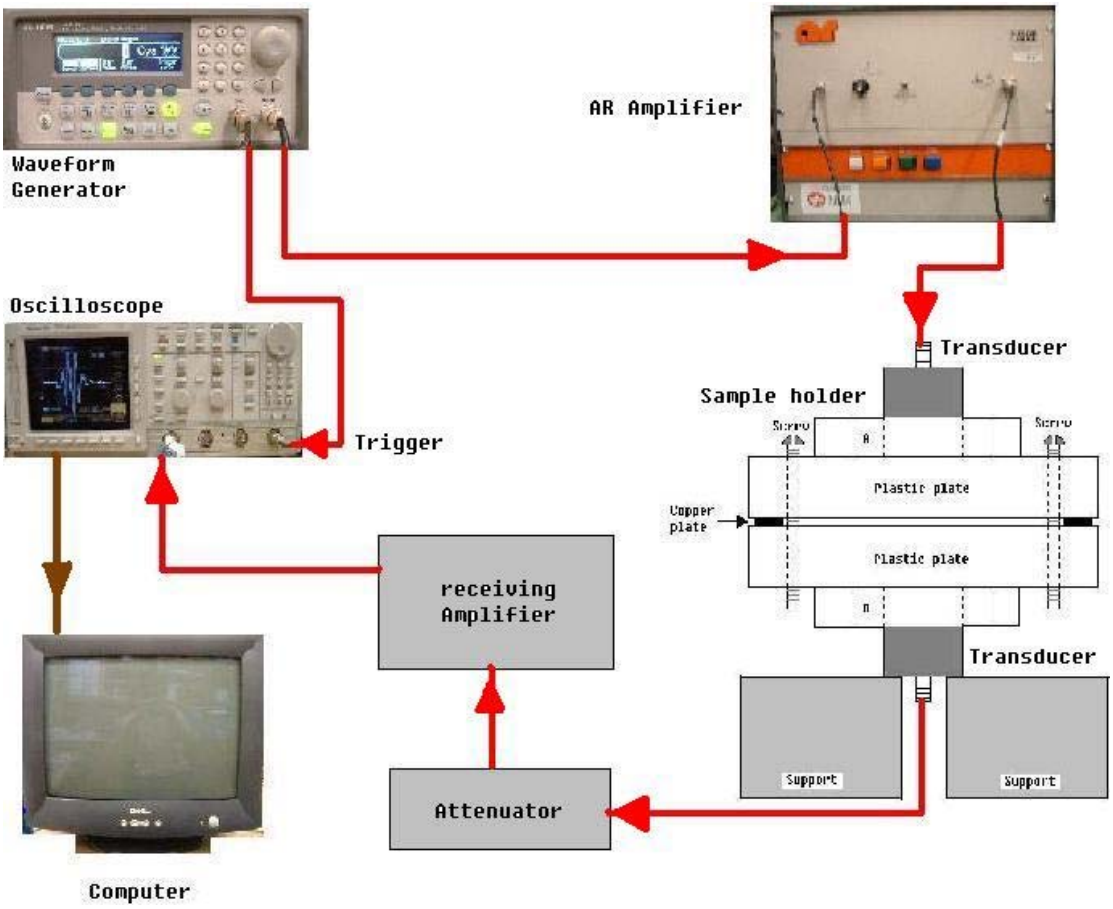

Figure 2.9. High frequency experiment setup.

In the high frequency experiments, a single cycle sinusoidal EM signal was generated by an Agilent 33220A Waveform Generator. The EM signal then was sent to an Amplifier Research (AR) power amplifier (model 250L). The amplified EM signal traveled to the generating transducer and was converted to an ultrasonic signal. After the acoustic signal propagated through the sample, it was transformed back to an EM signal by the other piezoelectric transducer. This signal was then attenuated by an attenuator that operated over a range from 0 to 100dB. Then the signal traveled through a High-Impedance Broadband Pre-Amplifier (model 253) and was amplified by a receiving amplifier. The final EM signal was displayed on a digital oscilloscope

(Tektronix TDS 544A) and was recorded on the computer by Matlab programs **fan1** or **fan2**.

In my experiments, I used two sets of transducer holders. One is called the contact measurement holder, which was used in all 40 kHz measurements, the vacuum dough high frequency measurements and the 20 MHz ambient dough measurements. The other one is a plastic delay measurement holder. It was used in high frequency measurements for ambient dough from 500 kHz up to 5 MHz.

2.2.1.1. Contact measurement holder

The following two figures show the structure (figure 2.10), and the top and bottom view (figure 2.11) of the contact measurement holder. The diameter of the hole in the center of the holder is the same as the diameter of the 40 kHz transducer. The surface of the transducer was set in the same plane as the steel plate. The three micrometers, with a range of 28 mm, determined the distance between the two steel plates and thus the transducers. The sample was sandwiched between the two transducers and compressed to the desired separation between transducers, which was controlled by the three micrometers. The screws were used to hold the system together and maintain the separation and hence sample thickness.

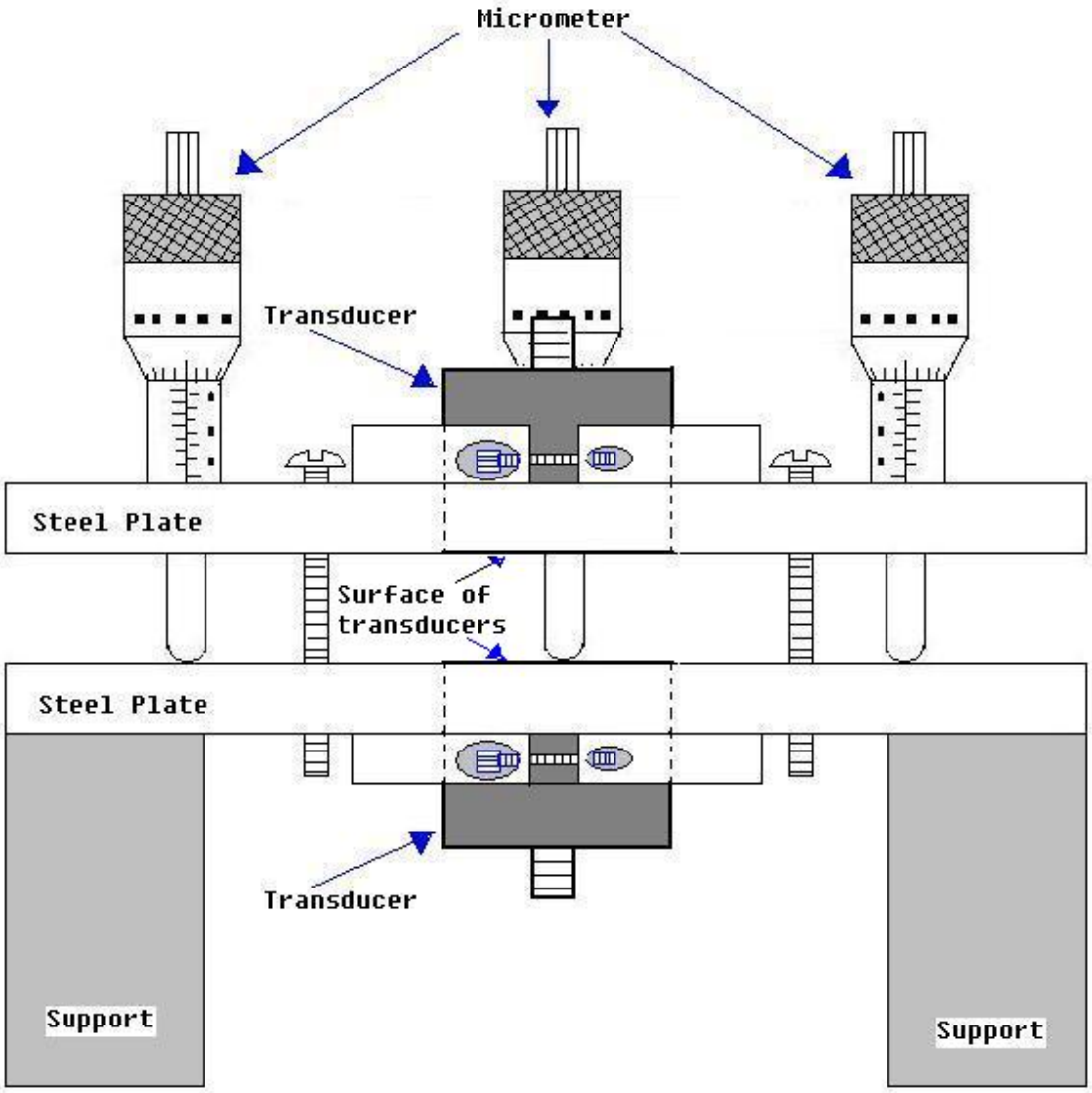

Figure 2.10. Transducer holder for contact measurements-side view.

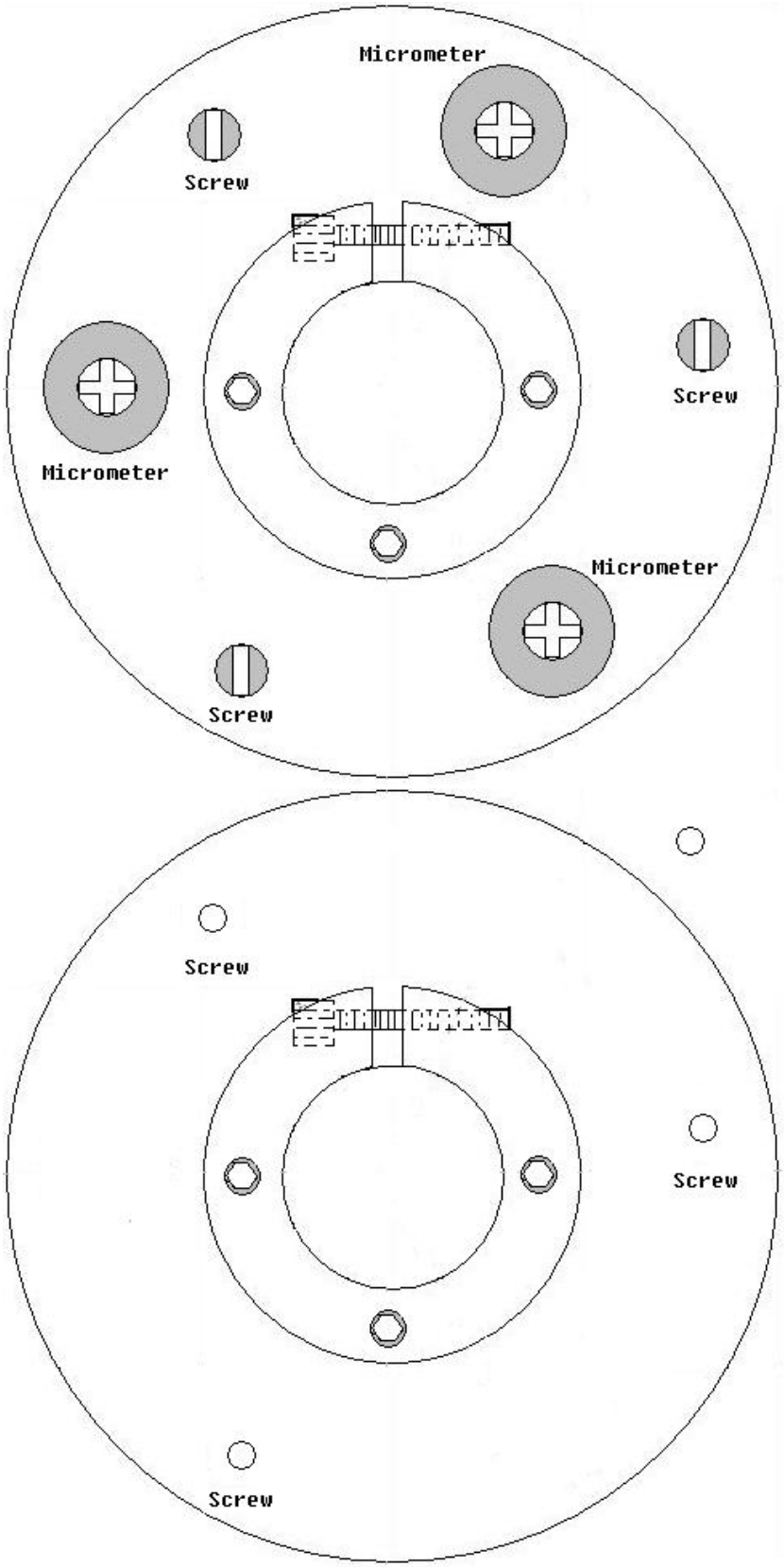

Figure 2.11. Top (top) and bottom (bottom) view of the contact measurements holder.

2.2.1.2. Plastic delay measurement holder

Figure 2.12 is a diagram of the plastic delay measurement holder. The copper plates inserted between the plastic plates controlled the thickness of the sample. In my experiments the copper plates were each 0.3 mm thick. To measure the properties of thicker samples, I simply used two copper plates together to get a 0.6 mm thick sample. The two transducers contacted the plastic plates and a coupling gel was used to ensure a reproducible and large signal. The alignment of the two transducers was controlled by clamp A. Clamp A was centered on the plastic plate and had an inner diameter which is the same as the diameter of the transducers for the range of frequencies from 500 kHz to 5 MHz used in my experiments.

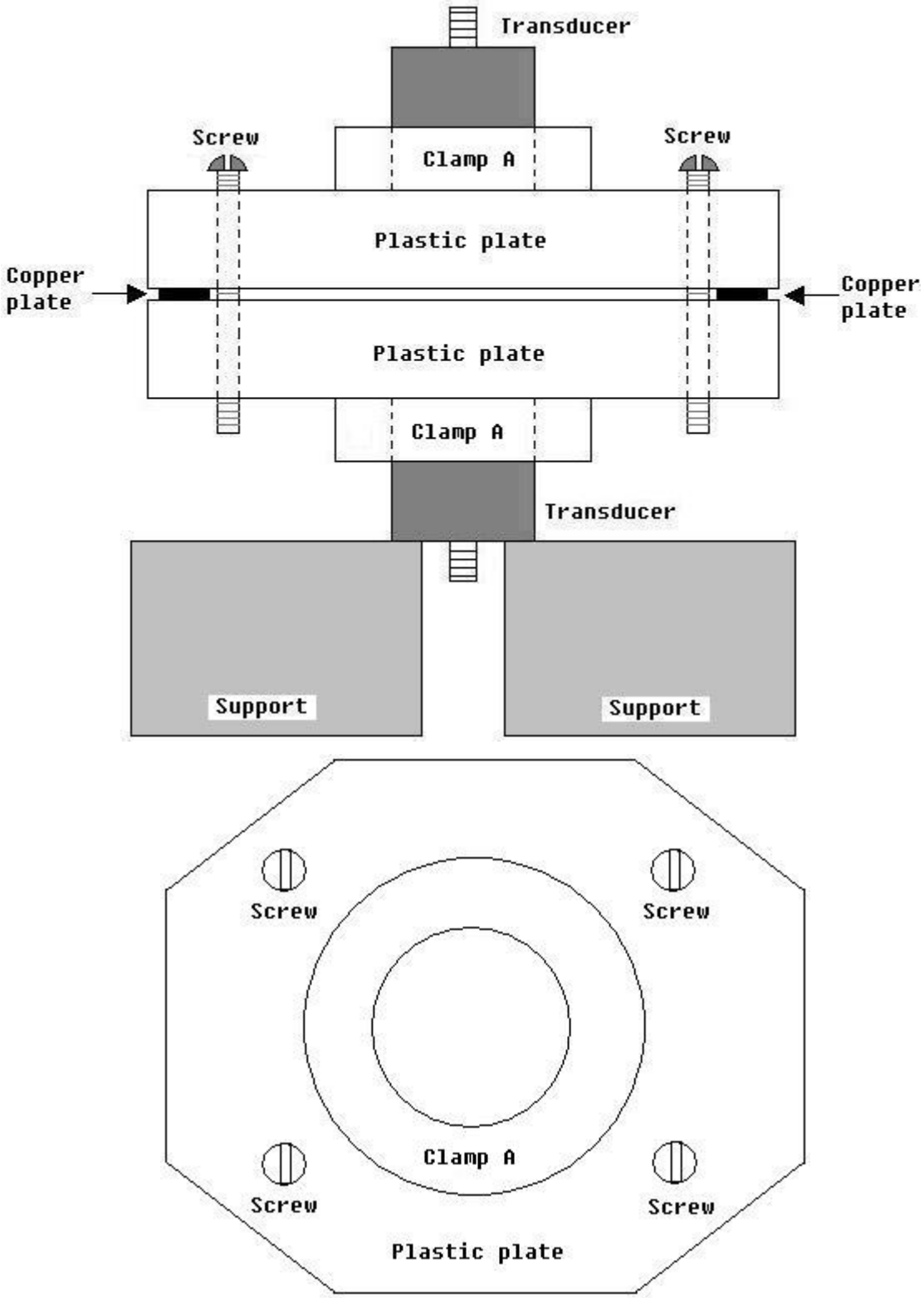

Figure 2.12. Side view (top) and top view (bottom) of the transducer holder for plastic delay plate measurements.

2.2.2. Sample preparation

The sample used in the ultrasonic measurements was taken from the dough as described in section 2.1.1. The sample was sandwiched between the two transducers or the two plastic plates and compressed to the desired thickness as shown in figure 2.13. During the measurement, the circumference of the holder was sealed by tape to keep the moisture content of the dough constant.

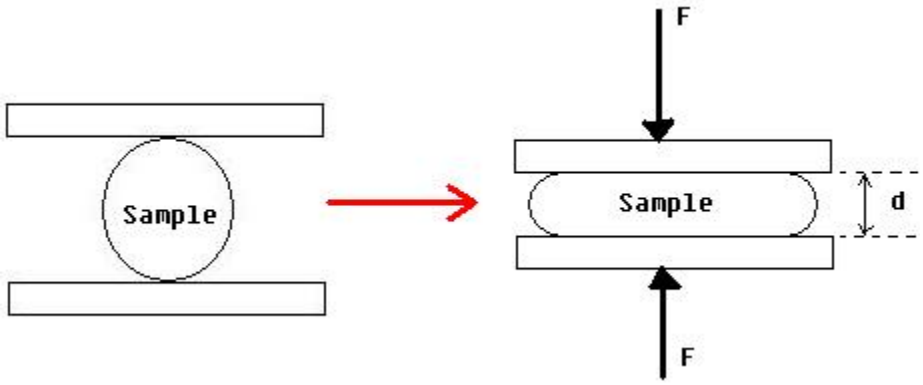

Figure 2.13. A diagram showing sample preparation for the ultrasonic measurements, where *d* is the thickness used in the experiment.

In the 40 kHz measurements, in order to make the area covered by the sample the same at different thickness, the mass of the sample used in the measurements was determined by

$$M = \pi R^2 d \rho , \qquad (2.1)$$

where R (2.2 cm for the 40 kHz transducer) is the diameter of the transducer, d is the thickness of the sample and ρ is the density of dough. To make sure that the dough covered the whole surface of the transducer, I used a bigger value of R (2.7cm). For the high frequency measurements, because the sample thickness is very thin (less than 1 mm),

the mass of the sample was not measured. The size of the sample was chosen by experience to ensure it covered the transducer surface well.

2.2.3. Data acquisition

TDSWAVE is a C program to acquire and transfer a waveform on the oscilloscope to a file which contains two columns of data. The first column is the x-axis transit time and the second one is the y-axis voltage.

In order to monitor the time evolution of the sample, I needed to record signals every several minutes. **fan1** and **fan2** were two Matlab programs designed to do this task. When running **fan1**, the program would ask the operator the number of signals needed to be acquired, the file prefix name to save these recording, and the value of the attenuator setting we used in the experiment.

Let's take an example as below. We would like to record 15 signals. The file name prefix was **foct10sam1** and we set 30dB on the attenuator. The program will record data every 2 minutes (This time interval between two recordings can be changed in the program). The output would be 15 files called **foct10sam1_N_30dB.dat,** where **N** is a number from 1 to 15 representing the order of the signal. In addition, there was an output file named **foct10sam1_time.dat**. This file saved all the clock times for each signal that was recorded. As a result, the file contained 7 columns and 15 rows. The columns are **[N year month day hour minute second]**. **N** is the order of the signal and other columns represented the time when this signal was saved.

Basically, **fan2** did the same job as **fan1**. The program **fan2** was written for very long time recording (like 10 hours). The program would ask the operator the same input parameters (file prefix name, number of acquisition, the attenuator value). When the number of acquisition **N** we input is less than 31, **fan2** is exactly the same as **fan1**. But if the acquisition number we input is larger than 31, taking 50 as an example, the program would record the first 31 signals every 2 minutes. After that, the time interval between two recordings became 30 minutes for the last 19 recording, since the changes happened more slowly. The file name had the same format as the file name from the program **fan1**. Also, there was a file like **foct10sam1_time2.dat** that contained the time when each signal was recorded.

Chapter 3 Data analysis method and a computational simulation for analyzing 40 kHz data

Part I : Data analysis method

3.1. The basic parameters of ultrasonic measurements

Ultrasonic research is based on the study and application of sound waves having frequencies higher than those to which the human ear can respond (about 16 kHz) (Blitz, 1963). Generally, the ultrasonic wave propagating through a fluid medium in the *x*-direction is written as a pressure wave, which can be expressed as follows:

$$P(x,t) = P_0 \cos(kx - \omega t) e^{(-\frac{\alpha x}{2})} \tag{3.1}$$

where $P(x,t)$ is the amplitude of the sound pressure at distance x and time t, P_0 is the original pressure at $x = 0$ and $t = 0$, $k = 2\pi/\lambda$ is the wave number, λ is the wavelength, and ω is the angular frequency. The two basic parameters that can be measured experimentally are phase velocity $v = \omega / k$ and attenuation coefficient α. These parameters can be related to the properties of food materials.

When ultrasound waves pass through a medium, the particles of that medium are set into vibrations at ultra-audible frequencies (Filipczynski, 1966). Let one of these particles be displaced from its equilibrium position as a result of an external force associated with the waves (Filipczynski, 1966). Because of the medium's elasticity, part of the energy of the vibrating particle is transmitted to neighboring particles, which, in turn, vibrate and transmit energy to their neighboring particles (Filipczynski, 1966).

Given that each particle starts its motion slightly later than the one before, the vibrational motion travels with a finite velocity v known as the wave velocity.

The 1-D equation of motion can be written (Létang *et al*., 2001)

$$M^* \frac{d^2U}{dx^2} + \rho\omega^2 U = 0\,, \tag{3.2}$$

where U represents the displacement of the particle, ρ is the density of the medium, M^* is an elastic modulus, equal to G^* for a shear wave, $K^* + \frac{3}{4}G^*$ for a compressional wave. K^* is the complex bulk modulus and G^* is the complex shear modulus. The relationship:

$$\frac{\omega}{k^*} = \left(\frac{M^*}{\rho}\right)^{1/2} \tag{3.3}$$

is verified, k^* being the complex wave number, defined by

$$k^* = \frac{\omega}{v} + i\alpha/2 \tag{3.4}$$

Attenuation of plane waves arises from:

(a) Deviation of energy from the parallel beam by regular reflection, refraction, diffraction and scattering;

(b) Absorption, for which mechanical energy is converted into heat by internal friction. (Blitz, 1963)

3.2. Measurement of the ultrasonic parameters from analysis in the time domain

This method was mainly used in the 40 kHz ultrasonic measurements. The pair of transducers that I used were PANAMETRICS X1021, 50kHz, with serial numbers 341260 and 341261. We measured the response of the transducers and found that the central frequency was approximately 40 kHz. The central frequency of the dough signal using this pair of transducers was normally 36 kHz. So in this thesis when we refer to 36 kHz results, it means that this pair of 40 kHz transducers was used in the experiment and data were analyzed at 36 kHz.

These low frequency transducers had a narrow bandwidth. Thus, we could suppose that the measurements would not be affected by the dispersion of ultrasound in the dough in this narrow frequency range. In this section, impedance mismatching of transducer and sample was not considered. The effect and correction of impedance mismatching is discussed in section 3.4.

Sections 3.2.1 and 3.2.2 describe the two methods I used to analyze the data at 40 kHz in the time domain. A computational simulation of the methods is described in the second part of this chapter.

3.2.1. Different sample thickness method

An example of an ultrasonic waveform transmitted through a sample is shown in Figure 3.1.

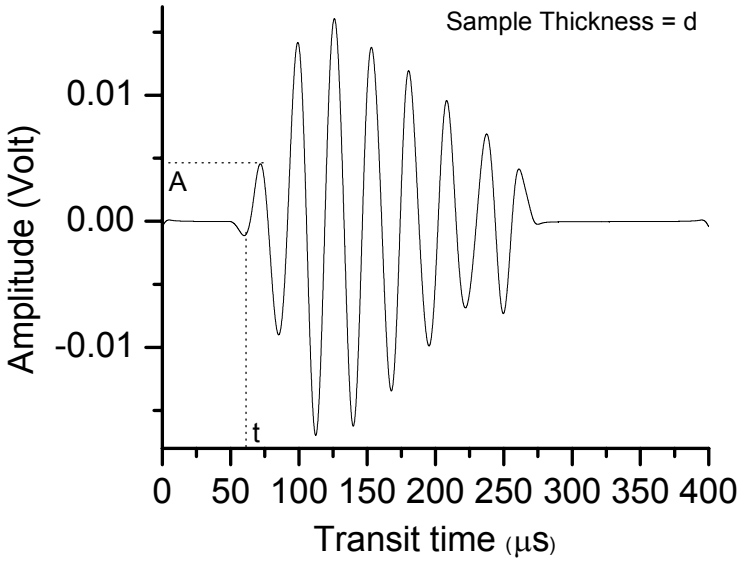

Figure 3.1. Waveform transmitted through a sample of thickness *d*.

If we were able to measure signals at different sample thicknesses, we could plot the transit time of the first minimum and the amplitude of the first maximum as a function of sample thickness using signals from samples of different thickness. Typical results are shown in figure 3.2.

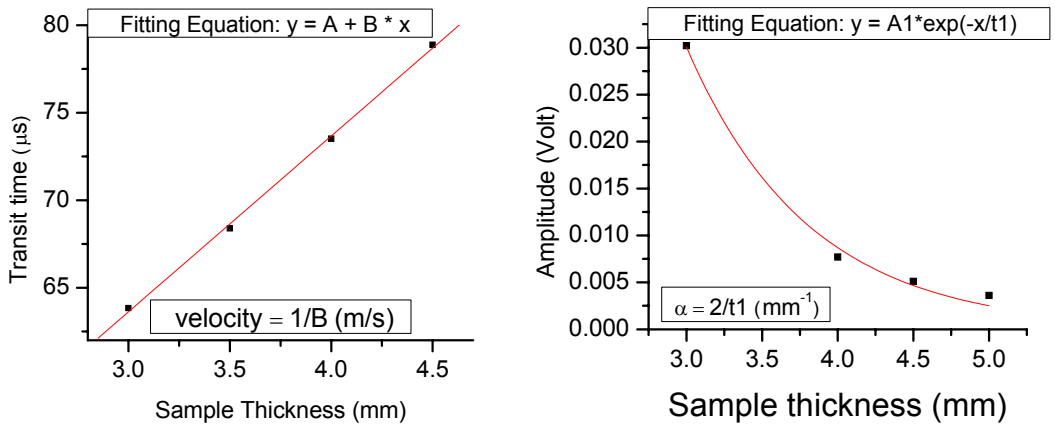

Figure 3.2. Transit time (left) and amplitude (right) as a function of dough sample thickness.

We fitted transit time data with a linear equation $y = A + Bx$ and the amplitude data by an exponential decay equation, $y = A_1 \exp(-x/t_1)$. If we assume that the sample is not dispersive in this frequency range, the velocity is equal to the inverse of the slope, $1/B$, and the attenuation coefficient equal to $2/t_1$ from the exponential decay.

3.2.2. Reference method

When we only had one thickness for the sample or we wished to observe the time evolution of the sample, we had to use the reference signal to get ultrasonic parameters. The reference waveform was measured with the two transducers in direct contact (*i.e.*, in the absence of the sample), or with a material of well-known acoustic properties inserted between them. Figure 3.3 is an example of a reference signal and sample signal.

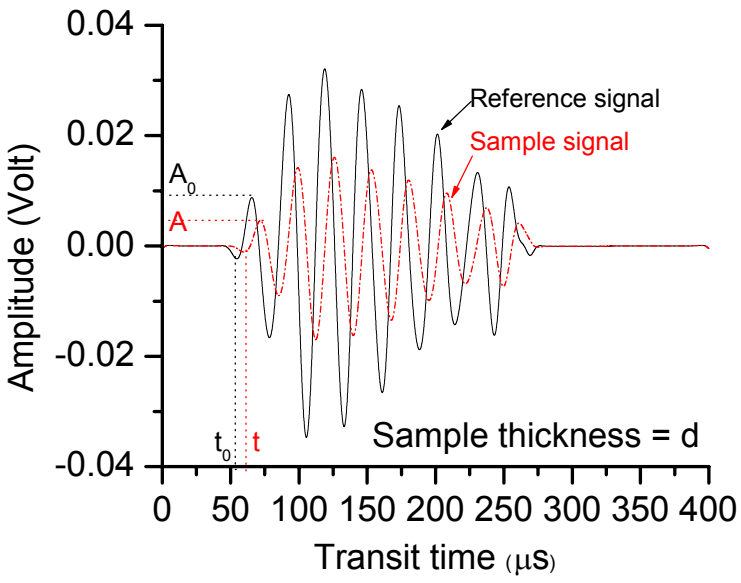

Figure 3.3. A reference signal and signal for the sample of thickness *d*.

The transit time of the first minimum is t_0 for the reference and t for the sample signal. The amplitude of the first maximum is A_0 for the reference and A for the sample signal. Initial estimates of the velocity and attenuation are then given by $v = \frac{d}{t - t_0}$ and $\alpha = \frac{2}{d}\ln(\frac{A_0}{A})$. However, these estimates neglect the effect of the impedance mismatch between the transducers and the dough sample, which can cause a reduction in the transmitted signal amplitude as well as a phase shift. The details of the effect and its calculation are discussed in section 3.4.1., where it is shown that the impedance mismatching correction is a significant one.

3.3. Measurement of ultrasonic parameters from analysis in the frequency domain

For high frequency measurements, namely 1 MHz to 20 MHz in my experiments, the transducers had a wide frequency range. We could not make the assumption that the dough was not dispersive. In other words, the phase velocity and attenuation coefficient became frequency dependent. So we could not use the method described in section 3.2 any more.

To analyze the ultrasonic data in the frequency regime, a Fast Fourier Transform (FFT) was used to analyze the data. The FFT gave us the frequency dependence of amplitude and phase. From the amplitude information we could get the attenuation coefficient and from the phase we could determine the phase velocity.

The FFT of the waveform signal was calculated using a C program, **fftfull**. The output file had three columns: frequency, amplitude and phase. Frequency was in MHz, amplitude had an arbitrary unit (proportional to the voltage detected by the transducer) and phase was in radians. We could also do exactly the same job in Matlab by using a program called **fourier**, which gave the same output file.

Figure 3.4 shows an ultrasound signal and its FFT. Part (a) is the ultrasonic signal; parts (b) and (c) are the FFT amplitude and phase.

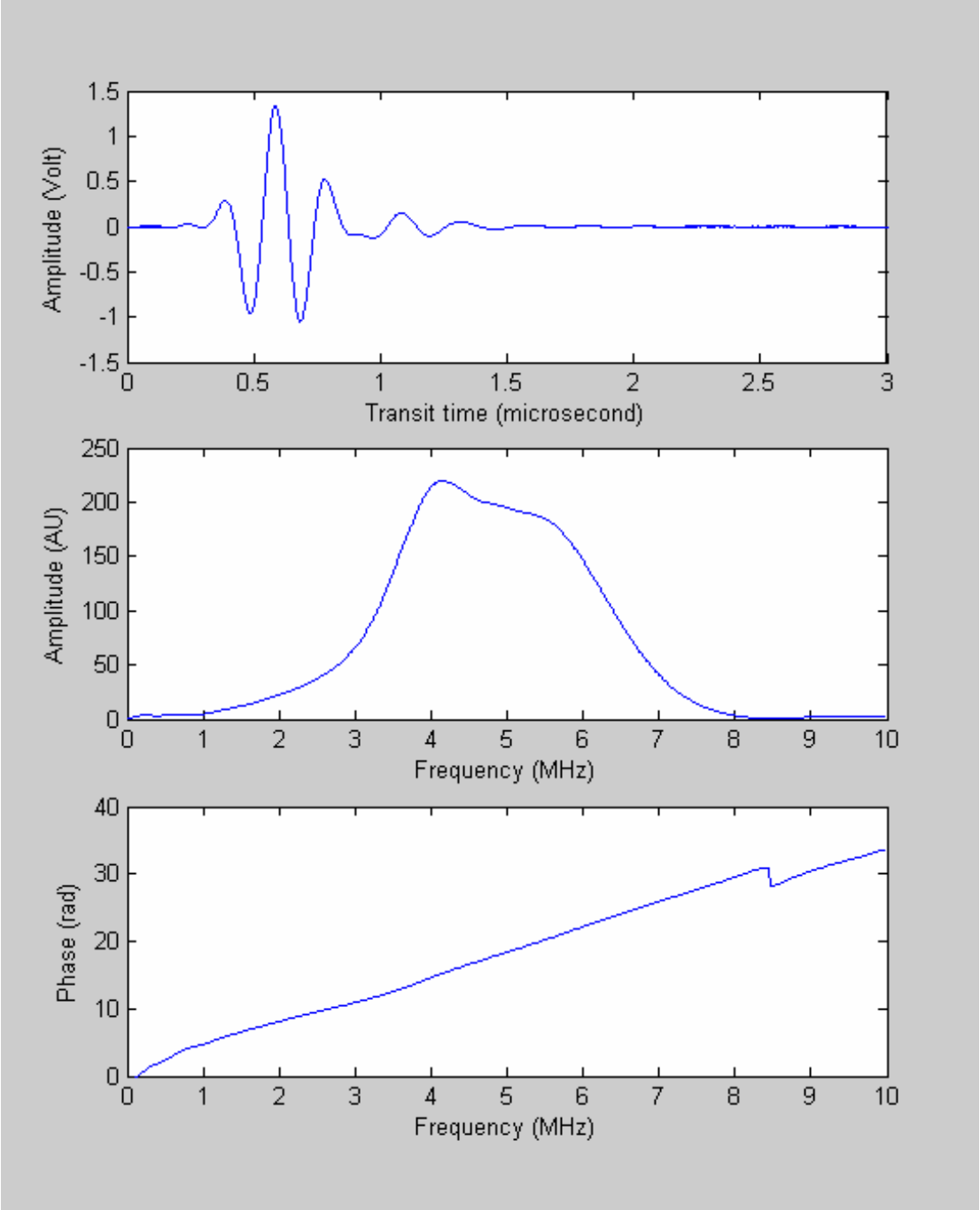

Figure 3.4. An ultrasonic signal (a) and its FFT, showing the amplitude (b) and phase (c) as a function of frequency. The central frequency of the transducers used in this example is 5 MHz.

Without considering impedance mismatch losses, when an incident signal $P_0 = e^{i\omega t}$ is transmitted through a sample with a thickness L (figure 3.5), the transmitted signal would be given by $P_{11} = e^{i\omega t} * e^{-\alpha L/2} * e^{-ikL}$.

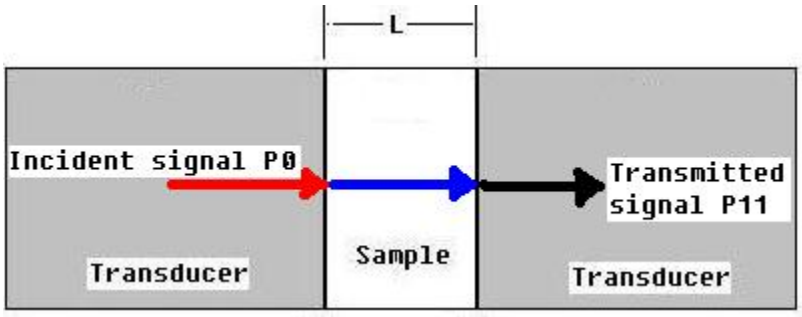

Figure 3.5. Incident signal P_0 and transmitted signal P_{11} neglecting impedance mismatching.

Therefore,

$$\frac{P_{11}}{P_0} = e^{-\alpha L/2} e^{-ikL} \tag{3.5}$$

Defining the parameter R_{11}

$$R_{11} = \frac{FFT(P_{11})}{FFT(P_0)} = \frac{|P_{11}|e^{i\phi_{11}}}{|P_0|e^{i\phi_0}} = \frac{|P_{11}|}{|P_0|} e^{i(\phi_{11}-\phi_0)} \tag{3.6}$$

Here $|P_0|$ and $|P_{11}|$ were the amplitudes from the FFT of the reference and transmitted signals, respectively, and ϕ_0 and ϕ_{11} were the phases from the FFT of the reference and transmitted signals.

Thus,

$$\begin{aligned} |R_{11}| &= \frac{|P_{11}|}{|P_0|} = e^{-\alpha L/2} \\ \triangle\phi &= \phi_{11} - \phi_0 = -kL \end{aligned} \tag{3.7}$$

We know that the phase velocity is given by

$$v = \frac{\omega}{k} \tag{3.8}$$

So from equation (3.7) we obtain

$$\alpha = \frac{-2\ln(|R_{11}|)}{L}$$
$$v = \frac{-\omega L}{\triangle\phi} \tag{3.9}$$

Because the amplitude and phase can both be frequency dependent, α and v will also be frequency dependent.

3.4. Impedance correction in ultrasound measurements

When a sound wave travels across the boundary from one material to another, due to their different physical properties, it is partially reflected from the boundary. The remainder of the wave energy is transmitted through the boundary. During the process of reflection and transmission, both the amplitude and phase of the wave are changed.

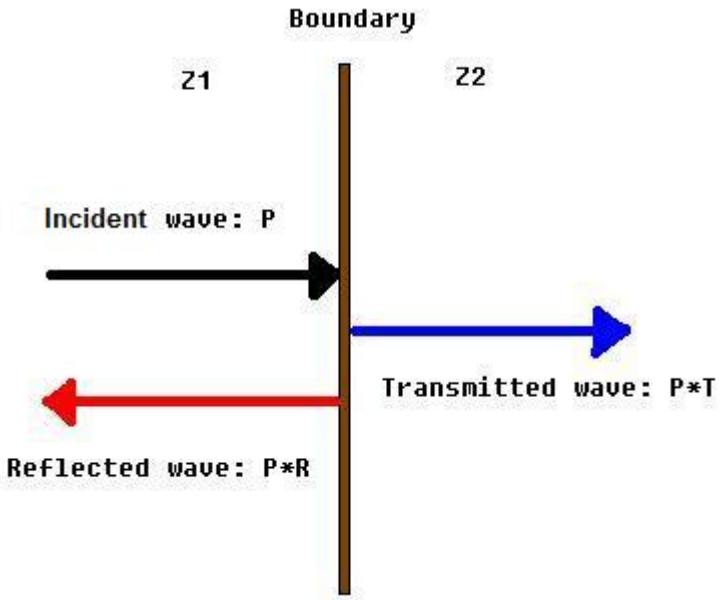

Figure 3.6. Schematic diagram showing reflected and transmitted waves when a wave is normally incident at a boundary.

Suppose we have a sound wave P normally incident at the boundary between material 1 and material 2 (figure 3.6). They have different acoustic impedances Z_1 and Z_2. The acoustic impedance Z of a material is normally defined as the product of density and acoustic velocity of that material:

$$Z = \rho v \tag{3.10}$$

When the material has significant attenuation, the impedance is complex, and is given by

the complete expression

$$Z = \frac{\rho v}{1 + i\frac{\alpha v}{2\omega}} \tag{3.11}$$

Equation (3.10) is a valid approximation of (3.11) when the term $\frac{\alpha v}{2\omega}$ is much less than 1. The reflection coefficient *R* is defined as the ratio of reflected wave amplitude and incident wave amplitude, and this ratio depends on the impedances of the two materials, given by

$$R = \frac{Z_2 - Z_1}{Z_2 + Z_1} \tag{3.12}$$

The transmission coefficient *T* is defined as the ratio of transmitted wave amplitude and incident wave amplitude and this ratio again depends on the impedances of the two materials.

$$T = \frac{2Z_2}{Z_2 + Z_1} \tag{3.13}$$

In my experiments I used three kinds of reference signal. They were contact transducer reference, water reference and plastic layer reference. Different kinds of impedance corrections were applied to each of them. These corrections are explained in the following sections.

3.4.1. Contact transducer reference

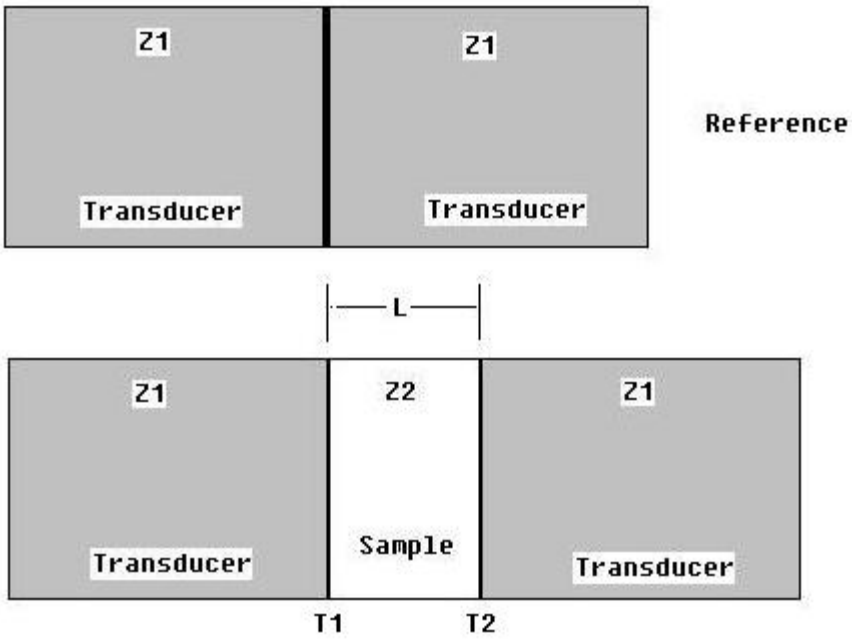

Figure 3.7. A measurement using a contact transducer reference.

If we have a wave $P_0 = e^{i\omega t}$ traveling from one transducer to the other one with identical impedances (figure 3.7), and we suppose that the coupling between them is perfect, the reference signal is

$$P_0 = e^{i\omega t} \tag{3.14}$$

Now if we have a sample with acoustic impedance Z_2 sandwiched between the transducers, the wave could be partially reflected at two boundaries of the sample. The signal we receive at the second transducer is

$$P_1 = e^{i\omega t} T_1 e^{-ikL} T_2 e^{-\alpha L/2} \tag{3.15}$$

T_1 and T_2 are the transmission coefficients at the two boundaries, k is the wave vector in this sample material, α is the attenuation coefficient of this sample and L is the sample

thickness. This expression does not account for multiple reflections inside the sample, since these can be neglected for highly attenuating materials such as dough. If we substitute equations (3.11) and (3.13) in (3.15), then it becomes

$$P_1 = e^{i\omega t} e^{-\alpha L/2} e^{-ikL} \frac{4Z_1 Z_2}{(Z_1 + Z_2)^2}$$
$$= e^{i\omega t} e^{-\alpha L/2} e^{-ikL} \frac{4Z_1 \dfrac{\rho v}{1 + i\,\alpha v/2\omega}}{\left(Z_1 + \dfrac{\rho v}{1 + i\,\alpha v/2\omega}\right)^2} \tag{3.16}$$

If we define

$$T = T_1 T_2 = \frac{4Z_1 \dfrac{\rho v}{1 + i\,\alpha v/2\omega}}{\left(Z_1 + \dfrac{\rho v}{1 + i\,\alpha v/2\omega}\right)^2} \tag{3.17}$$

we get

$$P_1 = e^{i\omega t} e^{-\alpha L/2} e^{-ikL} T = e^{i\omega t} e^{-\alpha L/2} e^{-ikL} |T| e^{i\theta} \tag{3.18}$$

$|T|$ is the magnitude of T and θ is its phase angle. In Matlab, we can simply get $|T|$ by using the command $|T|$ = abs(T) and θ by using θ = angle(T).

If there were no impedance mismatch between the transducers and the sample, P_{11} would be the received, transmitted signal, defined as $P_{11} = e^{i\omega t} e^{-\alpha L/2} e^{-ikL}$. However, in the experiment, the sample signal we measured was actually P_1.

$$P_1 = P_{11} |T| e^{i\theta} \tag{3.19}$$

Thus, the impedance effect $|T| e^{i\theta}$ should be taken into account. The correction for this effect in the high frequency ranges and in the 40 kHz range was different. These corrections are discussed in the following two sections (3.4.1.1 and 3.4.1.2).

3.4.1.1. High frequency range correction

The ratio of incident signal to the received signal (taking account of reflections from dissimilar material boundaries as well as acoustic losses in the sample) is given by:

$$\frac{P_1}{P_0} = \frac{|T|e^{i\theta}}{e^{\alpha L/2}e^{ikL}} \tag{3.20}$$

From above, the ratio of the FFTs is defined as:

$$R_1 = \frac{FFT(P_1)}{FFT(P_0)} = \frac{|P_1|e^{i\phi_1}}{|P_0|e^{i\phi_0}} = \frac{|P_1|}{|P_0|}e^{i(\phi_1-\phi_0)} \tag{3.21}$$

So we obtain

$$\begin{aligned} |R_1| &= \frac{|P_1|}{|P_0|} = \frac{|T|}{e^{\alpha L/2}} \\ \triangle\phi &= (\phi_1 - \phi_0) = \theta - kL \end{aligned} \tag{3.22}$$

From equation (3.22) we obtained

$$\begin{aligned} \alpha &= \frac{2\ln(\frac{|T|}{|R_1|})}{L} \\ v &= \frac{\omega L}{\theta - \triangle\phi} \end{aligned} \tag{3.23}$$

Equation (3.23) gives the correct way to determine the phase velocity and attenuation coefficient. But from equation (3.17), it can be seen that, in order to get T we have to know v and α. Thus (3.23) was an implicit equation. We had to solve it numerically. The other parameter used to solve T is the transducer impedance Z_1. We can use two liquids whose acoustic properties are known to measure Z_1. Take water and ethanol as an example. Defining the signal from a water layer with a thickness d_w as P_w and from an ethanol layer with a thickness d_e as P_e, the ratio of the two signals will be

$\frac{P_w}{P_e} = \frac{e^{ik_w d_w}}{e^{ik_e d_e}} \frac{Z_w}{(Z_1 + Z_w)^2} \frac{(Z_1 + Z_e)^2}{Z_e}$, in which the attenuation in these two liquids was neglected because they are small compared to other parameters. Z_w and Z_e are the acoustic impedances of water and ethanol, k_w and k_e are the wave vector of water and ethanol. Z_1 is the only unknown parameter in this equation and can be calculated easily.

The phase velocity and attenuation were determined by fixed-point iteration. Starting values were obtained from equation (3.9) (without the impedance mismatch), and used to obtain a first estimate of T. Equation (3.23) was then used to update v and α. This procedure was iterated to achieve convergence, which required only 3 to 4 iterations.

3.4.1.2. 40 kHz data correction

For 40 kHz data analysis we had two difficulties. One was that we did not know the impedance of the transducers. We contacted the company about the acoustic impedance of these transducers but unfortunately they would not give any useful information. The other problem was that the ringing of the transducer resulted in a noisy reference signal with a long tail. So we did not trust the FFT method. We therefore obtained v and α in the time domain using the method discussed in section 3.2. Normally we did not worry about the impedance effect because we calculated v and α from measurements at different thicknesses. But if we wanted to monitor the time evolution of the sample or if we only had one thickness, we had to use the reference signal and the impedance mismatch could potentially affect the results significantly.

Equations (3.10) to (3.19) could still be applied to the 40 kHz correction. From (3.17) we knew that we had to use Z_1, v and α in order to determine the transmission coefficient T. At the same time, if we knew v, α and T, it would be possible to use this information to determine the transducer impedance Z_1.

The following figure, 3.8, contains a set of data for dough mixed under ambient conditions. The thickness dependence of transit time and amplitude gives the phase velocity and attenuation coefficient. If we extrapolate the fitted exponential decay line back to zero thickness, we can estimate the transmission coefficient T from the ratio of the extrapolated value to the measured reference. Then it becomes possible to calculate the transducer impedance Z_1.

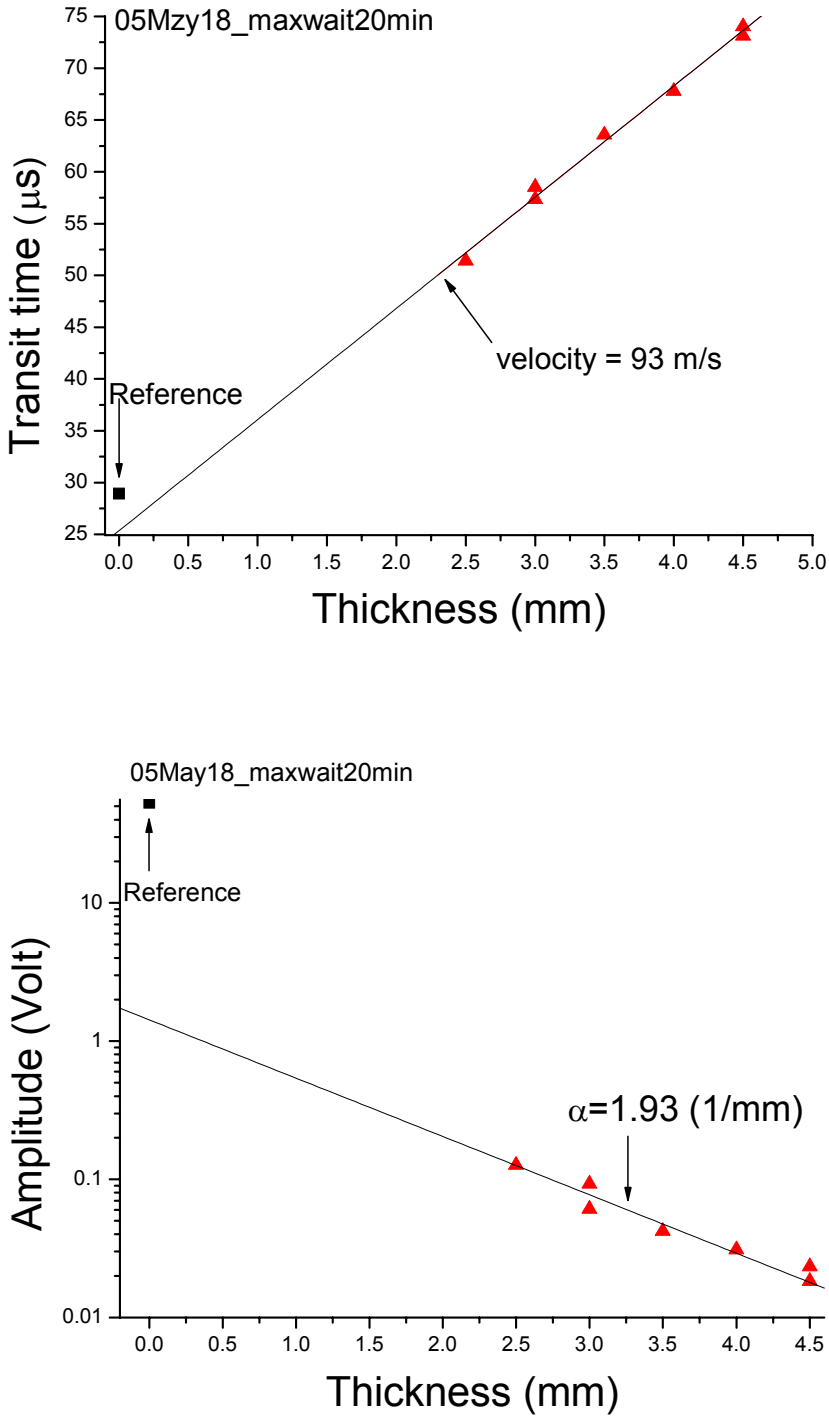

Figure 3.8. Transit time and amplitude (from the first maximum) as a function of sample thickness in a 36 kHz measurement.

From figure 3.8, we measured a velocity of 93 m/s and an attenuation coefficient of 1.93 mm^{-1}. If we extrapolate the amplitude data fitting curve back to zero thickness we get a value far below the reference amplitude.

If we call the experimental reference amplitude A_0 and extrapolated reference amplitude A_0', we have

$$A_0' = A_0 * |T|, \tag{3.24}$$

giving a way to determine $|T|$. Then α can be found using the reference amplitude, since

$$\alpha = \frac{2\ln\left(|T|\frac{A_0}{A(L)}\right)}{L}, \tag{3.25}$$

where *A(L)* is the amplitude of a signal received through a sample with a thickness *L*.

If we use the velocity and attenuation coefficient from the fits shown in figure 3.8, we can use equation (3.17) to predict the absolute value of the transmission coefficient *T* as a function of the transducer impedance Z_1.

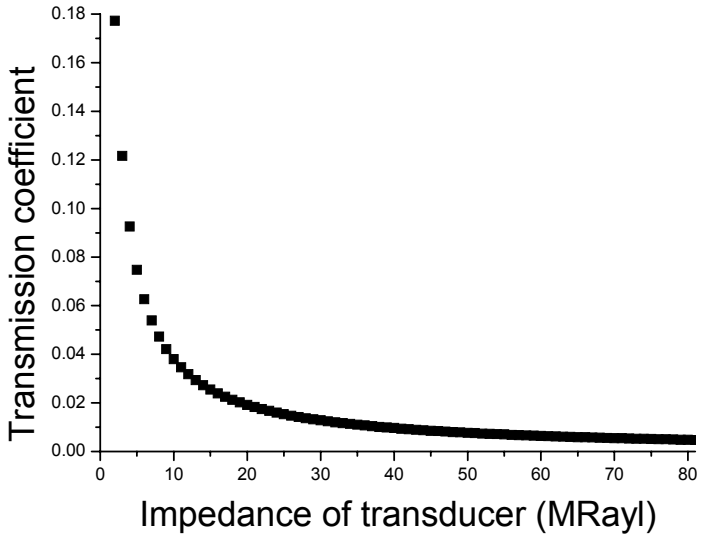

Figure 3.9. Transmission coefficients at 36 kHz as a function of transducer impedance. The velocity used was 93 m/s and attenuation coefficient was 1.93 mm^{-1}.

From figure 3.8 and equation (3.24) we found the transmission coefficient to be 0.026 ± 0.01, which corresponded to a transducer impedance from 10 to 24 MRayl in figure 3.9. Using the same procedure for the data from other runs, we found the value of the transducer impedance ranging from 7 to 41 MRayl. It seemed that we could not get an accurate determination of the transducer impedance from this method.

If we convert the velocity part of equation (3.23) to the time domain, we obtain

$$v = \frac{\omega L}{\theta - \triangle\phi} = \frac{L}{\theta/\omega - t_1 + t_0} \tag{3.26}$$

where t_1 is the transit time for the sample and t_0 is the transit time for the reference. θ is the phase angle of T and $\frac{\theta}{\omega}$ is the time shift of the signal due to the impedance mismatching. With the same v, α and T as used in figure 3.9, we can calculate the time shift at 36 kHz as a function of transducer impedance.

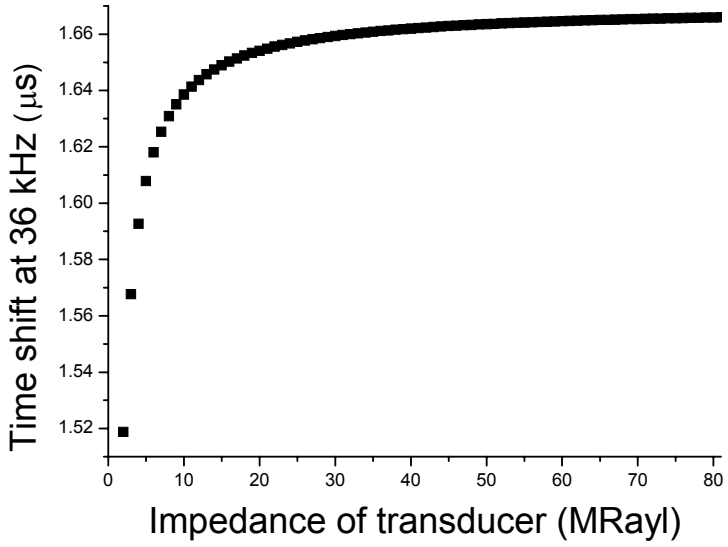

Figure 3.10. Time shift at 36 kHz as a function of transducer impedance. The velocity used was 93 m/s and attenuation coefficient was 1.93 mm^{-1}.

From figure 3.10 we can read that the time shift at 36 kHz was about 1.65 μs at the transducer impedance we got before. If we use this correction in the transit time data we obtain the correction as shown in figure 3.11.

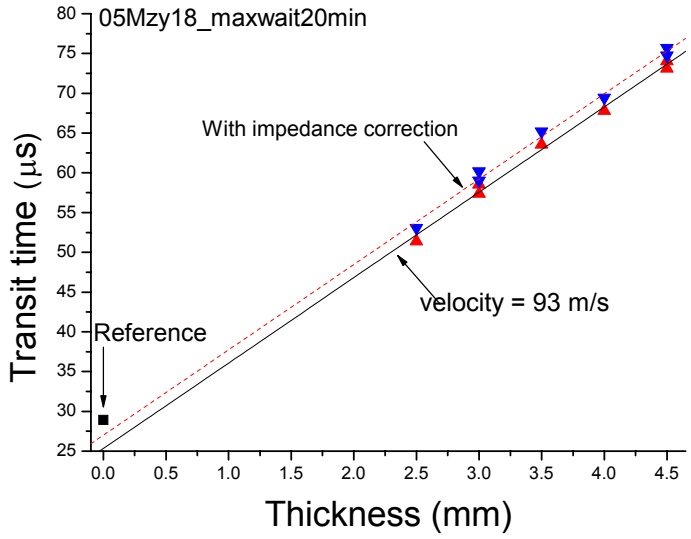

Figure 3.11. Transit time as a function of sample thickness in a 40 kHz measurement.

The red dashed line in figure 3.11 is the result after the time shift correction. Although this correction reduced the discrepancy between the experimentally measured reference and the extrapolated reference, we still had another 2 μs discrepancy between the experiment reference and the new extrapolated reference. Furthermore this additional discrepancy varied from one set of data to the other, with a range from 1 μs to 5 μs. We could not find the source of this discrepancy. Therefore the extrapolated reference (obtained from measurements at different sample thicknesses) was used instead of the measured reference when analyzing the ambient and nitrogen 40 kHz data to monitor the time evolution of phase velocity and attenuation coefficient, using the reference method as described in section 3.2.2.

For the vacuum mixed dough data analysis, the impedance correction becomes even harder. The time shift in the time domain due to the impedance mismatch affected the phase velocity much more than in ambient dough because of the higher phase velocity. Besides, we did not have different thickness data from different subsamples to extrapolate a reference as we did above for ambient dough. This is because a very thick sample was used in the vacuum dough measurement to avoid the multiple reflection effect and also we needed to choose a good part from the dough piece without artificially adding large air bubbles in the subsample. Figure 3.12 shows the velocity and attenuation coefficient in vacuum dough without impedance mismatching correction between the dough and transducers.

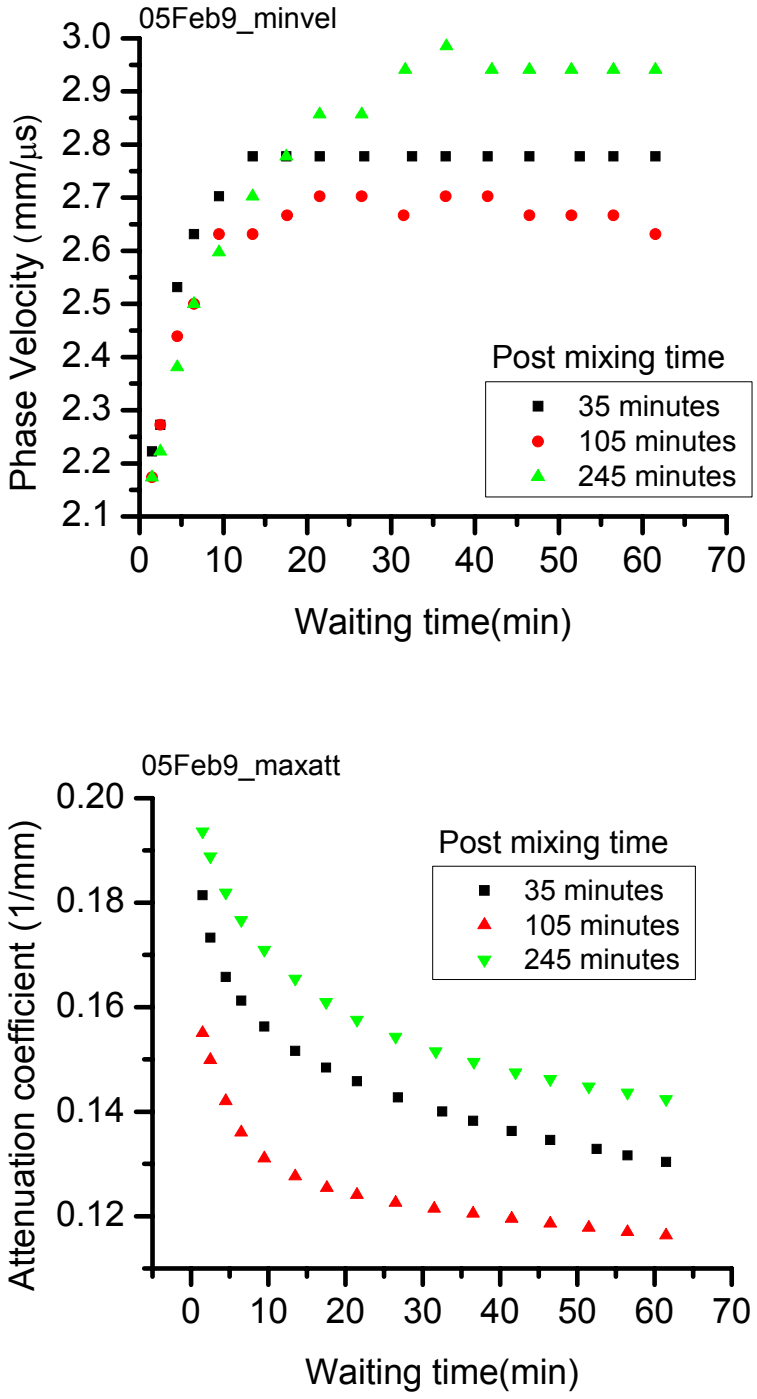

Figure 3.12. Velocity and attenuation coefficient in vacuum dough as a function of waiting time with no impedance mismatching correction.

The impedance of the 40 kHz transducer was estimated to be a value of 40 MRayl

based on the transducer's expected design characteristics as shown in figure 3.19 to make a correction for the results in figure 3.12. Using this value of transducer impedance, we calculated the time shift of the signal and transmission coefficient as a function of different values of the attenuation coefficient and phase velocity, as shown in figure 3.13 and 3.14. As shown in equation 3.17, the transmission coefficient is a complex function of velocity and attenuation. The phase of the transmission coefficient is related to the time shift of the signal in the time domain (see description of equation 3.26). So, with a constant velocity we can study the changing of the transmission coefficient and the time shift with the changing of attenuation and vice versa.

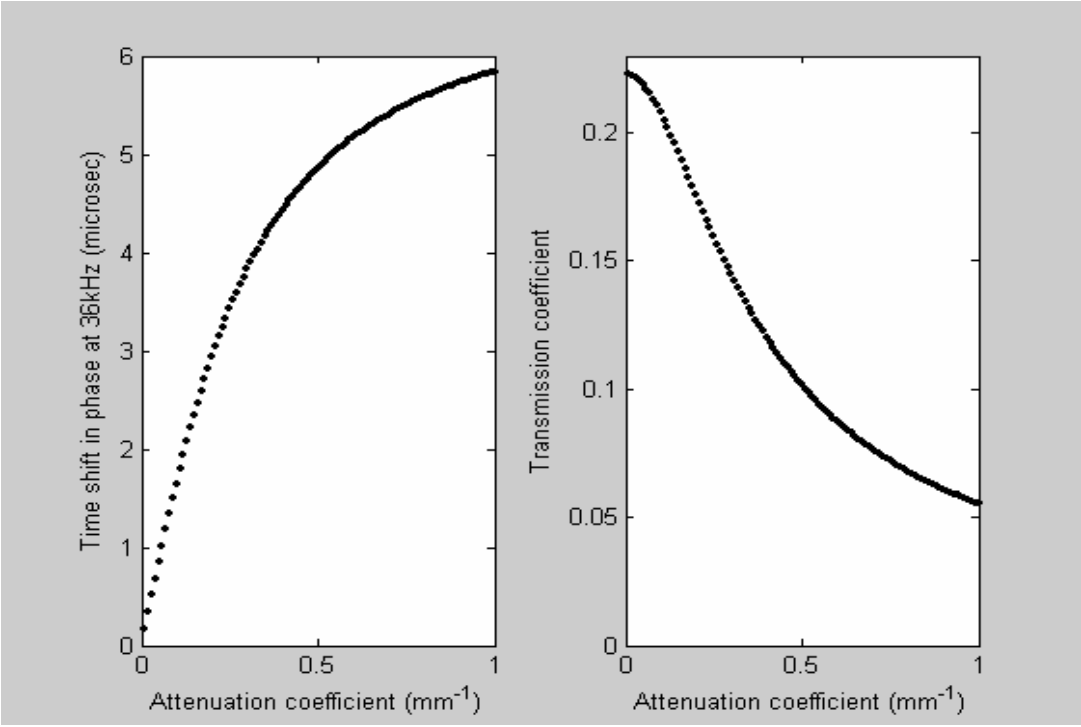

Figure 3.13. Calculated time shift and transmission coefficient at 36 kHz as a function of sample attenuation for vacuum mixed dough. The value of v used was 2 mm/μs, density 1.26 g/cm^3 and transducer impedance 40 MRayl.

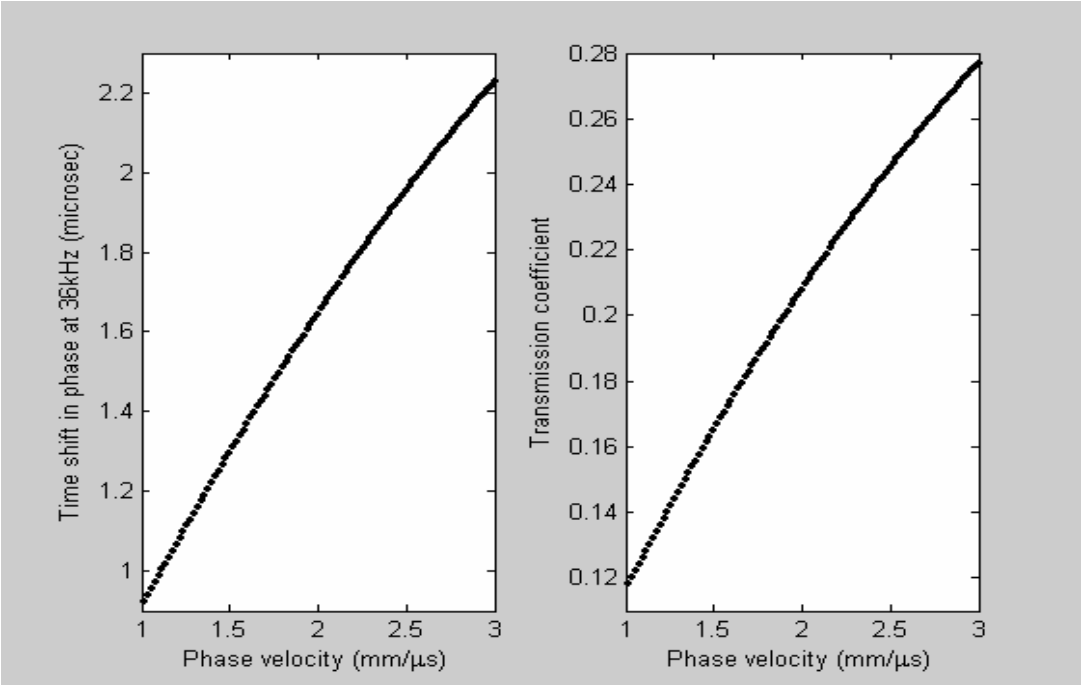

Figure 3.14. Calculated time shift and transmission coefficient at 36 kHz as a function of velocity for vacuum mixed dough. The value of α used was 0.1 mm^{-1}, density 1.26 g/cm^3 and transducer impedance 40 MRayl.

We roughly estimated the velocity to be around 2 mm/ μs and α to be approximately 0.1 mm^{-1} based on the different thickness measurement of the same subsample. From figure 3.14, we obtained a time-shift correction of 1.645 μs and a transmission coefficient of 0.208. If these corrections are applied to the results in figure 3.12, we find the results shown in figure 3.15.

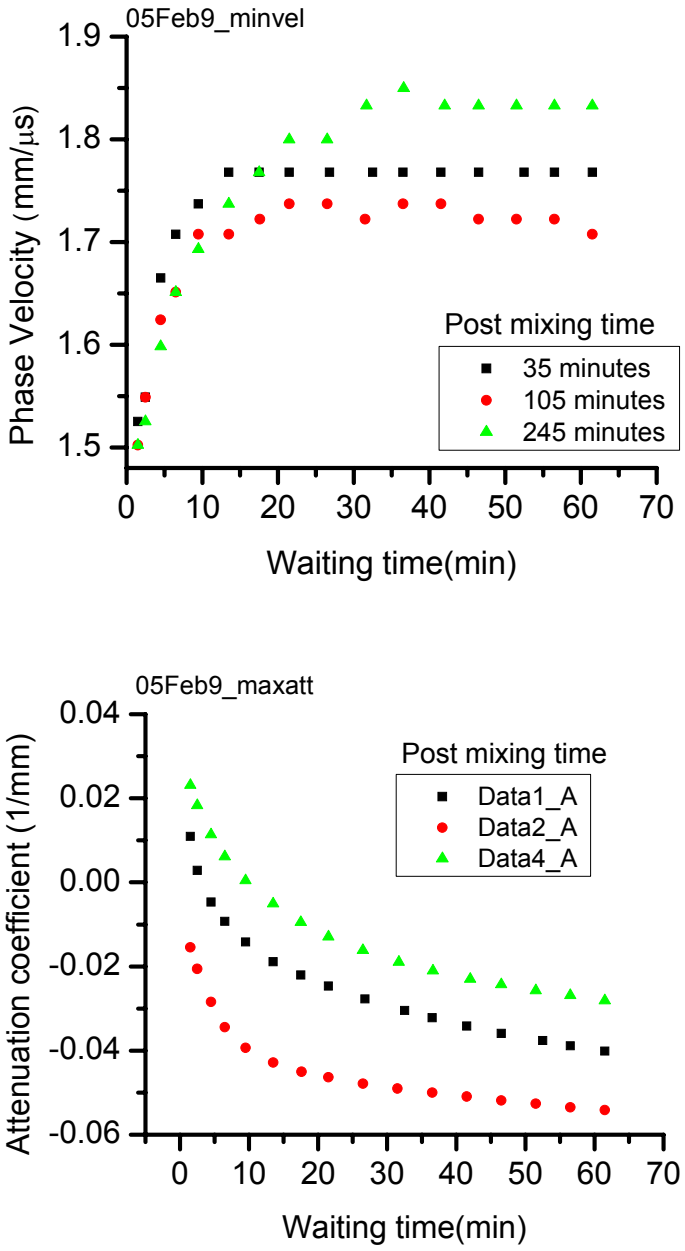

Figure 3.15. Velocity and attenuation coefficient as a function of waiting time with impedance correction using the parameters shown above.

We knew that the attenuation in the dough could not be negative. Therefore, it is clear that this correction did not work for the attenuation coefficient of vacuum dough and, as a result, we were also not confident in the correction for the phase velocity. In

any case, even though the actual values of v and α could not be accurately determined, it was certain that they should be lower than the values shown in figure 3.12. Despite these uncertainties, the overall trends shown by the time evolution of the vacuum dough could still be seen from these data.

In order to obtain a different measurement of the velocity in vacuum dough, we measured the signal velocity (Brillouin, 1960) as shown in figure 3.16, which is defined by the arrival time of the start of the pulse, $v_s = L/t_{start}$. Since many frequencies in the pulse are involved, the signal velocity cannot be associated with a specific frequency. However, if the phase velocity does not depend strongly on frequency, the signal velocity should have a similar value. For the data shown in figure 3.16, we obtain v_{signal} = 1.81 mm/μs.

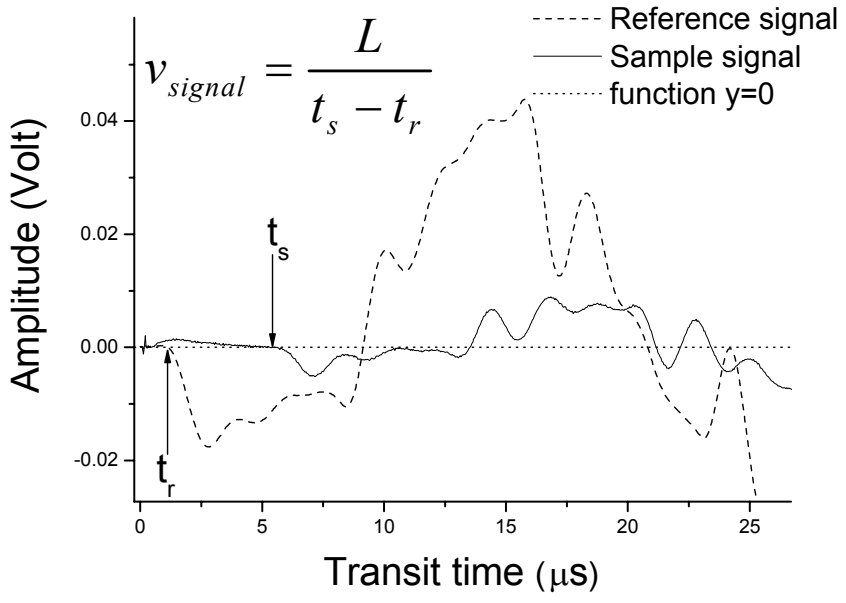

Figure 3.16. Determination of signal velocity. L in the figure is the sample thickness; t_s is the start time of the sample signal and t_r is the start time of the reference signal.

3.4.2. Water reference correction

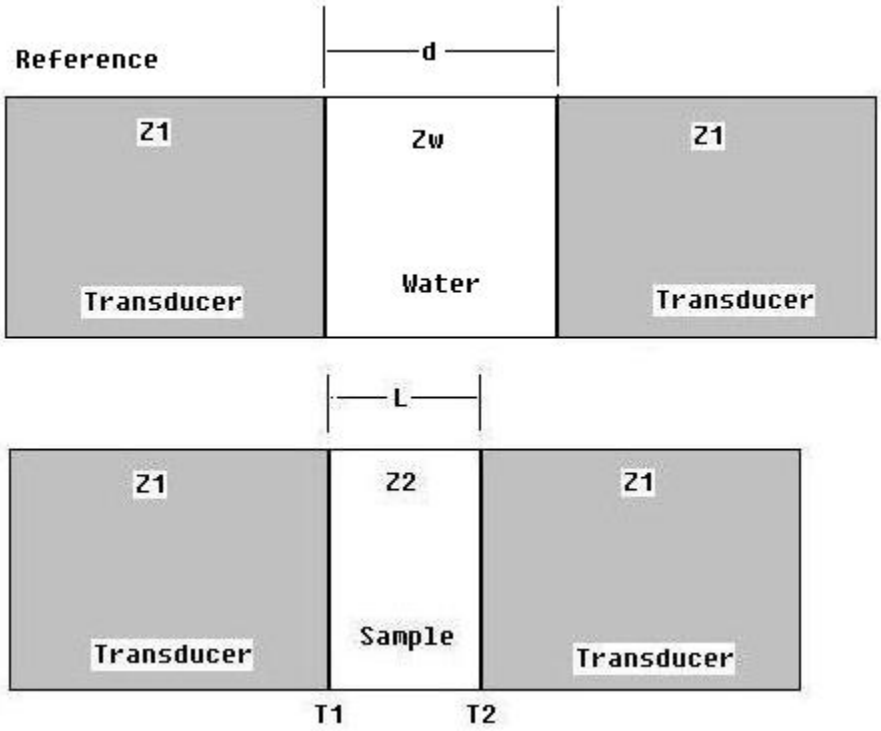

Figure 3.17. A water reference measurement.

The water reference was used only in the high frequency range, namely from 1 MHz to 20 MHz. The reference was measured as shown in figure 3.17, and may be represented as

$$P_0 = e^{i\omega t} T_w e^{-ik_w d} = e^{i\omega t} \frac{4Z_1 Z_w}{(Z_1 + Z_w)^2} e^{-ik_w d} \tag{3.27}$$

Z_w is the acoustic impedance of water, which is the product of its density and ultrasonic phase velocity, d is the thickness of the layer of water and k_w is the wave vector in water. We considered the attenuation coefficient of water to be negligible.

The sample signal could still be expressed according to equation (3.18)

$$P_1 = e^{i\omega t} e^{-\alpha L/2} e^{-ikL} T = e^{i\omega t} e^{-\alpha L/2} e^{-ikL} |T| e^{i\theta}$$

Therefore,

$$\frac{P_1}{P_0} = \frac{|T| e^{i\theta} e^{-ikL} e^{-\alpha L/2}}{T_w e^{-ik_w d}} = \frac{|T|}{T_w e^{\alpha L/2}} e^{-i(kL - k_w d - \theta)} \tag{3.28}$$

Following the approach in equation (3.21) for the contact reference measurement

$$R_1 = \frac{FFT(P_1)}{FFT(P_0)} = \frac{|P_1| e^{i\phi_1}}{|P_0| e^{i\phi_0}} = \frac{|P_{11}|}{|P_0|} e^{i(\phi_1 - \phi_0)}$$

We find

$$\begin{aligned} |R_1| &= \frac{|P_1|}{|P_0|} = \frac{|T|}{T_w e^{\alpha L/2}} \\ \triangle\phi &= (\phi_1 - \phi_0) = k_w d + \theta - kL \end{aligned} \tag{3.29}$$

From equation (3.29) we obtain

$$\begin{aligned} \alpha &= \frac{2 \ln\left(\frac{|T|}{T_w |R_1|} \right)}{L} \\ v &= \frac{\omega L}{\theta + k_w d - \triangle\phi} \end{aligned} \tag{3.30}$$

We can get $|R_1|$ and $\triangle\phi$ from the FFT of the reference and sample signal. Theoretically T_w, the transmission coefficient of the water layer, can be calculated from equation (3.27). As the high frequency transducers (> 500 kHz) were designed to match the impedance of water, the signal is believed to transmit totally. As a result, T_w was assumed to be one, which means the water signal was used as the reference. An observation to support the assumption of total transmission through the water layer is that the water signal was larger than the direct contact reference. Equation (3.30) is still an implicit function because T depends on the α and v of ultrasound in the dough. We

solved this equation numerically in the same way as we did in section 3.4.1.1.

3.4.3. Plastic delay plate reference correction

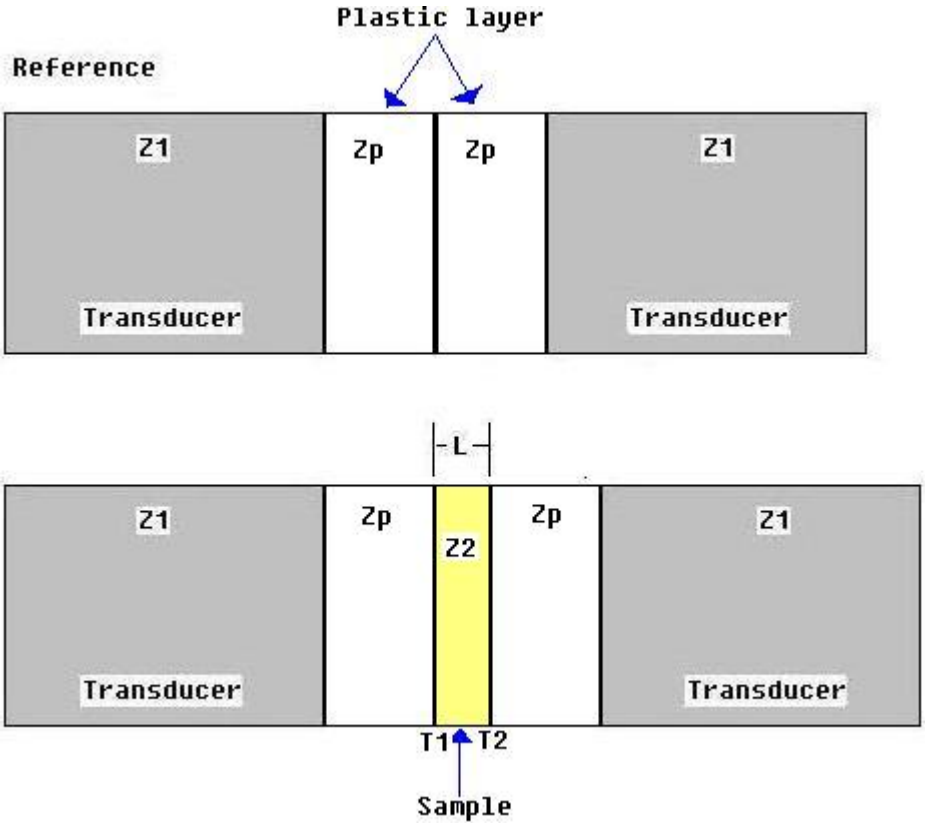

Figure 3.18. A plastic delay layer reference measurement.

The plastic delay-layer reference method involved the same principle as the contact reference method, but had the advantage that the material in contact with the sample had a well known impedance. This method was used only in the high frequency range. We could simply replace equation (3.17) by

$$T = T_1 T_2 = \frac{4Z_p \dfrac{\rho v}{1 + i\alpha v/2\omega}}{\left(Z_p + \dfrac{\rho v}{1 + i\alpha v/2\omega}\right)^2} \tag{3.31}$$

in which Z_p represents the acoustic impedance of the plastic layer. Then the impedance correction was made following the steps from equation (3.18) to (3.23).

Part II: A computational simulation for the 40 kHz analysis method

In order to examine the accuracy of the time domain analysis method that was described in section 3.2, a computational simulation of this method was created in Matlab, which was called Tdomain_simulation.

A Gaussian waveform was created as the input signal and transformed to the frequency domain by taking its fast Fourier transform (FFT). To describe the propagation of the signal through a sample with a thickness L, the input FFT was multiplied by the factor $e^{-ikL}e^{-\frac{\alpha}{2}L}$, in which k is a frequency dependent wave vector and α is the frequency dependent attenuation. The transmitted signal was transformed back into the time domain again by taking the inverse FFT. The velocity and attenuation values in these simulations were chosen to be close to those in dough.

Different analysis methods were tested and compared in this section. The effect of the complex impedance of the dough and the first reflected signal were included. The impedance of the transducer was estimated to be 40 MRayl (see figure 3.19).

The analysis methods used in this simulation were described in the sections 3.2.1 and 3.2.2. Results from the first minimum and the first maximum were compared. Different output parameters and their meaning are listed in table 3.1. The results had already been corrected for the impedance mismatch.

Vel_min	Phase velocity from comparing the first minimum of the reference and sample signal
Vel_max	Phase velocity from comparing the first maximum of the reference and sample signal
Alpha_min	Attenuation coefficient from comparing the first minimum of the reference and sample signal
Alpha_max	Attenuation coefficient from comparing the first maximum of the reference and sample signal
Fit_vel_min	Phase velocity from fitting the first minimum transit time of sample signal versus sample thickness
Fit_vel_max	Phase velocity from fitting the first maximum transit time of sample signal versus sample thickness
Fit_alpha_min	Attenuation coefficient from fitting the first minimum amplitude of sample signal versus sample thickness
Fit_alpha_max	Attenuation coefficient from fitting the first maximum amplitude of sample signal versus sample thickness

Table 3.1. Output parameters and their meaning from Tdomain_simulation.

ρ	Density of the sample
$\mathbf{Z_t}$	Impedance of the transducer
$\mathbf{Z_d}$	Impedance of the sample
$\boldsymbol{v}$	Phase velocity in the sample
α	Attenuation coefficient in the sample

Table 3.2. Input parameters and their meaning in Tdomain_simulation.

As was mentioned in section 3.4.1.2, the impedance of the 40 kHz transducer was very hard to determine experimentally. Therefore, we attempted to estimate its impedance, based on the transducer's expected design characteristics.

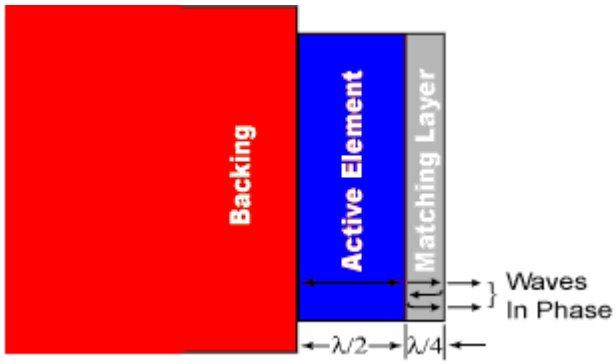

Figure 3.19. A cut away view of a typical contact transducer.

An active element of the contact transducer was PZT, which has an acoustic impedance of 35 MRayl. We knew the 40 kHz contact transducer was normally designed to match steel, which has an impedance of 46 MRayl. So from this, we could estimate the impedance of the matching layer to be about 40 MRayl. This estimate was based on the criterion for perfect matching that the impedance of the matching layer be equal to the square root of the geometric mean of the transducers and sample impedance (Kuttruff, 1991).

3.5. Simulation of ambient dough

3.5.1. No dispersion in *v* and α

The velocity and attenuation in the material were frequency independent in this case. The check was performed just to see the effect of the complex impedance of the sample on the results.

ρ (g/cm^3)	Z_t (MRayl)	Z_d (MRayl)	v (mm/μs)	α (mm^{-1})
1.12	40	$\frac{\rho v}{1+i\frac{\alpha v}{2\omega}}$	0.09	1.8

Table 3.3. The input parameters.

Thickness (mm)	Vel_min (mm/μs)	Alpha_min (mm^{-1})	Vel_max (mm/μs)	Alpha_max (mm^{-1})
2.5	0.0877	2.0462	0.0883	1.9909
3	0.0882	1.9755	0.0885	1.9382
3.5	0.0884	1.8577	0.0888	1.9163
4	0.0887	1.8282	0.0889	1.9118
4.5	0.0888	1.9331	0.0891	1.9264

Fit_vel_min (mm/μs)	Fit_vel_max (mm^{-1})	Fit_alpha_min (mm/μs)	Fit_alpha_max (mm^{-1})
0.090106	0.090106	1.7107	1.8432

Table 3.4. The output results

The output results showed that, with the effect of the complex impedance of the sample, Vel_min and Vel_max were less than 3 % smaller than the input value and the discrepancy decreased as the thickness became larger. Alpha_min and Alpha_max were about 2% to 14% different from the input α and it seemed that 4 mm gave the smallest discrepancy among these thicknesses.

Fit_vel_min and Fit_vel_max were the same and gave the most accurate results, about 0.1% larger than the input v. Fit_alpha_min was about 5% smaller and Fit_alpha_max was about 2% larger than the input value.

3.5.2. Dispersion in α

This test was to see the effect of complex impedance and frequency dependence of the attenuation.

ρ (g/cm^3)	Z_t (MRayl)	Z_d (MRayl)	v (mm/μs)	α (mm^{-1})
1.12	40	$\frac{\rho v}{1+i\frac{\alpha v}{2\omega}}$	0.09	50*frequency

Table 3.5. The input parameters. Frequency is with a unit of MHz.

Thickness (mm)	Vel_min (mm/μs)	Alpha_min (mm^{-1})	Vel_max (mm/μs)	Alpha_max (mm^{-1})
2.5	0.1231	2.9520	0.1087	2.3103
3	0.1250	2.9186	0.1099	2.2943
3.5	0.1268	2.8713	0.1107	2.2898
4	0.1286	2.7954	0.1120	2.2965
4.5	0.1300	2.6831	0.1133	2.3159

Fit_vel_min (mm/μs)	Fit_vel_max (mm^{-1})	Fit_alpha_min (mm/μs)	Fit_alpha_max (mm^{-1})
0.14009	0.11964	2.3628	2.3189

Table 3.6. The output results.

The output results showed that, with the effect of the complex impedance of the sample

and frequency dependent attenuation, Vel_min was about 37% to 44% larger than the input v and the discrepancy increased with increasing thickness. Vel_max was about 21% to 26% larger than the input v and the discrepancy increased with increasing thickness. Alpha_min and Alpha_max were about 14% to 48% different from the input α and it seemed that 4 mm gave the smallest discrepancy among these thicknesses.

Fit_vel_min and Fit_vel_max were about 56% and 33% larger than the input v. Fit_alpha_min was about 18% smaller, and Fit_alpha_max was about 16% larger than the input value.

3.6. Simulation of vacuum dough

The velocity and attenuation in the material were assumed to be frequency independent in this first case to see the effect of the complex impedance of the sample.

ρ (g/cm^3)	Z_t (MRayl)	Z_d (MRayl)	v (mm/μs)	α (mm^{-1})
1.26	40	$\frac{\rho v}{1+i\frac{\alpha v}{2\omega}}$	2	0.1

Table 3.7. The input parameters.

Thickness (mm)	Vel_min (mm/μs)	Alpha_min (mm^{-1})	Vel_max (mm/μs)	Alpha_max (mm^{-1})
8	1.8414	0.1759	1.9784	0.1627
9	1.7841	0.1621	1.8973	0.1499
10	1.7716	0.1531	1.8714	0.1420
11	1.7905	0.1470	1.8507	0.1370
12	1.7795	0.1428	1.8338	0.1338

Fit_vel_min (mm/μs)	Fit_vel_max (mm^{-1})	Fit_alpha_min (mm/μs)	Fit_alpha_max (mm^{-1})
1.6958	1.6129	0.076953	0.076406

Table 3.8. The output results.

The output results showed that, with the effect of the complex impedance of the

sample, Vel_min was about 10% and Vel_max were about 6 % smaller than the input value and the discrepancy became larger with increasing thickness. Alpha_min and Alpha_max were about 34% to 75% different from the input α and the discrepancy decreased with increasing thickness.

Fit_vel_min was about 15% smaller and Fit_vel_max was about 19% smaller than the input value. Fit_alpha_min and Fit_alpha_max were close and about 23% smaller than the input alpha.

One issue associated with the vacuum dough is the fast velocity, so that the first part of the reflected signal runs fast enough that it is superimposed on the directly transmitted signal. So, I assessed the effect of this reflected signal on the measured velocity and attenuation. If we ignored the first reflected signal, we would get Fit_vel_min, Fit_vel_max, Fit_alpha_min, and Fit_alpha_max to be exactly the same as the input values. It is clear that the first reflected signal affected the result even in this large thickness range with our input values. The following figure shows the signal parameters as a function of thickness over a wide range.

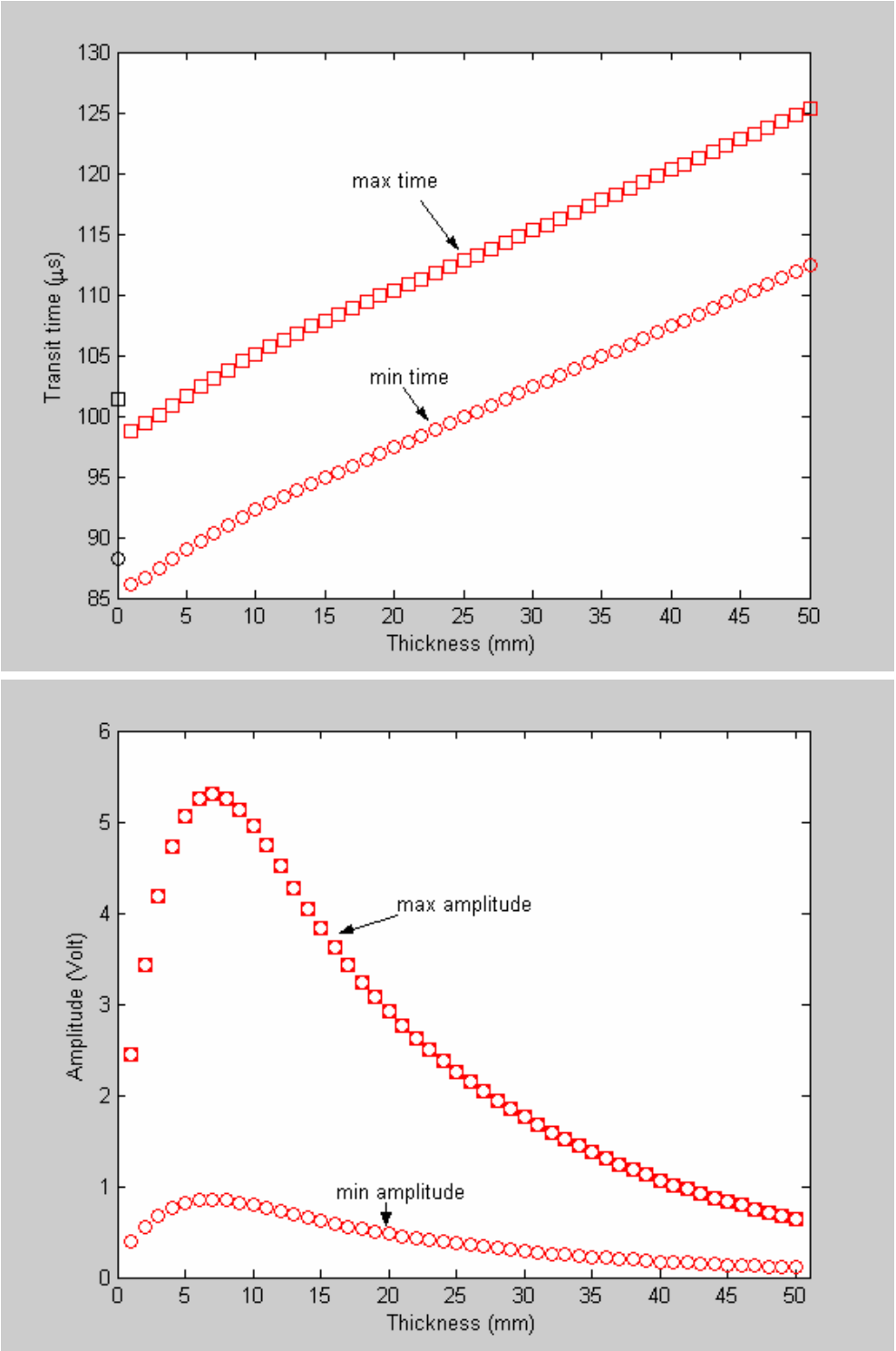

Figure 3.20. Transit time and amplitude as a function of sample thickness. The reflected signal affected the results with the low attenuation coefficient.

Chapter 4 Experimental Results and Discussion

The chapter consists of three parts: low frequency measurements and interpretation, high frequency measurements, and interpretation of the high frequency results. In the first part, two relaxations, relaxation due to the compression of the sample and relaxation following the mixing process, were studied for vacuum dough, ambient dough, nitrogen dough and the dough mixed at different reduced pressures.

The second part contains the data for the high frequency measurements of vacuum dough and ambient dough, from 1 MHz to 20 MHz. Both relaxation behaviors were studied and the spectra of phase velocity and attenuation were determined. In the third part, the spectra were explained by theoretical models. Two different models were used; one is for the results around the bubble resonance frequency, and the other one is applicable for higher frequencies, where the properties of the matrix itself dominate the behavior.

Part I: 40 kHz ultrasonic measurements

4.1. Ultrasound measurements of vacuum dough at 40 kHz

4.1.1. Variability in ultrasonic measurements of vacuum dough at 40 kHz

Ultrasonic measurements of ambient dough and reduced-pressure dough were well studied in Hussein Elmehdi's thesis (Elmehdi, 2001). The results reported in this chapter follow on from his ground-breaking research, by addressing questions that were not explicitly considered in his thesis. I started my work by improving the setup for vacuum mixing, so that dough samples mixed at higher vacuum could be prepared. If we consider absolute vacuum to be 0 inch Hg, I was able to obtain a reduced pressure in the range 1-2 inch Hg (about 3% to 7% atmospheric pressure). Previous work was done at 4-5 inch Hg, so this is a significant improvement.

The main parameters that we measured were the phase velocity and attenuation coefficient. Signals were recorded at 40 kHz for a range of different thicknesses. The method that we used to analyze the data was discussed in section 3.2.

In these initial measurements, I measured values of the velocity from 2000 to 2500 m/s and attenuation from 0.2 to 0.9 mm^{-1}. Also in these experiments, the data points for different thicknesses were very much scattered around the fitted curves (section 3.2). These results were not very consistent and therefore probably imprecise. In order to increase the accuracy, we needed more data points, which meant more thicknesses. For the vacuum dough, we found that signals still could be detected at a thickness of 20 mm. Since the attenuation was relatively low, one concern for measurements at small

thickness (like 3 mm) was the possibility that multiple reflections inside the sample would distort the measurements. Here we calculate the thickness at which the multiple reflections could affect the first minimum of the waveform. If we take the velocity to be 2.0 mm/μs and the frequency to be 0.036 MHz, the sample thickness L should satisfy the following inequality.

$$\frac{2*L}{v} > \frac{1}{4}*\frac{1}{f}$$

$$L > \frac{v}{8*f}$$

$$L > 6.9 \text{ mm}$$

Thus, we need to make the thickness of the vacuum dough larger than 6.9 mm for the 40 kHz ultrasonic measurements. In order to have a wider range of different thicknesses that satisfy this condition, while at the same time obtaining the maximum amount of information from one sample, I decided to start with a large thickness, like 18 mm, and progressively reduce the thickness to smaller values by squeezing the sample.

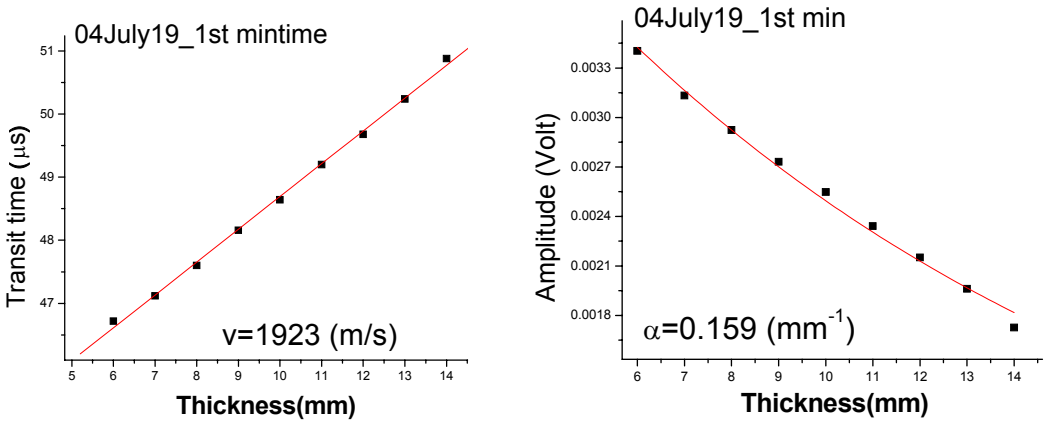

Figure 4.1. The transit time (left) and amplitude (right) as a function of sample thickness for one vacuum dough subsample that was squeezed from 14 mm to 6 mm.

For velocity, the data, shown in Figure 4.1, seem consistent with the expected behavior (transit time proportional to thickness), and a good fit of a straight line to the data was obtained. However, the amplitude data did not follow an exponential decay. Because dough is a viscoelastic material, we thought that the strain from the compression of the dough could affect the amplitude results, since over time, the strain stored in the dough would relax. To investigate this effect quantitatively, we designed an experiment to monitor the relaxation behavior of the dough after compressing to a certain thickness.

4.1.2. Relaxation behavior of vacuum-mixed dough at 40 kHz

4.1.2.1. Waiting time dependence

4.1.2.1.1. Short time relaxation

In the ultrasonic measurements, it was essential that the sample had good mechanical contact with the transducers, so that the ultrasonic signals could be effectively transmitted across the sample-transducer interfaces. In our experiment, this was achieved by squeezing a ball-shaped dough sample to a disc-shaped one with a certain thickness (see figure 4.2). Strain energy was stored in the sample after compression due to its viscoelastic properties.

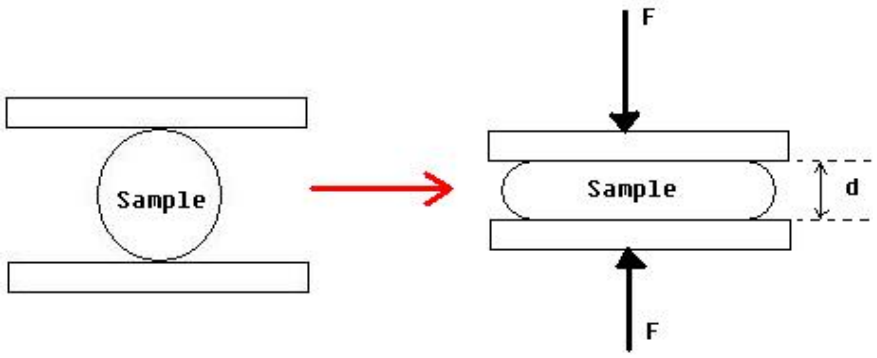

Figure 4.2. The change in sample shape during squeezing.

An example of the resulting ultrasonic behavior is shown in figure 4.3. Fifty minutes after mixing, a sample was compressed to 10 mm, and the changes in the transmitted ultrasonic signal were monitored as the sample was left to wait between the transducers for 5 minutes. Then the sample was compressed to a different thickness and was allowed to wait for 5 minutes at each thickness. We define the time during which the sample stayed at the same thickness between the transducers to be the waiting time. The signal was recorded at waiting times of 0, 1, 2.5 and 5 minutes.

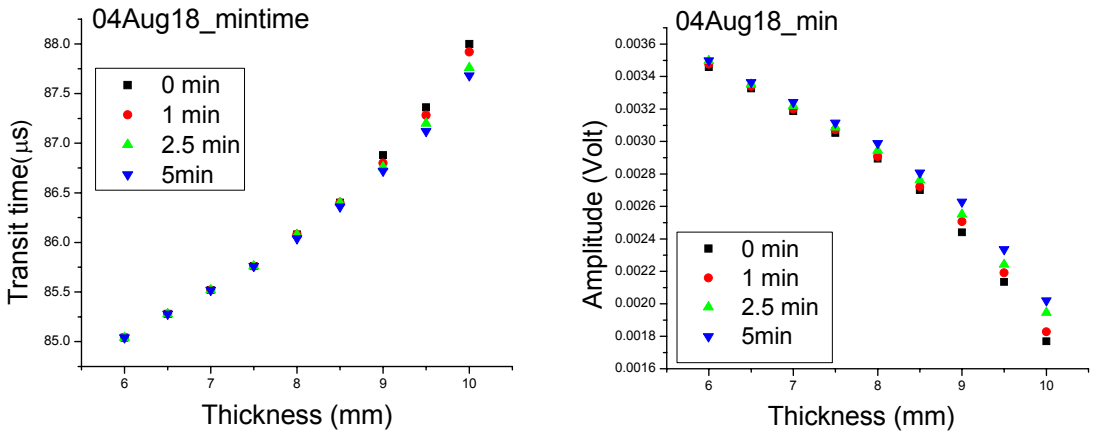

Figure 4.3. The transit time (left) and amplitude (right) as a function of sample thickness for a single vacuum dough subsample squeezed from 10 mm to 6 mm. The sample was allowed to wait for 5 minutes at each thickness.

It is clear from figure 4.3 that relaxation behavior was observed after the dough was compressed to a certain thickness. The transit time data curved upward and the amplitude data was still not an exponential decay. It seemed that five minutes was too short a time for full relaxation to occur at a given thickness. In the next section, I discussed what happened when the waiting time after compressing was longer.

4.1.2.1.2. Long time relaxation

Dough was mixed at 6% atmospheric pressure (1.8 inch Hg). The ultrasonic experiment was started about 60 minutes after the dough was mixed. The sample was compressed from 17 mm to different thicknesses. The waiting time at each thickness is recorded in table 4.1.

Thickness (mm)	17	16	15	14	13	12	11	10	9	8	7
Waiting Time (min)	120	40	20	10	5	5	5	5	5	45	5

Table 4.1. Sample thicknesses and waiting time at each thickness for the longer time relaxation experiments.

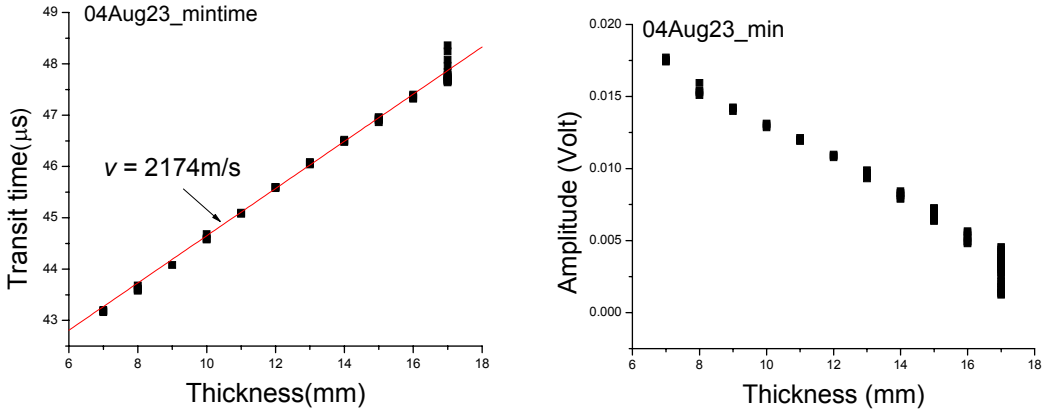

Figure 4.4. The transit time (left) and amplitude (right) as a function of sample thickness for a single vacuum dough subsample squeezed from 17 mm to 7 mm. A long waiting time was chosen at the first thickness.

Figure 4.4 shows that after a long initial waiting time at the first thickness, a good linear fit to the thickness dependence of the transit time data could be obtained, but the decrease in amplitude with thickness was still not exponential. To examine this behavior in more detail, it is worth plotting the relaxation behavior as a function of the waiting time after compression. In order to enlarge the scale and see the relaxation behavior clearly, I only present the data for thicknesses above 13 mm in the following figures (figure 4.5).

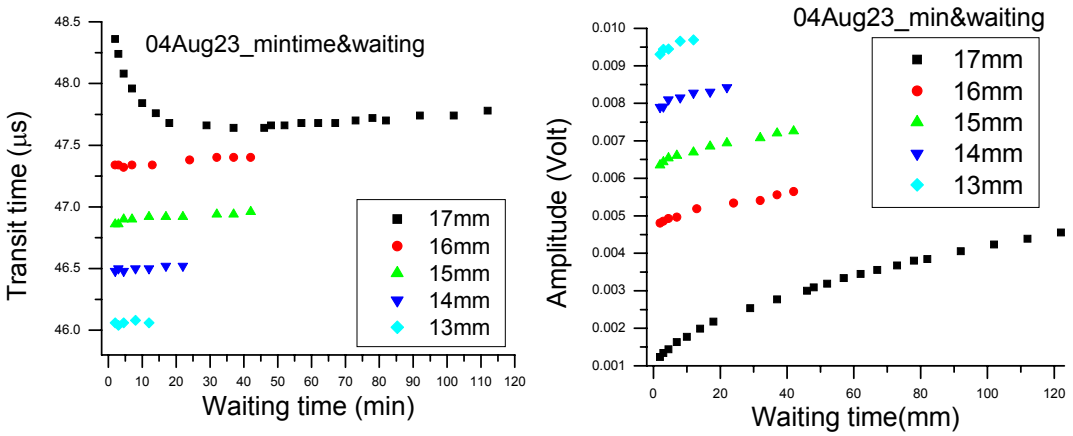

Figure 4.5. The transit time (left) and amplitude (right) as a function of waiting time at each thickness. The experimental data are the same as in Figure 4.4.

Figure 4.5 shows that the strain resulting from the compression does affect the ultrasonic properties. The relaxation behavior after the first compression was different from the behavior after the subsequent compressions. After the first compression, the transit time decreased quickly and then gradually started increasing. For the subsequent compressions, no initial decrease in transit time was observed and only the slow increase was seen. From the amplitude data, we found that after the first compression the amplitude increased quickly and then kept on increasing at a slower rate that appeared to be linear in time. From the amplitude data for the other thicknesses, we still see an initial rapid increase, which very quickly slowed down to a linear increase that was similar to the later time relaxation behavior after the first compression.

The data shown in figure 4.5 raise an interesting question: what is the origin of the difference between the data at the first thickness and the data at subsequent thicknesses? These data were measured for different amounts of compression but also for different

times after mixing. Could we detect a difference between subsamples resulting only from a different post mixing history?

4.1.2.2. Post mixing effect

To address the question raised in the last section, vacuum dough was mixed at 3.5% atmospheric pressure (1.05 inch Hg) and after 30 minutes ultrasonic measurements were started. The first subsample was compressed to 8 mm and left to wait between the transducers for 60 minutes. After that, a new subsample was placed between the transducers and measured for another 60 minutes. The same procedure was followed for the third and fourth subsamples. Each subsample had roughly the same mass. During the experiment the holder was sealed by plastic tape.

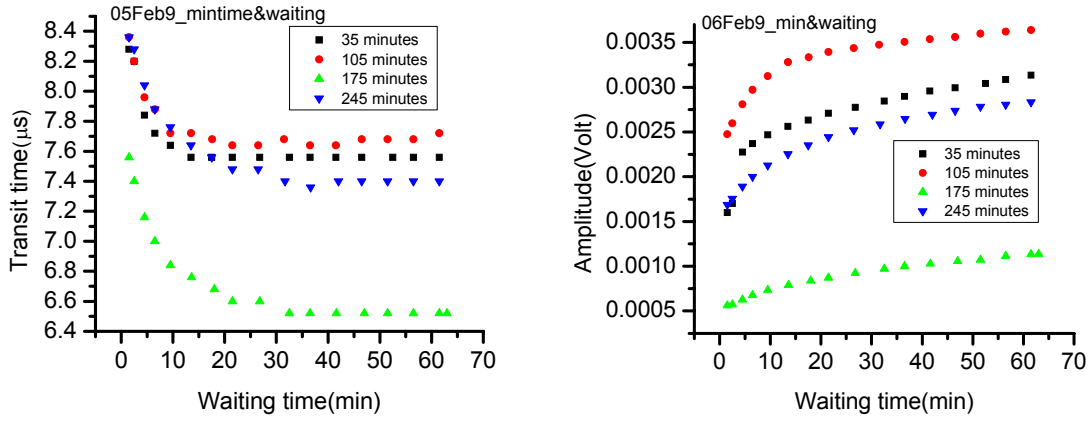

Figure 4.6. The transit time (left) and amplitude (right) as a function of waiting time for different subsamples with the same thickness but different post mixing times.

In figure 4.6 above, different symbols represent different subsamples with different post mixing times. The times shown in the figure are the post mixing times when each

subsample was taken from the container and inserted between the transducers. Consistently with the last section, both the transit time and amplitude changed with waiting time after the subsample was squeezed, but we did not see any systematic trend from one subsample to the next as the post mixing time increased. Note that there are quite large differences in the amplitude of the signals from the different subsamples, so that the uncertainty of these post mixing time relaxation measurements is also large. Thus, in the 40 kHz range, we were not able to detect any post mixing time relaxation of vacuum dough over times ranging from 30 to 300 minutes after mixing.

4.1.2.3. Imposition of tensile stresses

In section 4.1.2.1, I discussed the effect of compression stress on ultrasonic parameters. In this section, I will present data on the effect of stretching or tensile stress.

A vacuum dough was mixed, and its ultrasonic properties were measured starting 60 minutes after mixing. For this sample, the head space pressure in the mixer was only 12% atmospheric pressure; while this pressure is higher than for the data presented in Figure 4.6, the pressure was still low enough for vacuum type properties to be observed (see section 4.3). Evidence to support this assertion can be found by comparing the data for compressive stresses in figures 4.8 and 4.6, which clearly show similar behavior. The first subsample was compressed to 10 mm and then compressed to smaller thicknesses. Instead of progressively greater compressions, the sample was stretched

back to a less compressed state at some thicknesses. Table 4.2 lists the values of thickness selected, with the order of the measurements being from left to right, and the waiting time at each thickness. We could see that after being compressed to 9 mm, and again after first being compressed to 8 mm, the sample was stretched back by 0.5 mm.

Thickness (mm)	10	9	**9.5**	8	**8.5**	8	6
Waiting Time (min)	90	30	**20**	30	**30**	10	25

Table 4.2. Sample thicknesses and waiting time at each thickness.

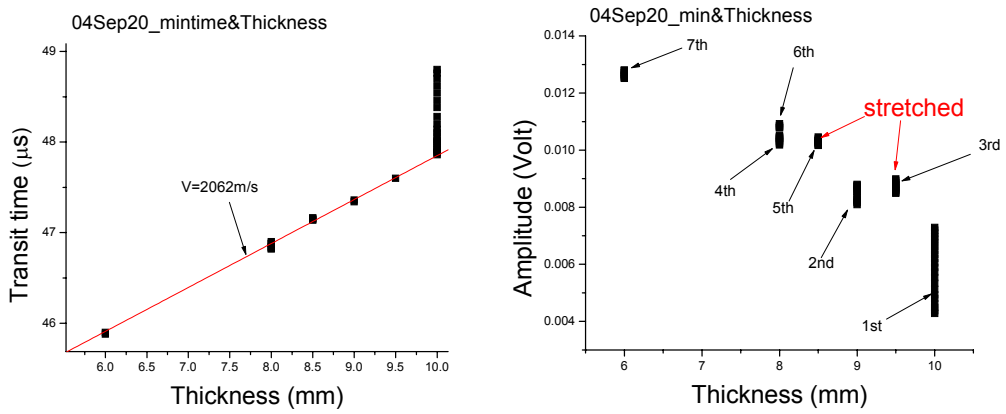

Figure 4.7. The transit time (left) and amplitude (right) as a function of thickness for the tensile experiment.

From the figures above (figure 4.7), it can be seen that the transit time data does not show any difference between the straight compression experiment and compressing-stretching experiment. However, from the amplitude data, we found that the stretching stress did affect the ultrasonic signal because the amplitude values at 9.5

mm and 8.5 mm are larger than the values extrapolated from other thicknesses during compression.

The time dependence of the relaxation effect is shown in the next figure (figure 4.8).

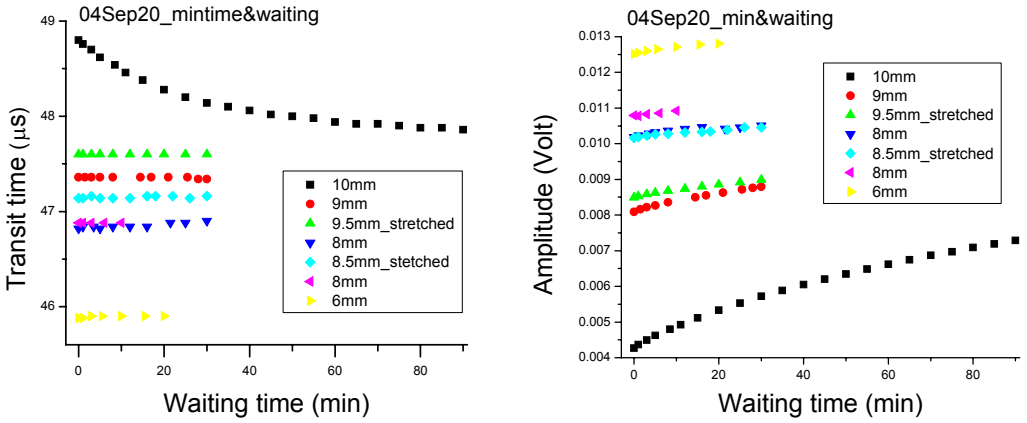

Figure 4.8. The transit time (left) and amplitude (right) as a function of waiting time at each thickness for the tensile experiment. The experimental data are the same as in figure 4.7.

The time dependence of the relaxation of both transit time and amplitude is similar to that observed in section 4.1.2.1, although the absolute value of the amplitude is affected by the stretching. What needs to be noticed here is the time dependence of the relaxation behavior of both transit time and amplitude is similar no matter whether the sample is compressed or stretched. In particular, the amplitude continues to increase after stretching as well as after compressing. This is different from the relaxation behavior of ambient dough, as will be shown in section 4.2.

4.1.2.4. Very long time relaxation effects

In order to better understand the relaxation behavior of vacuum dough after compression, a very long time relaxation experiment was performed. Thirty minutes after mixing, a vacuum dough sample was compressed to 10 mm and signals were recorded for about 28 hours. The transit time and amplitude data are shown below (figure 4.9).

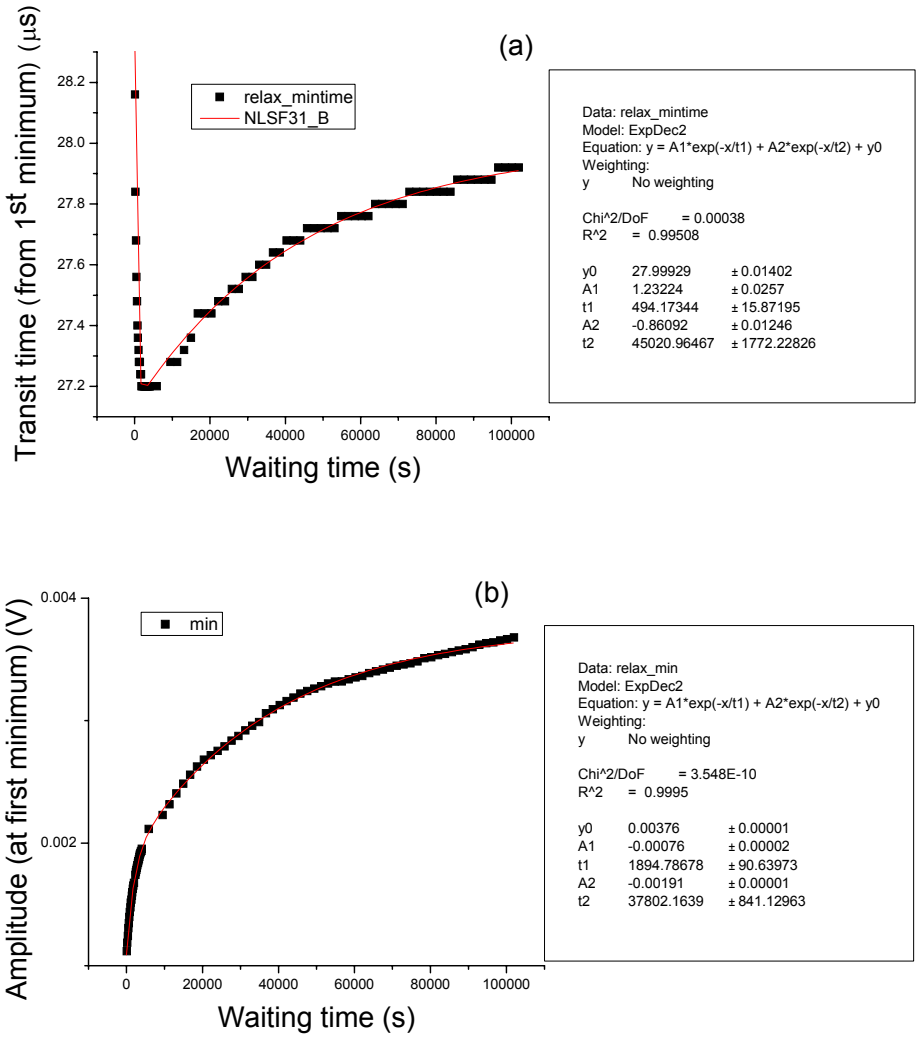

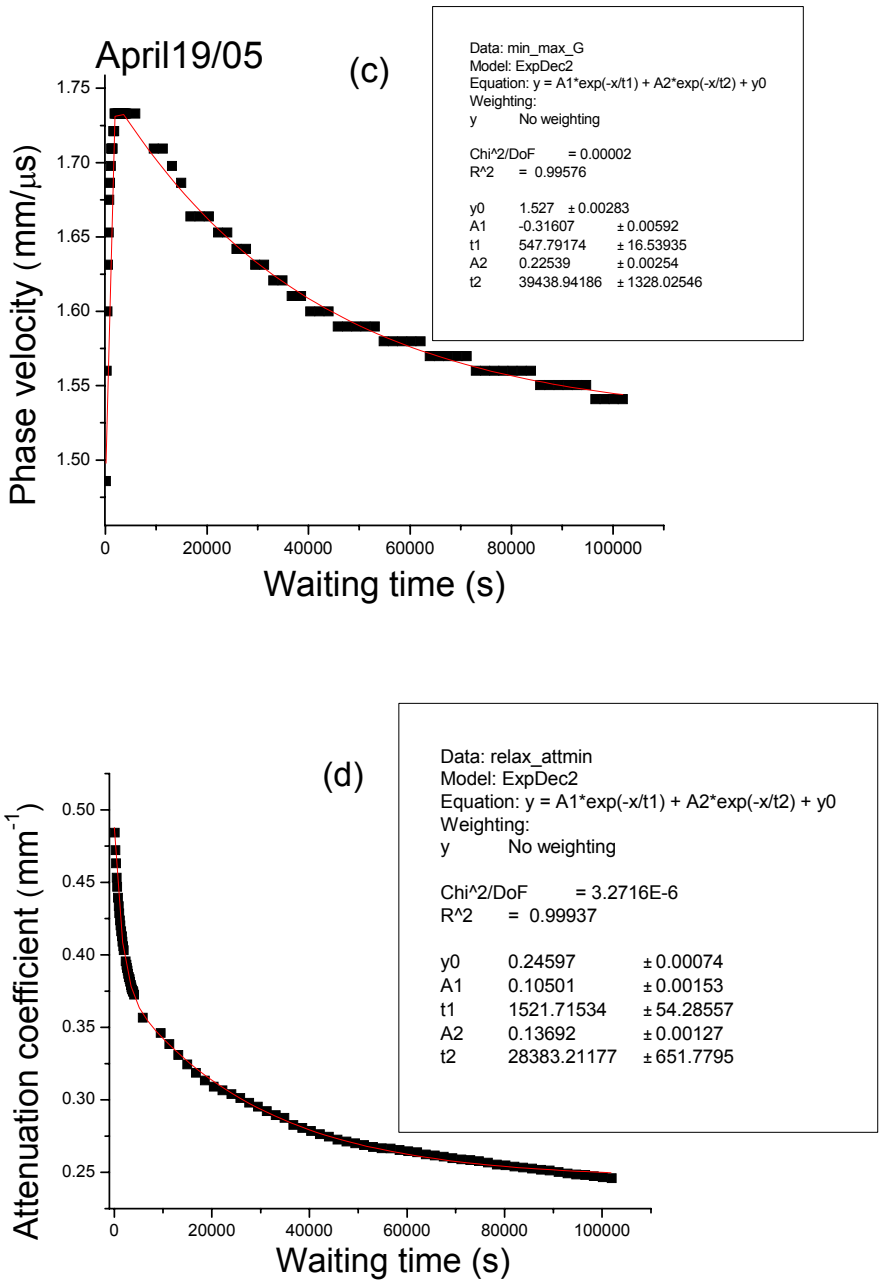

Figure 4.9. Very long waiting time relaxation effects in the vacuum dough. (a) and (b) show the transit time and amplitude data from the first minimum. (c) and (d) show the phase velocity and attenuation obtained by comparing the data from (a) and (b) with the reference signal measured with the two transducers in direct contact. The absolute value of the results shown in (c) and (d) might not have absolute accuracy because it was not possible to account fully for the effects of impedance mismatch between the transducer and sample (see section 3.4.1.2).

Both the amplitude and transit time could be well fitted by the sum of two exponential decay functions, which describe the combination of a rapid and a slow relaxation, $Y = A_1\exp(-T/t_1) + A_2\exp(-T/t_2) + Y_0$. The fitted parameters are listed in the table below.

Parameter / **Fit Data**	Y_0	A_1	**t_1 (s)**	A_2	**t_2 (s)**
Transit time	28	1.2	**500**	-0.86	**45000**
Amplitude	0.004	-0.008	**1900**	-0.002	**38000**
Phase velocity	1.53	-0.32	**540**	0.2	**40000**
Attenuation coefficient	0.246	0.11	**1520**	0.14	**28400**

Table 4.3. The double exponential decay fit of the very long waiting time vacuum data.

From above results, we find that the short relaxation has a relaxation time of around 500 to 2000s, while the long time relaxation is much longer, around 40,000s. The other thing to be noticed is that for the transit time data, the short relaxation causes the transit time to decrease but the long relaxation causes the transit time to increase. By contrast, both relaxations lead to increases in the amplitude. Also there is a discrepancy between the relaxation times of the transit time and amplitude, presumably reflecting the inadequacy of the model. Regardless of the limitation of this analysis, the big picture here is very clear, namely that two very different relaxation processes are involved after the vacuum sample is compressed. A challenge for future work will be to understand the mechanisms responsible for these two relaxations. The observed behavior also suggests that the amplitude of the transmitted signals from a vacuum sample will

eventually level off after a very long time, with a relaxation time of roughly 40,000s. Thus, it appears possible for equilibrium behavior to be attained in vacuum dough, providing one is prepared to wait long enough.

4.1.2.5. Summary of 40 kHz measurements on vacuum dough

For all the above experiments, it is clear that an exponential thickness dependence for the amplitude was never observed when a single subsample was compressed. One reason for this phenomenon is that the relaxation behavior of vacuum dough after the initial compression from a ball-shape to a disc-shape was larger that of the subsequent compressions and also had a significant very slow component (figures 4.5 and 4.9). Thus, the relaxation from the initial deformation was still continuing at the subsequent thicknesses. In addition, the subsequent compressions also changed the dough, as shown by the initially faster change in amplitude immediately after each compression. Thus, the dough continued to evolve during the measurement, and never reached an equilibrium amplitude at each thickness before the next compression was made. Therefore, the dynamic time-dependent attenuation that causes this behavior could not be measured accurately from the variation in amplitude of a single subsample with different thicknesses. A procedure for overcoming this limitation of the current measurements is proposed in Chapter 5.

By contrast, the relaxation of the transit time after the initial deformation seems shorter. As well the short and long time relaxation effects for velocity have opposite

sign, and therefore tend to cancel. Thus, almost no changes due to relaxation were apparent in the subsequent compressions of the sample, and so a linear relation was observed for transit time versus thickness after the initial relaxation had occurred (about an hour). Based on these linear fits from different experiments (e.g., see figures 4.4 and 4.7) we could derive a velocity of about 2070 ± 100 m/s for vacuum-mixed dough at 40 kHz. Because so few bubbles are present in the vacuum dough, this quite large value of velocity is expected to be representative of the properties of the dough matrix.

When different subsamples were used to measure the attenuation coefficient (Elmehdi, 2001), an exponential decay of amplitude with thickness was reported. This does not contradict the results reported in this thesis. Since these measurements were performed after the post-mixing time relaxation was complete, each different subsample at each thickness started from the same initial conditions, and each sample then experienced a similar initial relaxation after compression. So if we compare the amplitude for different thicknesses at the same waiting time after compression, an exponential decay should be observed. As mentioned above, this method is based on the assumption that no post mixing relaxation was occurring. From section 4.1.2.2, we can conclude that about 30 minutes after mixing, no post mixing relaxation could be observed for the vacuum dough, so this condition is easy to realize in practice. In such measurements, one would expect that the rate of exponential decay with thickness should change with waiting time, as the observed increase in amplitude indicates a decrease in the attenuation.

4.2. Ultrasound measurements of ambient dough at 40 kHz

In the last section, the effects of compressive and extensional strains on ultrasonic measurements of vacuum dough at 40 kHz were described. Vacuum dough is dough with very few air bubbles in it. In the next two sections, I describe the effects on the low frequency ultrasonic properties of adding air bubbles to dough, by studying dough mixed at both ambient and intermediate pressures.

4.2.1. Waiting time dependence

Dough was mixed at atmospheric pressure and half an hour after mixing, the ultrasonic measurements were started. One subsample was compressed and stretched to different thicknesses. The thicknesses are listed in table 4.4, along with the waiting times at each thickness, with the order in which the measurements were performed being given from left to right.

Thickness (mm)	4.5	4	**4.2**	3.8	**4**	3.5	**3.8**
Waiting Time (min)	32	32	**22**	32	**27**	32	**32**

Table 4.4. Sample thicknesses and waiting times at each thickness.

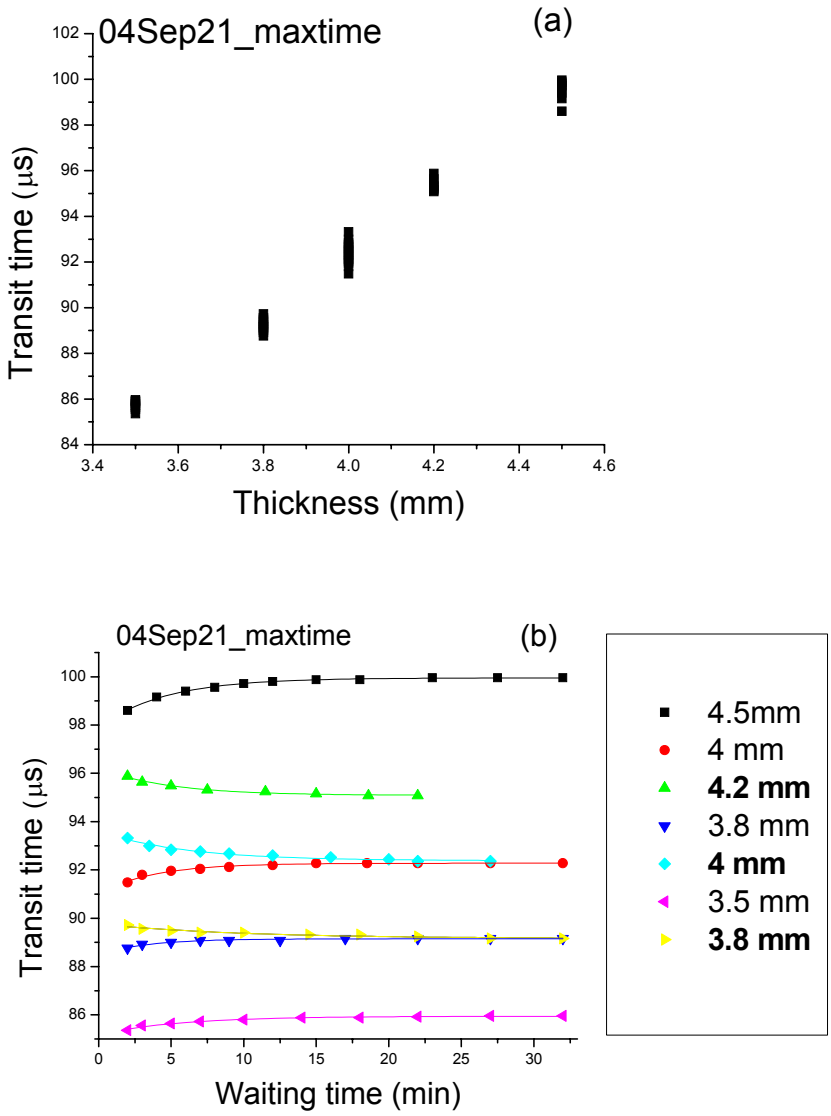

Figure 4.10. The transit time as a function of thickness (a) and waiting time (b) for ambient dough.

By comparing the figure above (figure 4.10) with Figs. 4.7 and 4.8, it can be seen that the relaxation behavior of ambient dough was different to that of vacuum dough. There are three main differences. First, after compression, the transit time increased with waiting time. From section 4.1.2.1, we know that transit time decreased with

waiting time immediately after compression for vacuum dough. Second, the relaxation behavior for the first thickness was similar to that of the compressed subsequent thicknesses. For the vacuum-mixed dough, they were very different. Third, the relaxation of the stretched dough induced transit time changes that were opposite to those in compressed dough. Also, at a given thickness, the transit time seemed to level off to the same value no matter whether the dough had just been compressed or stretched.

The data were fitted by an exponential decay function $Y = Y_0 + A_1 e^{(-T/t_1)}$ and the parameters for each thickness are listed in table 4.5.

Thickness (mm)	4.5	4	**4.2**	3.8	**4**	3.5	**3.8**
Y_0	100	92.3	95.1	89.1	92.4	85.9	89.2
A_1	-2	-1.24	1.14	-0.66	1.22	-0.76	0.6
t_1 (min)	4.6	3.8	4.8	3.3	6	5.6	3.5

Table 4.5. Exponential fitting parameters for the waiting time dependence of transit time at each thickness.

The next figure (figure 4.11) shows the amplitude results.

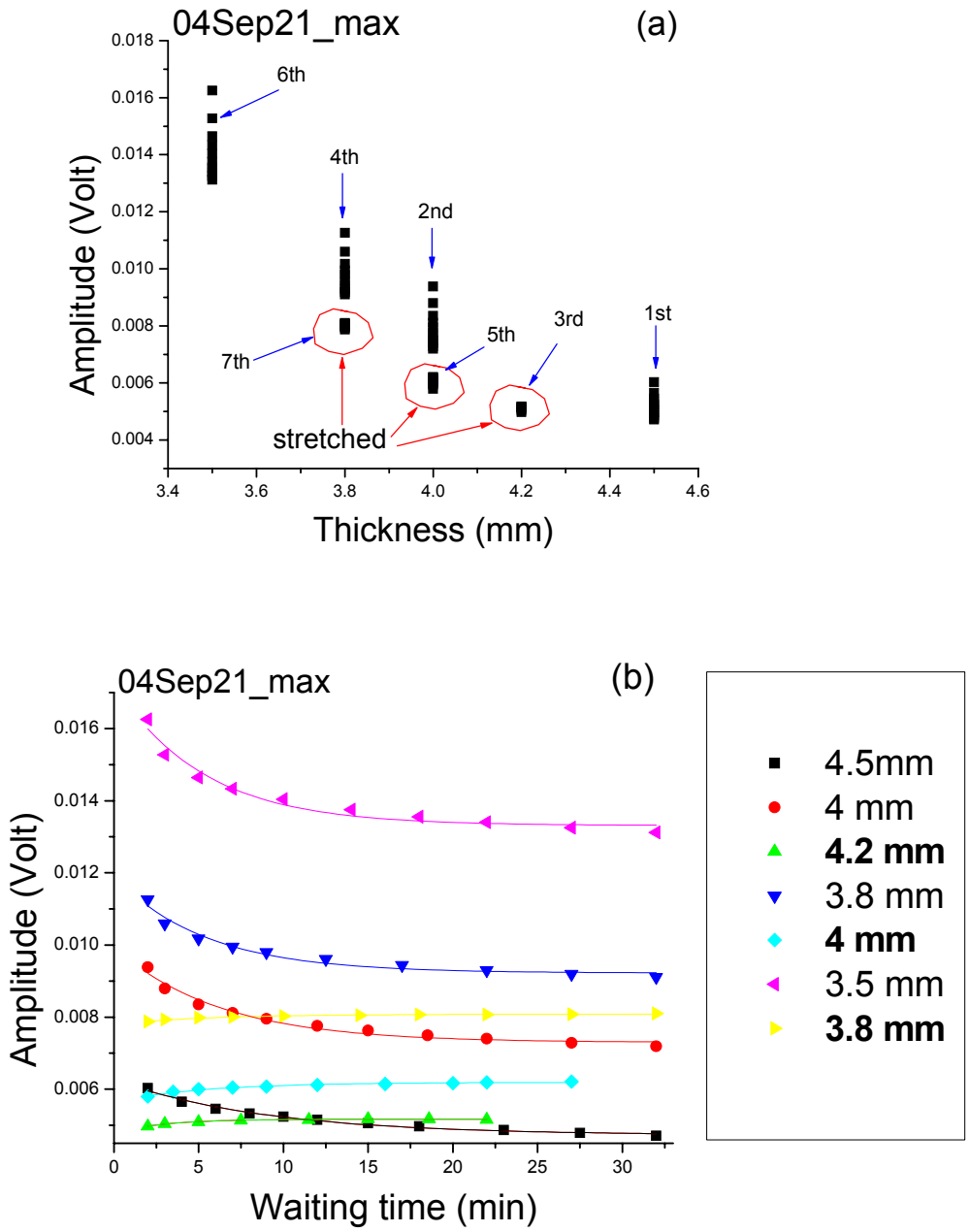

Figure 4.11. The amplitude as a function of thickness (a) and waiting time (b) for the tensile experiment for ambient dough.

Compared with the amplitude results for vacuum dough in section 4.1.2.3, there were also three differences in the behavior of the ambient dough. First, the change in amplitude during the relaxation was opposite: the amplitude decreased with waiting time

after compression instead of increasing with waiting time, as was found for vacuum dough. Second, the relaxation behavior at the first thickness was similar to that observed after compression to the other thicknesses. For the vacuum dough, they were very different. This difference for ambient dough could explain why consistent results could be obtained by squeezing one subsample to different thicknesses and compressing different subsamples to different thicknesses, as shown in the next figures. Figure 4.12 compares the experimental results obtained using these two methods. In this figure, the red square data were measured from a single subsample experiment, in which one subsample was compressed to different thicknesses, while the black triangle data were measured using the different subsample method, in which the measurements at each thickness were measured on different subsamples. All data were recorded immediately after each compression. Note the excellent agreement between the results obtained in these two experiments.

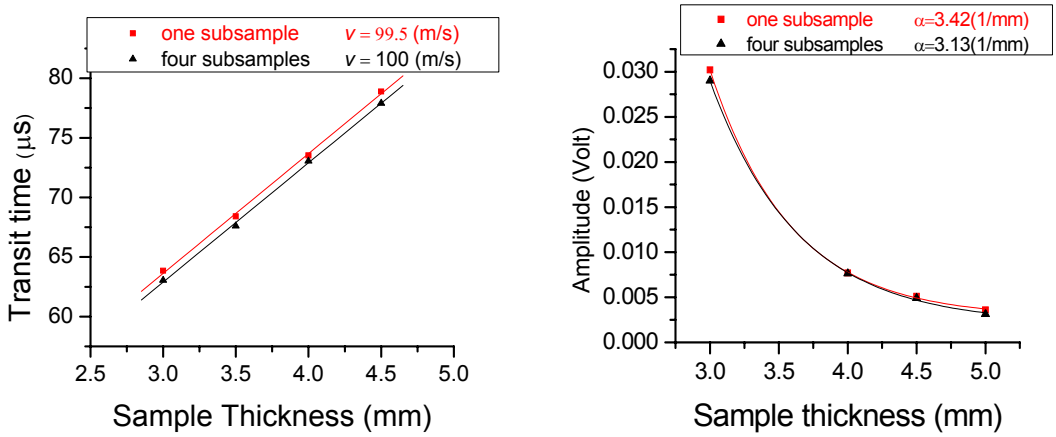

Figure 4.12. The transit time (left) and amplitude (right) as a function of sample thickness for the single subsample experiment (red squares) and for different subsamples experiment (black triangles). The data were recorded immediately after compression.

Third, the relaxation behavior seen in figure 4.11 at the stretched thicknesses behaved in the opposite way to that found for the compressed thicknesses. In addition, for a given thickness the amplitude appeared to level off to slightly different values for the compression and stretching stages of the experiment. The values for the stretched cases were somewhat smaller than for the compression cases.

The amplitude data were fitted by an exponential decay function $Y = Y_0 + A_1 e^{(-T/t_1)}$ and the parameters for each thickness are listed in table 4.6.

Thickness	4.5 mm	4 mm	**4.2 mm**	3.8 mm	**4 mm**	3.5 mm	**3.8 mm**
Y_0	0.005	0.007	0.005	0.009	0.006	0.013	0.008
A_1	0.002	0.003	-3.8E-4	0.003	-5.4E-4	0.004	-2.7E-4
t_1 (min)	8.9	6.2	2.9	5.4	5.4	5.2	5.7

Table 4.6. Exponential fitting parameters of amplitude at each thickness.

The fitting parameters in tables 4.5 and table 4.6 reveal several of the characteristics of ambient dough relaxation. First, the relaxation time t_1 is similar at all values of the thickness, with the value after initial squeezing not being significantly different to the value found after the subsequent compressions. This is consistent with what figure 4.12 is showing. The average value of t_1 is 5.1 ± 1.5 min. For the ambient dough, the value of t_1 for amplitude is a little larger than that for transit time, likely reflecting the

somewhat longer relaxation times that would be expected from fitting amplitude rather than attenuation (see table 4.3). The parameter A_1, which measures the magnitude of the relaxation changes, seems to increase with the post mixing time in both cases; this effect may be related to the greater compression of the samples at longer post mixing times (see also section 4.2.3). Second, comparing the results for squeezing and stretching deformations, we find that t_1 has similar values, while A_1 has the opposite sign. Another observation is that Y_0 at the same thickness in squeezing and stretching has almost the same value for the transit time but different values for the amplitude.

In order to learn more about the relaxation behavior of ambient dough after being compressed, a very long time waiting experiment was done, similar to the experiment for vacuum dough described in section 4.1.2.4. The results are shown in figure 4.13.

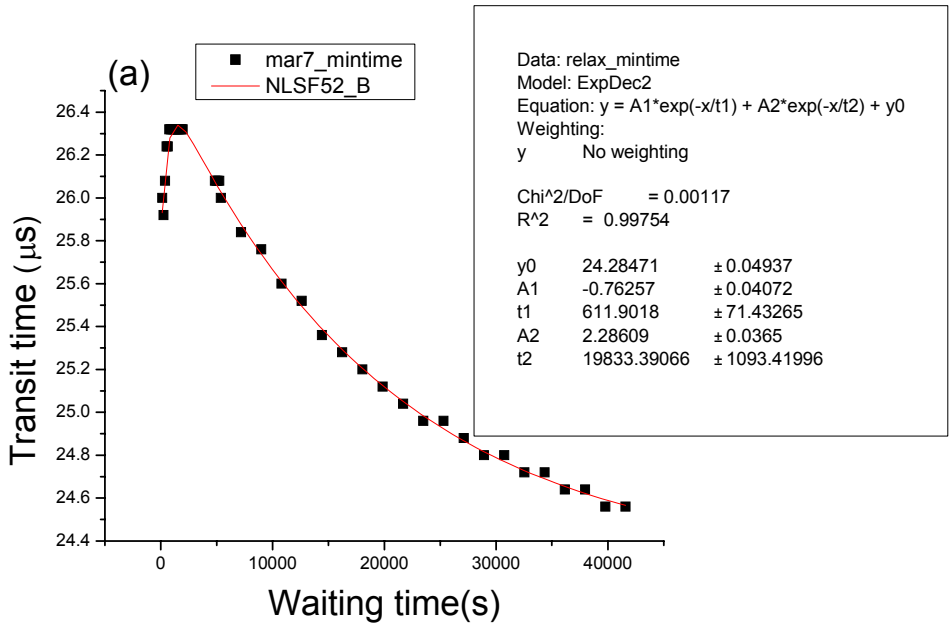

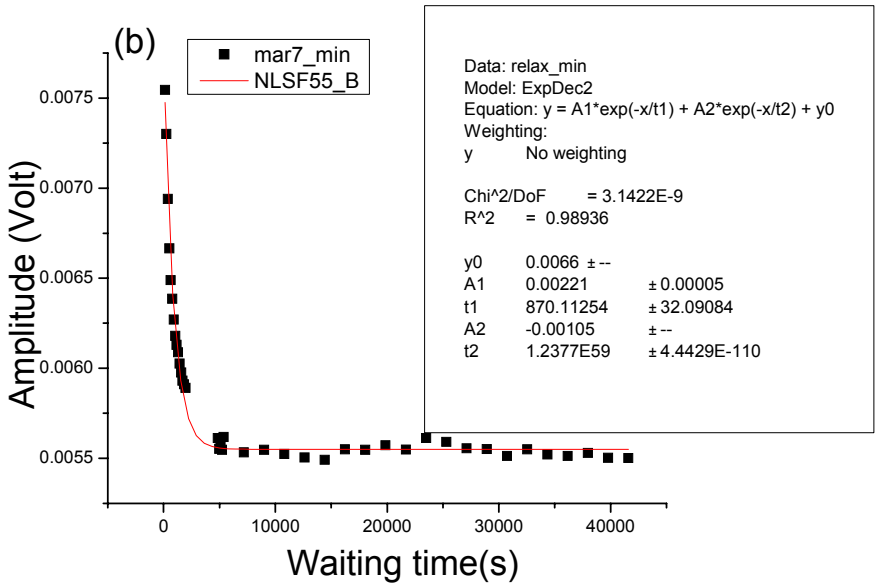

Figure 4.13. Change in transit time (a) and amplitude (b) for very long waiting time relaxation of ambient dough. The term "mintime" refers to the transit time of the first minimum in the waveform and "min" refers to the magnitude of the first minimum.

This very long waiting time measurement was started three and one-half hours after mixing. Both the amplitude and transit time were fitted by a double exponential decay function: $Y = A_1\exp(-T/t_1) + A_2\exp(-T/t_2) + Y_0$. The fitted parameters are listed in the table below (table 4.7).

Parameter / **Fit Data**	Y_0 (Volt)	A_1 (Volt)	**t_1 (s)**	A_2 (Volt)	**t_2 (s)**
Transit time	24.3	-0.8	610	2.29	20000
Amplitude	0.0066	0.002	870	-0.001	1.2377E59

Table 4.7. Double exponential fitting parameters for the data in figure 4.13.

Just as for the vacuum results, there is a fast relaxation and a slow relaxation process. The slow relaxation time for ambient dough is in the same range as that of vacuum, and is larger than the relaxation time found using a single exponential model. For the amplitude it seems that only the fast relaxation was observed, as the parameter t_2 is extremely large.

4.2.2. Post mixing effect

A second set of data was taken to enable the dependence of velocity and attenuation on post mixing time to be examined. For these measurements, a different subsample was used for each thickness. The ultrasonic measurements were started half an hour after the ambient dough was mixed. Table 4.8 summarizes the procedure and parameters for this experiment. In this table, the order in which the measurements at each thickness were performed is given from left to right, along with the waiting time at each thickness and the total post-mixing time at the end of the measurements at each thickness.

Thickness (mm)	4.5	3	4	4.5	3.5	2.5	3
Waiting Time (min)	32	32	32	32	32	32	692
Post-mixing Time (min)	35	79	131	172	214	258	298

Table 4.8. Sample thickness, total waiting time at each thickness, and post-mixing time at the start of each measurement for the dough mixed at atmospheric pressure.

Because each subsample had a different thickness, it would not make any sense to compare the transit time and amplitude for each subsample, as we did in section 4.1.2.2 for the vacuum dough post mixing effect. In order to study the post mixing effect with these data, we have to use the velocity and attenuation coefficient instead. The method for determining the velocity and attenuation for this set of data was described in section 3.4.1.2 in detail. An extrapolated reference, which is different from the experimentally measured reference, was chosen to determine the velocity and attenuation, thus allowing the offset due to the phase shift arising from the complex impedance of dough to be effectively taken into account.

In analyzing these data, a complication was encountered, namely that it was found that the extrapolated references are not the same for different values of the waiting time. As explained in section 3.4.1.2, the reference point was extrapolated from a linear fit of the transit time as a function of thickness. There are 15 different waiting times, so we obtained 15 different linear fits, and thus 15 different extrapolated reference times. However, if we were to use these different references for the data at each waiting time, even though they are very close to each other, we would not obtain the right trend for the time evolution with waiting time, as measured directly from the transit time evolution. The origin of this discrepancy lies in the difference in the magnitude of the waiting time dependence at each thickness, as well as the possibility that the velocity depends on post-mixing time, which for these data could result in inaccuracies in the linear extrapolation. However, these changes in the velocity and attenuation are quite small on

a percentage basis, so that the phase shift due to the complex impedance of the dough is not expected to change significantly during the time course of these experiments. Thus it is reasonable to take a fixed reference time for all the data, and to use the average extrapolated reference as the best estimate of this time. This approach for determining the velocity, using a fixed reference time, ensures that the correct trends in the velocity with waiting time and post mixing time will be reliably determined, even though the absolute value of the velocity may not be very accurately measured. Fortunately, the uncertainty in the absolute velocity can be estimated to be about 10% or less, which is comparable to the variation from sample to sample for ambient dough.

For the same reason, the attenuation coefficient was determined using the extrapolated amplitude reference, so that the reduction in amplitude due to interface reflections could be accounted for. As for velocity, a fixed amplitude reference was used, as determined by the averaged value from the different waiting times.

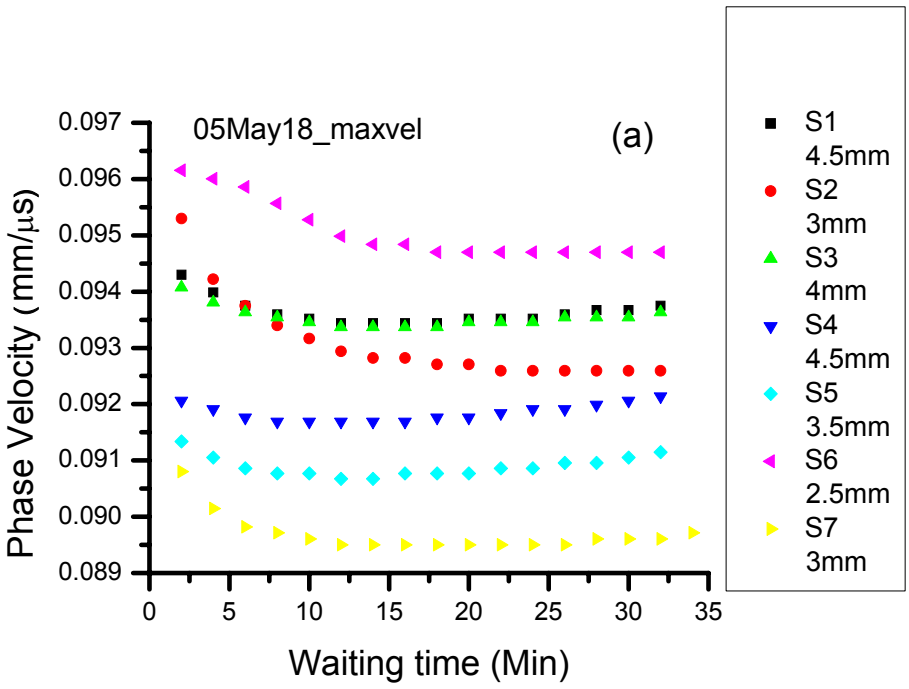
05May18_maxvel
(a)
Phase Velocity (mm/μs)
Waiting time (Min)
0.097
0.096
0.095
0.094
0.093
0.092
0.091
0.090
0.089
0
5
10
15
20
25
30
35
S1 4.5mm
S2 3mm
S3 4mm
S4 4.5mm
S5 3.5mm
S6 2.5mm
S7 3mm

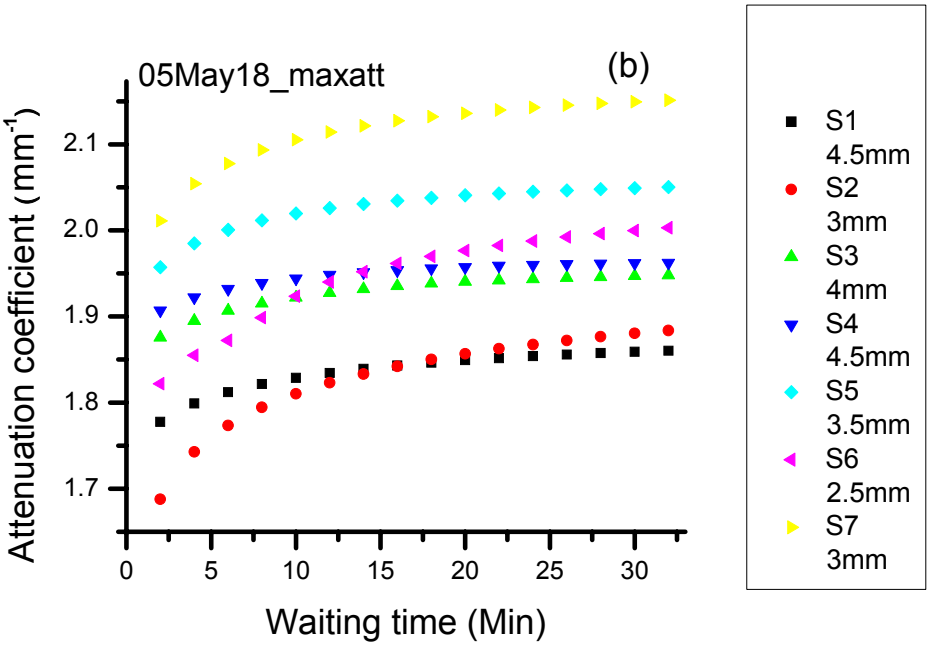
05May18_maxatt
(b)
Attenuation coefficient (mm-1)
Waiting time (Min)
2.1
2.0
1.9
1.8
1.7
0
5
10
15
20
25
30
S1 4.5mm
S2 3mm
S3 4mm
S4 4.5mm
S5 3.5mm
S6 2.5mm
S7 3mm

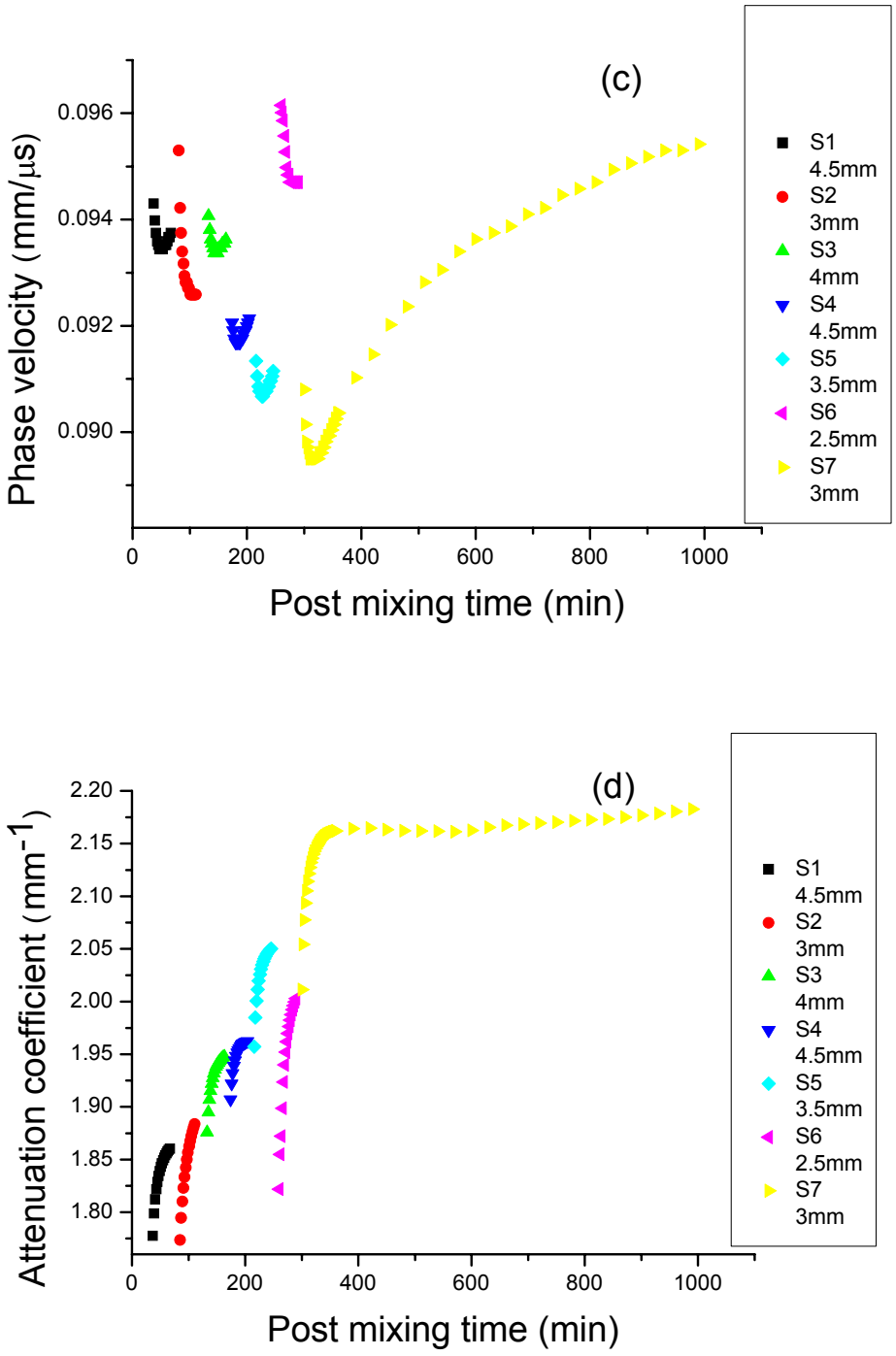

Figure 4.14. The phase velocity and attenuation coefficient as a function of waiting time at each thickness for different subsamples (a and b). The phase velocity and attenuation coefficient as a function of post mixing time at each thickness for different subsamples (c and d).

Figures 4.14 (a) and (b) show the relaxation behavior of ambient dough as a function of the waiting time after compression at different mixing times. From these figures, it appears that the change in both velocity and attenuation is greater for thinner samples, suggesting that the effects of the initial compression of the subsamples depend on sample thickness. Note that this effect occurs even though we had already chosen the mass of each subsample to attempt to minimize differences in compression as much as possible by making the final area of all the compressed subsamples to be almost the same. This effect is discussed in more detail in section 4.2.3.

Figures 4.14 (c) and (d) show the full time evolution of velocity and attenuation after mixing. From these figures, one might be tempted to infer that there is a systematic post mixing time evolution in both phase velocity and attenuation. To investigate this possibility, similar experiments were repeated on two other days, and the results shown in figure 4.15 were obtained. From figures 4.14 and 4.15, it is clear that no systematic post mixing evolution could be detected for velocity for times up to 300 minutes, although the long time increase in velocity for the last sample studied on each day is similar for all three data sets. For attenuation, however, there is a possibility that there could be a systematic increase of attenuation with post-mixing time during the first 300 minutes, although this effect is difficult to deconvolve from the waiting time relaxation, since the experiments for each subsample were terminated before the changes due to the waiting time evolution were complete. To investigate this post mixing effect in more detail, further experiments on different subsamples, in which the relaxation is

followed for longer times at each thickness, are required. This would be an interesting project for future work, especially as such a long-time trend is not expected based on previous experiments, which indicated that a relaxation time of roughly 15 minutes is characteristic of recovery from perturbations of the dough during mixing (e.g., see Elmehdi, 2001).

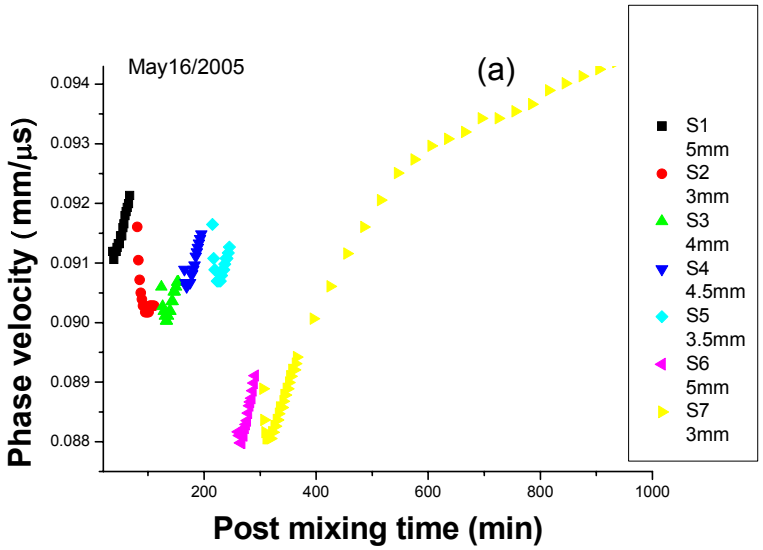

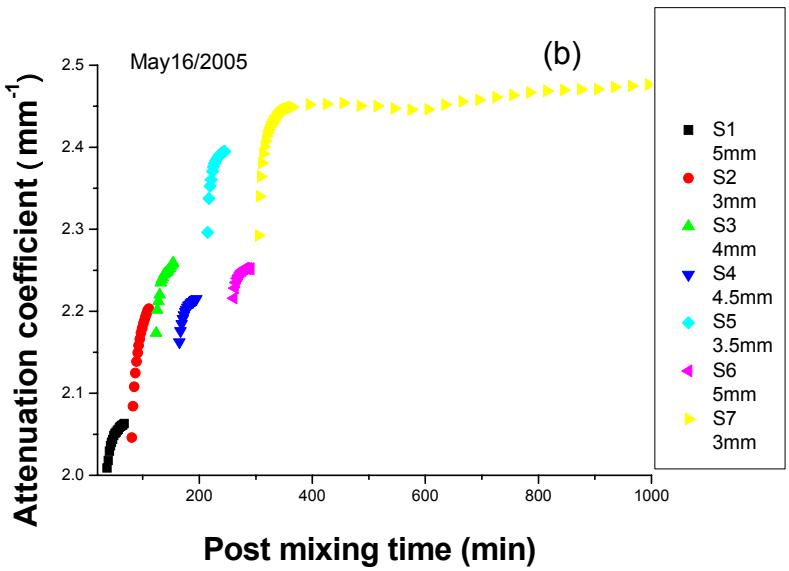

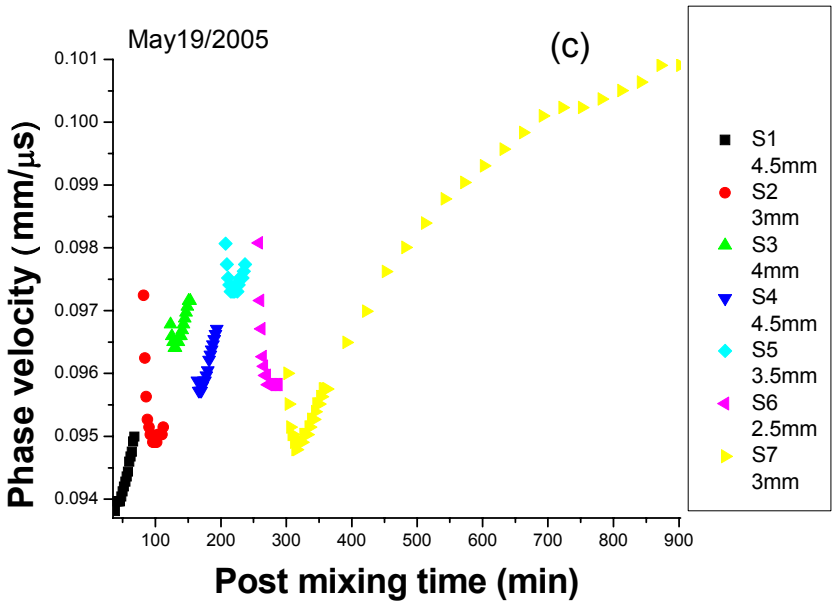

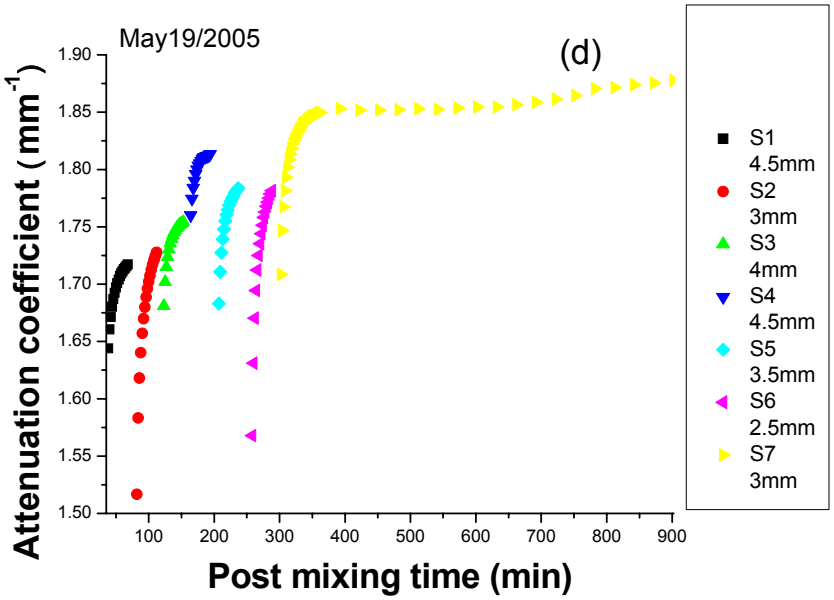

Figure 4.15. Repetitions of the experiments to investigate the phase velocity and attenuation coefficient as a function of post mixing time, showing the results at each thickness for different subsamples. The experiments were performed on May 16/2005 (a and b), on May 19/2005 (c and d).

4.2.3. Strain effect

In figures 4.14 and 4.15, it appears that the magnitudes of the changes in velocity and attenuation during the waiting time after compression are correlated with the thickness of the subsamples, and hence with the magnitude of the compressive stress that is applied. In particular, it can be seen that the changes in velocity and attenuation from the value after initial compression to the extreme values where the relaxation trend changed direction (for velocity) or leveled off (for attenuation) were different for different thicknesses. Even though the dough masses were carefully chosen for different thicknesses to reduce the strain difference at each thickness, it was still more difficult to compress a thinner sample than a thicker one. In this section, the change of velocity and attenuation as a function of the induced strain is studied.

To define a convenient measure of the response to compression, the change of velocity δv was defined as the difference between the initial value 2 minutes after compression and the minimum value where the relaxation behavior changed direction. The change of attenuation $\delta\alpha$ was taken to be the difference between the value 2 minutes after compression and the value 32 minutes after compression.

We can approximate the compression process in two steps as follows. First, the sphere-shaped sample was compressed to a cylinder. In this step, it is assumed that the stress exceeds the yield stress of the dough residing in the top and bottom portions of the sample, so that the dough "flows" without straining the bulk of the dough piece. Second, this cylindrically-shaped sample was compressed to its final dimensions. In this step,

because the stains were large in the experiment, the deformation should be described by true strain.

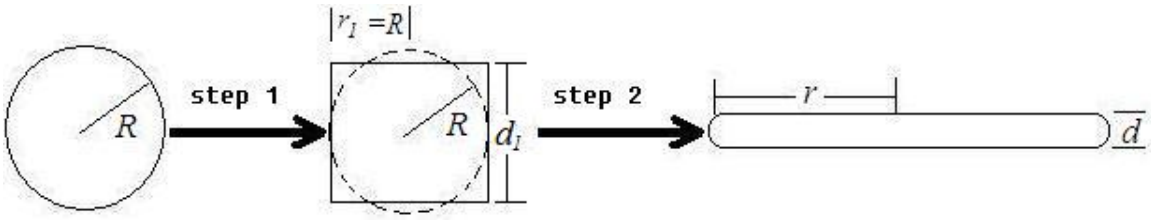

Figure 4.16. A diagram illustrating the two stages considered in the model for dough compression in the ultrasonic experiments. $d_1 = 4R/3$.

In the first step of the model, we assume that:

a. there is frictionless contact between the dough ball and the compression plates.

b. the material is an elastic-plastic material (and therefore can be approximated as a rigid plastic material) with a specific yield stress.

c. the material is incompressible.

d. the propensity of dough ball to "slump" is on a timescale that is long compared to the time of compression.

e. The initial stress will be large, due to point contact over a small surface area when the plate touches the points of the sphere. This stress will exceed the yield stress of the dough.

In this step, the dough flows outward from the point of contact, leading to an increase in flat surface area in contact with the transducer, and leading to a reduction in the applied stress. This process continues until the dough flows outward filling in the radius of curvatures of the dough ball until the thickness becomes $4R/3$. After this point, the

stress will essentially be uniform throughout the cylinder, and the dough cylinder as a whole will deform, rather than flowing to allow the displacement of portions of the dough away from regions of large stress.

Thus, "zero strain" can be defined at the point when $d = d_1 = 4R/3$. As we know the mass, m, and the density, ρ, of the dough piece, d_1 can be expressed as

$$d_1 = \frac{4^{2/3}}{3^{2/3}} \sqrt[3]{\frac{m}{\pi\rho}}.$$

In the second step of the model, each small change in the height, z, of the sample is considered as a fraction of the height it was just prior to this point of deformation. Thus the appropriate measure of the deformation is the true strain, which is defined as $\varepsilon_T = \int_{d_1}^{d} \frac{dz}{z} = \ln(d/d_1)$. For compression, as d is smaller than d_1, the true strain will be a negative quantity.

The change of velocity and attenuation as a function of the true strain is plotted in the next figure.

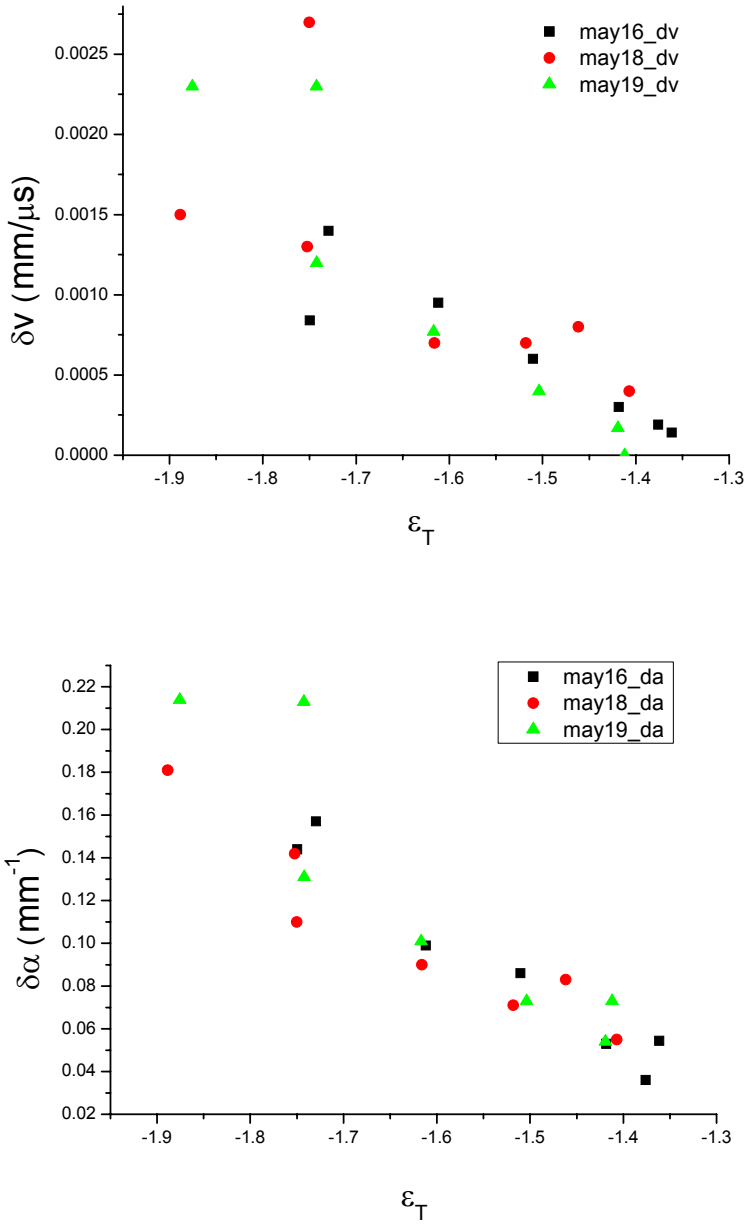

Figure 4.17. The change of velocity and attenuation as a function of true strain due to compression of dough subsamples.

From the above figure we can clearly see that the change in the velocity and attenuation after compression are both affected by the true strain from the deformation of the sample. The larger the absolute value of the true strain, the larger the change of

velocity and attenuation. This figure, therefore, provides unambiguous evidence that the relaxation effects observed immediately after the dough is placed between the transducers are due to the corresponding deformation of the samples during mounting. These experiments provide a controlled way of measuring changes in the mechanical properties of dough as a result of an applied uniaxial stress.

4.2.4. Discussion

The main conclusion that can be drawn from these experiments on ambient dough is that the relaxation mechanism that is responsible for the time dependence of velocity and attenuation must be different from that found in vacuum dough. For ambient dough, compression causes changes in the dough that show similar relaxation behavior, independent of the time after mixing. These changes also appear "reversible" in the sense that stretching reverses the sign of the time dependent changes in velocity and attenuation. These effects could, in principle, arise either from relaxation of the stretched polymers in the matrix, or from relaxation induced by changes due to bubbles. In the remainder of this section, we focus on the latter possibility.

A possible mechanism that could explain how bubbles determine the relaxation behavior caused by compression or extension is as follows. In this discussion it is helpful to refer to the waiting time dependence shown in Figs. 4.10 and 4.11, where the effects can be most clearly seen. As the dough is compressed or stretched, the bubbles are likely to be deformed from their initial spherical shape, as well as being reduced in

size. Thus, the volume fraction of the bubbles will be lowered, and the pressure inside the bubbles increased. Both these effects influence the velocity and attenuation at low ultrasonic frequencies, well below the bubble resonance frequency, which is the regime that applies to these experiments at 40 kHz. For example, it is known from the experiments of Elmehdi *et al*. and from effective medium theories that the velocity and attenuation are influenced only by the volume fraction of bubbles, rather than by their size or shape in this frequency regime [Elmehdi *et al*., 2004, Leroy *et al*., 2006], and that the velocity decreases but the attenuation increases as the volume fraction increases. Thus, it would be expected that a reduction in bubble size due to compression of the dough would reduce the volume fraction of gas in the bubbles and cause an instantaneous increase in the velocity and a decrease in the attenuation coefficient. However, this is not an equilibrium situation, because of the simultaneous increase in pressure inside the bubble resulting from compression, so that as time passes after compression, the pressure inside the bubbles would cause the bubbles to be restored towards their original size, until equilibrium is reached. Thus the relaxation effect observed for ambient dough in this range of times would correspond to an increase in bubble sizes and hence their volume fraction as the bubbles return towards their original configurations, causing a decrease in velocity (increase in transit time) and an increase in attenuation (decrease in amplitude) during the relaxation process. These trends during relaxation are consistent with the experimental data, suggesting that relaxation of the bubbles, rather than matrix effects due only to polymer relaxations, are responsible for the waiting time effects seen in Figs.

4.10 and 4.11. It is also worth noting that this bubble mechanism is also consistent with the behavior seen when the dough is stretched rather than compressed, since the bubble changes would be reversed in this case.

The underlying physics of these bubble effects lies in the very large compressibility of the bubbles relative to the dough matrix, and can be most easily appreciated in terms of Wood's approximation [Wood, 1941]. While this approximation is valid for bubbles in a liquid matrix, the basic idea is also relevant to bubbles in a viscoeleastic dough matrix, as can be shown by more sophisticated effective medium theories [Elmehdi, 2001, Leroy *et al*., 2006]. According to Wood's approximation, the velocity in a medium containing bubbles can be estimated from the volume-fraction-weighted average compressibilities of the bubbles (κ_a) and matrix (κ_m) :

$$\frac{1}{\rho v^2} = \kappa = \phi\kappa_a + (1-\phi)\kappa_m \tag{4.1}$$

Here ϕ is the volume fraction of bubbles. Since the compressibility of air is given by $\kappa_a = 1/\gamma P$, where γ is the heat capacity ratio and P is the pressure, the compressibility of the bubbles is much larger than that of the matrix, allowing the matrix term in the above equation to be neglected over the range of volume fractions for which measurements were made. Hence, a convenient approximate form for the velocity is

$$v \approx \sqrt{\frac{\gamma P}{\phi\rho}} \tag{4.2}$$

This equation shows that a sudden increase in P and decrease in ϕ on compression both cause v to instantaneously increase, while the more gradual relaxation back to

equilibrium, in which ϕ and P become restored towards their values before compression, is accompanied by a decrease in velocity. A similar relation between bubble volume fraction and ultrasonic properties is predicted by more complicated effective medium theories that include the viscoelastic properties of the matrix, but the increased complexity of these models obscures the essential idea that is shown by equation (4.2), and therefore will not be discussed here. It is also important to realize that while the bubble dynamics are the driving "force" for this mechanism, the relaxation times for bubble equilibrium to be re-established are determined by the viscoelastic response of the matrix. It remains an interesting challenge to develop a model that can predict these relaxation times quantitatively.

4.3. Relaxation behavior of dough at 40 kHz as the mixing pressure was varied

Since ambient dough and vacuum dough had opposite relaxation behavior after compression, it is interesting to investigate the relaxation behavior of dough that was mixed at pressures between atmospheric pressure and vacuum. In particular, we wanted to know whether there was a smooth crossover in the relaxation behavior from ambient-like to vacuum-like, and the headspace pressure at which this occurred. Thus, the relaxation behavior of dough mixed at 12%, 17% and 33% of atmospheric pressure was measured and is described in this section. The time evolution of the transit time and signal amplitude showed that dough mixed at 12% atmospheric pressure shows relaxation behavior similar to that of vacuum dough, while samples mixed at 17% and 33% atmospheric pressure exhibited relaxation effects that were more like those of an ambient dough.

4.3.1. Relaxation behavior of dough mixed at 12% atmospheric pressure

Dough was mixed at a headspace pressure equal to 12% atmospheric pressure. The ultrasonic measurements were started one hour after mixing. A single subsample was compressed and stretched to different thicknesses. The order of the measurements is given from left to right in table 4.9, which lists the thickness and waiting time at each thickness. Results for the transit time and amplitude as a function of waiting time are shown in figure 4.18.

Thickness (mm)	10	9	**9.5**	8	**8.5**	8	6
Waiting Time (min)	92	32	**22**	32	**32**	10	27

Table 4.9. Sample thickness and waiting time at each thickness for the dough mixed at 12% atmospheric pressure.

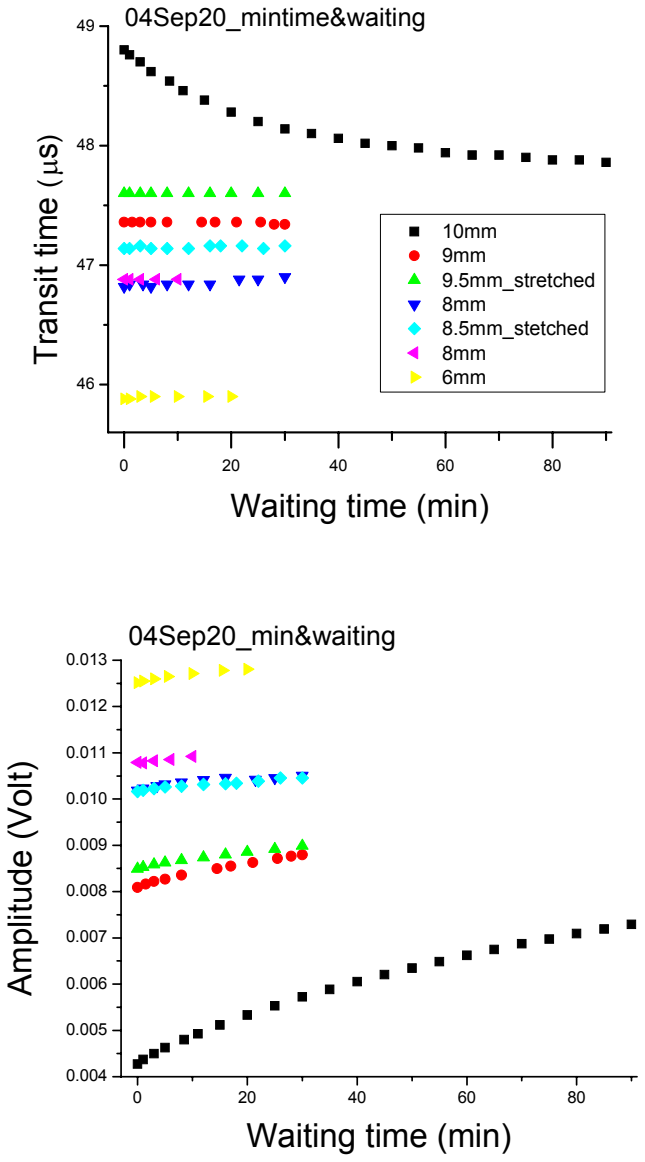

Figure 4.18. The transit time and amplitude as a function of waiting time at each thickness for dough mixed at 12% atmospheric pressure. (These data are the same as in Figure 4.8, but are replotted here to facilitate comparison with higher intermediate mixing pressures, and to emphasize that, by contrast with higher intermediate pressures, vacuum-like behavior is seen up to 12% atmospheric pressure.).

4.3.2. Relaxation behavior of dough mixed at 17% atmospheric pressure

The experimental procedure for the dough mixed at 17% atmospheric headspace pressure was the same as for the 12% atmospheric pressure measurements described in the previous section (Sec. 4.3.1). The values of the thicknesses used and the waiting time at each thickness are listed in table 4.10, and the transit time and amplitude data are shown in Figure 4.19. The ultrasonic measurements were started one hour after mixing. One subsample was compressed and stretched to different thicknesses.

Thickness (mm)	8	7	**7.5**	6.5	**7**	6
Waiting Time (min)	22	22	**18**	18	**18**	18

Table 4.10. Sample thickness and waiting time at each thickness for the dough mixed at 17% atmospheric pressure.

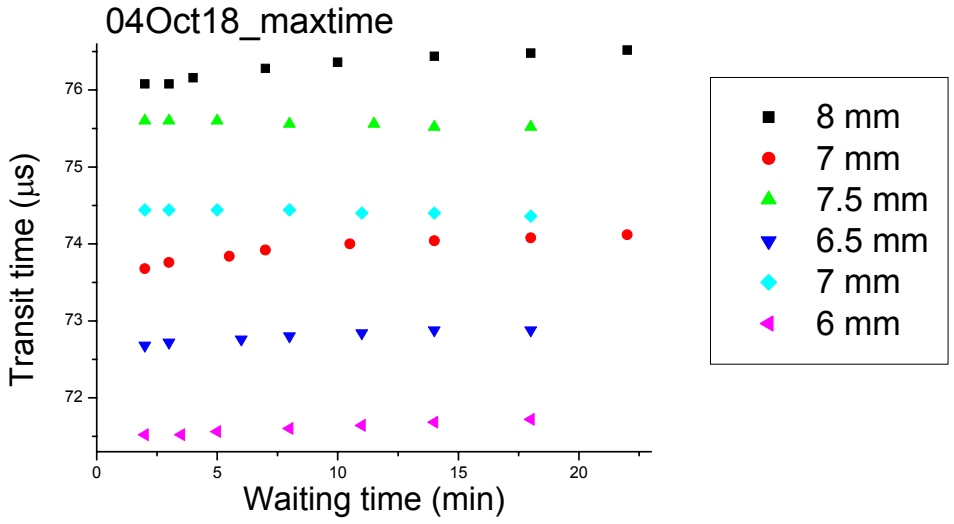

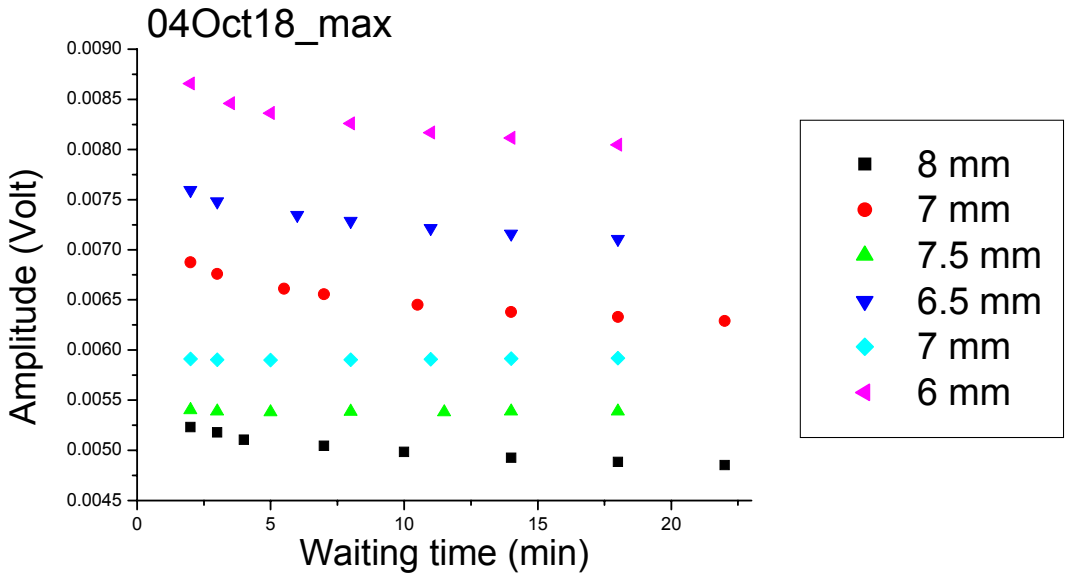

Figure 4.19. The transit time and amplitude as a function of waiting time at each thickness for measurements of the dough mixed at 17% atmospheric pressure.

4.3.3. Relaxation behavior of dough mixed at 33% atmospheric pressure

Dough was mixed at 33% atmospheric headspace pressure, and ultrasonic experiments were performed as described in sections 4.3.1 and 4.3.2. The experimental conditions are displayed in table 4.11 and the results in Figure 4.20.

Thickness (mm)	5.5	5	**5.2**	4.8	**5**	4	**4.2**	3.5	**4**	3.5
Waiting Time (min)	42	42	**32**	32	**37.5**	33	**32**	42	**36**	34

Table 4.11. Sample thicknesses and waiting time at each thickness for the dough mixed at 33% atmospheric pressure.

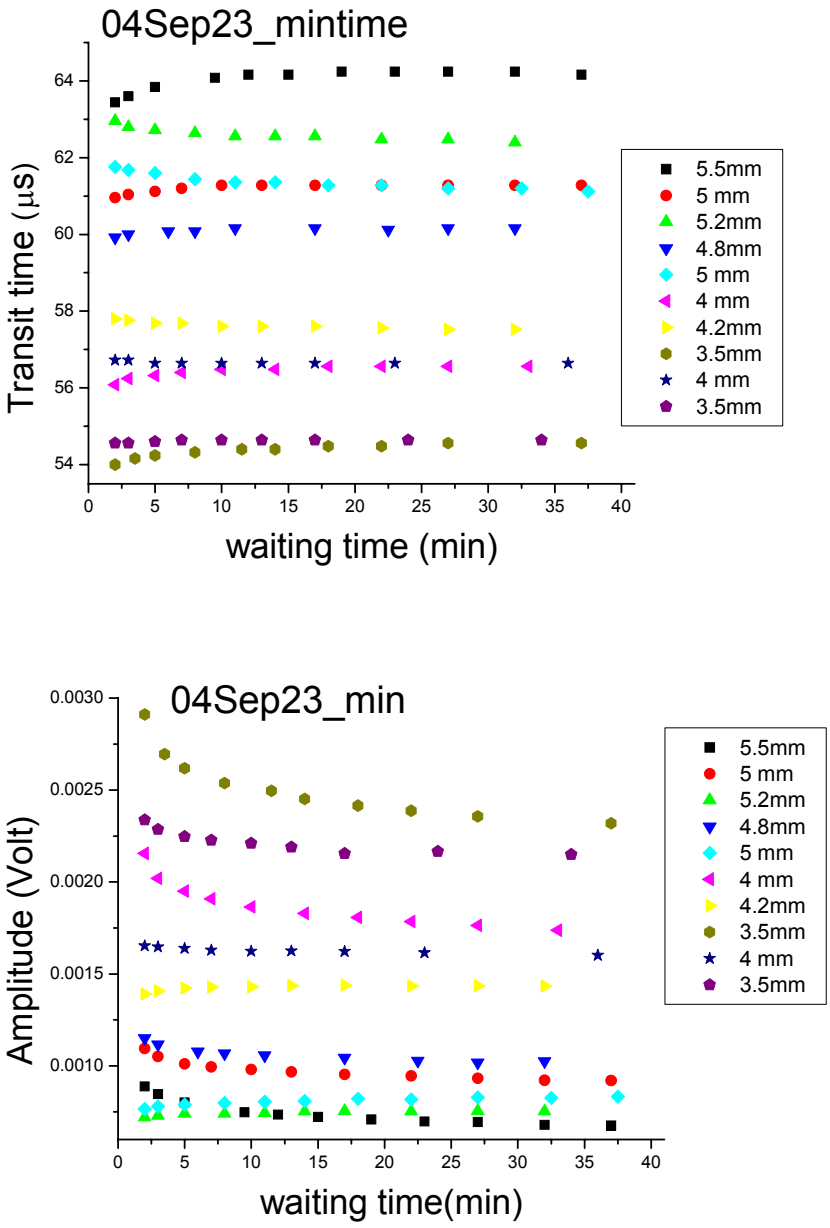

Figure 4.20. The transit time and amplitude as a function of waiting time at each thickness of the dough mixed at 33% atmospheric pressure.

4.3.4. Summary of the relaxation behavior of dough mixed at different headspace pressures

The purpose of this section is to discuss the relaxation behavior of dough mixed

under different pressures between vacuum and atmosphere in order to better characterize the crossover in the relaxation behavior from vacuum dough to ambient dough. For comparison, the relaxations of both the transit time and amplitude data for waiting times less than 30 minutes were fitted at each pressure by an exponential function $y = y_0 + A_1 * \exp(-T/t_1)$ for the initial thicknesses after compression. T represents the waiting time in this expression, the capital letter being used to distinguish waiting time T from propagation time t. From fitting this expression, we obtain the parameters A_1 and t_1 as a function of mixing pressure for both transit time and amplitude data. Because the thickness of each initial subsample for each pressure is different, the comparisons of A_1 and t_1 from the transit time and amplitude data may not accurately reflect changes in dough properties. Therefore, the fitting parameters for the transit time and amplitude were related to the velocity and attenuation changes, so that the comparison of data at different mixing pressures would be much more meaningful. In the following paragraphs, this relationship will be derived in detail.

The relaxation of the measured transit time t_m can be described as $t_m(T) = t_\infty + a_1 e^{-T/\tau}$, where t_∞ is the long time limiting value of the transit time, τ is the relaxation time, and a_1 is the total change in transit time due to the relaxation process. These parameters t_m, t_∞, a_1, and τ correspond to y, y_0, A_1 and t_1, respectively, in the fitting function. In terms of t_m, the corresponding velocity change is $v_m(T) = \frac{L}{t_m - t_R}$,

where t_R is the measured reference transit time. Hence, $v_m(T) = \frac{L}{t_\infty + a_1 e^{-T/\tau} - t_R}$

$= \frac{L}{(t_\infty - t_R)\left(1 + \frac{a_1}{t_\infty - t_R} e^{-T/\tau}\right)}$, and since the transit time change is much smaller than its absolute value ($a_1 \ll t_\infty - t_R$), we obtain $v_m(T) \approx \frac{L}{(t_\infty - t_R)}\left(1 - \frac{a_1}{t_\infty - t_R} e^{-T/\tau}\right)$. Thus, the velocity evolves in the same way as the transit time, $v_m(T) = v_\infty + \delta v\, e^{-T/\tau}$, with $v_\infty = \frac{L}{t_\infty - t_R}$ and $\delta v \approx -\frac{a_1 L}{(t_\infty - t_R)^2}$. In particular, the relaxation time τ of the transit time is the same as that of the velocity if the changes are small. It is convenient to write the total change in velocity δv in terms of the *total relative* velocity change, giving $\frac{\delta v}{v} \approx -\frac{a_1}{t_\infty - t_R} \approx -\frac{a_1}{t_m(0) - t_R}$. This relation simply states that the relative change in velocity is equal in magnitude, but opposite in sign, to the relative change in transit time so long as the changes are small, a condition that is certainly satisfied for these dough relaxation measurements. The negative of the total relative velocity change and the corresponding relaxation time are plotted as a function of mixing pressure in figure 4.21

The measured amplitude can be written two ways, either as $A_m(T) = A_\infty + A_1 e^{-T/t_1}$, or as $A_m(T) = A_R e^{-\frac{\alpha L}{2}} = A_R e^{-\frac{(\alpha_0 + \Delta\alpha(T))L}{2}}$. Here A_R is the reference amplitude after making the correction for the impedance mismatch at the interface, and α is the attenuation coefficient. The amplitude at zero waiting time is $A(0) = A_\infty + A_1$. From the first expression for the measured amplitude, one can derive $\frac{A_m(T) - A(0)}{A(0)} = \frac{A_1}{A(0)}(e^{-T/t_1} - 1)$,

while the second expression gives $\frac{A_m(T)-A(0)}{A(0)} = e^{-\frac{\Delta\alpha L}{2}} - 1 \approx -\frac{\Delta\alpha L}{2}$ if the change in attenuation is small. Combining these two results, we obtain a new expression for the change of the attenuation as $\Delta\alpha(T) = \frac{2A_1}{LA(0)} - \frac{2A_1}{LA(0)} e^{-T/t_1}$. This expression contains two important results. One is that $-\frac{2A_1}{LA(0)}$ gives the total attenuation change at each pressure. The other one is that the relaxation time of the amplitude and attenuation coefficient are the same if the change is small. figure 4.22 shows how both the total change of the attenuation, $\delta\alpha - \frac{2A_1}{LA(0)}$, and the attenuation relaxation time t_1 vary as the mixing pressure is increased.

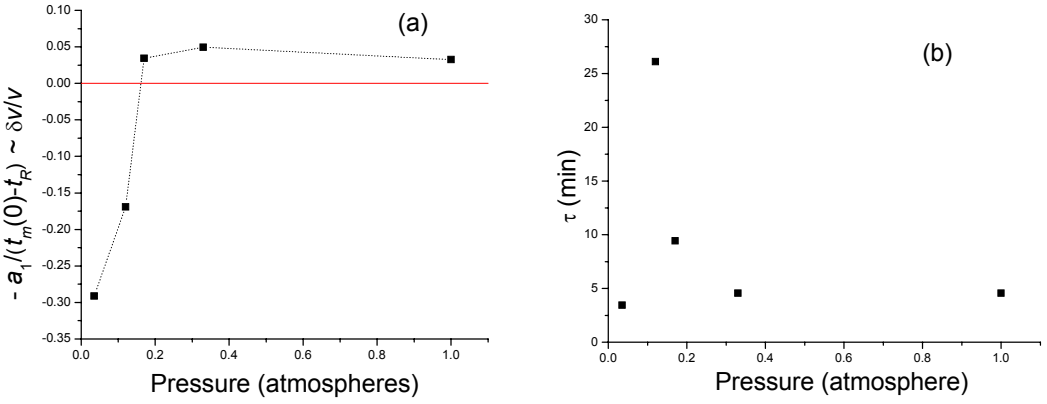

Figure 4.21. The fitting parameters of the phase velocity relaxation as a function of mixing pressure. The results are accurate only when the change of velocity is small.

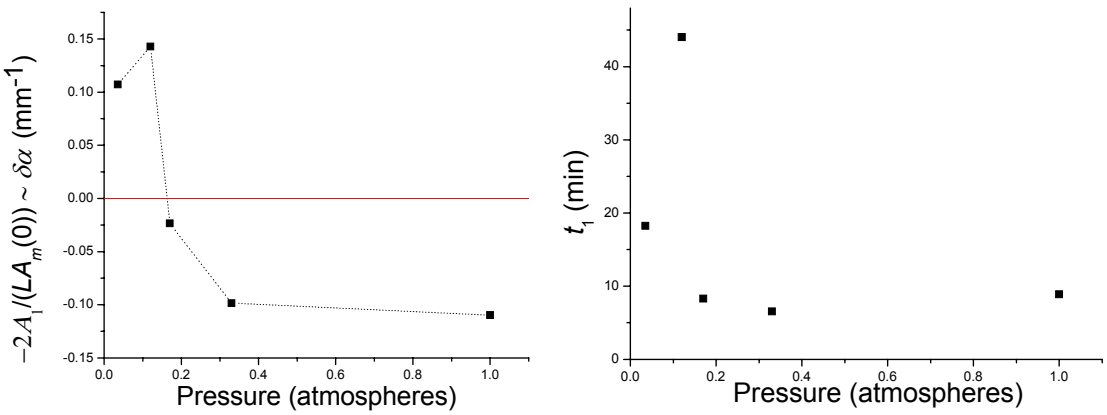

Figure 4.22. The fitting parameters of the attenuation coefficient relaxation as a function of mixing pressure. These results were obtained from fits to the amplitude variation, and are accurate so long as the change in attenuation is small.

From figures 4.21 and 4.22, we can see that both $\frac{\delta v}{v}$ and $\delta\alpha$ change sign between mixing pressures of 0.12 to 0.17 atmospheric pressure. Thus, we can estimate that the transition from vacuum-like dough to ambient-like dough occurs at a crossover pressure around 0.16 atmospheres. The relaxation time for both the velocity and attenuation coefficient has small values at both high mixing pressures and very low pressures, while a peak appear close to where the transition from vacuum-like to ambient-like dough occurs. This peak in the relaxation time also indicates the transition between the two kinds of dough. One possible reason for the occurrence of the peak could be as follows. Because the waiting time relaxation for vacuum-like and ambient-like dough is opposite in sign, we can infer that there are two different mechanisms involved in these relaxations. At high mixing pressures, one mechanism dominates (possibly associated with bubble relaxations, as discussed in section 4.2.4) and at low pressures, the other mechanism determines the relaxation behavior. Thus at both

high and low pressures, the relaxation times were similar because only one of the relaxation mechanisms was dominant, and both mechanisms happen to have similar relaxation times. However, close to the crossover pressure, the two opposite relaxations start competing with each other and tend to cancel out, so that the two relaxations can not be distinguished in the fit and a very long effective relaxation time is found.

4.4. Ultrasound measurements of nitrogen dough at 40 kHz

Ultrasonic measurements were not only performed on dough mixed under different headspace pressures, but they were also used to study dough mixed in a different gas that did not contain oxygen. In this section, dough mixed in a headspace containing nitrogen gas was studied. The motivation for these measurements was to see if oxygen, or lack of it in vacuum dough, played a role in the relaxation behavior described in the previous three sections. It had previously been surmised that the lack of oxygen in vacuum dough was responsible for the large values of the shear modulus that were determined from low frequency ultrasonic measurements [Elmehdi *et al*., 2004]. Thus, replacing air by nitrogen could modify relaxation effects dominated by the dough matrix, although it would not be expected to play an important role in the bubble relaxation mechanism postulated in section 4.2.4.

The density of the samples was measured 20 min after mixing and the ultrasonic measurements were started about 35 minutes after mixing. Different subsamples were used at each thickness. Table 4.12 lists the values of thickness that were selected, the waiting times at each thickness and the post-mixing time at the beginning of each measurement.

Thickness (mm)	**4.5**	**3**	**4**	**4.5**	**3.5**	**2.5**	**3**
Waiting Time (min)	32	32	32	32	32	32	940
Post mixing (min)	35	79	122	162	203	245	290

Table 4.12. The sample thickness (with the order of the measurements being left to right), the waiting time at each thickness, and the post mixing time for each thickness for dough mixed in nitrogen.

The same kind of experiment was repeated on three different days for different batches of nitrogen dough so that the results could be compared with similar data for ambient dough. The following figure (figure 4.23) shows typical phase velocity and attenuation coefficient results for nitrogen dough. The phase velocity and attenuation were analyzed based on an extrapolated reference from different thickness data. This extrapolated reference was averaged over the values obtained for different waiting times. The reason for analyzing the data in this way is that this approach gives the most reasonable estimate of the extrapolated reference for these data. Recall that it is very difficult to eliminate the offset of the experimental reference unambiguously, and that, if we analyze the data for each waiting time based on the corresponding extrapolated reference using data for the different thicknesses at that waiting time, the time evolution of the results would be obscured (see the detailed discussion in section 3.4.1.2) The corresponding figures for ambient dough are shown in section 4.2.2.

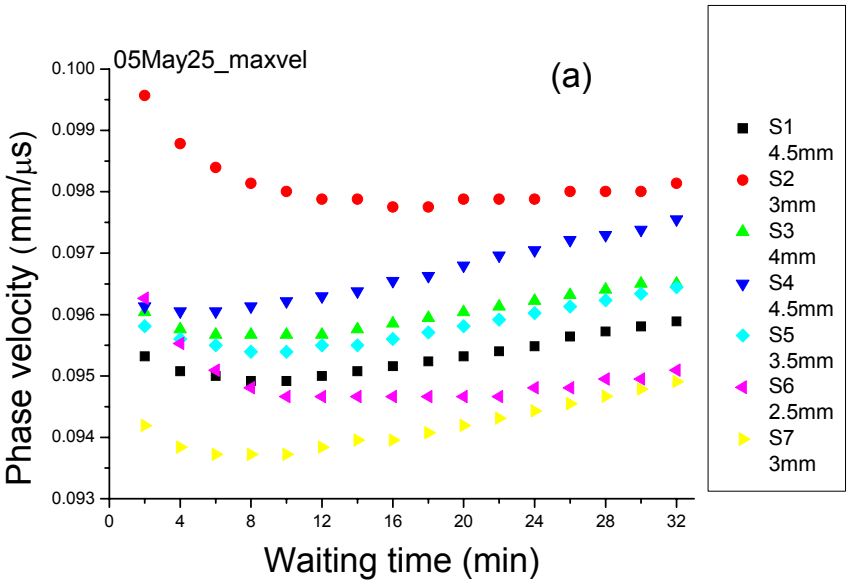
05May25_maxvel
(a)
Phase velocity (mm/μs)
Waiting time (min)
S1 4.5mm
S2 3mm
S3 4mm
S4 4.5mm
S5 3.5mm
S6 2.5mm
S7 3mm

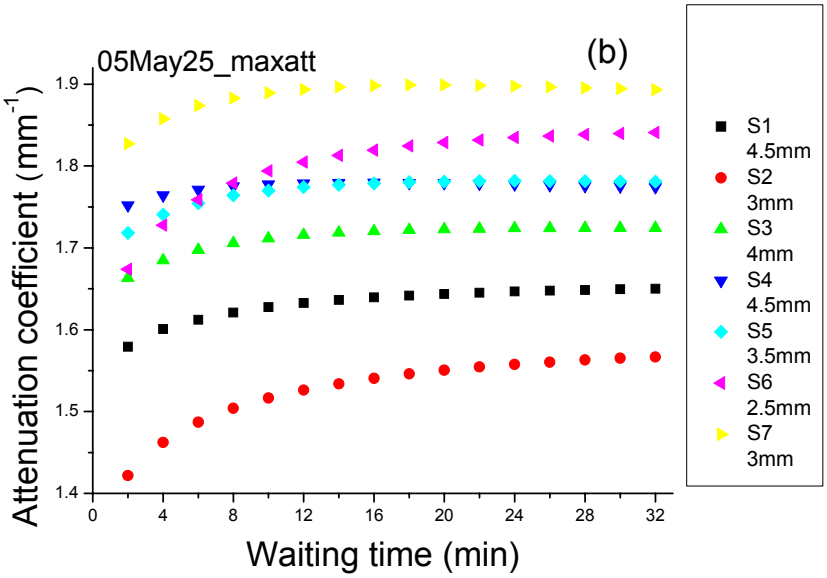
05May25_maxatt
(b)
Attenuation coefficient (mm-1)
Waiting time (min)
S1 4.5mm
S2 3mm
S3 4mm
S4 4.5mm
S5 3.5mm
S6 2.5mm
S7 3mm

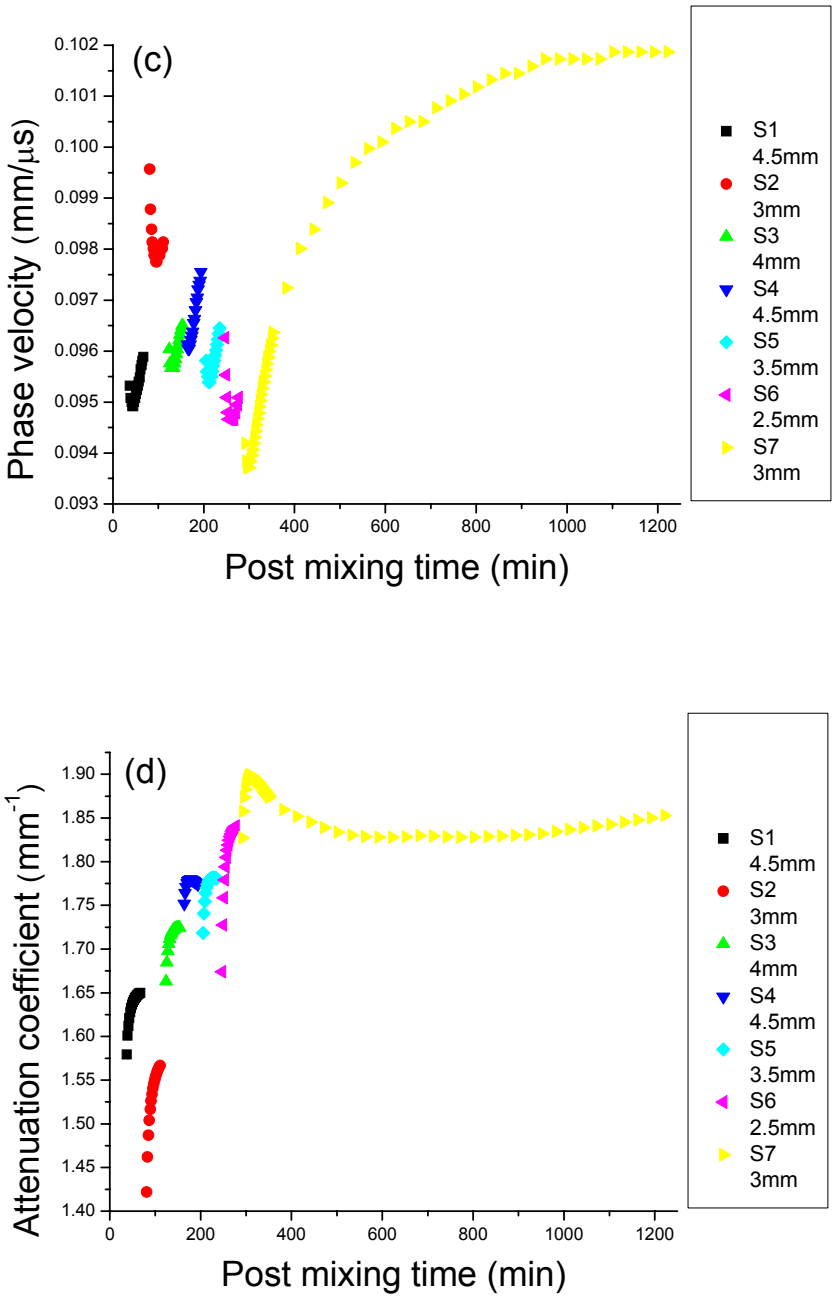

Figure 4.23. The phase velocity and attenuation coefficient as a function of waiting time for nitrogen dough at each thickness for different subsamples measured at different post-mixing times (a and b). The phase velocity and attenuation coefficient as a function of post mixing time at each thickness for the different subsamples (c and d).

From the above figure, it can be seen that the variation of the velocity and

attenuation with post mixing time, as well as the dependence on waiting time, is similar to ambient dough, rather than vacuum dough.

To further examine the similarities and differences between the relaxation behavior of nitrogen and ambient dough, we also investigated the long-time dependence of velocity and attenuation on waiting time for the last subsample studied in the measurements illustrated in figure 4.23. The results are shown in the next figure (figure 4.24). These long-time relaxation experiments reveal that there is a second relaxation process that dominates the behavior of both nitrogen and ambient doughs at times greater than about 10 minutes. This additional relaxation process causes the velocity to increase rather than to decrease with time, and therefore must originate from a different mechanism to the early time behavior. However, there are also some notable differences in this long-time relaxation effect for ambient and nitrogen doughs, as discussed in more detail below.

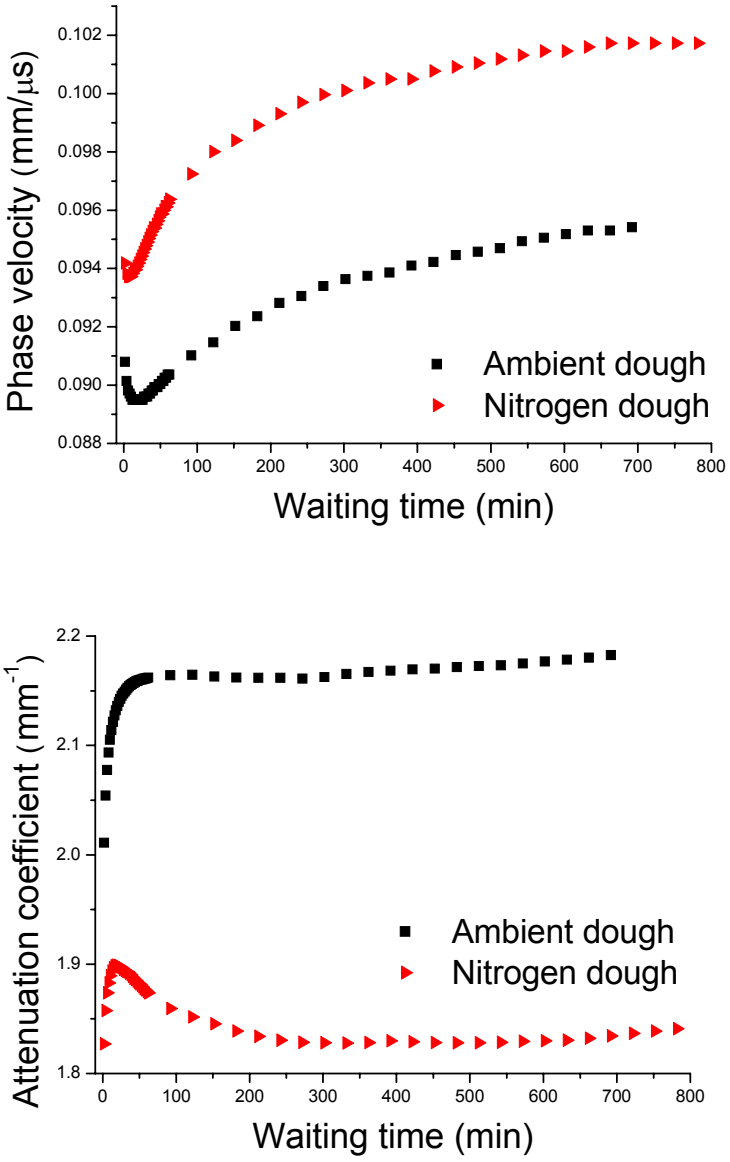

Figure 4.24. The very long waiting time relaxation of ambient dough and nitrogen dough.

From these experiments we found that:

(a). $\rho_{nitrogen} = 1.16 \pm 0.01$ g/cm^3 is larger than $\rho_{ambient} = 1.12 \pm 0.01$ g/cm^3. This implies that the bubble volume fraction is smaller in nitrogen dough than in ambient dough. The volume fraction of ambient dough is about 12 % and, using the same gas free density,

the volume fraction of nitrogen dough would be 9%.

(b). If we compare the samples at similar post mixing times (about 300 minutes) and waiting times (about 3 minutes), using data averaged over three identical experiments performed on different days, we find that the phase velocity of nitrogen dough was about 9% larger than that of ambient dough. In addition, the attenuation coefficient of nitrogen dough was about 10% smaller than that of ambient dough. These larger values of velocity and smaller attenuation coefficients are consistent with a lower volume fraction of bubbles in the nitrogen dough, as can be seen by comparing these differences with the volume fraction dependence of velocity and attenuation found by Elmehdi *et al*. (2004) for air-mixed doughs at various headspace pressures

(c). The overall relaxation behavior of nitrogen dough was similar to that of ambient dough, although there were two significant differences. First, the variation of both velocity and attenuation at early waiting times was less for nitrogen dough than for ambient dough, a result that is also consistent with the bubble relaxation mechanism proposed in section 4.2.3, since the volume fraction of bubbles is smaller in the nitrogen dough. This smaller initial change in velocity and attenuation for nitrogen dough also has the effect of moving the turning point, where the slope of the waiting time dependence of the velocity and attenuation changed sign, to earlier times. Second, for the relaxation behavior at very long waiting times, the attenuation coefficient decreased

with time and leveled off to a value close to the initial attenuation for the nitrogen dough, while the attenuation showed no significant long time decrease for ambient dough, remaining approximately independent of time for times greater than 30 minutes. This decrease in the attenuation coefficient for nitrogen dough at long times is reminiscent of the decrease seen in vacuum dough (see figure 4.9), suggesting there may be a somewhat similar matrix relaxation effect, possibly due to oxygen depletion in the matrix, in the nitrogen dough. However, this mechanism, if present in nitrogen dough, is certainly weaker than in vacuum dough, and does not significantly affect the velocity changes in the same way, since the long-time velocity changes are not similar in the nitrogen and vacuum doughs (see figure 4.9) Thus, it is evident from these low frequency ultrasonic experiments that the mechanisms underlying the matrix relaxation effects in three dough systems are remarkably complex, and their elucidation will require additional work that unfortunately lies beyond the scope of this thesis.

Part II: High frequency ultrasonic measurements

In part II of this chapter, I present the experimental results that I obtained over the frequency range from 1 MHz to 20 MHz. These experiments were performed on both vacuum dough and ambient dough. The goals of these experiments were both to investigate the effects of bubble resonance on the velocity and attenuation (1-5 MHz), and to measure the frequency dependence of these ultrasonic parameters at frequencies well above resonance (near 20 MHz), where additional information on the matrix properties was expected. In part II, the results are presented in their entirety without interpretation, to give as complete a picture as possible of the data that could be measured. The interpretation of these measurements in terms of theoretical models is therefore postponed until part III.

4.5. Vacuum mixed dough

Vacuum dough was measured over a wide range of frequencies, from 1 MHz to 20 MHz. Four pairs of transducers were used with central frequencies of 1 MHz, 2.25 MHz, 5 MHz and 20 MHz. Each pair of transducers was used on a different day for different, freshly mixed samples. Because the vacuum level could vary from one day to the next, each sample may have been slightly different. Table 4.13 gives the results of density measurements for each sample, along with the frequency of the transducers used for the ultrasonic measurements.

Transducer	1 MHz	2.25 MHz	5 MHz	20 MHz
Sample density	1.265 g/cm^3	1.26 g/cm^3	1.26 g/cm^3	1.265 g/cm^3

Table 4.13. Sample density measured in the different frequency experiments.

The data from these measurements were analyzed in the frequency domain using the method described in section 3.3 and the impedance mismatch correction was applied as discussed in section 3.4.2. The results from the different frequency ranges are listed individually from sections 4.5.1 to 4.5.4 and a wide frequency spectrum is shown in section 4.5.5. These results are interpreted in the third part of this chapter.

4.5.1. 1 MHz measurements

Ultrasonic measurements on the vacuum dough that was prepared for the 1 MHz experiments were started 10 minutes after mixing. The post mixing time and the waiting time for each sample investigated are listed in the following table (table 4.14).

Sample	Sample1	Sample2	Sample3	Sample4	Sample5
Thickness	4 mm	4 mm	4 mm	4 mm	4 mm
Post mixing	10 min	43 min	67 min	133 min	187 min
Waiting time	20 min	20 min	40 min	40 min	60 min

Table 4.14. The sample thickness, waiting time at each thickness and post mixing time at the start of measurements for each thickness for the 1MHz measurements.

The phase velocity and attenuation coefficient measured for each thickness (and

corresponding post mixing time) are shown in the following figures.

4.5.1.1. Post mixing effect

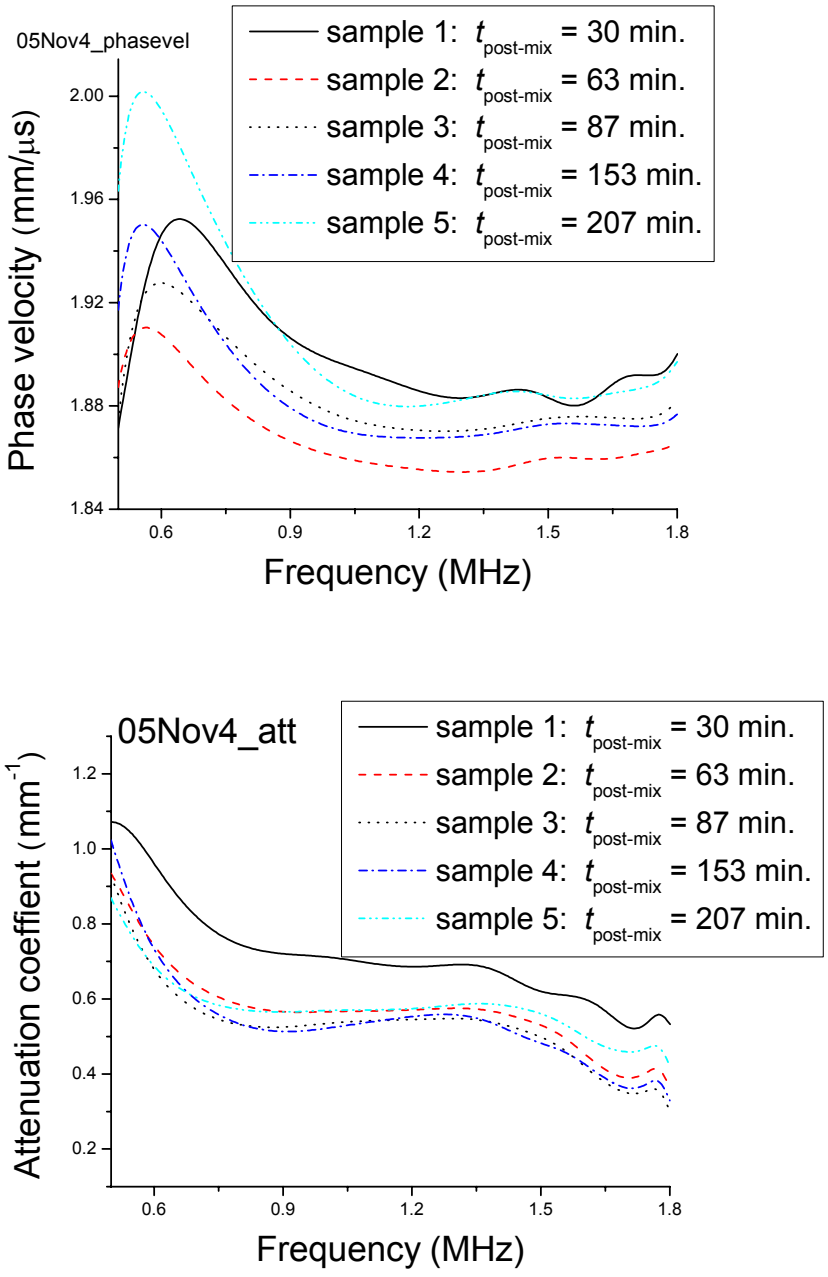

Figure 4.25. Frequency dependence of the phase velocity and attenuation coefficient of vacuum dough for the 1 MHz measurements with different post mixing times. The results were obtained 20 minutes after compressing.

4.5.1.2. Waiting time effect

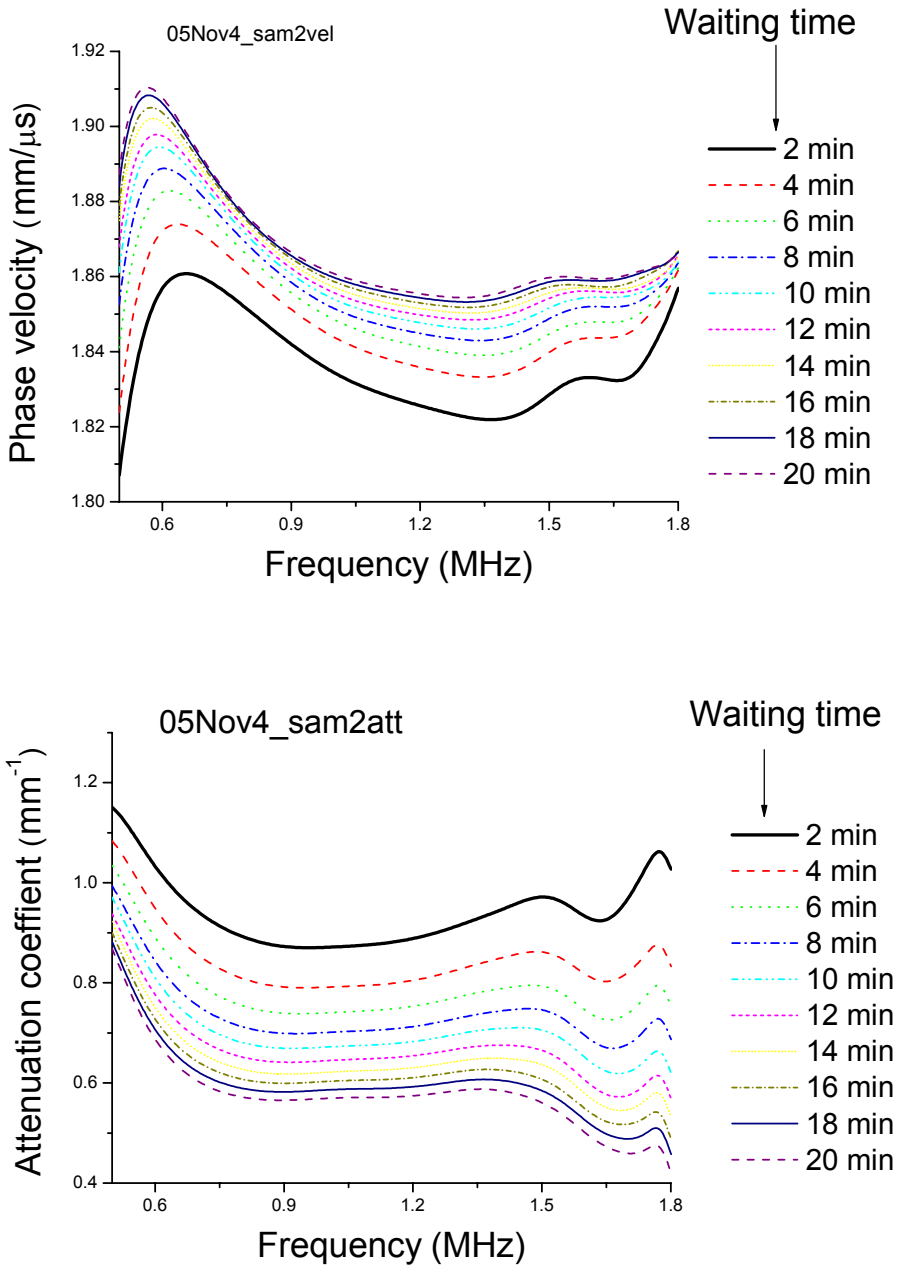

Figure 4.26. Frequency dependence of the phase velocity and attenuation coefficient of vacuum dough at different waiting times for the 1 MHz measurements. The results were from the same subsample with a 43 minutes post mixing time at the start of the measurements. Similar waiting time relaxation behavior was observed at other post mixing times.

4.5.2. 2.25 MHz measurements

Ultrasonic experiments at 2.25 MHz were started 40 minutes after mixing. The post mixing time and the waiting time for each sample are listed in the following table.

Sample	Sample1	Sample2	Sample3	Sample4
Thickness	3 mm	3 mm	3 mm	3 mm
Post mixing	40 min	79 min	131 min	259 min
Waiting time	30 min	30 min	120 min	60 min

Table 4.15. Thickness and measuring times for each sample in the 2.25 MHz measurements.

The phase velocity and attenuation coefficient measured for each sample are shown in the following figures.

4.5.2.1. Post mixing effect

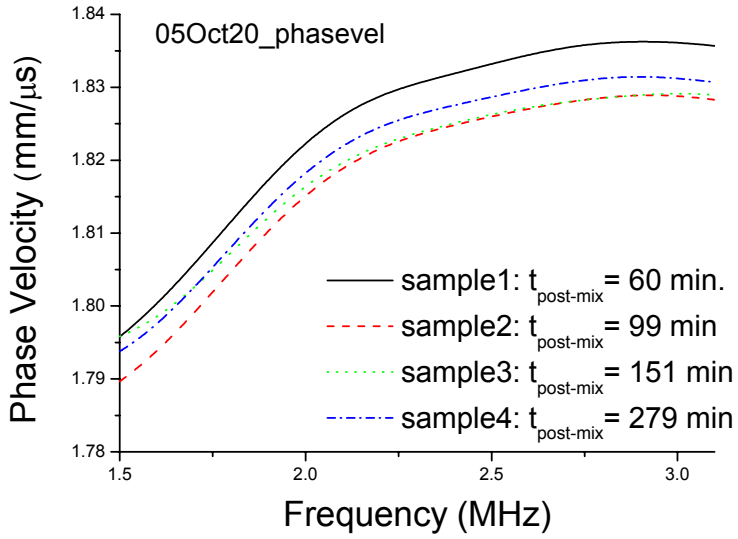

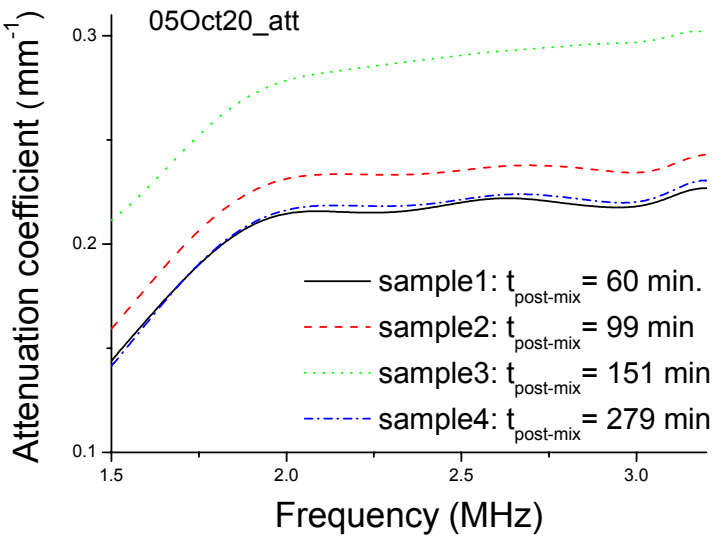

Figure 4.27. Frequency dependence of the phase velocity and attenuation coefficient of vacuum dough in the 2.25 MHz measurements with different post mixing times. The results were obtained 20 minutes after compressing.

4.5.2.2. Waiting time effect

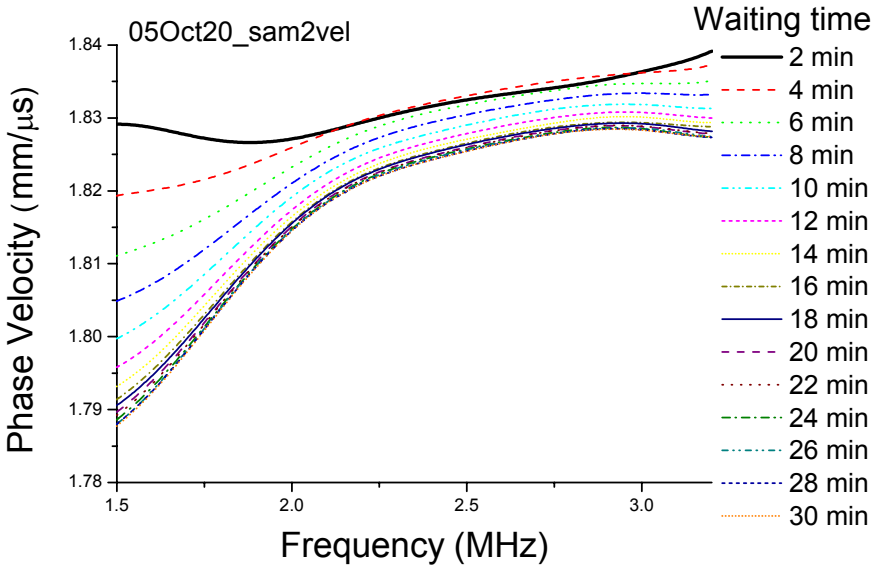

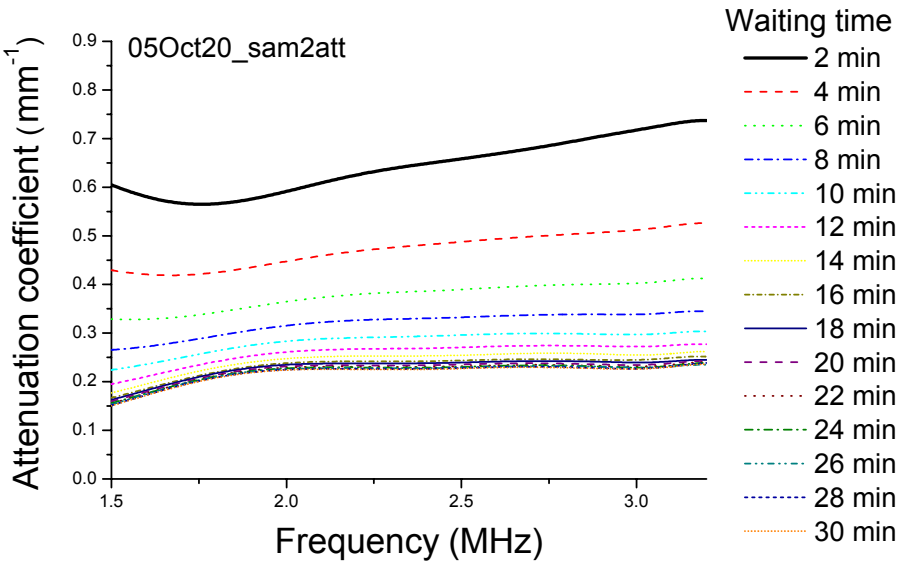

Figure 4.28. Frequency dependence of the phase velocity and attenuation coefficient of vacuum dough in the 2.25 MHz measurements with different waiting times. The results were obtained from the same subsample with a 79 minutes post mixing time at the start of the measurements. Similar waiting time relaxation behavior was observed at other post mixing times.

4.5.3. 5 MHz measurements

Ultrasonic experiments at 5 MHz were started 30 minutes after mixing. The post mixing time and the waiting time for each sample are listed in the following table.

Sample	Sample1	Sample2
Thickness	10 mm	2 mm
Post mixing	35 min	128 min
Waiting time	60 min	60 min

Table 4.16. Thickness and measuring times for each sample in the 5 MHz measurements.

The phase velocity and attenuation coefficient measured at each thickness are shown in the following figures.

4.5.3.1. Post mixing effect

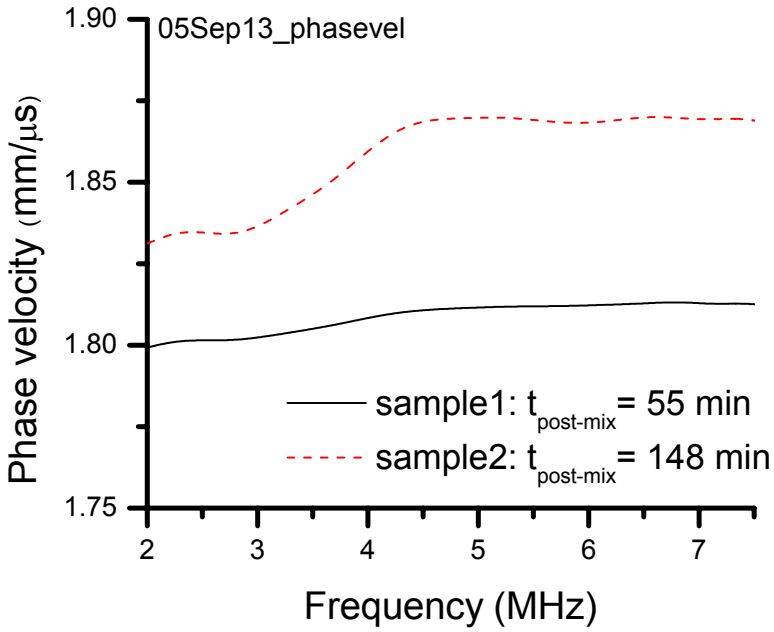

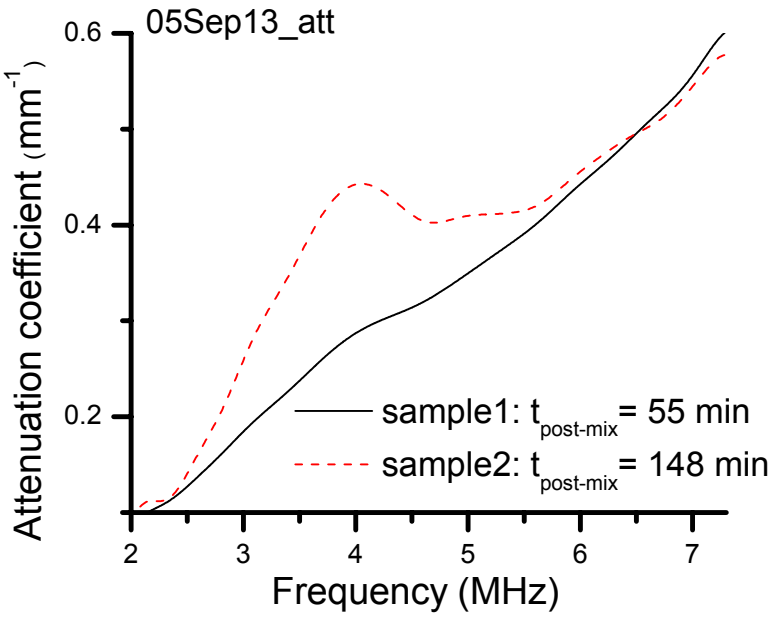

Figure 4.29. Frequency dependence of the phase velocity and attenuation coefficient of vacuum dough in the 5 MHz measurements with different post mixing times. The results were obtained 20 minutes after compressing.

4.5.3.2. Waiting time effect

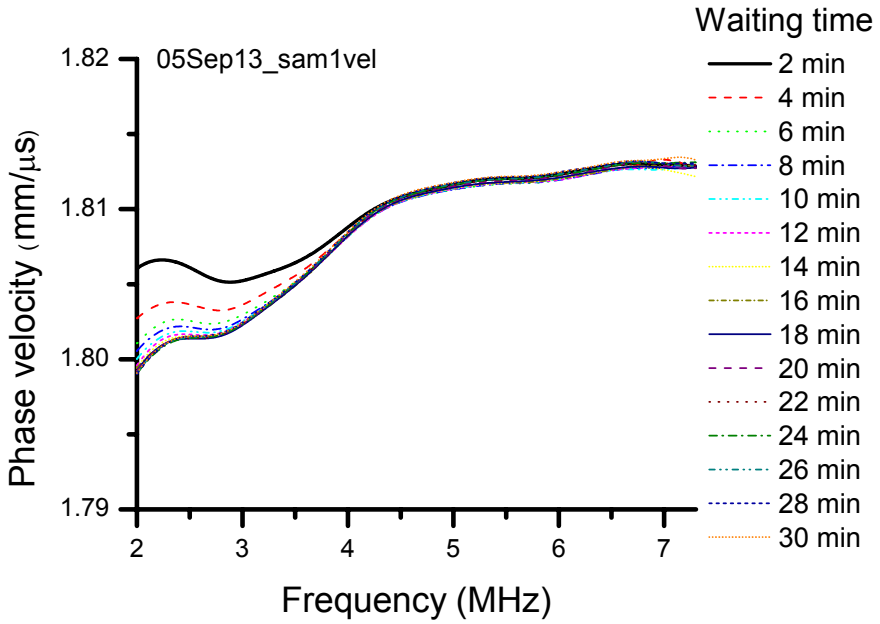

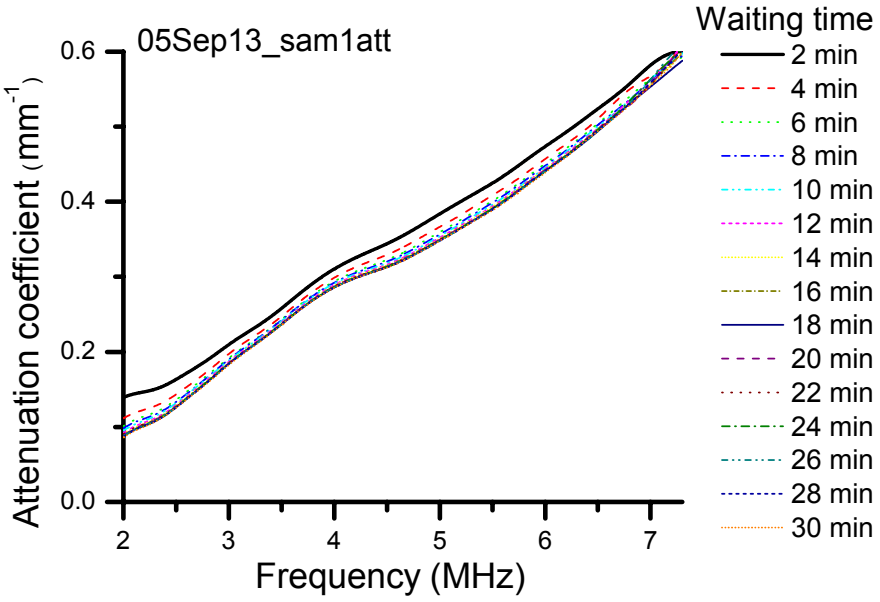

Figure 4.30. Frequency dependence of the phase velocity and attenuation coefficient of vacuum dough in the 5 MHz measurements with different waiting times. The results were obtained from the same subsample with a 35 minutes post mixing time at the start of the measurements. Similar waiting time relaxation behavior was observed at other post mixing times.

4.5.4. 20 MHz measurements

Ultrasonic experiments at 20 MHz were started 10 minutes after mixing. The post mixing time and the waiting time for each sample are listed in the following table.

Sample	Sample1	Sample2	Sample3	Sample4	Sample5	Sample6
Thickness	2 mm	2 mm	2 mm	2 mm	1.5 mm	1.5 mm
Post mixing	10 min	47 min	83 min	115 min	147 min	181 min
Waiting time	20 min	20 min	20 min	20 min	20 min	20 min

Table 4.17. Thickness and measuring times of each sample for the 20 MHz measurements.

The phase velocity and attenuation coefficient measured for each sample is shown in the following figures.

4.5.4.1. Post mixing effect

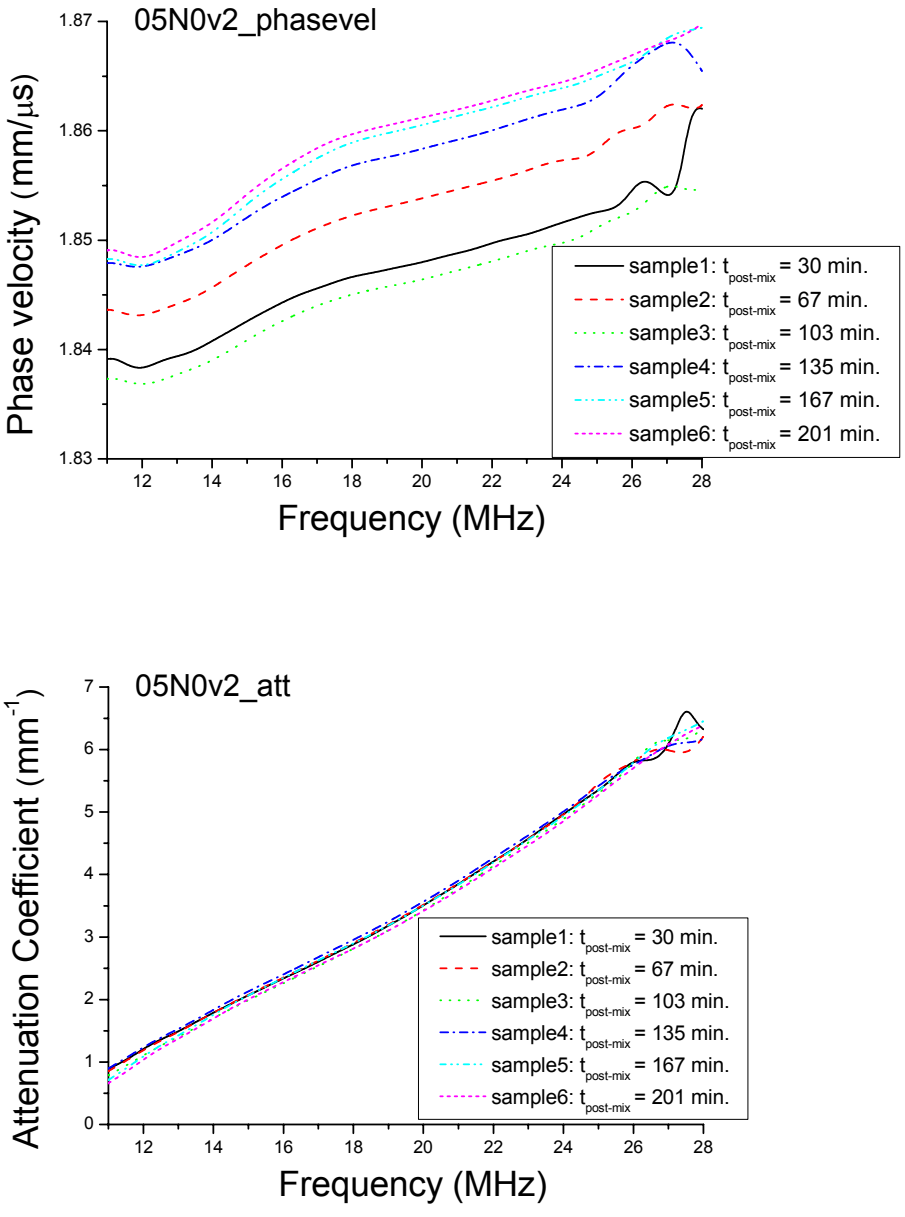

Figure 4.31. Frequency dependence of the phase velocity and attenuation coefficient of vacuum dough in the 20 MHz measurements with different post mixing times. The results were obtained 20 minutes after compressing.

4.5.4.2. Waiting time effect

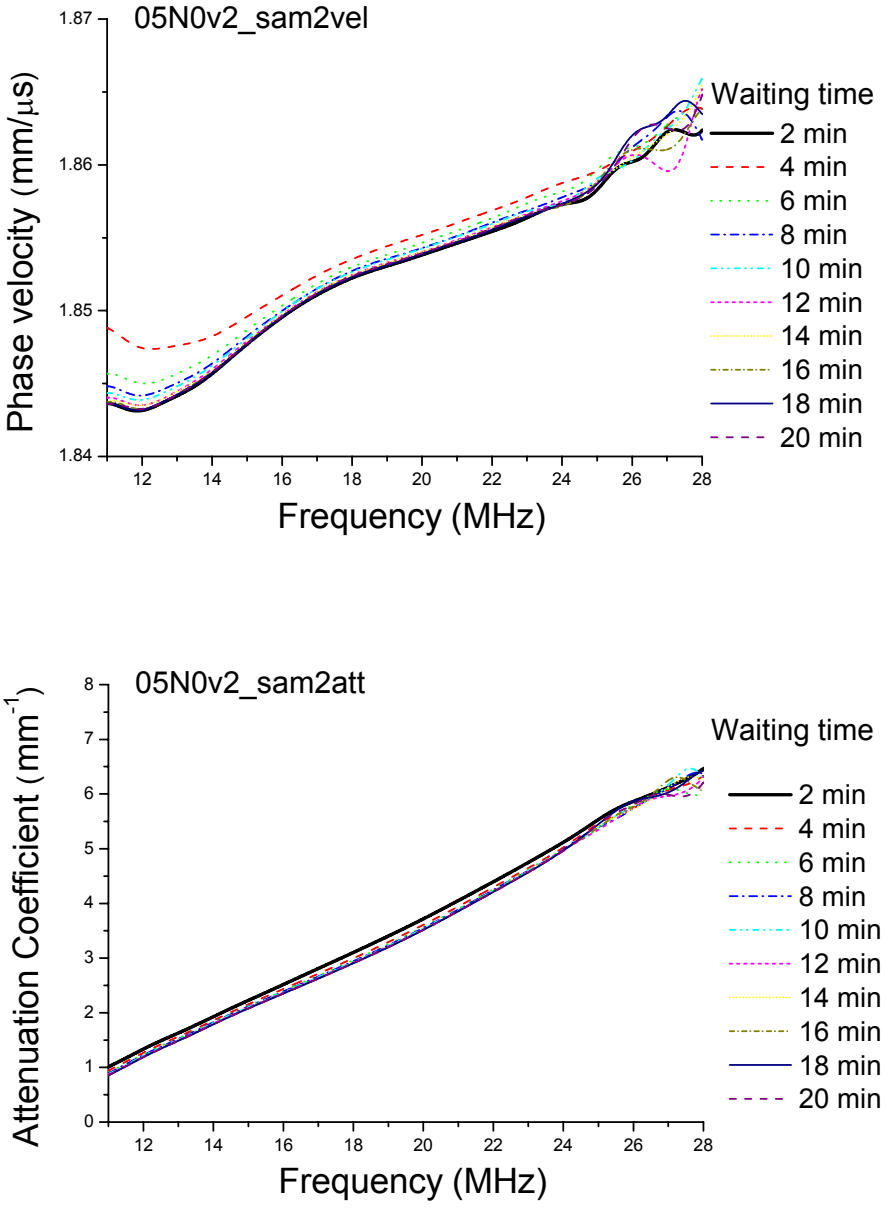

Figure 4.32. Frequency dependence of the phase velocity and attenuation coefficient of vacuum dough in the 20 MHz measurements with different waiting times. The results were from the same subsample with a 47 minutes post mixing time at the start of the measurements. Similar waiting time relaxation behavior was observed at other post mixing times.

4.5.5. Data over the whole frequency range for vacuum dough

Data from the different frequency ranges studied, having similar post mixing times and the same waiting time, were collected together to show the behavior over a wide frequency spectrum (figure 4.33). The post mixing time for the data from each frequency range is listed in the following table.

Frequency	**500 kHz**	**1 MHz**	**2.25 MHz**	**5 MHz**	**20 MHz**
Post mixing	73 min	67 min	79 min	35 min	83 min

Table 4.18. Post mixing time for each frequency range.

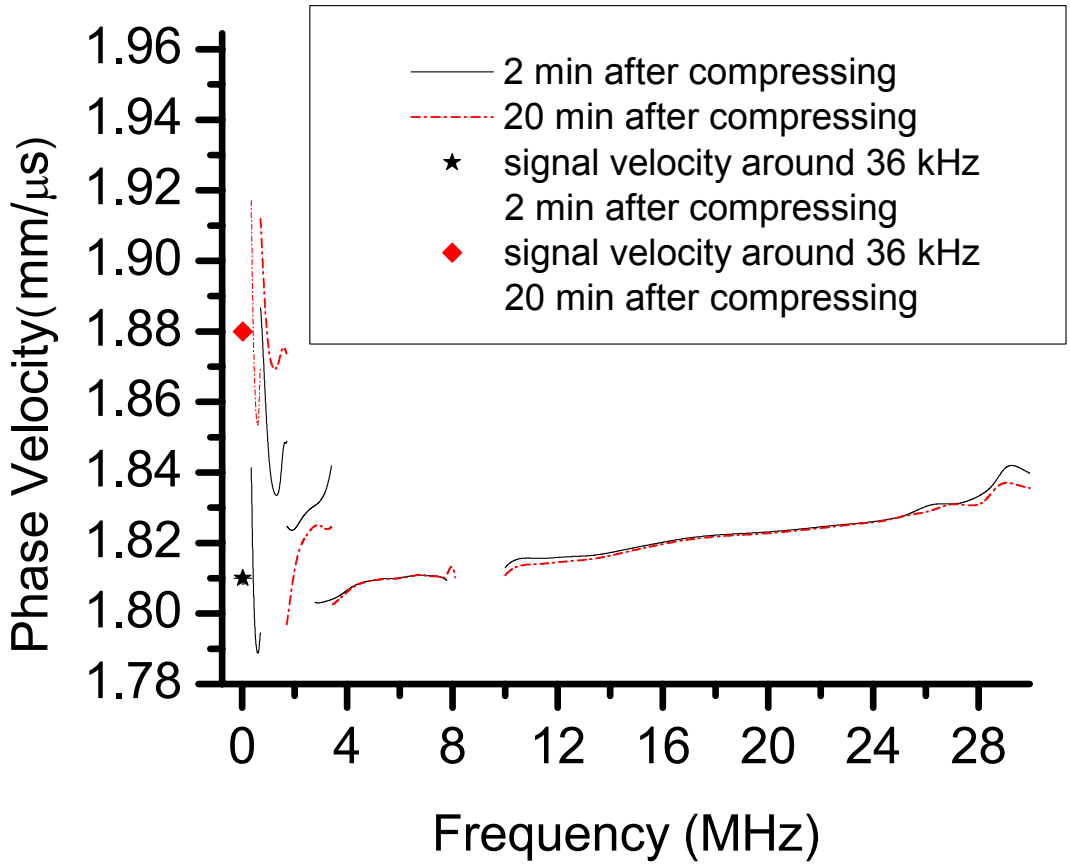

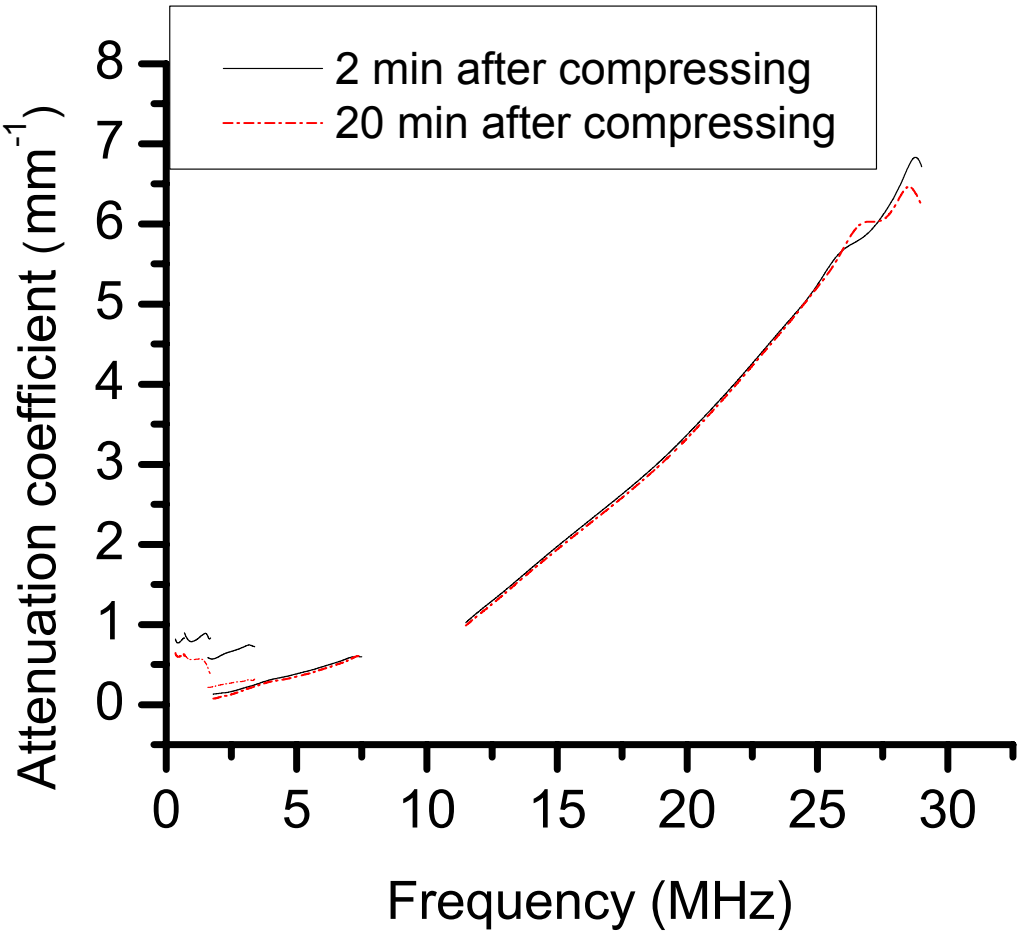

Figure 4.33. Phase velocity and attenuation coefficient as a function of frequency for vacuum mixed dough.

4.6. Ambient mixed dough

As was done for vacuum dough, ambient dough was also measured over a wide range of frequencies, from 1 MHz to 20 MHz. Five pairs of transducers were used including 1 MHz, 2.25 MHz, 3.5 MHz, 5 MHz and 20 MHz. Each pair of transducers was used on a different day for each different sample.

The data from these measurements were analyzed in the frequency domain, using the method described in section 3.3. For the measurements from 1 to 5 MHz, because of the large impedance mismatch between the sample and transducer in this frequency range and the difficulty in accurately determining the impedance of the transducers, the plastic delay layer method was used. Thus, the impedance mismatch was corrected in the way described in section 3.4.3. For the 20 MHz measurements, because the ultrasound was attenuated significantly by the plastic layer, the contact reference method was used, and the impedance mismatch was corrected in the way described in section 3.4.1.1. The results from the different frequency ranges are presented individually in sections 4.6.1 to 4.6.5, and a wide frequency spectrum is shown in section 4.6.6. These results are interpreted in the third part of this chapter.

4.6.1. 1 MHz measurements

Ultrasonic experiments were started 20 minutes after mixing. The post mixing time and the waiting time for each sample are listed in the following table.

Sample	Sam1	Sam2	Sam3	Sam4	Sam5
Thickness	0.3 mm	-	0.3 mm	0.6 mm	0.3 mm
Post mixing	20 min	61 min	103 min	151 min	191 min
Waiting time	30 min	30min	30 min	30 min	30 min

Table 4.19. Thickness and measuring time of each sample in the 1 MHz measurements.

4.6.1.1. Post mixing effect

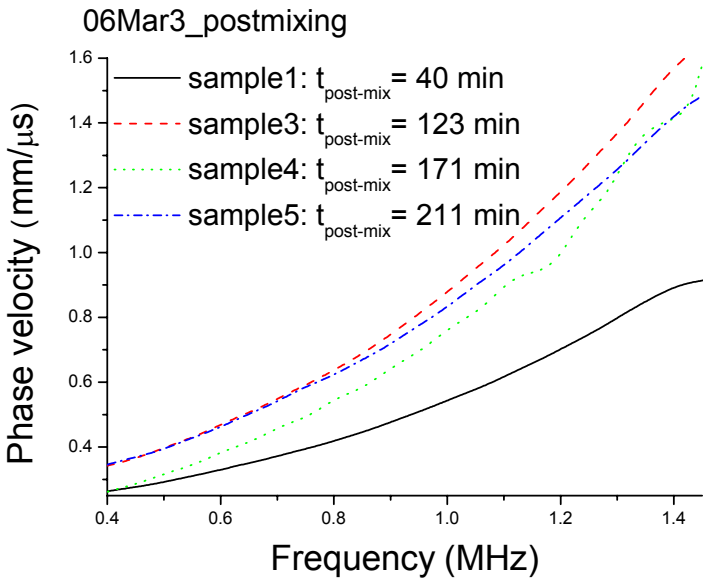

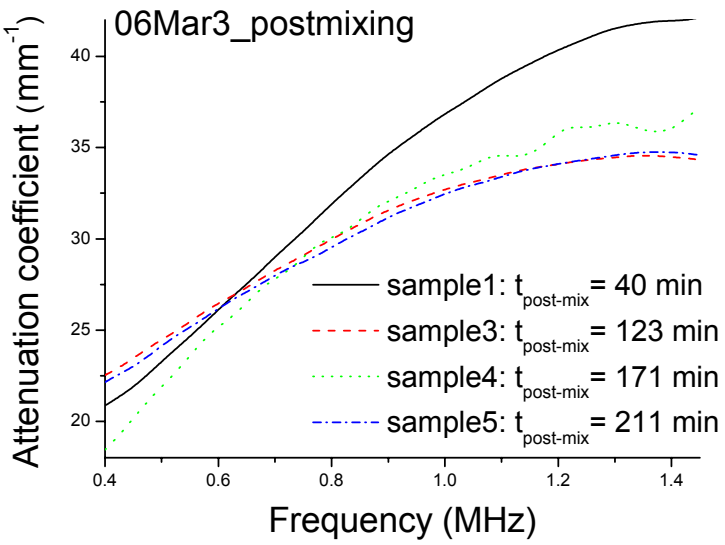

Figure 4.34. Frequency dependence of the phase velocity and attenuation coefficient of ambient dough in the 1 MHz measurements with different post mixing times. The results were obtained 20 minutes after compressing.

4.6.1.2. Waiting time effect

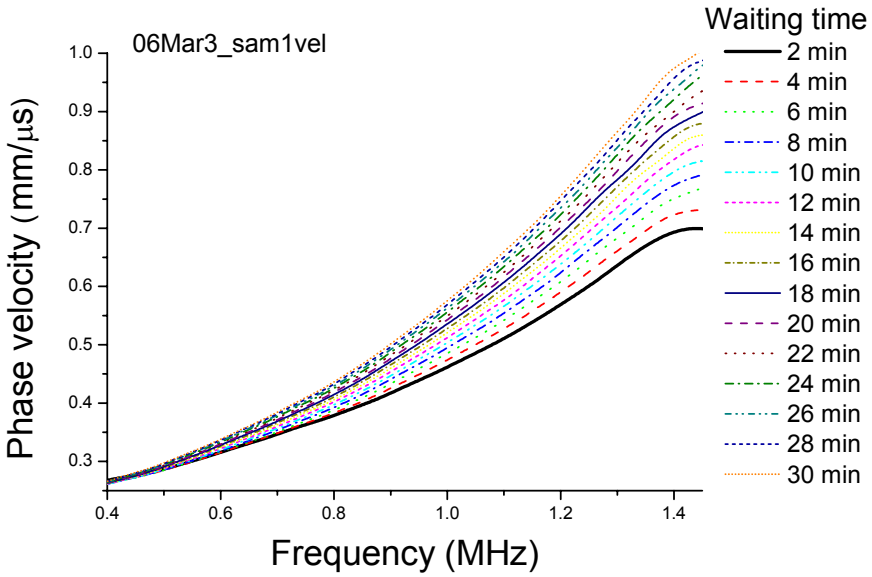

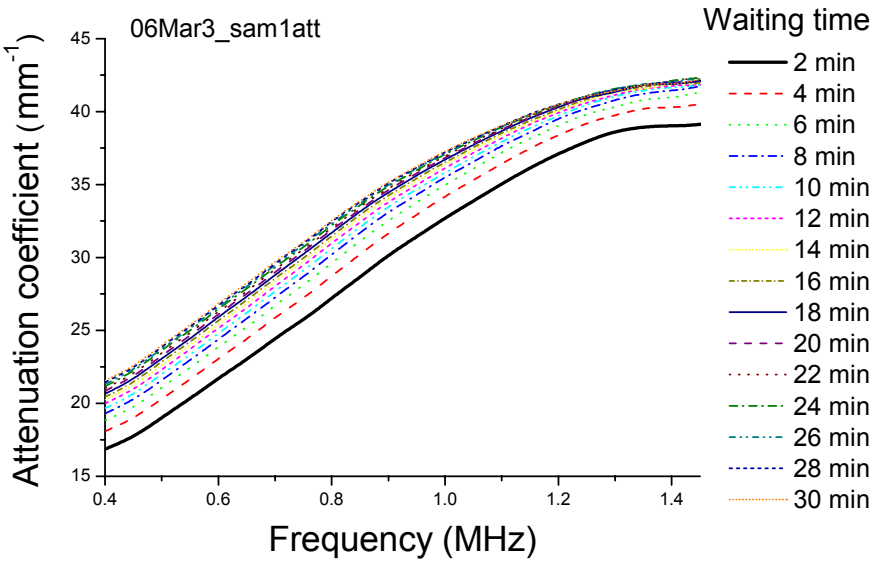

Figure 4.35. Frequency dependence of the phase velocity and attenuation coefficient of ambient dough in the 1 MHz measurements with different waiting times. The results were obtained from the same subsample with a 40 minutes post mixing time at the start of the measurements. Similar waiting time relaxation behavior was observed at other post mixing times, although the magnitude of the changes become smaller as the post mixing time increased.

4.6.2. 2.25 MHz measurements

Ultrasonic experiments were started 23 minutes after mixing. The post mixing time and the waiting time for each sample are listed in the following table.

Sample	Sam1	Sam2	Sam3	Sam4	Sam5	Sam6
Thickness	0.3 mm	0.3 mm	0.6 mm	0.3 mm	0.3 mm	0.3 mm
Post mixing	23 min	65 min	109 min	116 min	160 min	203 min
Waiting time	30 min	30 min	3 min	30 min	30 min	645 min

Table 4.20. Thickness and measuring time of each sample in the 2.25 MHz measurements.

4.6.2.1. Post mixing effect

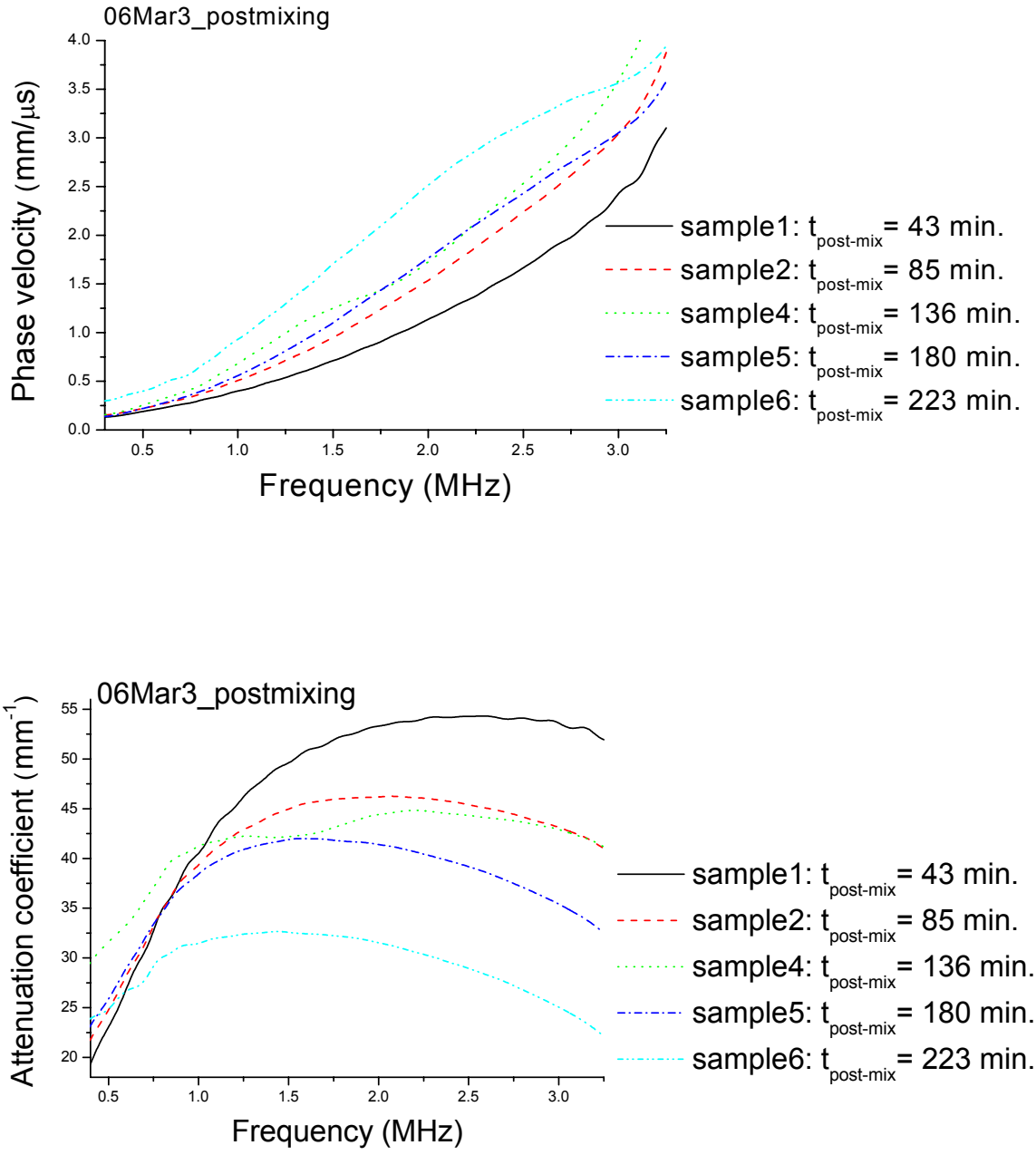

Figure 4.36. Frequency dependence of phase velocity and attenuation coefficient of ambient dough in the 2.25 MHz measurements with different post mixing times. The results were obtained 20 minutes after compressing.

4.6.2.2. Waiting time effect

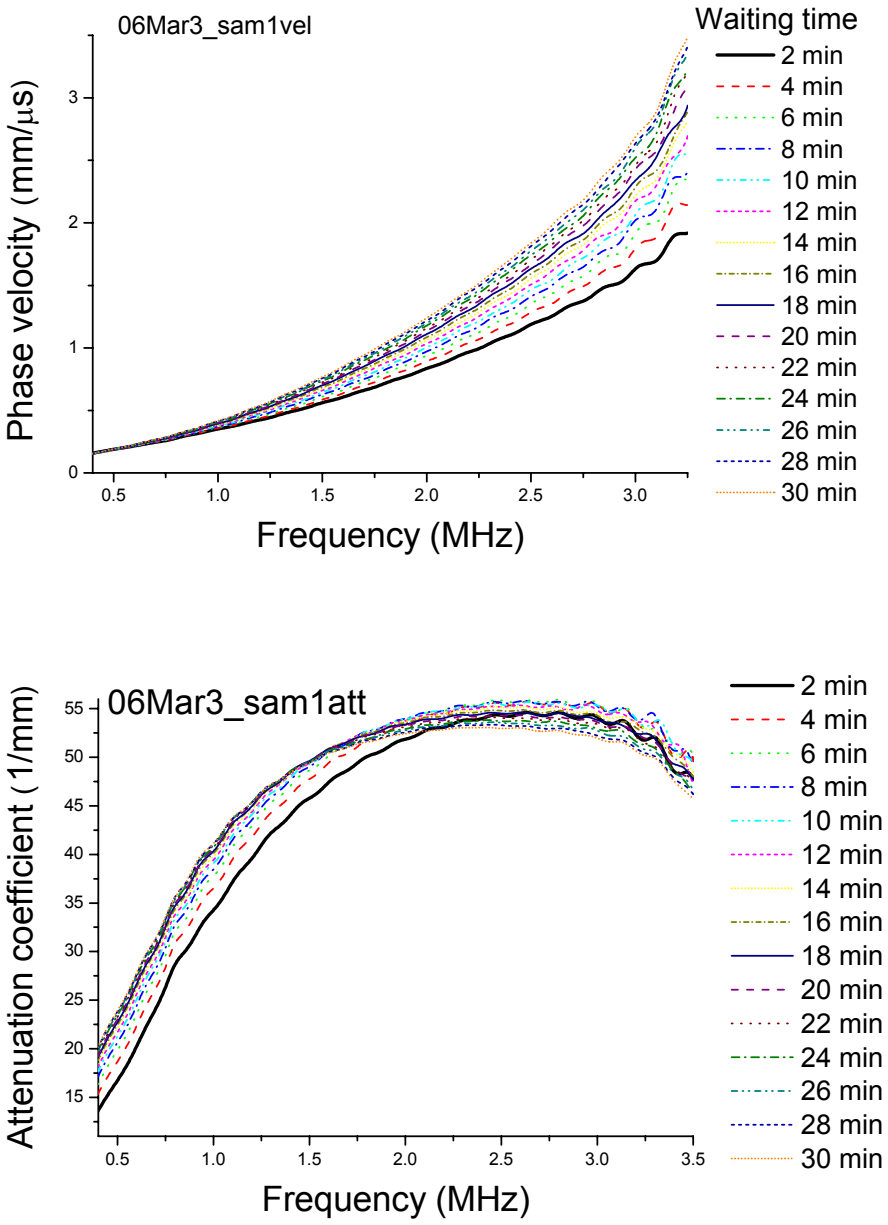

Figure 4.37. Frequency dependence of the phase velocity and attenuation coefficient of ambient dough in the 2.25 MHz measurements with different waiting times. The results were measured in the same subsample with a 23 minutes post mixing time at the start of the measurements. Similar waiting time relaxation behavior was observed at other post mixing times, although the magnitude of the changes become smaller as the post mixing time increased.

4.6.3. 3.5 MHz measurements

Ultrasonic experiments were started 26 minutes after mixing. The post mixing time and the waiting time for each sample are listed in the following table.

Sample	Sam1	Sam2	Sam3	Sam4	Sam5	Sam6
Thickness	0.3 mm	0.3 mm	0.6 mm	0.3 mm	0.6 mm	0.3 mm
Post mixing	26 min	67 min	109 min	150 min	192 min	230 min
Waiting time	30 min	30 min	30 min	30 min	30 min*	60 min

Table 4.21. Thickness and measuring time of each sample in the 3.5 MHz measurements. (For sample 5, the ultrasonic signal was not recorded every 2 minutes. Only 2 measurements were taken, the first one after 2 minutes and the second one after 30 minutes.)

4.6.3.1. Post mixing effect

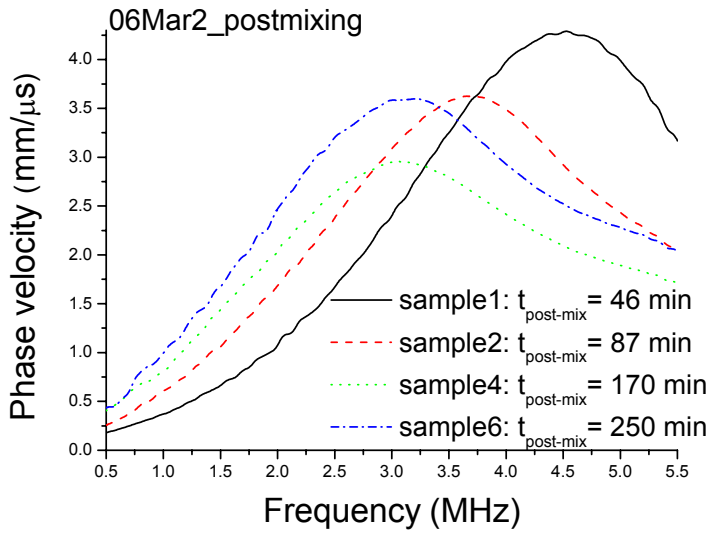

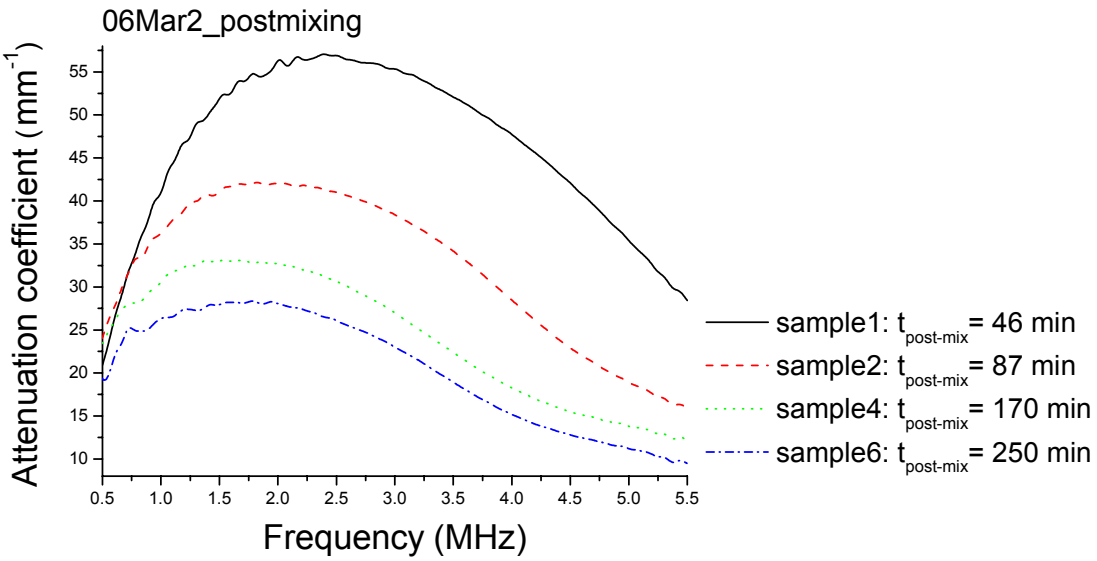

Figure 4.38. Frequency dependence of the phase velocity and attenuation coefficient of ambient dough in the 3.5 MHz measurements with different post mixing times. The results were obtained 20 minutes after compressing.

4.6.3.2. Waiting time effect

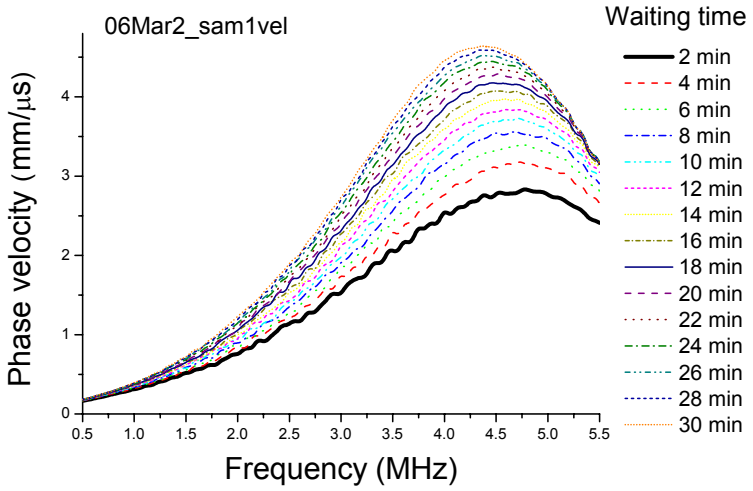

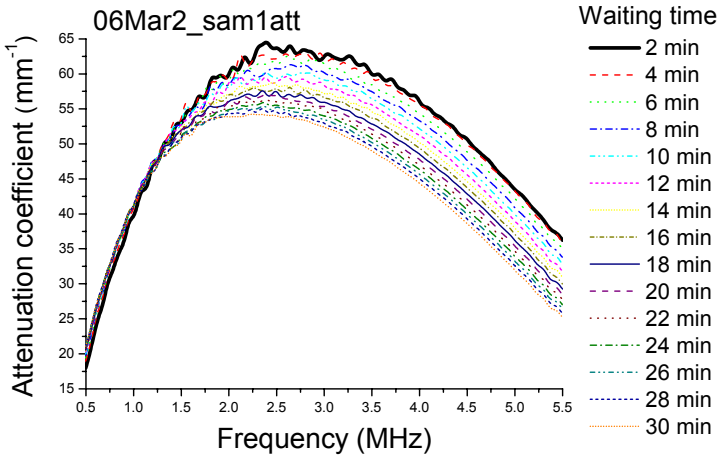

Figure 4.39. Frequency dependence of the phase velocity and attenuation coefficient of ambient dough in the 3.5 MHz measurements with different waiting times. The results were obtained from the same subsample with a 26 minutes post mixing time at the start of the measurements. Similar waiting time relaxation behavior was observed at other post mixing times, although the magnitude of the changes become smaller as the post mixing time increased.

4.6.4. 5 MHz measurements

Ultrasonic experiments were started 21 minutes after mixing. The post mixing time and the waiting time for each sample are listed in the following table.

Sample	Sam1	Sam2	Sam3	Sam4	Sam5	Sam6
Thickness	0.3 mm	0.3 mm	0.6 mm	0.6 mm	0.9 mm	0.6 mm
Time after mixing	21 min	65 min	109 min	152 min	197 min	245 min
Waiting time	30 min	30 min	30 min	30 min	30 min	30 min

Table 4.22. Thickness and measuring times of each sample in the 5 MHz measurements.

4.6.4.1. Post mixing effect

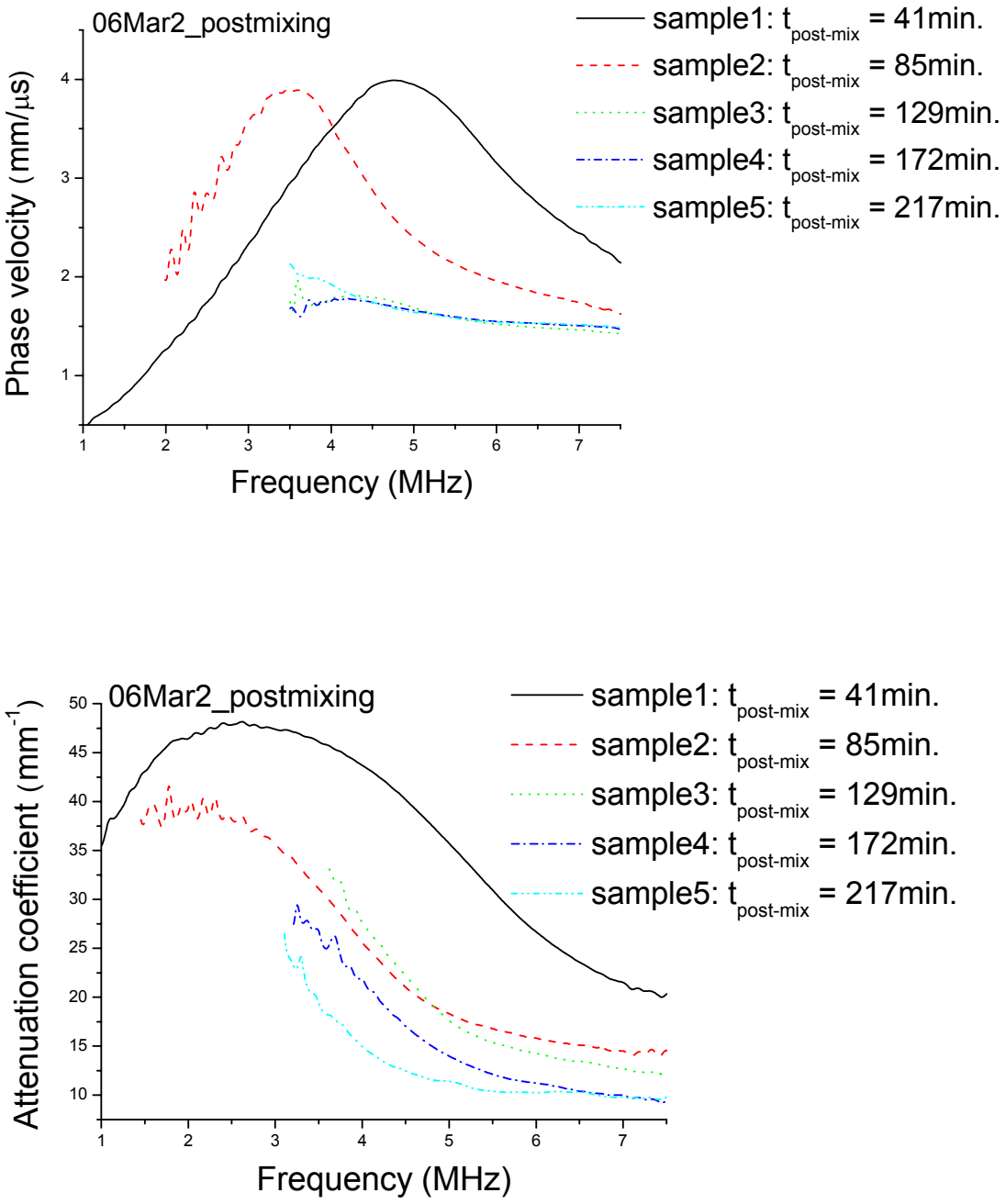

Figure 4.40. Frequency dependence of the phase velocity and attenuation coefficient of ambient dough in the 5 MHz measurements with different post mixing times. The results were obtained 20 minutes after compressing.

4.6.4.2. Waiting time effect

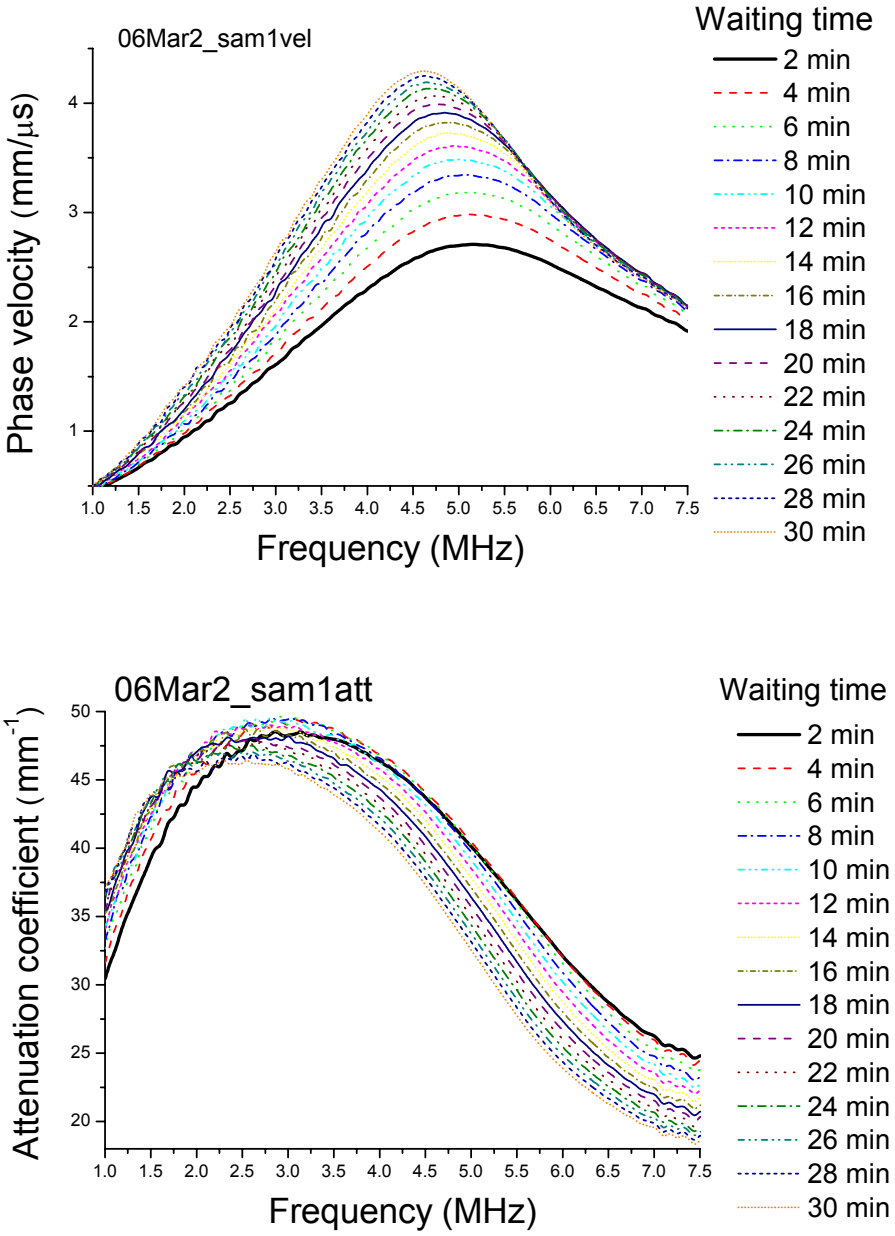

Figure 4.41. Frequency dependence of the phase velocity and attenuation coefficient of ambient dough in the 5 MHz measurements with different waiting times. The results were obtained from the same subsample with a 21 minutes post mixing time at the start of the measurements. Similar waiting time relaxation was observed at other post mixing times, although the magnitude of the changes become smaller as the post mixing time increased.

4.6.5. 20 MHz measurements

Ultrasonic experiments at 20 MHz were started 23 minutes after mixing. The post mixing time and the waiting time for each sample are listed in the following table.

Sample	Sam1	Sam2	Sam3	Sam4	Sam5	Sam6	Sam7	Sam8	Sam9
Thickness	0.5 mm	0.5 mm	0.5mm	0.5 mm	0.5 mm	0.5 mm	0.6 mm	0.4 mm	0.5 mm
Post mixing	35 min	74 min	112 min	148 min	202 min	238 min	376 min	402 min	447 min
Waiting time	30 min	30 min	30 min	30 min	30 min	30 min	30 min	30 min	30 min

Table 4.23. Thickness and measuring time of each sample in the 20 MHz measurements.

4.6.5.1. Post mixing effect

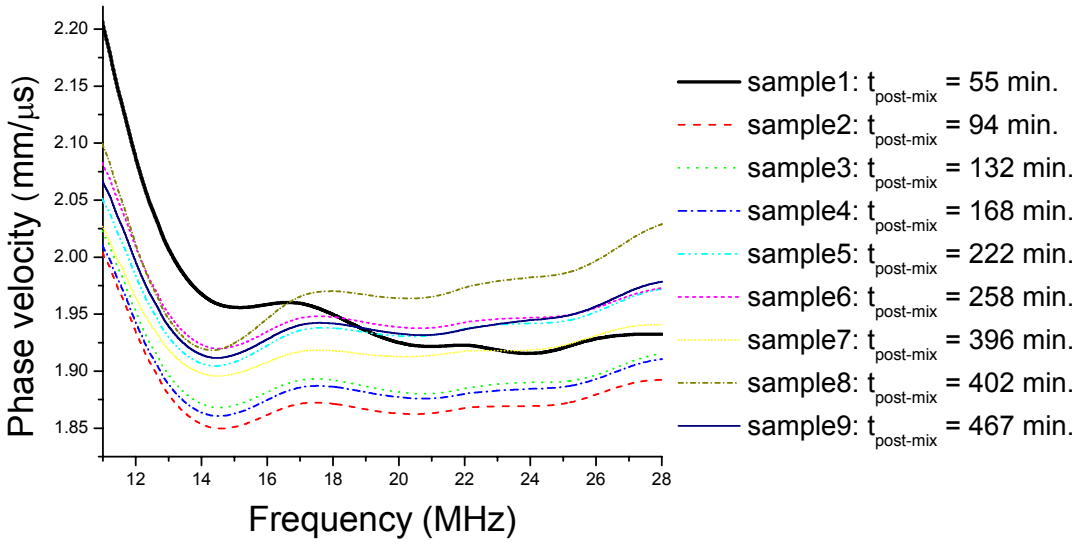

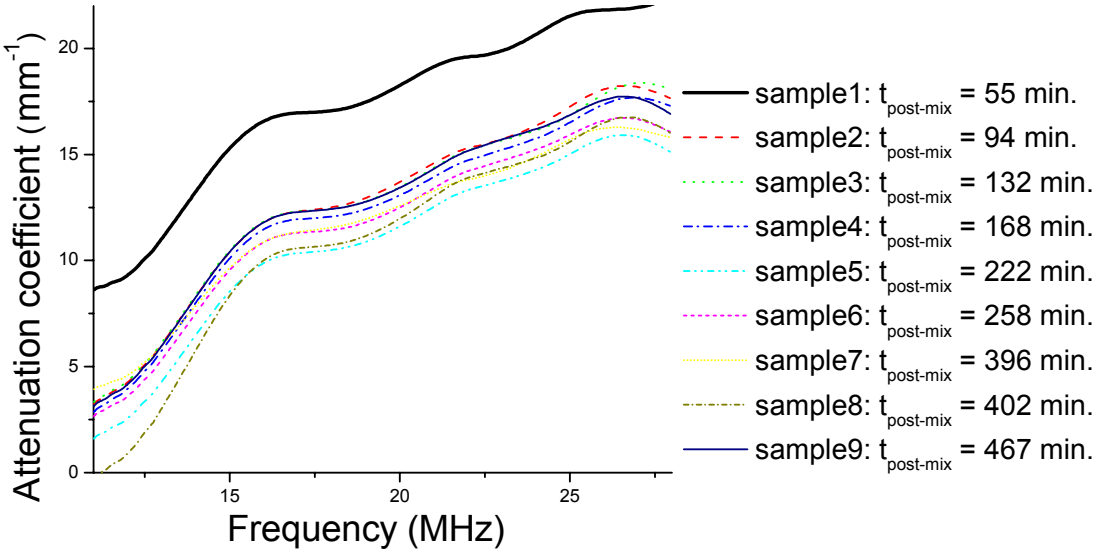

Figure 4.42. Frequency dependence of the phase velocity and attenuation coefficient of ambient dough in the 20 MHz measurements with different post mixing times. The results were obtained 20 minutes after compressing.

4.6.5.2. Waiting time effect

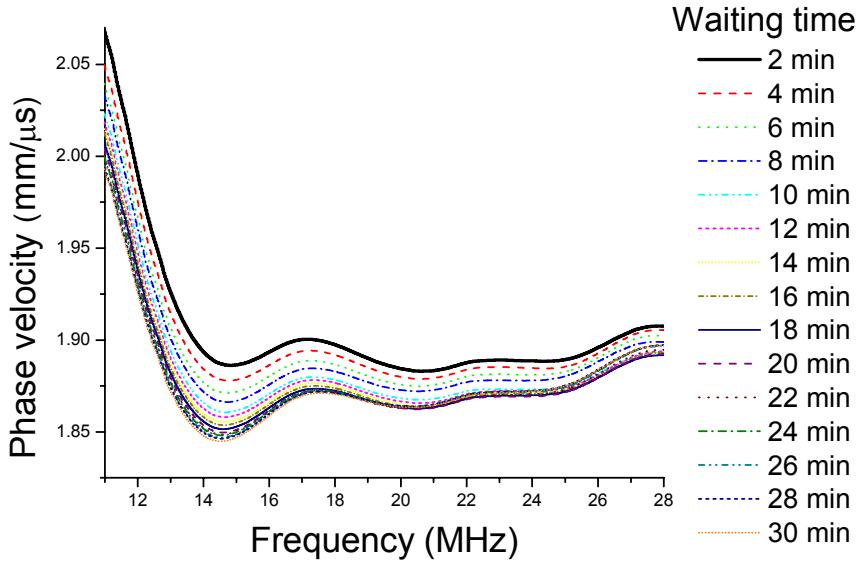

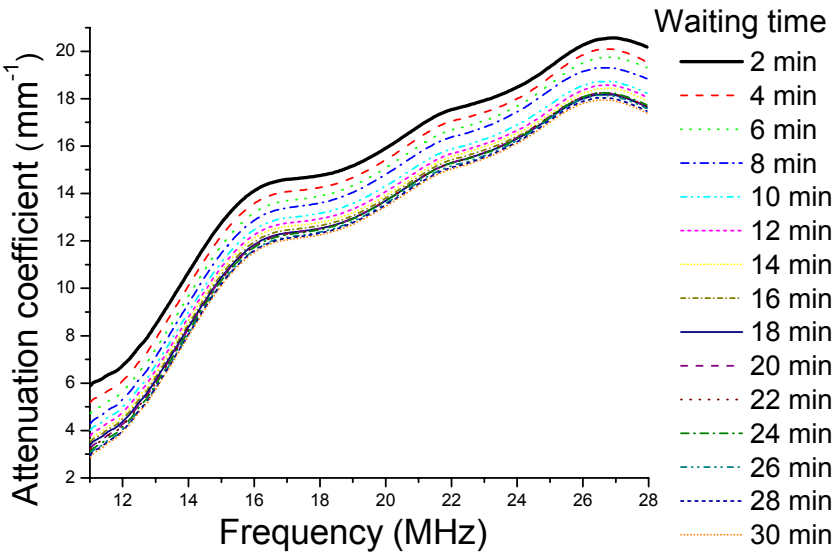

Figure 4.43. Frequency dependence of phase velocity and attenuation coefficient of ambient dough in the 20 MHz measurements with different waiting times. The results were obtained from the same subsample with a 35 minutes post mixing time at the start of the measurements. Similar waiting time relaxation was observed at other post mixing times, although the magnitude of the changes become smaller as the post mixing time increased.

4.6.6. Measurements over the whole frequency range for ambient dough

4.6.6.1. Post mixing effect

Data from the different frequency ranges studied, having similar post mixing times and the same waiting time, were collected together to show the behavior over a wide frequency spectrum. Two post mixing times were chosen here to show the time evolution of the results after mixing. All of the results had the same waiting time of 20 minutes.

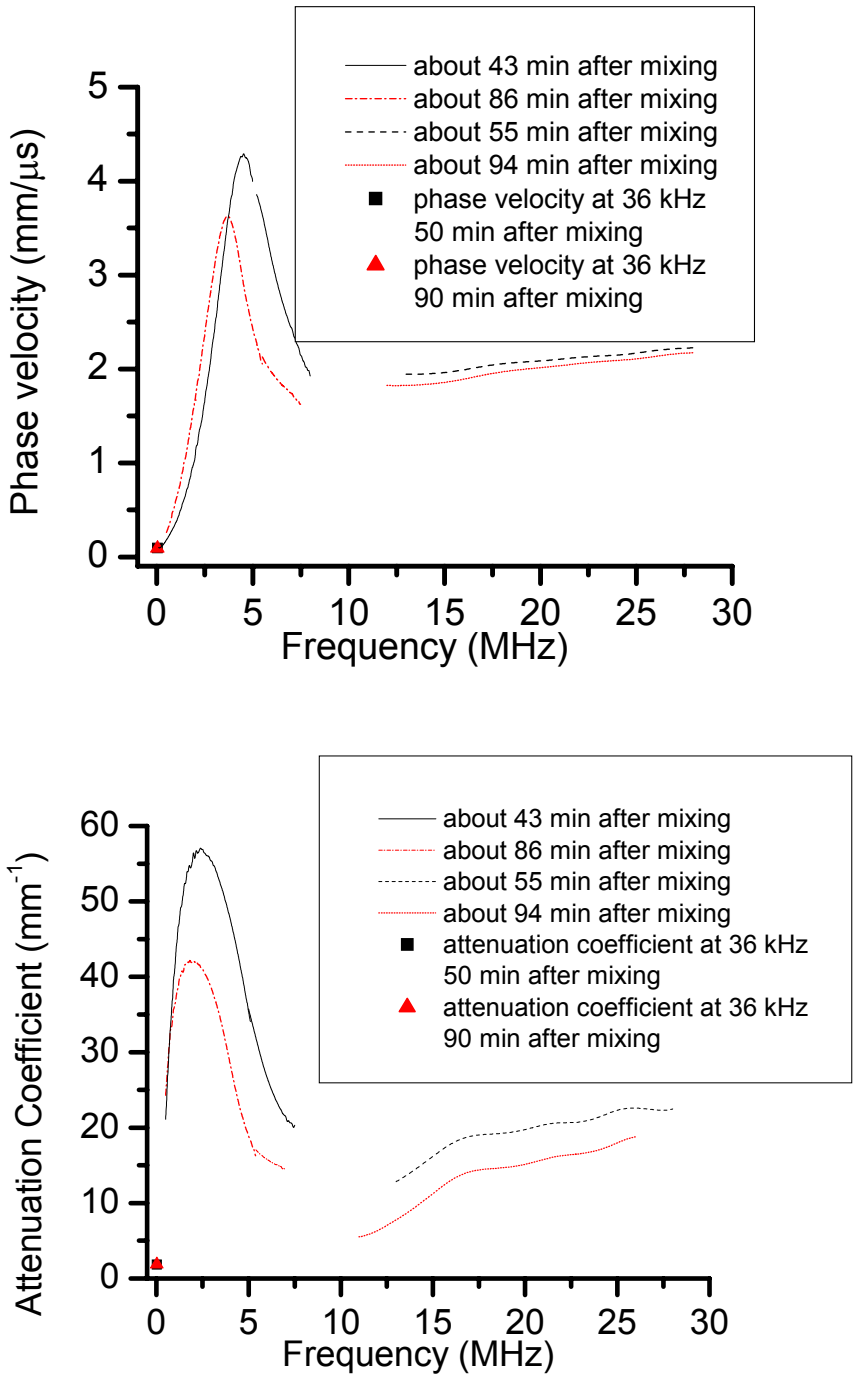

Figure 4.44. The post mixing effect on the phase velocity and attenuation coefficient as a function of frequency for ambient mixed dough. (This post mixing time was the total time after mixing, including both the time when the subsample was taken from the container plus the waiting time after it was compressed.)

From the figure above, we can clearly see the peak of the phase velocity as well as the attenuation coefficient shifted to lower frequencies, and the magnitude of the attenuation decreased, with the time after mixing. The process was also observed at a longer post mixing time (about 250 minutes), as shown in sections 4.6.3 and 4.6.4. At the high frequency end (around 20 MHz), both the phase velocity and the attenuation coefficient decreased as the post mixing time increased from 55 minutes to 94 minutes.

4.6.6.2. Waiting time effect

Data from the same subsample but with different waiting time are shown in figure 4.45. The post mixing time of this subsample at the start of the measurements is listed in table 4.24.

Frequency	**36 kHz**	**3 MHz**	**5 MHz**	**20 MHz**
Post mixing	60 min	67 min	65 min	74 min

Table 4.24. Post mixing times for the data at each frequency range. (This post mixing time was the time after mixing when the subsamples were taken from the container)

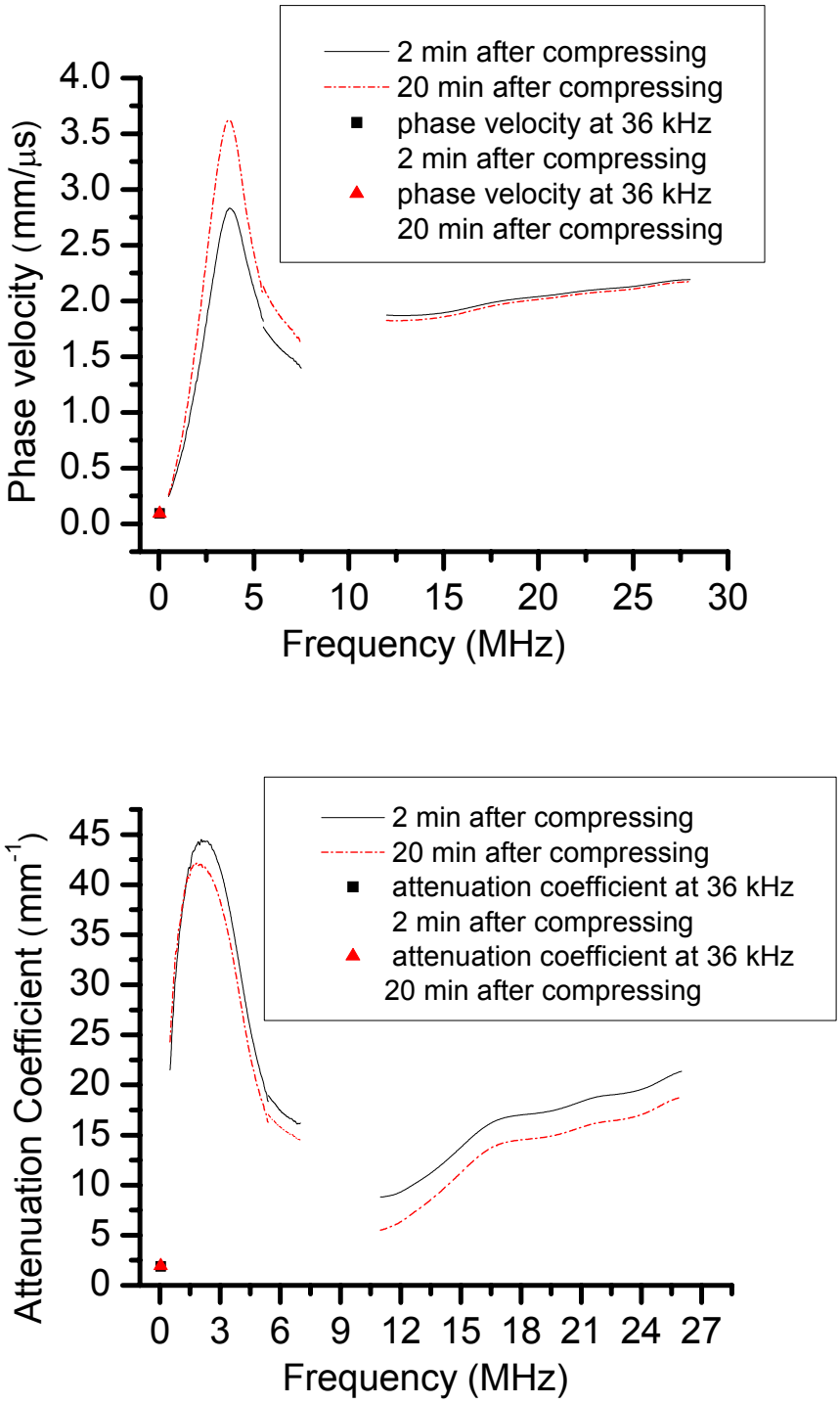

Figure 4.45. The waiting time dependence of the phase velocity and attenuation coefficient as a function of frequency for ambient mixed dough.

From the figure above (figure 4.45), we can see that the peak of the phase velocity increased with time and slightly shifted to lower frequency. This increase in the magnitude of the velocity peak with waiting time is larger than the changes seen as the post mixing time increased (see section 4.6.6.1). As the waiting time evolved, the attenuation coefficient decreased and the peak shifted to the low frequency end, which is consistent with the relaxation behavior observed when the post mixing time increased.

At the high frequency end, the phase velocity almost did not change while the attenuation coefficient decreased as the waiting time became longer.

Because the two measurements also had 20 minutes difference in the post mixing time, post mixing relaxation should also be involved. But as we observed different relaxation behavior in the peak value of the phase velocity, we would say this waiting time relaxation is real. In order to investigate this relaxation more accurately, more samples are suggested to be made so that subsamples with similar post mixing times and different waiting times could be measured.

Part III: Interpretation of the high frequency results

Two different kinds of model were used to interpret the frequency dependence of the phase velocity and attenuation coefficient. One explained the results close to the bubble resonance frequency. The other one explained the results above the bubble resonance (near 20 MHz), enabling new information on the properties of the matrix to be determined.

4.7. The theoretical models

4.7.1. Model used to explain the results near the bubble resonance frequency

In 1945, Leslie L. Foldy published a paper in Physical Review about the multiple scattering of waves (Foldy, 1945). This was the first detailed study of the multiple scattering of waves by a randomly distributed collection of scatterers, and its effect on velocity and attenuation. Before this, all the studies of the multiple scattering of waves were in the "geometrical optics limit", which considered wave rays as the trajectories of particles, neglecting interference phenomena characteristic of waves. The basic idea of this theory is presented below. To be consistent with the original paper, the same symbols are used.

This theory deals with scalar waves in the limit of isotropic scattering by a random distribution of scatterers. At a single frequency ω, the wave at position r and time t can be represented as $\psi(r)e^{i\omega t}$. In the absence of scatterers, $\psi(r)$ satisfies the wave

equation

$$\Delta\psi + k_0^2\psi = 0 \tag{4.3}$$

where $k_0 = \omega / v_0$ and v_0 is the wave velocity in the scatterer-free medium. In the presence of scatterers, the wave function becomes the sum of the incident field and the scattered fields. Thus, for a particular configuration of the scatterers at positions r_j, the value of the wave function at point r can be represented as

$$\psi(r) = \psi_0(r) + \sum_j A_j E(r, r_j), \tag{4.4}$$

where $A_j = g(s_j, \omega)\psi^j(r_j)$, $\psi^j(r_j)$ is the external field at the j^{th} scatterer, and $g(s_j, \omega)$ is the scattering function for the j^{th} scatterer whose scattering parameter is s_j. (For the gas bubbles discussed in this section, the scattering parameter s is the radius.) E is defined as

$$E(r, r') = \frac{\exp(-ik_0 |r - r'|)}{|r - r'|}. \tag{4.5}$$

The external field acting on the j^{th} scatterer is then

$$\psi^j(r) = \psi_0(r) + \sum_{j'(\neq j)} A_{j'} E(r, r_{j'}). \tag{4.6}$$

Equation (4.4) and (4.6) represent the fundamental equations of multiple scattering.

For a large number of scatterers, the exact calculation of $\psi(r)$ is impossible but Foldy showed that the configurational average of the wave field, $\langle\psi(r)\rangle$, satisfies the wave equation

$$\Delta\langle\psi(r)\rangle + k^2(r)\langle\psi(r)\rangle = 0\,, \tag{4.7}$$

with

$$k^2(r) = k_0{}^2 + 4\pi\int g(s,\omega)n(r,s)ds\,. \tag{4.8}$$

Here, $n(r,s)ds$ is the number of scatterers per unit of volume with scattering parameter between s and $s+ds$, at point r. Note that derivation of equation (4.5) requires the following statement to be true: the average field that a scatterer experiences at a given position would be the same if the scatterer were not there. This hypothesis is usually fulfilled for dilute systems.

The model we used to describe the propagation of ultrasonic waves in the bubbly viscoelastic medium was based on this multiple scattering theory. In our case the scatterers are the gas bubbles in the dough. For the whole material, we assume that the wave vector is independent of position. Then we could rewrite equation (4.8) as

$$k^2 = k_0{}^2 + 4\pi\int g(s,\omega)n(s)ds\,. \tag{4.9}$$

We see that the effective wave vector k depends on the scattering coefficient $g(s,\omega)$ of a bubble with a radius s and angular frequency ω, and the number of bubbles per unit volume whose radius is between s and $s+ds$.

From research on the bubble size distribution in dough (Bellido *et al*., 2006; Campbell *et al*., 1991), we consider a log-normal distribution of bubble radii:

$$n(s) = \frac{N_{tot}}{\sqrt{2\pi}\varepsilon s}\exp\left[-\frac{\left(\ln\left(s/s_0\right)\right)^2}{2\varepsilon^2}\right], \tag{4.10}$$

where N_{tot} is the total number of bubbles per unit volume, s_0 is the median radius, and ε is the logarithmic standard deviation. In practice we can represent N_{tot} as a function of volume fraction of bubbles ϕ.

$$N_{tot} = \frac{3\phi}{4\pi \times s_0^3 \times \exp\left(9\varepsilon^2/2\right)}. \tag{4.11}$$

When the bubble radius is much less than the wavelength of the sound wave $\left(\omega s / v_0 << 1\right)$, the bubble can be modeled by a harmonic oscillator (Leroy *et al*. (2005)). The scattering coefficient can be represented as

$$g(s,\omega) = \frac{s\omega^2}{\omega_0^2 - \omega^2 - i\omega\Gamma}, \tag{4.12}$$

where ω_0 is the resonance angular frequency and Γ is the damping rate of the harmonic oscillator. The full expression for ω_0 is very complicated (Leighton, 1994, pages 172 to 188). A good approximation for ω_0 is (Alekseev and Rybak, 1999):

$$\omega_0 \approx \frac{1}{s}\sqrt{\frac{3\gamma P_0 + 4\mu'}{\rho}}, \tag{4.13}$$

where γ is the ratio of the specific heat capacities of the gas in the bubble, P_0 is the static pressure of the gas, ρ the mass density of the matrix, and μ' the real part of its shear modulus.

The damping rate of the bubble arises from three different loss mechanisms ($\Gamma = \Gamma_{rad} + \Gamma_{vis} + \Gamma_{th}$) (Prosperetti, 1977). $\Gamma_{rad} = \omega^2 s / v_0$ accounts for the loss of energy in the bubble due to radiating ultrasonic waves. $\Gamma_{vis} = 4\mu'' / \rho\omega s^2$ accounts for viscous losses, which occur at the interface of the bubble and the surrounding medium. Here

μ'' is the imaginary part of the shear modulus. Thermal dissipation contributes to the damping Γ_{th} in a more complicated way, which can be represented as $\Gamma_{th} = -\frac{P_0 \,\mathrm{Im}(\tilde{\phi})}{\omega \rho s^2}$, with

$$\tilde{\phi}(\omega, s) = \frac{3\gamma}{1 - 3(\gamma - 1) i \frac{D}{\omega s^2}\left[1 - s\sqrt{-i}\sqrt{\frac{\omega}{D}}\coth(s\sqrt{-i}\sqrt{\frac{\omega}{D}})\right]} \tag{4.14}$$

Here D is the thermal diffusion coefficient of the gas. Using equation (4.14), the effects of thermodynamics of the gas can be taken into account. This leads to a more complete description of the angular resonance frequency, equation (4.13), can be written as $\sqrt{\frac{P_0 \,\mathrm{Re}(\tilde{\phi}) + 4\mu'}{\rho s^2}}$.

Using this model, we can calculate the effective wave vector $k(\omega)$. The angular frequency ω divided by the real part of $k(\omega)$ gives the phase velocity of the whole material, and twice the imaginary part is the attenuation coefficient.

4.7.2. Model used to explain the results around 20 MHz

The model used in this section is a classical ultrasonic relaxation model that describes how the frequency dependence of the velocity and attenuation is influenced by molecular relaxations. The largest changes occur when the relaxation time is comparable to $1/\omega$. The description of this model follows the review given by Litovitz and Davis (Litovitz and Davis, 1965). One good application of this model was carried out by Verdier *et al.* (Verdier *et al.,* 1998).

For longitudinal waves, the phase velocity v and attenuation coefficient α are related to the complex longitudinal modulus M^* as follows:

$$M^* = M' + iM'' = \rho v^{*2}. \tag{4.15}$$

Here $v^* = v' + iv''$ is the complex velocity and ρ is the density. The complex velocity v^* can be expressed in terms of the complex wave vector k^* as in the following expression.

$$k^* = \frac{\omega}{v^*} = \frac{\omega(v' - iv'')}{v'^2 + v''^2}. \tag{4.16}$$

Therefore, the real and imaginary part of the wave vector can be written as

$$k' = \frac{\omega}{v} = \frac{\omega v'}{v'^2 + v''^2} \quad \text{and} \quad k'' = \frac{-\omega v''}{v'^2 + v''^2}. \tag{4.17}$$

Thus, the measured velocity and attenuation are given by

$$v = \frac{v'^2 + v''^2}{v'} \quad \text{and} \quad \alpha = \frac{2\omega v''}{v'^2 + v''^2}. \tag{4.18}$$

Then equation (4.15) can be written as

$$M^* = \rho(v' + iv'')^2 = \rho(v'^2 - v''^2) + 2i\rho v' v'' \tag{4.19}$$

Therefore

$$M' = \rho(v'^2 - v''^2) \quad \text{and} \quad M'' = 2\rho v' v'' \tag{4.20}$$

From (4.20) we can express v' and v'' in terms of M' and M''. Then, using equation (4.18), v and α can be written in terms of M' and M'' as follows:

$$v = \sqrt{\frac{2}{\rho}\left(\frac{M'^2 + M''^2}{M' + \sqrt{M'^2 + M''^2}}\right)}$$

$$\alpha = \omega\sqrt{2\rho\left(\frac{\sqrt{M'^2 + M''^2} - M'}{M'^2 + M''^2}\right)} \tag{4.21}$$

Also M' and M'' can be expressed in terms of v and α as

$$M' = \rho v^2\left[\frac{1-\left(\frac{\alpha v}{2\omega}\right)^2}{\left[1+\left(\frac{\alpha v}{2\omega}\right)^2\right]^2}\right] \quad \text{and} \quad M'' = \frac{2\rho v^2\left(\frac{\alpha v}{2\omega}\right)}{\left[1+\left(\frac{\alpha v}{2\omega}\right)^2\right]^2} \tag{4.22}$$

When the value of $\left(\frac{\alpha v}{2\omega}\right)^2$ is much smaller than 1, equation (4.22) can be written as

$$M' = \rho v^2 \quad \text{and} \quad M'' = \frac{2\rho v^3 \alpha}{\omega} \tag{4.23}$$

For longitudinal waves, M^* is a function of the complex bulk or compressional modulus K^* and the complex shear modulus G^*:

$$M^* = K^* + \frac{4}{3}G^* \tag{4.24}$$

When a pressure is applied to a viscoelastic medium, its response may involve both volume and shear relaxations, with corresponding relaxation times τ_v and τ_s, respectively. Then, for the case where the static shear modulus is zero, the complex moduli take the form:

$$K^* = K_0 + \frac{K_r\omega^2\tau_v^{\,2}}{1+\omega^2\tau_v^{\,2}} + i\frac{K_r\omega\tau_v}{1+\omega^2\tau_v^{\,2}} \tag{4.25}$$

$$G^* = \frac{G_\infty\omega^2\tau_s^{\,2}}{1+\omega^2\tau_s^{\,2}} + i\omega\frac{G_\infty\tau_s}{1+\omega^2\tau_s^{\,2}} \tag{4.26}$$

where K_0 is the static compressional modulus, $K_r = K_\infty - K_0$ (with K_∞ being the high-frequency modulus of compression), is the relaxation modulus, and G_∞ is the high-frequency shear rigidity.

Combining (4.23), (4.24), (4.25) and (4.26) gives

$$v = \sqrt{\frac{K_0 + \frac{K_r \omega^2 \tau_v^{\,2}}{1+\omega^2 \tau_v^{\,2}} + \left(\frac{4}{3}\right)\frac{G_\infty \omega^2 \tau_s^{\,2}}{1+\omega^2 \tau_s^{\,2}}}{\rho}} \tag{4.27}$$

and

$$\alpha = \frac{\omega^2}{\rho v^3}\left(\frac{K_r \tau_v}{1+\omega^2 \tau_v^{\,2}} + \left(\frac{4}{3}\right)\frac{G_\infty \tau_s}{1+\omega^2 \tau_s^{\,2}}\right) \tag{4.28}$$

Therefore, if acoustic energy is absorbed by molecules in the dough, and this process requires some finite amount of time for the exchange of energy, then the velocity and the attenuation will be expected to vary in this characteristic way as a function of the frequency of the ultrasound wave propagating through the dough.

4.8. Interpretation of the results near the bubble resonance frequency

4.8.1. Ambient dough

The dough parameters, which are used in the model described in section 4.7.1, are listed in the following table.

Parameters	**Physical meaning**
r_0	Typical radius of the log-normal distribution of the air bubbles
ε	Width of the log-normal distribution
ϕ	Void fraction of gas in the medium
ρ_m	Mass density of the matrix
v_0	Velocity of sound in the matrix
μ'	Real part of the shear modulus
μ''	Imaginary part of the shear modulus

Table 4.25. Dough parameters used in the bubble resonance model and their physical meaning.

For the log-normal distribution that describes the bubble sizes, r_0 and ε are the parameters that determine the mean radius of the distribution $r_{mean} = r_0 \exp(0.5\varepsilon^2)$ and the position of the maximum of the distribution $r_{\max} = r_0 \exp(-\varepsilon^2)$. The void fraction ϕ is defined as

$$\phi = 1 - \frac{\rho}{\rho_m} \tag{4.29}$$

Here ρ is the dough density, which is influenced by the mixing pressure, and ρ_m is

the density of the matrix. Thus, the void fraction ϕ can be obtained from density measurements.

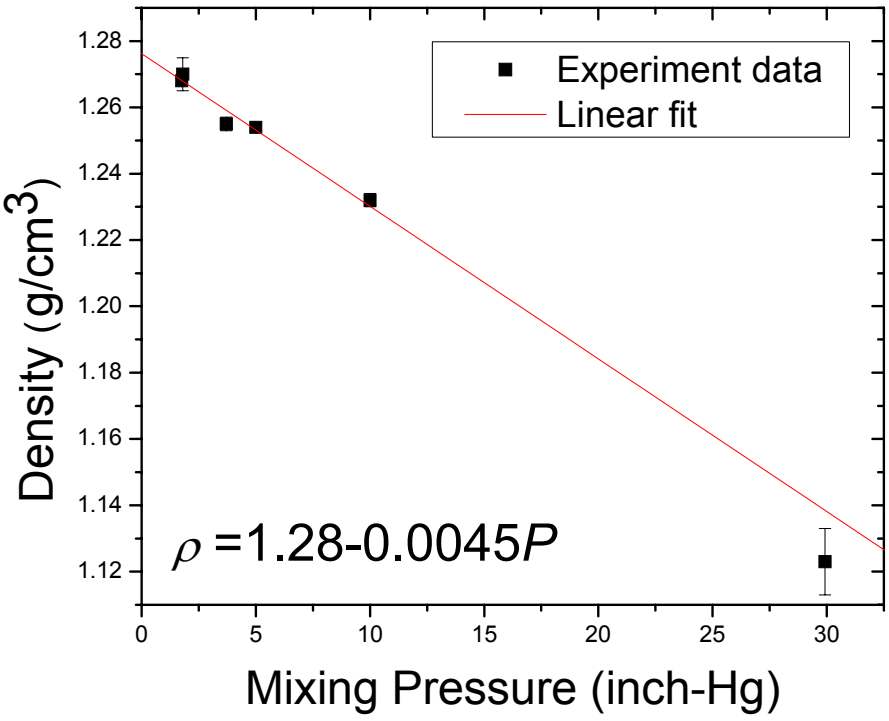

Figure 4.46. The density of dough as a function of mixing pressure.

Figure 4.46 shows the measured density as a function of the mixing pressure for my samples. The matrix density, ρ_m, is the y-intercept in the figure, which is 1.275 g/cm^3 in this case. Using this value, we obtain a void fraction of 12% (±1%) for the ambient dough we used. The velocity of sound in the matrix is hard to know directly, but it can be inferred from the comparison of the resonance model to our data, since above resonance, the theory predicts that the velocity approaches the matrix value. From this comparison, we find that v_0 is about 1.6 mm/μs near the bubble resonance frequency.

The shear modulus of dough was more difficult to estimate, especially for the high frequencies used in the experiments (Letang *et al*., 2001). From measurement of the phase velocity at 36 kHz (see figure 4.14), the real part of the shear modulus could be obtained by using the equation for the velocity in the low frequency limit well below resonance: $v = \sqrt{(3P_0 + 4\mu')/(3\rho\phi)}$ (Leroy et al., (2006)). This gives $\mu' = 800\,\text{kPa}$ at 36 kHz. According to low frequency rheological measurements (0.01-100 Hz), the shear modulus of dough scales with frequency as $f^{1/3}$, and μ''/μ' roughly equals 0.7 (Keentok *et al*., 2002). By making the assumption that these results can be extrapolated to high frequencies, the following expressions can be used to estimate the real and imaginary parts of the shear modulus in the dough samples:

$$\mu' = 800\ \text{kPa} \times \left(f / 36\ \text{kHz}\right)^{1/3} \tag{4.30}$$

and

$$\mu'' = 560\ \text{kPa} \times \left(f / 36\ \text{kHz}\right)^{1/3} \tag{4.31}$$

They are equivalent to

$$\mu' = 24 \times f^{1/3}\ \text{kPa} \tag{4.32}$$

and

$$\mu'' = 17 \times f^{1/3}\ \text{kPa} \tag{4.33}$$

with *f* expressed in Hz.

Using the above values for ϕ, ρ, the parameters for gas properties (diffusion coefficient and heat capacity ratio) and the parameters for dough matrix properties (gas free velocity and attenuation), the bubble model was fit to the data in figure 4.47. The best fit gave somewhat larger values for the shear modulus than those in equations (4.32) and (4.33).

$$\mu' = 50 \times f^{1/3} \text{ kPa} \tag{4.34}$$

and

$$\mu'' = 35 \times f^{1/3} \text{ kPa} \tag{4.35}$$

From this fit, the bubble distributions for the two sets of data were obtained. For the data 43 minutes after mixing, $r_0 = 17.5\,\mu\text{m}$, $\varepsilon = 0.37$ and for the data 86 minutes after mixing, $r_0 = 22$ μm and $\varepsilon = 0.35$. We can see that as the time after the dough was mixed became longer, the bubble size increased and the distribution became narrower. This is consistent with the disproportionation of the bubbles in the dough, an effect that has been suggested by previous researchers (van Vliet, 1999).

These results from fitting the model to our data are significantly different to the bubble size distribution measured by x-ray tomography (Bellido *et al.*, 2006). The x-ray data was obtained for a sample that had rested for 90 minutes after mixing, and is displayed in figure 4.47(c) (dashed curve).

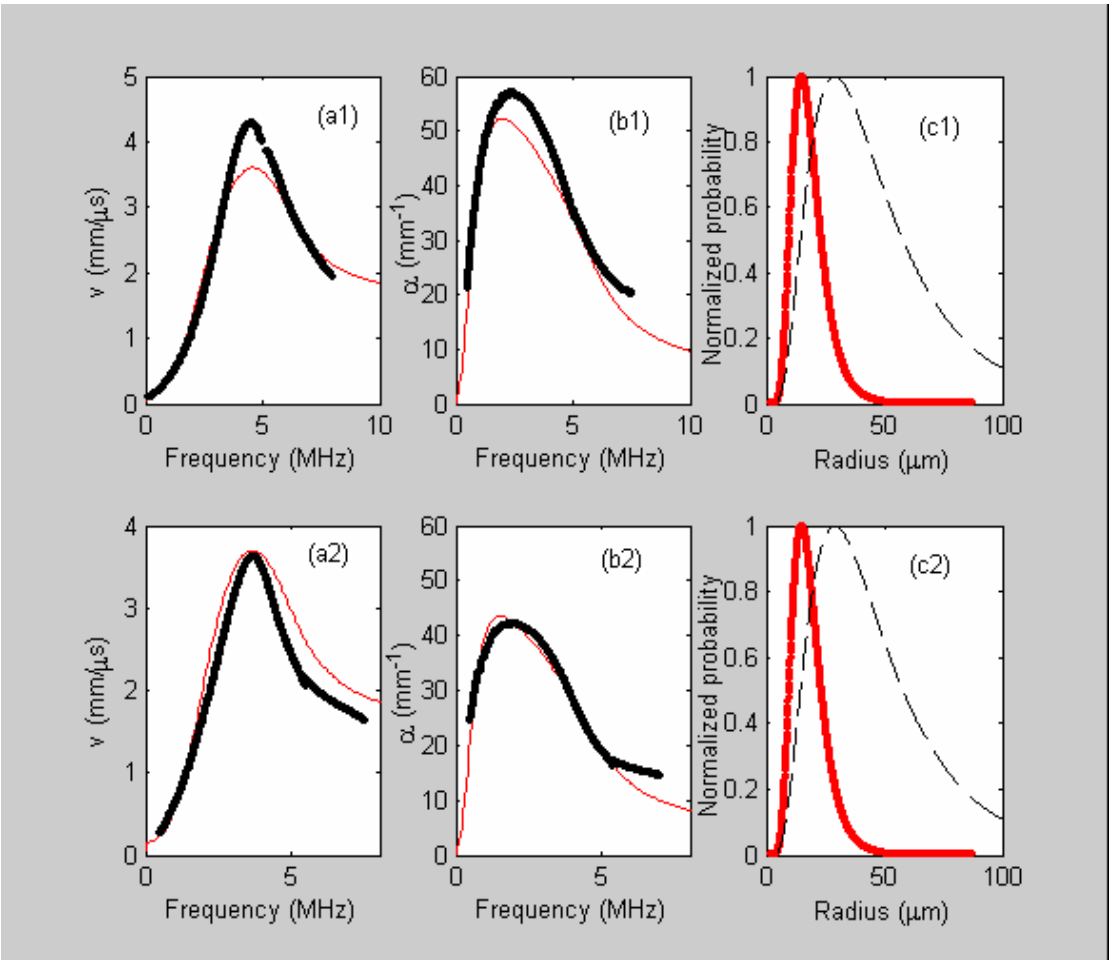

Figure 4.47. The theoretical fit (thin red lines) of the resonance model to the ambient data (symbols). Attenuation (a), phase velocity (b) and inferred size distribution of bubbles (thick red curve in (c)) obtained from a sample of dough analysed 43 minutes after mixing (1) and 86 minutes after mixing (2). The dashed curve in (c) corresponds to the size distribution measured by x-ray tomography for a sample of dough rested for 90 minutes after mixing (Bellido *et al.*, 2006).

Some possible reasons for this discrepancy could be:

a. The conditions of sample preparation were not the same in both cases: the ultrasound samples were compressed to obtain 0.3 mm thick slices (because the attenuation is high, the thickness had to be small enough for the transmitted pulse to be measurable), whereas samples analyzed by tomography were not compressed to the same extent (2.17 mm).

b. The model was developed for a low void fraction of bubbles (less than 1%), while the void fraction in the ambient dough we measured was 12%.

c. The shape of the gas cells could be changed when the sample was compressed to be very thin. The model does not take the effect of bubble shape into account.

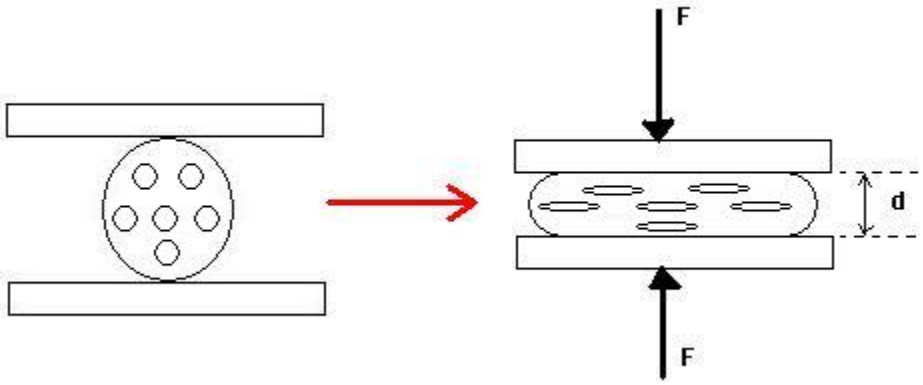

Figure 4.48. The squeezing of the air bubbles in the ambient dough.

Although we could fit the results from 20 minutes after compressing with this model, it was very hard to find a set of parameters which could fit the results from 2 minutes after compressing. The possible reasons could be those as listed above, especially reason c. The gas cells were most distorted immediately after compression and would be expected to go back to their original shape after relaxation.

In order to watch the time evolution of the dough after mixing and compressing, the change of the phase velocity and attenuation coefficient peaks in the frequency domain are shown below in figures 4.49 and 4.50. The data used here were from the 3.5 MHz measurements.

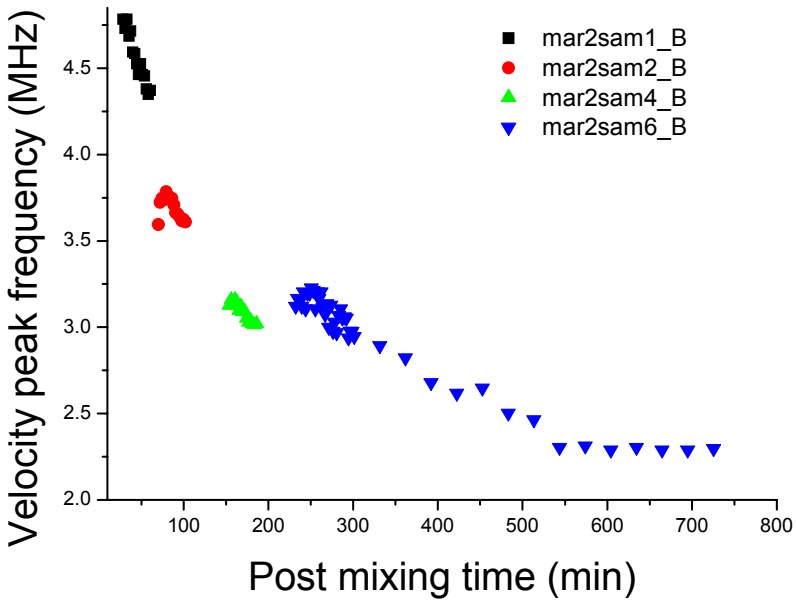

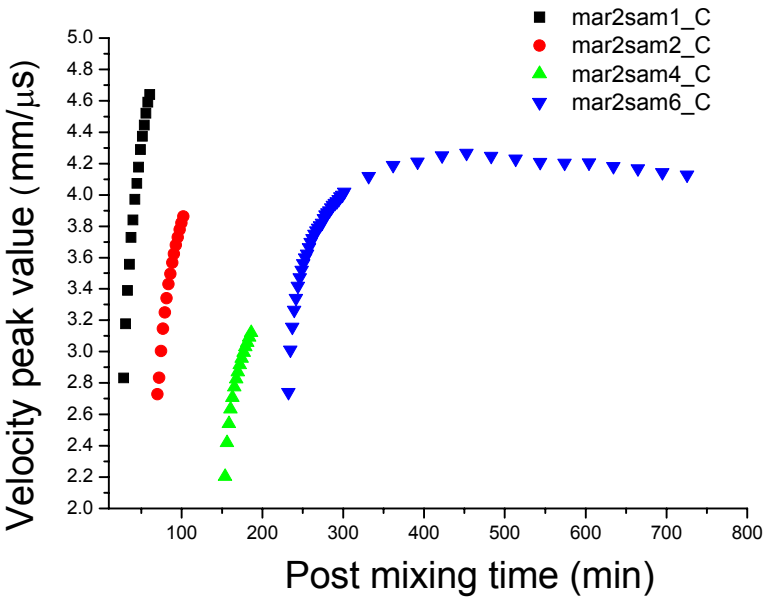

Figure 4.49. Time evolution of the velocity peak in the frequency domain. Each symbol represents one subsample.

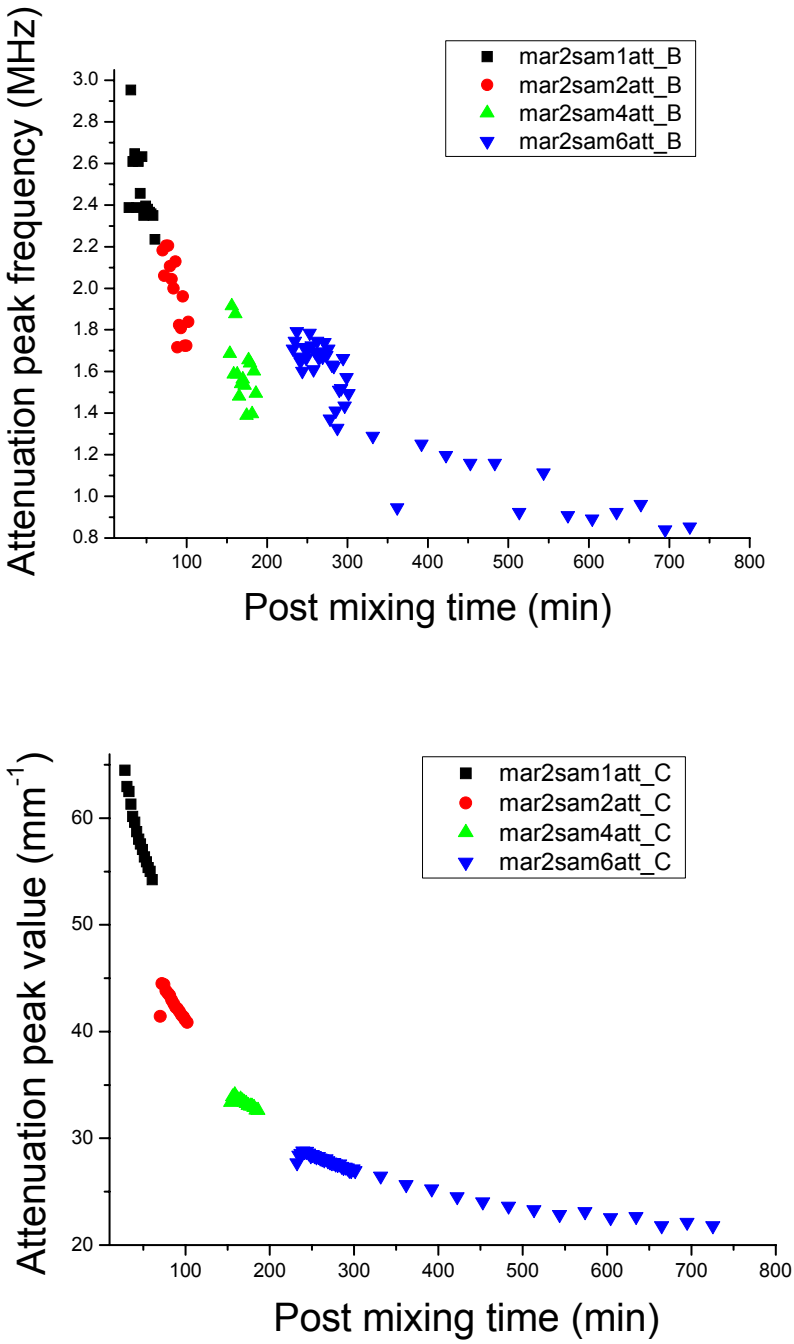

Figure 4.50. Time evolution of the attenuation peak in the frequency domain. Each symbol represents one subsample.

Because the peak frequency of the attenuation coefficient and phase velocity can be

related to the average size and width of the bubble size distribution, with higher peak frequencies corresponding to smaller bubble sizes, we can infer from the above figures that the bubble size grows with the time after mixing.

4.8.2. Vacuum dough

There is considerable scatter in the data for vacuum dough near the bubble resonance frequency (figure 4.51). Therefore, post-mixing relaxation could not be observed near the bubble resonance in the vacuum dough within the uncertainty of the data from different subsamples (see section 4.5 for the complete set of data). For a given subsample, however, the variation of velocity and attenuation with waiting time could be clearly seen, and was investigated using the bubble resonance model. The phase velocity and attenuation results are from figure 4.33. The void fraction was 0.5% and shear modulus at the best fit was

$$\mu' = 300kPa \times f^{1/3} \tag{4.36}$$

and

$$\mu'' = 210kPa \times f^{1/3} \tag{4.37}$$

Based on the analysis of low frequency velocity and attenuation data by Elmehdi (2001), it is expected that the values of μ' and μ'' for vacuum dough will be larger than the corresponding values for ambient dough.

The data were very difficult to fit because of the large scatter near the bubble resonance. The data were measured using the direct contact method. One possible reason for the scatter could be the difficulty in accurately correcting for the effects arising

from the transducer impedance. Even though we measured the transducer impedance in the experiment using two lossless liquids, water and ethanol, it still is difficult to account fully for the transducer impedance when the transducers were in contact with a material having complex impedance such as dough.

The best fit by eye to the data enabled the following values of the size distribution parameters to be estimated: $r_0 = 50\mu m$, $\varepsilon = 0.42$ for 2 minutes after compressing; $r_0 = 70\mu m$, $\varepsilon = 0.38$ for 20 minutes after compressing. However the uncertainty in these values is much larger than that for ambient dough, since the vacuum data, taken with the different transducers, are very scattered.

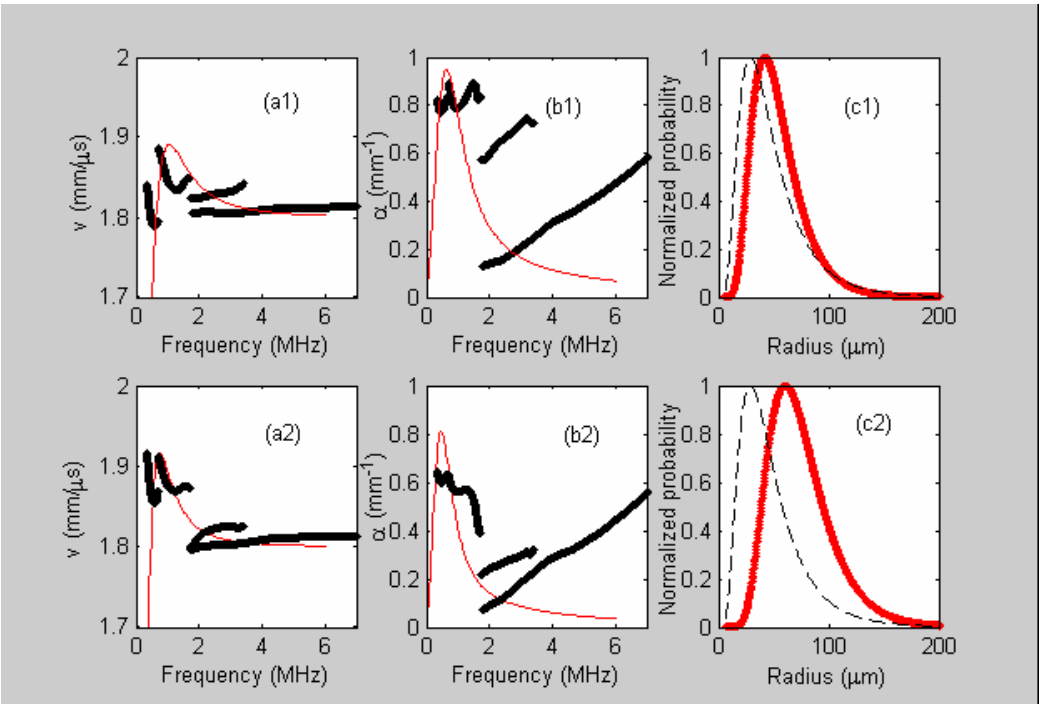

Figure 4.51. The theoretical fit (thin red lines) of bubble resonance model to the vacuum data (solid symbols). Attenuation (a), phase velocity (b) and inferred size distribution of bubbles (thick red curves in (c)) obtained from a sample of dough analyzed 2 minutes after compression (1) and 20 minutes after compression (2). The dash curve in (c) corresponds to the size distribution measured by x-ray tomography for a sample of dough rested for 90 minutes after mixing (Bellido *et al*., 2006).

Because of the low void fraction, the model may be more reliable for the vacuum dough than ambient dough. Also, the thickness of the vacuum dough sample (3 to 4 mm) was normally much larger than that of ambient dough (0.3mm), so that the possible distortion of the gas cells due to mounting the samples between the transducers would be expected to be much smaller in the vacuum sample than in the ambient dough as the thickness of vacuum dough measured at these frequencies is about 10 time larger than that of ambient dough and therefore the true strain is smaller.

We note that the bubble size distribution inferred from the ultrasonic data for vacuum dough was quite different from that of the ambient dough. According to the literature (Campbell *et al.*, 1998), dough mixed in a reduced pressure should have fewer bubbles, but the size of the bubbles should be similar to the values for ambient dough. This expectation does not seem to be in accord with our data, as the bubble sizes determined from the model for the vacuum and ambient doughs are different, however, one should be cautious about inferring too much from this comparison given the experimental uncertainties. For the ambient dough, we have better data, but the void fraction is much higher than 1% (a range of concentrations where the model has not been tested independently) and the subsamples used in the experiment were very thin (0.3 mm, so that the bubble size distribution could be affected by the compression of the samples). For the vacuum data, the void fraction is low and subsamples were less deformed, but the contact measurement used included the effect of the transducer impedance, which was difficult to eliminate. In future work, it would be very good to perform an experiment

near the bubble resonance frequency on the vacuum dough using the plastic delay layer method, as this should give us more accurate measurements of the bubble size distribution of the dough.

The theoretical *v* and α results in figure 4.51 above are compared in the next figure.

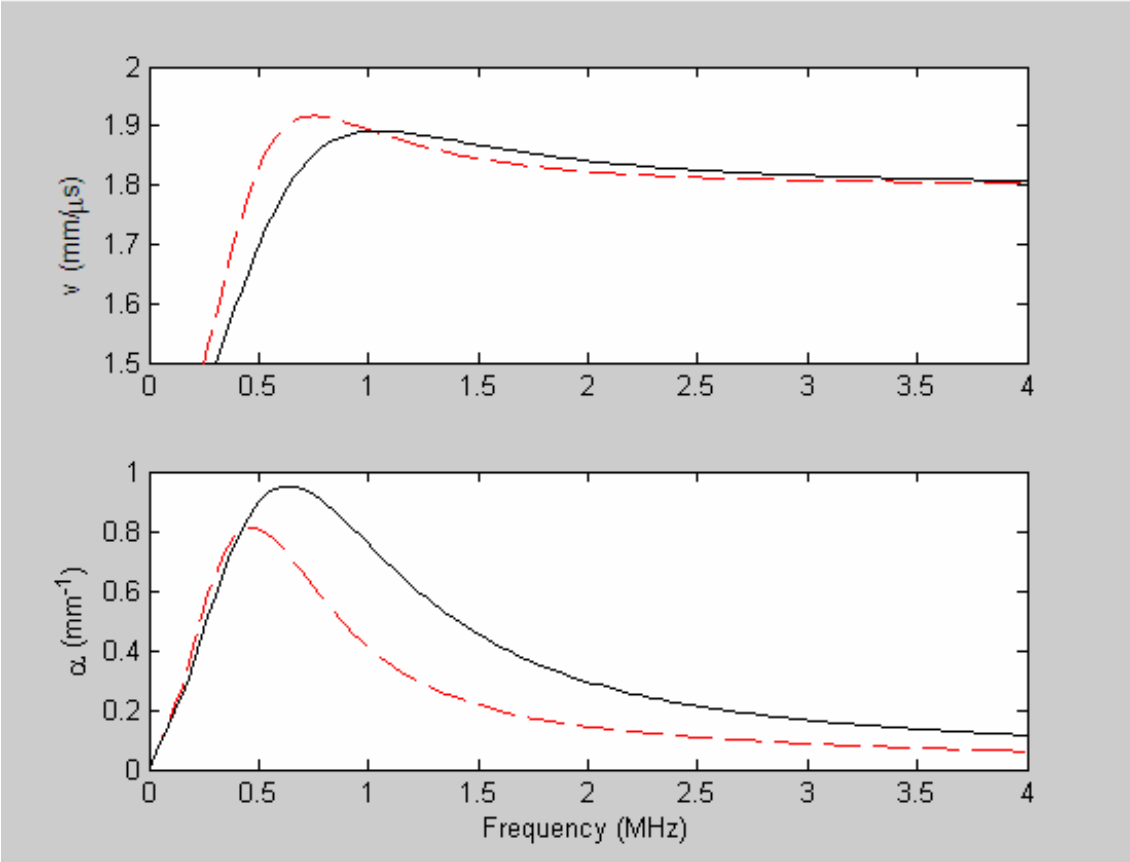

Figure 4.52. The theoretical *v* and α results from figure 4.51. The black solid line represents 2 minutes after compression while the red dashed line repreents 20 minutes after compression.

This figure shows that the peak of the phase velocity is shifted to a lower frequency as the waiting time increases, and the peak value also increases with time after compression. The peak of the attenuation decreases and shiftes to a low frequency. The peak

frequency of the velocity is at a higher frequency than that of attenuation, a result that is characteristic of bubble resonances.

The behavior shown in figure 4.52 could explain the relaxation behavior found in the 1 MHz and 2.25 MHz measurements (see figure 4.26 and figure 4.28 from sections 4.5.1 and 4.5.2). The phase velocity around 1 MHz increased with waiting time while velocity around 2 MHz decreased as the waiting time increased, consistent with the trends seen in figure 4.52 as the resonance becomes shifted to lower frequencies. Attenuation decreased with waiting time for both frequency ranges, which is again consistent with the behavior indicated in figure 4.52. Although the frequency dependence of the data is not exactly as shown in the theoretical result, the model still gives a reasonable qualitative interpretation of the experiment.

4.9. Interpretation of the results at frequencies far above bubble resonance

A Matlab graphic user interface (see figure 4.53) was designed to facilitate the theoretical fitting of Eqns (4.27) and (4.28) to the data. The sliders on the left side of the interface were used to adjust the parameters in the equations. The new theoretical curves with the adjusted parameters were then plotted with the experimental data in the two figures on the right-hand side.

4.9.1. Ambient dough

4.9.1.1. Post mixing effect

The data from figure 4.47 was compared with the predictions of the model (equations (4.27) and (4.28)). Both data sets were selected from ultrasonic analyses performed 20 minutes after compression. Since the bulk modulus is orders of magnitude larger than the shear modulus in dough, it is expected that the data would only be sensitive to the relaxation time at constant volume τ_v. Thus, equations (4.27) and (4.28) were simplified before fitting the data by retaining only the terms involving τ_v (i.e., by setting the shear relaxation time τ_s and G_∞ to zero in the fitting). The fitting of this model to the results for the dough analyzed 55 minutes after mixing is shown in figure 4.53 and for the dough 96 minutes after mixing in figure 4.54. The best combinations of parameters found from the model for these high frequency data are given in table 4.26 and in figures 4.53 and 4.54.

Parameters / Post mixing	ρ (g/cm^3)	K_0 (GPa)	K_r (GPa)	τ_v (μs)
55 minutes	1.12	3.08	7.04	0.0045
94 minutes	1.12	3.08	4.88	0.005

Table 4.26. Model fitting parameters at two different post mixing times for ambient dough.

From the table above we can see that the value of K_r decreases significantly with the increase in post mixing time, consistent with the fact that both the attenuation and velocity are smaller at the longer time. These results (see also figures 4.53 and 4.54) are consistent with a material that stiffens with increases in frequency, with a relaxation time of approximately 5 ns. There is a significant difference in the value derived for $K_\infty = K_0 + K_r$ as post-mixing time increases, with K_∞ decreasing from 10 GPa to 8 GPa over the range of post mixing times investigated.

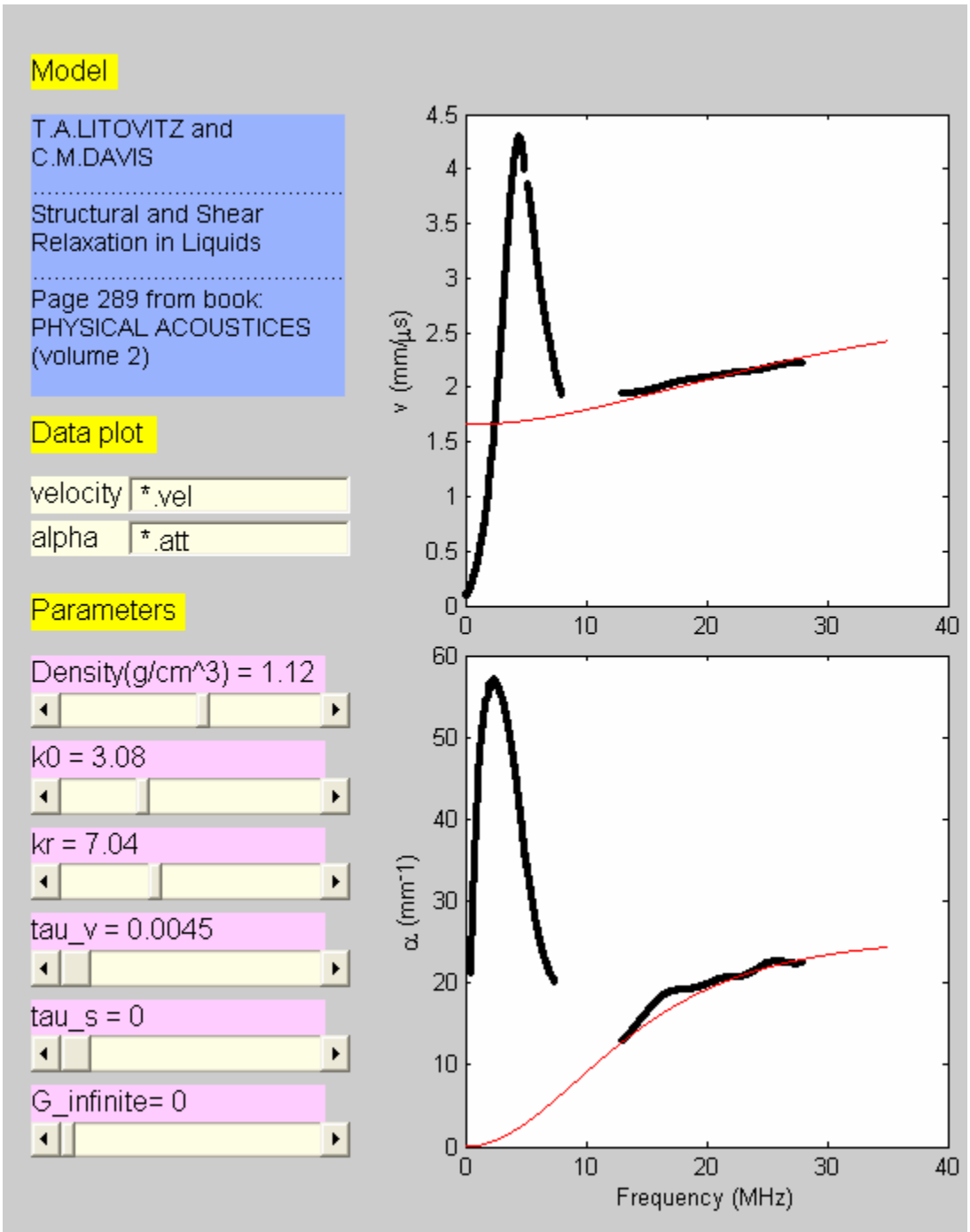

Figure 4.53. Theoretical fits (thin red curves) to the high frequency ambient dough data (solid symbols) measured 55 minutes after mixing.

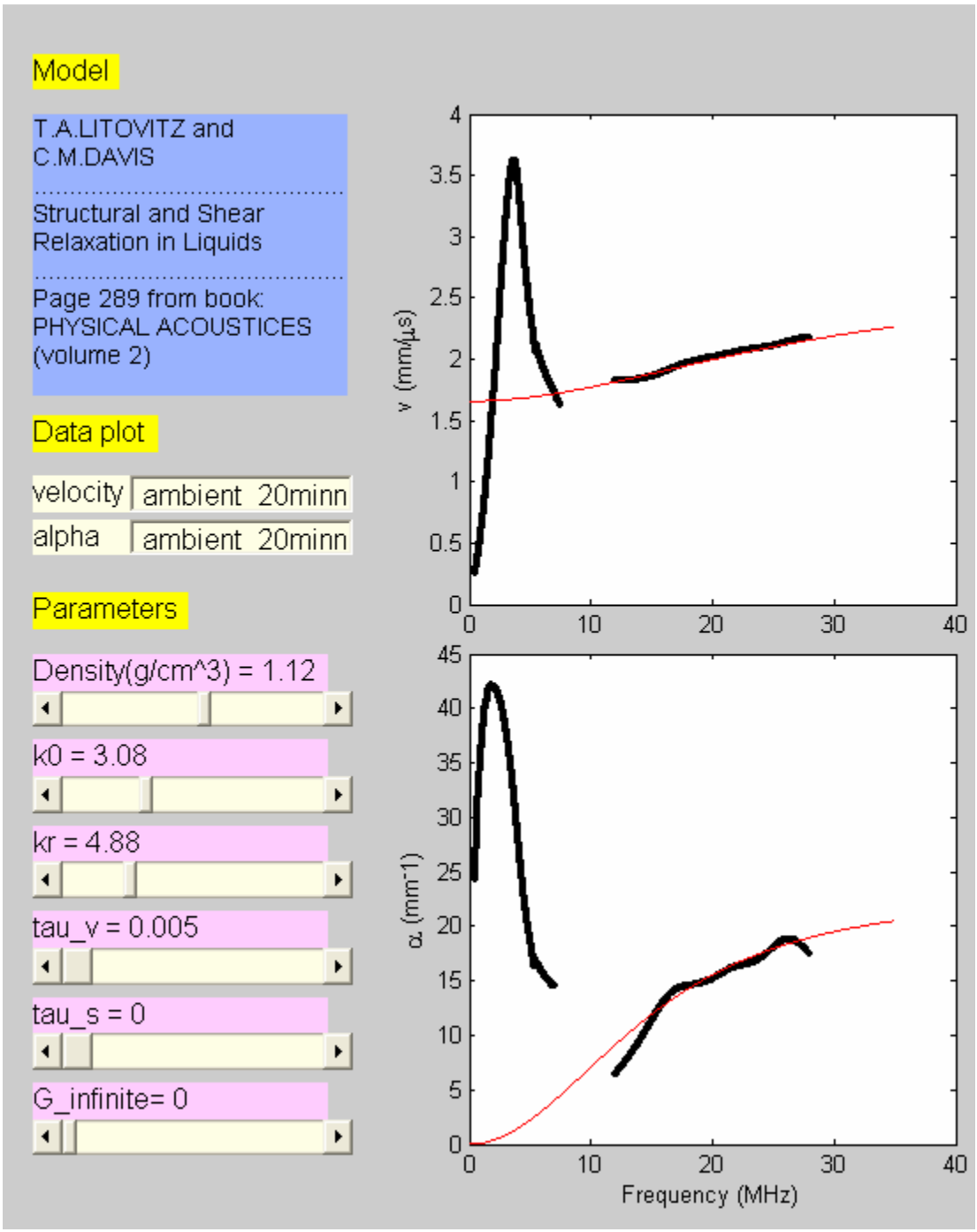

Figure 4.54. Theoretical fit of the high frequency range ambient dough results from 94 minutes after mixing.

4.9.1.2. Waiting time dependence

The data from figure 4.45 were also fitted by the molecular relaxation model. The corresponding post mixing times are 76 and 94 minutes. Both data sets were from the same subsample, but with different waiting times. The fitting for the results measured 2 minutes after compression are shown in figure 4.55, and the results 20 minutes after compression are shown in the previous figure, figure 4.54. The results of the modeling of these high frequency data are shown in table 4.27.

Parameters / Waiting time	ρ **(g/cm^3)**	K_0 **(GPa)**	K_r **(GPa)**	τ_v **(μs)**
2 minutes	1.12	3.08	5.92	0.0046
20 minutes	1.12	3.08	4.88	0.005

Table 4.27. Model fitting parameters at two different waiting times for ambient dough.

These results are also consistent with a material that stiffens with increases in frequency, with a relaxation time at constant volume centred at approximately 5 ns. There is a slight decrease in the value derived for K_∞, with K_∞ decreasing from 9 GPa to 8 GPa as post-compression time increases. Comparison of figures 4.53-4.55, and tables 4.26 and 4.27, show that both K_r and K_∞ decrease with both waiting time after compression and the time after mixing, showing that the magnitude of the change in K and thus also the high frequency limit K_∞ are evolving to lower values as the dough ages.

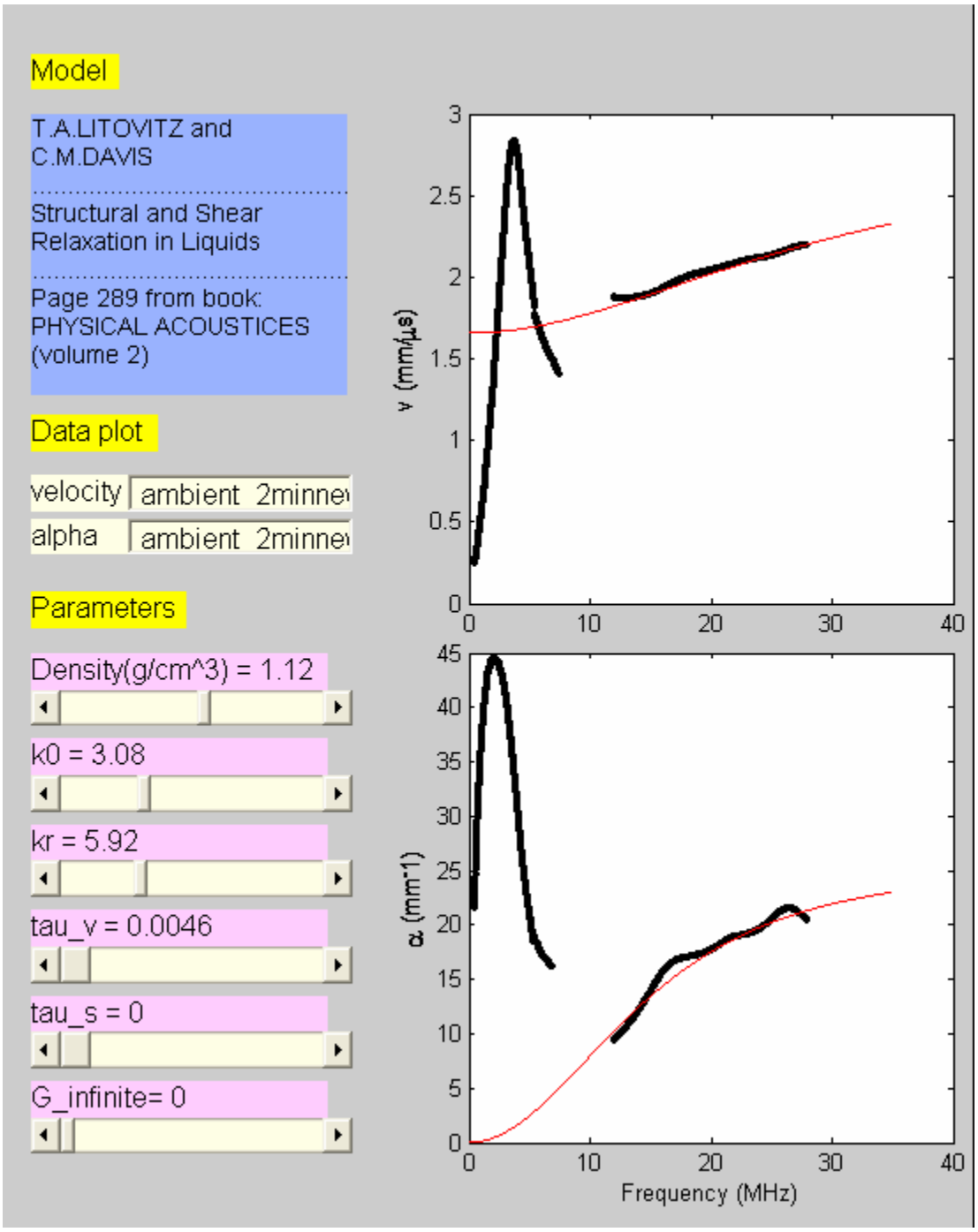

Figure 4.55. Theoretical fit (thin red lines) of the data for ambient dough (solid symbols) at high frequencies measured 2 minutes after compression.

4.9.2. Vacuum dough

For the vacuum dough data, no post-mixing time relaxation effect was found in this frequency range (see section 4.5 in part 2 of this chapter). We used the model to fit the data from figure 4.33. There was no difference between the model fits for data from dough tested 2 minutes after compression and the dough tested 20 minutes after compression. Figure 4.56 shows the results of fitting the theory to the experimental data. The fitting parameters are listed in table 4.28.

ρ (g/cm^3)	K_0 (GPa)	K_r (GPa)	τ_v (μs)
1.26	4.13	3.48	0.00096

Table 4.28. Model fitting parameters at two different waiting times for vacuum dough.

It is apparent that the vacuum dough does not change its properties with time in this frequency range, but that like the ambient mixed dough, the vacuum dough stiffens with increases in frequency. The value derived for K_∞ is very similar to that of the ambient mixed dough (7-8 GPa). However, the relaxation time at constant volume is substantially lower, with a value of approximately 1 ns.

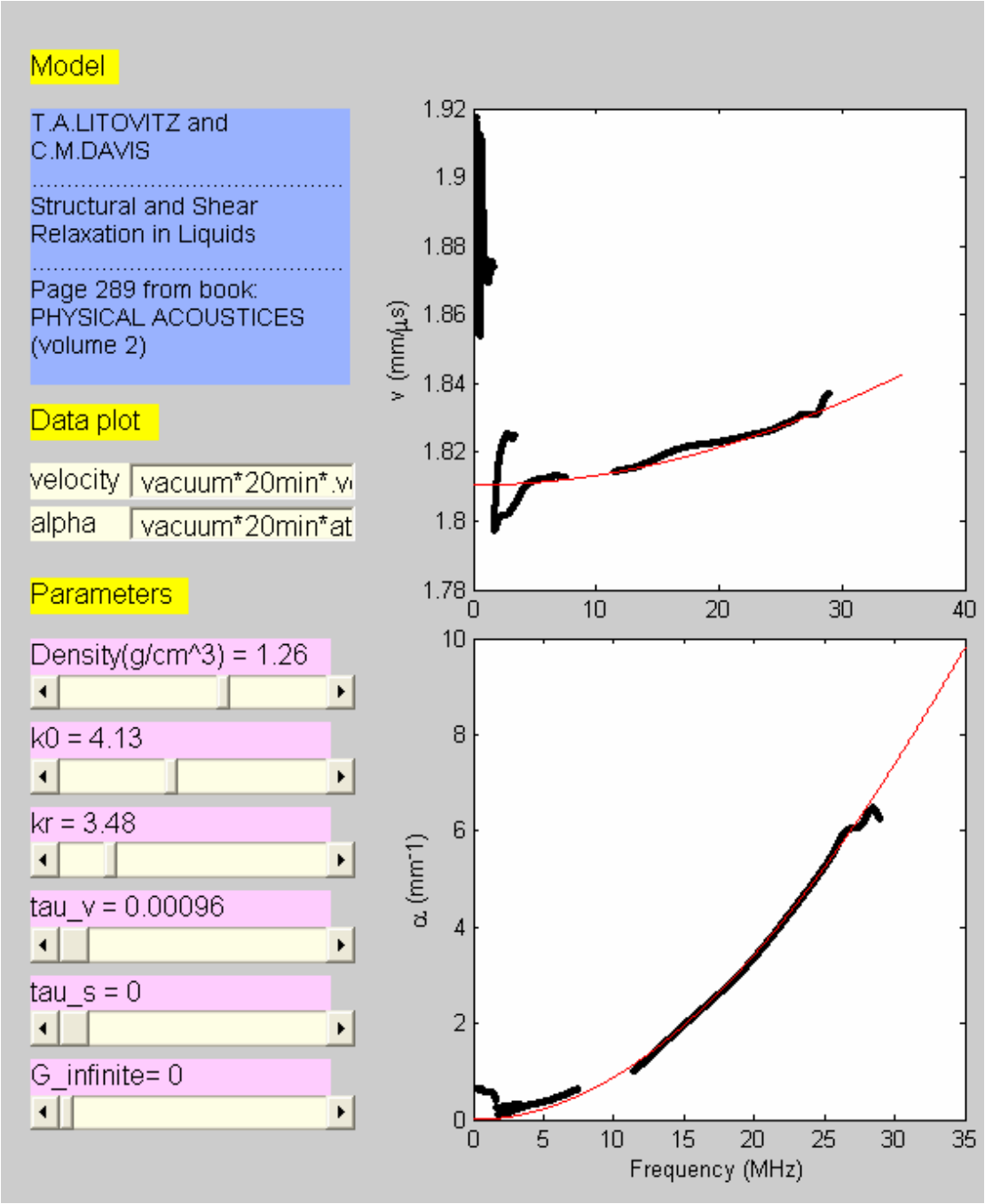

Figure 4.56. Theoretical fit (solid red curve) of the relaxation model to the high frequency data for vacuum dough (solid symbols).

4.9.3. Summary of the results for the high frequency measurements

The best combinations of the parameters were found that fit both the magnitude and the frequency dependence of the data. In the molecular relaxation model, only the relaxation time at constant volume τ_v could be determined from my data, since the shear modulus is believed to be too small for the shear relaxation to have a significant effect on the longitudinal ultrasound data. Thus, the parameters determined from fitting the model to the data are only ρ, K_0, K_r and τ_v.

For vacuum dough, no time evolution of parameters in the model was observed.

For ambient dough, though we found some difference in K_r for different times, it is hard to ascribe this difference to the slow relaxation of the matrix. The main changes over time in the data are the slopes of the velocity data and the overall magnitude of the attenuation, both of which could still be affected by the bubble resonance (figure 4.47) at early times before much Oswald ripening has occurred. The fact that there appears to be a decrease in K_∞ to a value that is determined from the model fit to the vacuum mixed dough (7-8 GPa) also suggests that there is a common value for K_∞ at high frequency, regardless of the means by which the dough was mixed.

Comparing ambient dough and vacuum dough, the most important discovery we found is the very different fast relaxation time τ_v between ambient dough (about 0.005 μs) and vacuum dough (about 0.001 μs). K_0 for ambient dough (3.08) was found to be less than that of the vacuum dough (4.13), which means that the zero frequency velocity in the ambient dough is smaller than that of vacuum dough. At long times after mixing,

$K_\infty = K_0 + K_r$ (the square root of which when divided by the square root of density corresponds to the high frequency limit of the velocity), seems very similar between ambient dough (7.96) and vacuum dough (7.61). Therefore, the differences in properties between these doughs occurs in K_0 and τ_v suggesting that the matrix of ambient dough and vacuum dough are indeed different.

4.9.4. Interpretation of the structural and/or molecular basis for the high frequency ultrasonic relaxations

The structure of wheat flour doughs is undeniably complex. As well as being a composite material comprised of a matrix carrying a high volume fraction of inert filler materials (Scanlon and Zghal, 2001), the matrix material itself is a composite, consisting of a hydrated gluten complex. This hydrated gluten complex is primarily composed of storage proteins, and these proteins have a wide distribution of molecular weights. The gluten complex is stabilized by hydrogen bonds, salt bridges, van de Waals forces and dynamically changing di-sulfide-thiol covalent interchanges (Phan-Thien et al., 2000). It is also believed that lipids native to the wheat flour are essential to the formation of this gluten complex (Bloksma 1990). It has been suggested that the proteins of this gluten matrix are organized into a supermolecular structure comprised of "glutenin particles" that aggregate to form the gluten matrix. These glutenin particles are thought to represent the vestiges of protein bodies of the growing endosperm of the grain in which the storage proteins are deposited (Don *et al*., 2003). Therefore, there are a considerable number of mechanisms that could be responsible for the molecular relaxations in the dough matrix observed in the 1 to 5 ns time range described above. Since detailed physico-chemical investigations were not part of my MSc project, I will only suggest possible mechanisms that might be responsible for the reduction in relaxation times as observed at the high frequency end of the mechanical spectrum.

It is conceivable that, just as there is a resonance peak associated with the interaction of ultrasound of a specific frequency with gas bubbles of specific sizes, that ultrasound in the megahertz frequency range interacts with the glutenin particles of a specific size to cause an additional mechanical resonance in the dough. Since glutenin particles range in size from 5-30 um (Don *et al*., 2003), the wavelength of sound would be similar to the radius of the particles at frequencies of 100-700 MHz (taking the velocity of sound to be 1700 m/s). Although these frequencies might agree with the peak of the molecular relaxations deduced from these studies, a number of factors discount the occurrence of a resonance of the glutenin particles as being responsible for the relaxation peaks observed in the mechanical spectra. Firstly, the characteristic frequency dependence of relaxation and resonance phenomena are different, and, even though the entire frequency range could not be explored in these measurements, the broad frequency response seen in the data could be very well fitted by the classic relaxation form, rather than a resonance expression, for velocity and attenuation. Secondly, the contrast in density between the glutenin particles and the rest of the gluten matrix will not be as sharp as that between air and dough matrix. Therefore, we would not expect a signature as strong as that suggested by the rise in velocity at the high frequency end of the spectrum. Thirdly, it is not clear why the glutenin particles from air-mixed doughs would be approximately 5 times bigger than the size of those from the vacuum mixed doughs (as deduced from the position of the maximum in the peak of the relaxation). Fourthly, there is an increase in the value of the modulus at faster rates of testing of the dough that is difficult to reconcile

with the presence of a resonance peak associated with structural components in the dough matrix. For these reasons, it is not believed that there is a supermolecular structural basis for the peaks at high frequency, but rather the peak arises from molecular relaxation within the dough.

To relate the high frequency ultrasonic relaxations to a specific molecular relaxation in the dough matrix, I will summarize the outcomes of the velocity and attenuation results of the experiments on air-mixed and vacuum-mixed doughs: there is no difference in the value of K_∞ for the two types of doughs at long times after mixing, whereas the value of K_0 is slightly larger for the vacuum mixed dough (4 vs 3 GPa), that this change in mechanical properties as a function of frequency can be modeled with a single relaxation mechanism and the molecular relaxation responsible is relatively long when the dough is mixed in air (5 vs 1 ns). To assign a mechanism that incorporates all of these facts, and given the complexity of dough described above, it is probably easier to rule out molecular relaxation phenomena that cannot be responsible, rather than to definitely assign a given mechanism in the absence of corroborating evidence from other techniques.

Firstly, it is not a mechanical relaxation associated with configuration rearrangements of free water molecules within the dough. These relaxations occur over picosecond timeframes (Caliskan *et al.* 2003; Gottschalk *et al.* 2001; Halle 2004) and so would not be assessed by the ultrasonic techniques used in this study. However, since water molecules associated with proteins can undergo rotation at much slower timescales (Gottschalk *et al* 2001; Halle 2004), the role of "bound" water in the mechanical

relaxation cannot be ruled out.

Secondly, it is not a molecular relaxation time associated with rotation or tumbling of the protein molecules in the aqueous environment in which they reside. The classical equation relating rotational correlation times (τ_R) to molecular volume (V) in a solvent of given viscosity (η) is given by (Gottschalk *et al*., 2001; Halle 2004;Yeboah *et al*., 1994):

$$\tau_R = \eta V/k_B T \tag{4.38}$$

in which k_B is the Boltzmann's constant and T is the absolute temperature. Given the large molecular volume associated with gluten proteins (Bloksma 1990; Phan-Thien *et al*., 2000; Wellner *et al* 2005), we cannot ascribe a mechanical relaxation in the 1-5 ns time range to tumbling of the glutenin or gliadin molecules that make up the gluten proteins within the dough matrix. For example, (Yeboah *et al.,* 1994) found from time-resolved fluorescence analyses that the rotational correlation time of γ-gliadins in 70% ethanol were of the order of 50 ns. Since the γ-gliadins are one of the smallest storage proteins found in the dough matrix (Autran 1994), full-scale rotation of the protein molecules can be ruled out as the basis for the observed ultrasonic relaxations.

Thirdly, the time scale is also too small for the full-scale folding of the protein into a new conformation as a result of the mechanical disturbance by the ultrasonic pulses. For large proteins, such conformational changes take place over milliseconds to seconds (Guo *et al.,* 2005; Naganathan *et al.,* 2006). Even longer timescales have been associated with conformational changes of proteins that reside at interfaces (Martin *et al.,* 2003).

Therefore, intermediate length scale folding motions in the gluten proteins or the protein-water complex must be responsible for the 1-5 ns timescale relaxations that are observed with ultrasound. One likely candidate is ultrasonic stress-induced changes in the secondary structure of gluten proteins. A number of different spectroscopic analyses have shown evidence of such conformational changes (Alberti *et al.,* 2002; Calucci *et al.,* 2001; Georget and Belton 2006; Yeboah *et al.,* 1994). Especially, the interconversion from P_{II}, disordered or β-turn structures to the β-sheet structure is a means of storing the elastic energy (Shi *et al.,* 2006; Wellner *et al.,* 2005) that is put into the system by the ultrasonic pulses. The timescale for such conformational rearrangements is of the order of nanoseconds (Kudryashova *et al.,* 2003; Yeboah *et al.,* 1994), and so matches the relaxation times obtained from these studies. There remains the need to explain why this conformational rearrangement occurs five times faster in doughs mixed under vacuum compared to air-mixed doughs if we are to assign secondary structural rearrangements to the ultrasonic results.

One potential mechanism for the time difference that can be discounted is that the difference in dough viscosity arises from moisture content differences between the doughs, and this is responsible for the difference in ultrasonic properties at these frequencies. Elmehdi (2001) reported that vacuum mixed doughs lose more moisture than doughs mixed at atmospheric pressure, and decreasing dough moisture content will increase the viscosity of the dough matrix (Masi *et al.,.,* 1998). However, based on equation (4.38), one would expect longer relaxation times for the vacuum mixed dough,

not the shorter time as observed. Nevertheless, it is hypothesized in this thesis that water does indeed play a role in the relaxation time difference between the doughs, but one must consider the molecular structure of the two dough systems to understand how this difference arises.

In this thesis I take the viewpoint put forward by Belton and colleagues that the loop and train model well describes the structure of wheat glutenins (Belton, 1999). Also, I suggest that ultrasonic strain energy at lower frequencies induces the disordered (hydrophilic) to *β*-sheet transition in glutenin described above, and thus stores elastic energy. The creation of a greater amount of *β*-sheet structure in the glutenin leads to loss of water from the loop regions of the glutenin polymers (Alberti *et al.,* 2002; Georget and Belton 2006). Schematically, this can be illustrated as in figure 4.57.

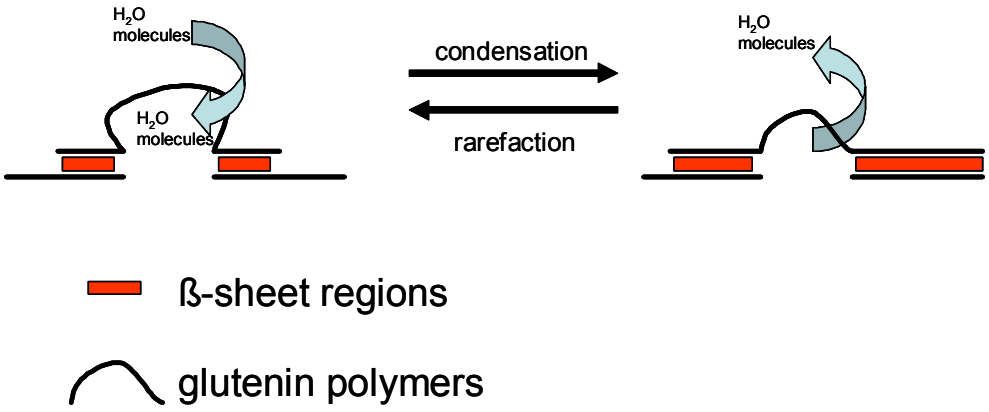

Figure 4.57. A scheme of conformational rearrangements in glutenin induced by a sinusoidally varying ultrasonic pulse.

In the condensation phase, water molecules that are hydrogen bonded to the many

glutamine side-chains on the polymers are squeezed out of the loops so that strain energy can be stored in the β-sheet regions (trains) where glutamine hydrogen bonds to glutamine on an adjacent chain, and this hydrogen bonded structure gets reinforced by hydrophobic bonds (Alberti *et al.,* 2002). At sufficiently low frequencies, the influx of water molecules into the loops during the condensation phase is fast enough that it acts in phase with the ultrasonic waves and so attenuation losses arising from this process are negligible. In this low frequency regime, the dough with more train regions will be stiffer than its counterpart that possesses more loop regions. The stiffer dough will be the dough with less moisture (Georget and Belton. 2006), i.e., the dough that has been mixed under vacuum. As a result, the drier vacuum-mixed dough will have a higher velocity at lower frequencies, as observed here, and as corroborated by Létang *et al*, (2001), who examined the ultrasonic velocity of doughs made from a weaker breadmaking flour made up with varying amounts of water.

At high frequencies (likely > 100 MHz) the structural transition induced by ultrasonic condensation cannot take place since the frequency is too high to allow time for the water to move out of the loops and for the creation of a greater amount of β-sheet regions. In this case, I do not expect there to be a difference in the K_∞ values for the two types of doughs, a result that is observed, i.e., at high frequencies the stiffness of the dough is independent of its water content.

In the intermediate timescales the loop to train transition does occur, but there is a phase lag between the ultrasonic wave and the movement of water back into the loops

during the rarefactions. As a result, there is a greater loss of acoustic energy, with the peak of the attenuation centered about a frequency which is close to the reciprocal of the relaxation time for water movement into and out of the loops (which will be determined by the structure of the dough matrix). But, which structures in the glutenin polymers might cause the relaxation time to be five times slower in the dough mixed in air compared to the dough mixed under vacuum?

I cannot suggest a definite mechanism for the difference, but two possible mechanisms might be responsible. Firstly, the slower relaxation time for the air-mixed doughs could be due to the presence of the bubbles. The loop to train transition is harder to induce in the air-mixed doughs because the polymers that undergo this transition are tethered by the presence of the bubbles. Certainly, wheat gluten proteins are surface-active polymers, and would be expected to lower their overall free energy state by adopting a conformation where hydrophobic regions of the polymer reside at the air-aqueous interface (Wilde 2003). It has been reported that when ovalbumin adsorbs to an air-aqueous interface, substantial changes in protein mobility occur with protein movement at the nano-second timescale becoming more restricted (Kudryashova *et al*., 2003). If this also occurs for the surface active storage proteins in dough, then the considerable amount of interfacial area in doughs (Carlson and Bohlin, 1978) would be expected to delay the conversion of loops to trains and so increase the relaxation time in doughs mixed under air that have this large interfacial area. Secondly, the structure of gluten polymers in the vacuum-mixed dough is such that glutenin polymers in

vacuum-mixed doughs more readily adopt the β-sheet structure at a faster timescale. Two possible mechanisms could account for this in the vacuum-mixed dough: there is less water, and so there are fewer loops (Georget and Belton 2006), making the loop to train transition occur faster; alternatively, mixing under vacuum creates a more parallel alignment of the glutenin polymer chains so that again there is a faster loop to train transition in the vacuum-mixed doughs. The latter mechanism is consistent with the ideas advanced by Elmehdi *et al.* (2004) in attempting to explain the differences in low frequency velocities between vacuum and air-mixed doughs; they suggested that the presence of di-sulfide linkages between glutenin polymers disrupts the parallel alignment of polymers induced by the work input of the mixing process. Some support for this comes from Alberti *et al.* (2003), who compared the structure of specific glutenin sub-units with their alkylated counterparts (alkylation knocks out the potential for di-sulfide bond formation) by ^{13}C and ^{1}H NMR, and concluded that the absence of cross-links allowed for closer packing of glutenin polymers.

Chapter 5 Conclusions

There are three main parts in this chapter, a summary of the dough measurement and analysis method, conclusions from the different frequency measurements, and recommended future work. In the first part, measurement procedures that allowed me to obtain reasonable results are described, as well as the methods for analysis of the raw data. The second part consists of three parts: the reporting of results at a frequency much lower than the bubble resonance, results at frequencies around the resonance, and results acquired at frequencies much higher than the bubble resonance. For the low frequencies and at frequencies around the bubble resonance, the bubble resonance model was applied, and we may infer how ultrasonic measurements relate to the bubble evolution in the dough. From the measurements at much higher frequencies than the bubble resonance frequency, information on the properties of the dough matrix was determined. The last part of the conclusion discusses recommended future work. Based on the experience gained from our studies, additional experiments are suggested to enable a deeper understanding of the properties of dough to be obtained.

5.1. Dough measurement and analysis method

Dough is a very complicated biomaterial. Its properties change with time after mixing or after any deformation that is needed to study the dough. This time dependent behavior raises a lot of difficulties when performing accurate measurements of its properties. As a result, new or improved experimental procedures and analysis had to

be devised to cope with these difficulties and enable quantitative measurements to be performed. In this section, the progress made in these measurement and analysis methods, for the different frequency ranges, is summarized.

For the 40 kHz measurements, the biggest difficult in this study was the lack of impedance information on the 40 kHz transducer. Thus, it was very hard to estimate the impedance mismatch of the 40 kHz transducer and the sample, and therefore to make appropriate corrections for the effects of boundary reflections. For this reason, different subsamples with different thickness were used to obtain the velocity and attenuation for dough mixed under ambient conditions and dough mixed under nitrogen. This method was based on the assumption that the acoustic properties of the dough were the same for measurements at different thicknesses. But from our study, the time evolution after subsample preparation deformation was found to depend on the sample thickness, even though the mass of the subsample was adjusted at different thicknesses to eliminate the effect from the strain stored during the compression of the dough (section 4.2.3). So we found that if the different thickness method was used to analyze velocity and attenuation for different waiting times, the waiting time relaxation for both velocity and attenuation were opposite to those we inferred from the relaxation trend of the transit time and amplitude. This also suggested that very thin thicknesses of dough should not be used. From our measurements and results, thicknesses less than 3 mm are not recommended for the ambient and nitrogen doughs. The best approach, based on knowledge at this moment, is to use an extrapolated reference to calculate the phase velocity and

attenuation. Different values of the extrapolated reference were obtained from the different waiting time data and so an averaged value of this reference was used for all data.

For the different thickness method, another systematic error arose from the frequency dependence of the measured attenuation values. A detailed study was presented in part 2 of Chapter 3. This effect could cause an error of about 5% in the measured values, based on the estimated transducer impedance.

For the vacuum dough, subsamples of large thickness were used to avoid multiple reflections. Data from compressing one subsample to different thicknesses did not give the correct velocity and attenuation (see figure 4.3). Because of the difficulty in correcting the impedance mismatch at this frequency (40 kHz), and lack of data from different subsamples, the phase velocity and attenuation from the reference might not be accurate (see figure 3.12, figure 3.15). Thus at 40 kHz, the velocity in vacuum dough was estimated as a signal velocity (see figure 3.16). We were still able to use these results to study the relaxation behavior of vacuum dough at this frequency.

For the higher frequency measurements (from 500 kHz up to 20 MHz), the transducer impedance was measured by using water or another liquid which has negligible attenuation. This made the analysis of the data easier and more accurate, since the effects of impedance mismatch could then be accurately taken into account.

However, the generating voltage pulse was picked up electrically by the receiving transducer, giving an early time signal coincident with the trigger pulse, and this electromagnetic signal overlapped with the real transmitted ultrasonic signal and had comparable amplitude. For this reason, plastic delay layers were used to separate the real signal from the initial generating pulse signal. Plastic layers eliminated the complexity of the transducer response arising from the complex impedance of materials such as dough. Because plastic layers were not used for vacuum dough, the velocity and attenuation are more scattered in this higher frequency range (see figure 4.51). For understanding the vacuum dough more clearly, future work is suggested in section 5.5.

One important point in all the measurements was that the sample holder should be sealed to maintain the moisture content of the sample. By doing this, the dough samples between the two transducers were found to be still wet even after an overnight measurement.

5.2. Low frequency (40 kHz) measurements

Doughs mixed at different head space pressures and different gas environments were studied at this frequency, including ambient dough, vacuum dough, dough mixed at pressures between ambient and vacuum pressure, and dough mixed in nitrogen.

For ambient dough, the measured phase velocity was about 90 m/s and attenuation coefficient about 2 mm^{-1}. The uncertainty in these values is around 10%.

The main observation was the time evolution of the phase velocity and attenuation coefficient. One evolution was associated with the relaxation of the sample after its insertion, and resulting compression, between the transducers. It was referred to as waiting time evolution in this thesis. The other evolution depended on the time after dough had been mixed, and it was called post mixing evolution.

With the waiting time evolution of ambient dough, the phase velocity decreased and attenuation coefficient increased in the initial 25 minutes after compression. This was explained as follows. When the subsample was compressed from a ball shape to a plate shape, the bubbles inside could be compressed to a smaller size and the pressure in them became larger. With this decrease of void fraction and increase of bubble pressure, the phase velocity became larger and the attenuation smaller instantaneously. As the waiting time increased, relaxation allowed the bubbles to return to their initial state before compression, because of the viscoelastic properties of the sample. Thus, the phase velocity dropped and the attenuation increased with waiting time. This explanation was also consistent with behavior when the subsample was stretched, since the relaxation behavior became opposite, because the bubbles were deformed in the opposite way. A detailed discussion can be found in section 4.2.4. When the waiting time exceeded about 25 minutes, the time evolution behavior changed, with the phase velocity increasing (instead of decreasing) and the attenuation leveling off to a time independent value. The mechanism of this very long waiting time relaxation is still not very clear.

The waiting time relaxation was also found to be thickness dependent (section 4.2.3). Even though the mass of the subsample was carefully chosen to reduce the difference in strain that was stored in the dough as a result of the deformation of the subsamples to different thickness, the true strain resulting from the compression to different thickness is still different. The waiting time at which the relaxation changed direction for phase velocity varied with the true strain - the larger the strain, the later the change. Another observation is that the absolute value of the change in velocity from the initial value to the turning point depends on the true strain applied in the sample preparation. A similar trend was also apparent for the attenuation.

With the time after mixing, no systematic time evolution was found for velocity, and likely also for attenuation, for times longer than 30 minutes after mixing. This suggests either that the magnitude of the strains induced by mixing, and their effect on ultrasonic properties of the dough, is small compared with those applied during subsample preparation for ultrasonic testing, or that the strains have been relaxed in the first 30 minutes after mixing.

For the vacuum dough, opposite waiting time relaxation behavior at early times was observed compared to the ambient dough. After the initial compression of the dough, the phase velocity rapidly increased for about 60 minutes and then started to decrease. Initially, the attenuation coefficient rapidly decreased and then started to decrease at a

slower rate. This waiting time relaxation behavior was found to be very different after the initial compression to the behavior after subsequent compressions, i.e., when the initial ball shaped sample was compressed to a disk shape versus when the disk shaped sample was subsequently compressed to a thinner disk shaped sample (see figure 4.5). This partially explains why the one subsample method fails to measure velocity and attenuation in the vacuum dough measurements (see figure 4.3).

For the very long waiting time relaxation (see figure 4.9), a double exponential function was used to model these relaxations. We found that the short relaxation has a relaxation time around 500 to 2000s, while the long time relaxation is much longer, around 30,000 to 40,000s. The mechanisms of these two relaxations are still not very clear. Thirty minutes after mixing, no post mixing relaxation was found in our experiment (as the experiments were started 30 minutes after mixing).

For the dough mixed at a head space pressure between ambient and vacuum pressures, both ambient-like relaxation and vacuum-like relaxations were observed, depending on pressure. For the pressure close to that used to prepare the vacuum dough, the relaxation behavior was more like vacuum dough, while when the pressure was higher, the relaxation behavior was closer to that of ambient dough, with the relaxation rate changing with pressure. The crossover pressure was found to be between 0.12 to 0.17 atmospheres. This suggests that there are two different relaxation mechanisms involved, one being due to relaxation arising from bubble shape and volume changes, and

the other one being from relaxation of polymers in the dough matrix. At higher mixing pressures, bubble relaxation is dominant but when pressure decreases, we started to see the relaxation arising from the matrix. The crossover pressure also corresponds to the bubble void fraction below which velocity increases rapidly as the void fraction is lowered (Elmehdi *et al*., 2004). The detailed discussion can be found in section 4.3.4.

Nitrogen dough was also studied in this thesis. Compared with ambient dough, there are several differences. First, the density is higher: $\rho_{nitrogen} = 1.16 \pm 0.01$ g/cm^3 is larger than $\rho_{ambient} = 1.12 \pm 0.01$ g/cm^3. This implies that the bubble volume fraction is smaller in nitrogen dough than in ambient dough. The volume fraction of ambient dough is about 12 % and, using the same gas free density, the volume fraction of nitrogen dough would be 9%. Second, using the same measurement process as for ambient dough (different subsamples for each thickness; same sequence of different thicknesses, waiting times and post mixing times; same analysis for v and α using the average extrapolated reference), the phase velocity of nitrogen dough was found to be about 9% larger than that of ambient dough. In addition, the attenuation coefficient of nitrogen dough was about 10% smaller than that of ambient dough. These larger values of velocity and smaller attenuation coefficients are consistent with a lower volume fraction of bubbles in the nitrogen dough, as can be seen by comparing these differences with the volume fraction dependence of velocity and attenuation found by Elmehdi *et al*. (2004) for doughs mixed in air at various headspace pressures. Third, although the overall

relaxation behavior of nitrogen dough was similar to that of ambient dough, the variation of both velocity and attenuation from the initial value to the turning point at early waiting times was less for nitrogen dough than for ambient dough. As there is a lower volume fraction of bubbles in nitrogen dough, this result is also consistent with the bubble relaxation mechanism proposed in section 4.2.3. This smaller initial change in velocity and attenuation for nitrogen dough also has the effect of moving the turning point, where the slope of the waiting time dependence of the velocity and attenuation changed sign, to earlier times. Fourth, for the relaxation behavior at very long waiting times, the attenuation coefficient decreased with time and leveled off to a value close to the initial attenuation for the nitrogen dough, while the attenuation showed no significant long time decrease for ambient dough, remaining approximately independent of time for times greater than 30 minutes. This decrease in the attenuation coefficient for nitrogen dough at long times is reminiscent of the decrease seen in vacuum dough (see figure 4.9), suggesting there may be a somewhat similar matrix relaxation effect, possibly due to oxygen depletion in the matrix, in the nitrogen dough. However, this mechanism, if present in nitrogen dough, is certainly weaker than in vacuum dough, and does not significantly affect the velocity changes in the same way, since the long-time velocity changes are not similar in the nitrogen and vacuum doughs (see figure 4.9).

5.3. Measurements near the bubble resonance

The bubble resonance frequency in ambient dough is in the 1 to 5 MHz range.

Both ambient and vacuum dough were studied in this frequency range.

For ambient dough, peaks in both the phase velocity and the attenuation were observed around the bubble resonance frequency. The attenuation peak is at a lower frequency compared with the velocity peak. Based on multiple scattering theory, a bubble resonance model was used to interpret the data. The description of the theoretical model can be found in section 4.7.1.

From the fitting of the experimental data based on this model, a log-normal bubble distribution in the dough was found to be consistent with the data. For the dough 43 minutes after mixing, parameters $r_0 = 17.5$ μm, $\varepsilon = 0.37$ were found. (For the log-normal distribution that describes the bubble sizes, r_0 and ε are the parameters that determine the mean radius of the distribution $r_{mean} = r_0 \exp(0.5\varepsilon^2)$ and the radius at the maximum of the distribution $r_{\max} = r_0 \exp(-\varepsilon^2)$. ε is called the geometric standard deviation in bubble size.) For the dough 86 minutes after mixing, $r_0 = 22$ μm and $\varepsilon = 0.35$. We found that as the time after the dough was mixed became longer, the average bubble size increased and the distribution became narrower. This indicates that there is disproportionation of the bubbles occurring in the dough. A clearer picture of the evolution of the bubble size can be seen in the variation of the velocity and attenuation peak frequency and peak value with post mixing time (figure 4.49 and 4.50). Because the peak frequency of the attenuation coefficient and phase velocity can be related to the average size and width of the bubble size distribution, with higher peak frequencies corresponding to smaller bubble sizes, we can infer that the bubble size

grows with the time after mixing.

Comparing these results with those obtained with x-ray tomography for a sample of dough that had rested for 90 minutes after mixing, the peak radius of our bubble distribution is smaller and the width is narrower (figure 4.47). The discussion of the discrepancies can be found in section 4.8.1.

For vacuum dough, there is considerable scatter in the data near the bubble resonance frequency (figure 4.51). No post-mixing relaxation could be observed near the bubble resonance within the uncertainty of the data from different subsamples (see section 4.5 for the complete set of data). Using the bubble resonance model, parameters $r_0 = 50\mu m$, $\varepsilon = 0.42$ were found for dough 2 minutes after compressing and $r_0 = 70\mu m$, $\varepsilon = 0.38$ at 20 minutes after compressing. This is larger than the bubble size inferred for ambient dough from ultrasonic measurements, as well as from the x-ray tomography.

For both ambient and vacuum doughs, there are several factors that contribute to the uncertainties in determining the bubble size distribution using this model. For the ambient dough, we have better data, but the void fraction is much higher than 1% (a range of concentrations where the model has not been tested independently) and the subsamples used in the experiment were very thin (0.3 mm, so that the bubble size distribution could be affected by the compression of the samples). For the vacuum data, the void fraction is low and subsamples were less deformed, but the contact measurement was influenced by the effect of the transducer impedance, which was difficult to

eliminate unambiguously.

5.4. Measurements above bubble resonance

At frequencies much higher than the bubble resonance frequency (namely those around 20 MHz), a classical ultrasonic relaxation model, which describes how the frequency dependence of the velocity and attenuation is influenced by molecular relaxations, was used to interpret the results. Both ambient and vacuum dough were studied. A description of the model is given in section 4.7.2.

For vacuum dough, the fitting parameters do not change with time. Although we found some difference in K_r for different times, it is hard to ascribe this difference to the slow relaxation of the matrix. We believe this effect is due to the tail of the bubble resonance, even though there are few bubbles in vacuum dough.

The most important discovery we found is the existence of fast relaxations in the dough matrix on the nanosecond timescale, with relaxation times τ_v that differ in magnitude between ambient dough (about 0.005 μs) and vacuum dough (about 0.001 μs). Also, the results suggest there is a common value of K_∞ at high frequency for both ambient and vacuum dough. K_0 for ambient dough (3.08 GPa) was found to be less than that of the vacuum dough (4.13 GPa) which means that the zero frequency velocity in the ambient dough is smaller than that of the vacuum dough. This difference in K_0 suggests that the matrix of ambient dough and vacuum dough are different.

It was suggested in section 4.9.4 that intermediate length scale folding motions in

the gluten proteins or the protein-water complex are responsible for the 1-5 ns timescale relaxations that are observed in our ultrasonic experiments. One likely candidate is ultrasonic stress-induced changes in the secondary structure of gluten proteins. Research shows that the interconversion from disordered or β-turn structures to the β-sheet structure is a means of storing the elastic energy (Shi *et al.,* 2006; Wellner *et al.,* 2005) that is put into the system by the ultrasonic pulses. In the condensation phase, water molecules that are hydrogen bonded to the many glutamine side-chains on the polymers are squeezed out of the loops, so that strain energy can be stored in the β-sheet regions (trains) where glutamine hydrogen bonds to glutamine on an adjacent chain, and this hydrogen bonded structure gets reinforced by hydrophobic bonds (Alberti *et al.,* 2002). The timescale for such conformational rearrangements is of the order of nanoseconds (Kudryashova *et al.,* 2003; Yeboah *et al.,* 1994), and therefore is similar to the relaxation times obtained from these studies.

Although it is hard to give a definite mechanism to explain why the relaxation time is five times slower in the ambient dough compared to the dough mixed in vacuum, two possible mechanisms were given in this study. First, the slower relaxation time for the air-mixed doughs could be due to the presence of the bubbles. The loop to train transition is harder to induce in the air-mixed doughs because the polymers that undergo this transition are tethered to the bubbles. Second, it may be easier for the structure of glutenin polymers in the vacuum-mixed dough to adopt the β-sheet structure. This could happen for two reasons. One is that in the vacuum dough, the water content is

less, so that the loop to train transition occurs faster. Secondly, the process of mixing under vacuum creates a more parallel alignment of the glutenin polymer chains, so that again there is a faster loop to train transition in the vacuum-mixed doughs.

5.5. Recommendations for future work

a. Experiment to measure the acoustic impedance of the 40 kHz transducers

The lack of information on the 40 kHz transducer acoustic impedance caused a lot of uncertainties in our study. Therefore, it would be worthwhile to perform an experiment to measure the impedance of the 40 kHz transducer directly. A material with well known acoustic properties, such as Acrylic could be chosen as the sample. Signals could be recorded from samples with different thickness. The minimum thickness should be chosen so that the first arrival could be separated from the multiple reflections. Theoretically, if we have signals from two different thicknesses, we can calculate the impedance of the transducer.

b. Very long waiting time experiment with a short post mixing time

In this thesis, very long waiting time experiments were performed for different kinds of dough. A common feature of these experiments is the very long post mixing time at which these measurements were started; this happened because this kind of experiment was normally done for the last subsample. An interesting question is whether the long waiting time relaxation behavior is the same for short post mixing time as for very long

post mixing time. This experiment will give us a more complete picture of the very long waiting time relaxation for different doughs.

c. Different thickness experiments for vacuum dough performed on different subsamples

My experiments showed that an exponential decay of amplitude with thickness can never be observed for vacuum dough if only one subsample was squeezed to different thicknesses, because the waiting time relaxation is very different for the initial compression and the subsequent compressions. Therefore, it would be of interest to measure different subsamples of different thicknesses. Because large thicknesses are required to eliminate multiple reflections for vacuum dough, on account of the large velocities, and the subsample should also be chosen from the inner part of the dough piece (since surface of the dough piece is not smooth) to avoid trapping air bubbles from the surface of the dough piece, a single mixed dough piece might not be enough for the experiment. This problem can be overcome by mixing several doughs and choosing subsamples of different thicknesses from different dough pieces. Although no post mixing relaxation was found for vacuum dough in our study, we can chose the same post mixing time for different subsamples more precisely using this approach. Then, we can measure the waiting time dependence of the transit time and amplitude for each thickness. It would be important that the mass of the samples for different thickness be chosen so that the compression would be similar for each thickness. Unless the samples of

different thickness are really different, it should then be possible to plot the thickness dependence of the amplitude, as well as transit time, for different waiting times. From this group of experiments, we will obtain the attenuation and velocity as a function of waiting time for the vacuum dough.

d. Different thickness experiments for doughs mixed at intermediate pressures performed on different subsamples

In order to understand the properties of dough mixed at the intermediate pressures, instead of compressing one subsample to subsequent thickness, different subsamples should be used for different thickness measurements. Basically, the same experiment as was done for ambient dough in section 4.2.2 should be done for the doughs mixed at intermediate pressures. Doing this will help to reveal more clearly the waiting time and post mixing time relaxations for these pressures, and therefore to better understand how the volume fraction of bubbles affects the relaxation behavior of the dough.

e. Additional experiments on dough mixed in a nitrogen environment

In the research performed for this thesis, when mixing nitrogen dough, there was a step in which air was pumped out of the mixing bowl before the nitrogen flow was started (see details in section 2.1.3). It could be argued that this procedure might lower the void fraction of gas in the nitrogen dough, a result which is consistent with the experimental observations. Therefore, in order to be certain of the quality of the nitrogen dough, it

would be better if the whole mixer was put inside a larger nitrogen environment. For example, the mixer could be put into a large glove box or a sealed tank. The nitrogen atmosphere inside the mixing bowl could then be created by slowly flowing nitrogen gas through the glove box or sealed tank, without the need to evacuate the mixing bowl first. This procedure will enable a better comparison between ambient dough and nitrogen dough to be made.

f. High frequency measurements for nitrogen dough

After performing the above experiment (experiment e.), it would be worthwhile to measure nitrogen dough in the high frequency range, just as we did for ambient and vacuum dough. This would give us a more complete picture of the connection between these three types of dough. In particular, it might then be possible to learn more about the role of oxygen on the properties of the dough matrix, especially how oxygen affects the bubble size distribution, disproportionation of the bubbles, and fast molecular relaxations in the matrix.

g. High frequency measurements for vacuum dough with a plastic delay layer

As was discussed in section 4.8.2, where we infer bubble size distributions by using the bubble resonance model for ambient dough and vacuum dough, both measurements face difficulties. The ambient data is of better quality, but the bubble volume fraction is much higher than the range of volume fractions for which independent tests of the model

have been carried out. Thus it is not known yet whether the model is reliable for such high volume fractions. For the vacuum dough, the bubble volume fraction is small, but because of the complexity of the data analysis, due to the impedance mismatch between the transducer and the sample, the phase velocity and attenuation are more scattered around the bubble resonance frequency and the data are less reliable (see figure 4.51). Therefore it would be very good to perform an experiment near the bubble resonance frequency on the vacuum dough using the plastic delay layer method. This experiment will give better data, so that we can infer the bubble size distribution more accurately for the vacuum dough. Because the bubble size distribution is not considered to change with the mixing pressure, this experiment should give information that is relevant to the bubble size distribution of dough mixed at any pressure.

References

Enrica **Alberti**, Simon M. Gilbert, Arthur S. Tatham, Peter R. Shewry and Ana M. Gil (2002). "Study of high molecular weight wheat glutenin subunit 1Dx5 by 13C and 1H solid-State NMR Spectroscopy. I. Role of Covalent Crosslinking", *Biopolymers (Biospectroscopy),* **67***,* 487–498.

V. N. **Alekseev** and S. A. Rybak (1999). "Gas bubble oscillations in elastic media", *Acoustical Physics*, **45**, 535-540.

William A. **Atwell** (2001). *Wheat Flour* (American Association of Cereal Chemists, Inc. St Paul, USA).

J.-C. **Autran** (1994). "Size-Exclusion High-Performance Liquid Chromatography for Rapid Examination of Size Differences of Cereal Proteins", in *High-Performance Liquid Chromatography of Cereal and Legume Proteins*, ed. by J. E. Kruger and J. A. Bietz (AACC Press, St Paul, MN) pp. 326-372.

W. R. **Aykroyd** and Joyce Doughty (1970). *Wheat in Human Nutrition* (Food and Agriculture Organization of the United Nations)

J. C. **Baker** and M. D. Mize (1941). "The origin of the gas cell in bread dough", *Cereal Chemistry*, **18**, 19-34.

G. G. **Bellido**, M. G. Scanlon, J. H. Page and B. Hallgrimsson (2006). "The bubble size distribution in wheat flour dough", *Food Research International,* **39**, 1058-1066.

P. S. **Belton** (1999). "On the elasticity of wheat gluten", *J. Cereal Sci.,* **29**, 103-107.

J **Blitz**. (1963). *Fundamentals of Ultrasonics* (Butterworths Scientific Publications, Ltd., London).

A. H. **Bloksma** (1971). in *Wheat Chemistry and Technology*, ed. by Y. Pomeranz (The American Association of Cereal Chemists, Inc., St. Paul, Minnesota).

A. H. **Bloksma** (1990). "Rheology of the bread making process", *Cereal Foods World,* **35** 228–236.

A.H. **Bloksma** and W. Bushuk (1988). "Rheology and chemistry of dough", in: *Wheat chemistry and technology, 3rd ed.,* ed. by. Y. Pomeranz, (American Association of Cereal Chemists, Inc., St. Paul, Minnesota) Vol. 2, pp. 131–218.

Léon. **Brillouin** (1960). *Wave propagation and group velocity*, (Academic Press Inc., New York).

Betty A. **Bugusu**, Bartlomiej Rajwa and Bruce R. Hamaker (2002). "Interaction of Maize Zein with wheat gluten in composite dough and bread as determined by confocal laser scanning microscopy", *Scanning,* **24**, 1-5.

G. **Caliskan**, A. Kisliuk, A. M. Tsai, C. L. Soles, A. P. Sokolov (2003). "Protein dynamics in viscous solvents", *J. Chem. Phys.,* **118** (9), 4230-4236.

Lucia **Calucci,** Calogero PFilipczynskiino, Antonella Capocchi, Luciano Galleschi, Silvia Ghiringhelli, Franco Saviozzi and Maurizio Zandomeneghi (2001). "Structure and dynamics of high molecular weight glutenin subunits of durum wheat (triticum durum) in water and alcohol solutions studied by electron paramagnetic resonance and circular dichroism spectroscopies", *J. Agric. Food Chem*., **49**, 359-365.

G.M. **Campbell**, C.D. Rielly, P.J. Fryer and P.A. Sadd (1991). "The measurement of bubble size distribution in an opaque food fluid", *Transactions of the Institution of Chemical Engineers, Part C, Food and Bioproducts Processing,* **69**, 67-76.

G. M. **Campbell**, D. D. Rielly, P. J. Fryer, and P. A. Sadd (1998), "Aeration of bread dough during mixing: effect of mixing dough at reduced pressure", *Cereal Foods World,* **43**, 163-167.

T. **Carlson** and L. Bohlin (1978). "Free surface energy in the elasticity of the wheat flour doughs", *Cereal Chemistry,* **55**, 539-544.

N. L. **Chin**, Peter J. Martin and Grant M. Campbell (2005). "Dough aeration and rheology: Part3. Effect of the presence of gas bubbles in bread dough on measured bulk rheology and work input rate", *J. Sci. Food Agric.*, **85**, 2203-2212.

K. W. **Commander** and A. Prosperetti (1989). "Linear pressure waves in bubbly liquids: comparison between theory and experiments", *J. Acoust. Soc. Am.*, **85**, 732-746.

C. **Don**, W. Lichtendonk, J. J. Plijter and R. J. Hamer (2003). "Glutenin Macropolymer: a Gel Formed by Glutenin Particles", *Journal of Cereal Science*, **37**, 1-7.

H. M. **Elmehdi** (2001). *An ultrasonic investigation of the effect of voids on the mechanical properties of bread dough and the role of gas cells in determining the cellular structure of freeze-dried breadcrumb,* Ph.D. Thesis, University of Manitoba.

H. M. **Elmehdi**, J. H. Page and M. G. Scanlon (2004). "Ultrasonic investigation of the effect of mixing under reduced pressure on the mechanical properties of bread dough", *Cereal Chemistry*, **81**, 504-510.

Hamed **Faridi** and Jon M. Faubion (1995). *Wheat end uses around the world* (American Association of Cereal Chemists, St. Paul, Minnesota, USA).

J. M. **Faubion** and R. Carl Hoseney (1989). "The Viscoelastic Properties of Wheat flour Doughs", in *Dough Rheology and Baked Product Texture* ed. by Hamed Faridi and Jon M. Faubion (Van Nostrand Reinhold, New York).

Leszek **Filipczynski**, Zdzislaw Pawlowski and Jerzy Wehr (1966). *Ultrasonic Methods of Testing Materials,* translated [from the Polish] by K. R. Schlachter and edited by J. Blitz (Butterworths, London).

L. L. **Foldy** (1945). "The multiple scattering of waves", *Physical Review*, **67**, 107-119.

I. S. **Forrest** (1996). "The use of ultrasonics of in-line measurement in beer and wort", *Cerevisia,* **21**, 51-54.

J. **Garcia-Alvarez**, J. M. Alava, J. A. Chavez, A. Turo, M. J. Garcia, J. Salazar (2006). "Ultrasonic characterization of flour-water systems: A new approach to investigate dough properties", *Ultrasonics,* **44***,* 1051-1055.

Dominique M. R. **Georget** and Peter S. Belton (2006). "Effects of temperature and water content on the secondary structure of wheat gluten studied by FTIR spectroscopy". *Biomacromolecules,* **7**, 469-475.

Michael, **Gottschalk**, Norbert A. Dencher and Bertil Halle (2001). "Microsecond exchange of internal water molecules in bacteriorhodopsin", *J. Mol. Biol.,* **311**, 605-621.

Weihua. **Guo**, Joan-Emma Shea, and R. Stephen Berry (2005), "The Physics of the

interactions governing folding and association of proteins", *Ann. N. Y. Acad. Sci.,* **1066**, 34–53.

Bertil **Halle** (2004). "Protein hydration dynamics in solution: a critical survey", *Phil. Trans. R. Soc. Lond. B* **359**, 1207-1224.

I. **Hlynka** and J. A. Anderson (1955). "Laboratory dough mixer with an air-tight bowl", *Cereal Chem.,* **32**, 83-87.

M. **Kaczmarek**, M. Pakula and J. Kubik (2000). "Multiphase nature and structure of biomaterials studied by ultrasounds", *Ultrasonics,* **38**, 703-707

S. G. **Kargl** (2002). "Effective medium approach to linear acoustics in bubbly liquids", *J. Acoust. Soc. Am.*, **111**, 168-173.

Elena V. **Kudryashova**, Marcel B. J. Meinders, Antonie J. W. G. Visser, Arie van Hoek and Harmen H. J. de Jongh (2003). "Structure and dynamics of egg white ovalbumin adsorbed at the air/water interface", *Eur. Biophys. J.*, **32**, 553–562.

Heinrich **Kuttruff** (1991). *Ultrasonics: Fundamentals and Applications* (Elsevier Applied Science, London and New York).

T. G. **Leighton** (1994). *The Acoustical Bubble* (Academic Press, London).

C. **Létang**, M. Piau, C. Verdier (1999). "Characterization of wheat flour-water doughs. Part 1: Rheometry and microstructure", *Journal of Food Engineering,* **41**, 121-132.

C. **Létang**, M. Piau, C. Verdier, L. Lefebvre (2001). "Characterization of wheat flour-water doughs: a new method using ultrasound", *Ultrasonics*, *133-141.*

V. **Leroy**, M. Devaud, T. Hocquet and J.-C. Bacri (2005). "The bubble cloud as an

N-degree of freedom harmonic oscillator", *Eur. Phys. J. E*, **17**, 189-198.

Valentin **Leroy**, Yuanzhong Fan, A. L. Strybulevych, G. G. Bellido, J. H. Page, M. G. Scanlon (2006). "Investigating the bubble size distribution in dough using ultrasound", in *Bubbles in Foods2*, ed. by G. Campbell, in press.

T. A. **Litovitz** and C.M. Davis (1965). "Structural and Shear Relaxation of Liquids", in *Physical Acoustics* Volume II, Part A (Academic Press, London) pp 281-349.

F. **MacRitchie** (1985). "Physicochemical Processes in Mixing", in *Chemistry and Physics of Baking*, ed. by J. M. V. Blanshard, P. J. Frazier and T. Galliard (Royal Society of Chemistry, London).

Anneke H. **Martin**, Marcel B. J. Meinders, Martin A. Bos, Martien A. Cohen Stuart and Ton van Vliet (2003). "Conformational Aspects of Proteins at the Air/Water Interface Studied by Infrared Reflection-Absorption Spectroscopy", *Langmuir* **19**, 2922-2928

P. **Masi**, S. Cavella, and M. Sepe (1998). "Characterization of Dynamic Viscoelastic Behavior of Wheat Flour Doughs at Different Moisture Contents", *Cereal Chemistry*, **75**, 428-432.

D. J. **McClements**, M. J. W. Povey (1990). "Ultrasonic characterization of a food emulsion", *Ultrasonics* **28**, 266-272.

Athi N. **Naganathan**, Urmi Doshi, Adam Fung, Mourad Sadqi, and Victor Muñoz (2006). "Dynamics, Energetics, and Structure in Protein Folding", *Biochemistry,* **45**, 8466-8475.

Nhan **Phan-Thien**, Marcus Newberry and Roger I. Tanner (2000). "Non-linear

oscillatory flow of a soft solid-like viscoelastic material", *J. Non-Newtonian Fluid Mech.,* **92**, 67–80.

A. **Prosperetti** (1977). "Thermal effects and damping mechanisms in the forced radial oscillations of gas bubbles in liquids", *J. Acoust. Soc. Am.*, **61**, 17-27.

E. J. **Pyler** (1973). *Baking: Science and Technology* Vol. I (Sosland Publishing, Merriam, KS, USA), pp. 246-252.

R. **Saggin** and J. N. Coupland (2001). "Non-contact ultrasonic measurements in food materials", *Food Res. Int.*, **34**, 865-870.

M. G. **Scanlon** and M. C. Zghal (2001). "Bread properties and crumb structure", *Food Res. Int.,* **34**, 841-864.

Zhengshuang **Shi**, Kang Chen, Zhigang Liu, and Neville R. Kallenbach (2006). "Conformation of the backbone in unfolded proteins", *Chem. Rev.*, **106**, 1877-1897.

M. **Strasberg** (1953). "The pulsation frequency of nonspherical gas bubbles in liquids", *J. Acoust. Soc. Am.*, **25**(3), 536-537.

C. O. **Swanson**, and E. B. Working (1933). "Testing the quality of flour by the recording dough mixer", *Cereal Chem.*, **10**(1), 1-29.

Katherine A. **Tilley**, Rachel E. Benjamin, Katherine E. Bagorogoza, B. Moses Okot-Kotber, Om Prakash, and Haidoo Kwen (2001), "Tyrosine Cross-Links: Molecular Basis of Gluten Structure and Function", *J. Agric. Food Chem.,* **49**, 2627-2632.

T. **Van Vliet** (1999). "Physical factors determining gas cell stability in a dough during

bread making", in *Bubbles in Food* ed. by G. M. Campbell, C. Webb, S. S. Pandiella, and K. Niranjan (Eagan Press, St. Paul, MN) pp. 121-127.

C. **Verdier** and M. Piau (1996). "Analysis of the morphology of polymer blends using ultrasound", *J. Phys. D: Appl. Phys*., **29**(6), 1454-1461.

Claude **Verdier**, Pierre-Yves Longin and Monique Piau (1998). "Dynamic shear and compressional behavior of polydimethylsiloxanes: Ultrasonic and low frequency characterization", *Rheol. Acta*, **37**, 234-244.

C. E. **Walker** and J. L. Hazelton (1996). "Dough rheological tests", *Cereal Foods World,* **41**(1), 23-28.

C. E. **Walker**, J. L. Hazelton, and M. D. Shogren (1997). *The mixograph handbook* (National Manufacturing Division, TMCO, 507 "J" St., Lincoln, NE, USA).

Nikolaus **Wellner**, E. N. Clare Mills, Geoff Brownsey, Reginald H. Wilson, Neil Brown, Jacqueline Freeman, Nigel G. Halford, Peter R. Shewry, and Peter S. Belton (2005). "Changes in Protein Secondary Structure during Gluten Deformation Studied by Dynamic Fourier Transform Infrared Spectroscopy", *Biomacromolecules,* **6**, 255-261.

P. **Wilde** (2003). *Breadmaking: Improving Quality*, ed. by S. P. Cauvain (Woodhead Publishing Ltd, Abington, England) pp. 321-351.

P. S. **Wilson**, R. A. Roy, W. M. Carey (2005). "Phase speed and attenuation in bubbly liquids inferred from impedance measurements near the individual bubble resonance frequency", *J. Acoust. Soc. Am.*, **117**, 1895-1910.

A. B. **Wood** (1941). *A Textbook of Sound* (Bell, London)

N. A **Yeboah**, R. B. Ferredman, Y. Popineau, P. R. Shewry and A. S. Tatham (1994). Fluoresence studies of 2 Gamma-Gliadin fractions from bread wheat", *Journal of Cereal Science*, **19**, 141-148.